

Czech Technical University in Prague
Faculty of Electrical Engineering

Doctoral Thesis

June 2019

Petra Matunová

Czech Technical University in Prague

Faculty of Electrical Engineering

Department of Physics

***STUDY AND SIMULATION OF
MOLECULAR INTERACTIONS ON
DIAMOND SURFACES***

Doctoral Thesis

Petra Matunová

Prague, June 2019

Ph.D. Programme: (P2612) Electrical Engineering and Information Technology
Branch of study: (2602V009) Electrotechnology and Materials

Supervisor: *Doc. RNDr. Bohuslav Rezek, Ph.D.*
Supervisor-Specialist: *Ing. Vít Jirásek., Ph.D.*

Keywords

density functional theory, nanodiamonds, polypyrrole, photovoltaics

Klíčová slova

teorie funkcionálu hustoty, nanodiamanty, polypyrol, fotovoltaika

Acknowledgments

I would like to thank my supervisor doc. RNDr. Bohuslav Rezek, Ph.D. for his professional guidance during my work on the thesis, his excellent organization skills and willingness. I thank to my supervisor-specialist Ing. Vít Jirásek, Ph.D. for all the fruitful discussions. Next, I am thankful to Prof. Alexanfer Holleitner, Prof. Ursula Wurstbauer, and Prof. Alessio Garliardi for supervising and facilitating me my exchange study at the Technical University of Munich. As well, my thank belongs to Ing. Daria Miliaieva, Waldemar Kaiser, M.Sc., Mohammed Darwish, M.Sc., and Dr. Diego López Carballeira for inspirative discussions. Last but not least, I would like to thank my family for their support.

Honest declaration

I declare that I carried out this doctoral thesis independently, and only with the cited sources, literature and other professional sources.

Annotation

Finding novel flexible materials for renewable energy generation is increasing in importance to meet modern society requirements. Diamond nanoparticles denoted as nanodiamonds (NDs) possess numerous beneficial material properties and are envisioned for a wide range of applications. Blending NDs with organic materials into organic-inorganic composites could provide new beneficial properties for solar cells, in contrast with the well-established but not ideally cost-effective and adaptable silicon photovoltaics. This thesis is focused on studying interactions of polypyrrole (PPy) with NDs by computational methods in order to reveal and better understand effects possibly brought about by the nanoscale features. First principles density functional theory (DFT) is employed, particularly the B3LYP and ω B97X-D functionals with the 6-31G(d) basis set are used. We compare PPy in chemisorbed and physisorbed configurations on the most probable reconstructed (111) and (100) ND surface slabs as well as amorphous surfaces with the most common hydrogen- and oxygen-surface functional groups. Consistently for hydrogenated and oxidized ND surfaces, calculated binding energies (E_b) indicate exothermic and endothermic character for physisorbed and chemisorbed structures, respectively. For the oxidized ND surfaces, though, the analysis reveals significant role of hydrogen bonds in the physisorption of PPy. The covalent or non-covalent nature of the bond type is confirmed by the interaction energies (E_{int}). For a substantial number of the cases, high values of charge transfer (Δq) between PPy and ND are observed. We observe spatially separated HOMO and LUMO and favorable energetic level alignment at the ND-PPy interface for the majority of the oxidized NDs. The computed features are also retained for NDs with the amorphous surface layer. Excited states are computed by time-dependent DFT (TDDFT) to analyze how the electronic configuration can promote dissociation of excitons, for instance in photovoltaic applications. In a number of the cases, the transition from HOMO to LUMO turns out to be dominant. The obtained results thus provide guidance for the synthesis of real ND-PPy composites.

Anotace

Nalezení nových flexibilních materiálů pro výrobu energie z obnovitelných zdrojů nabývá na významu pro splnění požadavků moderní společnosti. Diamantové nanočástice označované jako nanodiamanty (NDs) mají řadu příznivých materiálových vlastností a mají potenciál pro širokou škálu aplikací. Kombinace NDs s organickými materiály do organicko-anorganických kompozitů by mohlo poskytnout nové výhodné vlastnosti pro solární články, na rozdíl od dobře zavedené, ale nikoli ideálně nákladově efektivní a přizpůsobitelné křemíkové fotovoltaiky. Tato práce je zaměřena na studium interakcí polypyrolu (PPy) s ND pomocí výpočetních metod s cílem odhalit a lépe porozumět efektům, které jsou důsledkem nanostruktury. Konkrétně je použita teorie funkcionálu hustoty (DFT) vycházející z prvotních principů a B3LYP a ω B97X-D funkcionály s 6-31G(d) bázev sadou. Porovnáváme PPy v chemisorbovaných a fyzisorbovaných konfiguracích na nejpravděpodobnějších rekonstruovaných (111) a (100) ND površích a také na amorfních površích s nejběžnějšími vodíkovými a kyslíkovými funkčními skupinami na povrchu. Konzistentně pro hydrogenované a oxidované ND povrchy, vypočtené vazebné energie (E_b) indikují exotermní charakter pro chemisorbované struktury a endotermní charakter pro fyzisorbované struktury. Pro oxidované ND povrchy analýza odhalila významnou roli vodíkových vazeb pro fyzisorpci PPy. Kovalentní nebo nekovalentní charakter vazby je potvrzen interakčními energiemi (E_{int}). Pro značný počet případů jsou pozorovány vysoké hodnoty přenosu náboje (Δq) mezi PPy a ND. Dále jsou pozorovány prostorově oddělené hraniční orbitály (HOMO a LUMO) a příznivé vyrovnání energetické hladiny na rozhraní ND-PPy pro většinu oxidovaných ND. Vypočtené vlastnosti jsou zachovány i pro ND s amorfní povrchovou vrstvou. Excitované stavy jsou počítány časově závislým DFT (TDDFT) k analýze, jak může elektronová konfigurace podpořit disociaci excitonů, například ve fotovoltaických aplikacích. V řadě případů se ukazuje, že přechod z HOMO na LUMO je vůči ostatním přechodům dominantní. Získané výsledky tak poskytují návod pro syntézu reálných ND-PPy kompozitů.

Contents

Aims of the thesis	2
1 Introduction	3
1.1 Diamond	5
1.2 Theoretical approaches	9
1.2.1 Units	9
1.2.2 Basic principles	9
1.2.3 Born-Oppenheimer approximations	10
1.2.4 Basis set	10
1.2.5 Approximative methods in quantum theory	10
1.2.6 Hartree-Fock method	11
1.2.7 Density functional theory	14
2 Results	16
2.1 Computational details	17
2.2 Adsorption of PPy on H-terminated NDs	21
2.2.1 Structural analysis	21
2.2.2 Binding and Interaction energies	25
2.2.3 Electronic properties and charge transfer	26
2.3 Adsorption of PPy on O-terminated NDs	29
2.3.1 Structural analysis	29
2.3.2 HOMO and LUMO distribution and energies	33
2.3.3 Binding and interaction energies	35
2.3.4 Charge transfer	37
2.3.5 Excited states	38
3 Conclusion	41
Bibliography	43
List of Abbreviations	52
List of Publications	53
List of Activities	55
Attached Publications	57

Aims of the thesis

The goal of this thesis is to investigate feasibility and nature of the bonding between polypyrrole (PPy) and diamond nanoparticles (NDs) using computational approaches, guide the experimental synthesis of the composites of PPy with detonation nanodiamonds (DNDs), and provide a better understanding of the system's properties and function. Particularly, the thesis aims to explore the interactions of PPy with surfaces of NDs on theoretical basis using density functional theory (DFT) computations. Inherent part is a thorough review the background knowledge and state of the art, and present the progress of our research so far. Regarding the possible applications, the goal is to analyze properties pointing out the practicability and possible usability of the PPy-ND systems for solar cell and photovoltaic applications. More generally, the aim of the thesis is to perform basic research of a representative of organic-inorganic interfaces.

1. Introduction

Solar energy production and in particular photovoltaics (PV) is one of the key elements to support the energy transition from fossil to renewable energy sources, thus directly contributing to solving the climate change problem. From more than half a century ago, when the first solar cells were manufactured, up till now bulk silicon wafers have been the most commonly used material for solar cells. In the last ten years, PV has seen exponential growth, with an installed capacity of over 100 GW in Europe alone. Mass realization and further exponential growth are expected when integrated PV becomes common, i.e. in roofs, facades, windows and other objects. However, the current silicon-based PV devices have limitations preventing their ubiquitous application: Although they reach efficiency up to 26.7% in a single-junction [1] the efficiency to cost ratio remains unsatisfactory as higher efficiencies are reached only for multiple-junction cells. They also realize their full potential (energy conversion efficiency) only under high and direct solar irradiation, which is not coinciding with the areas of the highest energy consumption in the developed countries. Silicon nanoparticles are considered as an alternative to the traditional bulk silicon material [2,3] owing to charge carrier multiplication, low toxicity, and possibility to rely on well-established silicon industry. However, the synthesis and stabilization of Si nanocrystal surfaces is complicated.

Organic PV (OPV) is a promising area in particular owing to the ability to cover large surface areas and better performance under low-light conditions. The development of high-performance organic semiconductors has enabled OPV to become an important source of alternative energy over the past few years. The newly developed active materials used in OPV are non-toxic and enable cost-effective and eco-friendly roll-to-roll manufacturing with orders of magnitude lower energy consumption compared to the manufacturing process for classic PV. However, current OPV technology still suffers from fundamental issues. Those are mostly degradation, higher cost of some key components, and relatively low efficiency of only up to 11 % [4].

Worldwide research and development efforts are thus put into investigating newly combined inorganic and organic materials [5-7], which would provide a breakthrough for OPV-type solar cells performance and wider application. One of the main challenges is to increase the efficiency while decreasing the production and installation costs. Diamond nanoparticles – nanodiamonds (NDs) – represent an inexpensive (~ 1 EUR/g) carbon nanomaterial possessing a unique set of material, chemical, and electronic properties, e.g., superb hardness, chemical inertness, non-toxicity, biocompatibility, high carrier mobility, efficient heat dissipation, and luminescence. Various carbon nanostructures were already studied as charge transporting material and additives within a light harvesting material [8-10]. However, the potential of NDs in photovoltaics and the connected light to energy conversion remains mostly unexplored. NDs could be beneficial alternative to silicon and other traditional photovoltaic materials,

e.g., TiO₂, GaAs, and CdS [2,3,11].

The possible beneficial functionalization of NDs is diverse, NDs are capable to bind a wide array of surface groups, and it changes the electrical properties of the structures [12]. Combination of NDs with organic materials can lead to novel electronic semiconductor-organic functional systems. Polypyrrole (PPy) is a typical representative of organic semiconductors, PPy is chemically stable conjugated polymer [13] absorbing well the visible light (hence called organic dye), its conductivity and energy band gap (typically 1.3 – 3.2 eV) can be controlled by the method of preparation [14,15]. Structurally, PPy contains an amino group within its heterocycle, and it can be a linker to biomolecules [16]. In this respect, NDs modified with PPy could be used as a sensor. Combining PPy with nanodiamonds has a potential use in photovoltaic (PV) applications based on an experimentally measured transfer of photogenerated charge between bulk diamond and PPy observed by Kelvin force microscopy and optical spectroscopy [17-19]. These results showed that merging diamond and organics provides an efficient interface for exciton dissociation and electron transfer [19,20]. Such hybrid organic-inorganic interfaces are considered perspective for novel photovoltaic systems [21,22]. For these purposes, chemical modification and investigation of interaction of diamond surface with molecules is important. Previous experimental studies also showed various configurations of PPy binding with NDs [23]. Moreover, carbon allotropes in junction with polymers turned out to be promising material for solar cells [7,24,25].

The nanoscale properties of functionalized and sensitized NDs would be difficult to understand based purely on experimental techniques. Therefore, computational approach involving first-principles calculations is essential. In this work, we present a comprehensive computational study of chemisorbed (grafted) and physisorbed (merely adsorbed) PPy oligomers on hydrogenated or oxidized ND surfaces including also additional hydrogenated or oxidized amorphous carbon layer with view to possible photovoltaic applications.

1.1 Diamond

Diamond has been known to humans for centuries, and its applications are still expanding. Since the middle of the 20th century, diamond has been commercially manufactured as industrial material. Nowadays, most technologies are moving to the nanoscale, where demand for nanodiamonds is emerging [26,27].

Bulk diamond has a number of unique properties including high electron and hole mobilities, both of about $2000 \text{ cm}^2/\text{Vs}$, thermal conductivity of $25 \text{ W/cm}\cdot\text{K}$, electric breakdown field of 10^7 V/cm , hardness of 104 kg/mm^2 , and Debye temperature of 1860 K [27]. Undoped intrinsic diamond is an electric insulator with the band gap of 5.47 eV . However, under doping, diamond could be transformed into a p- or n-type semiconductor. The near-surface region of H-terminated diamond shows p-type semiconductivity, negative electron affinity, and it is positively charged. While the surface of O-terminated diamond exhibits insulating properties, positive electron affinity, and it is negatively charged.

Diamond is an allotrope of carbon, which is a base for a rich variety of forms owing to its electronic structure. The electron configuration of carbon in the ground state is $1s^2 2s^2 2p^2$. The four valence electrons in the $2s$ and $2p$ valence shells can participate in chemical bonds, the valency of carbon is 4. The energy difference between the valence shells is small, therefore the electron wave function of their electrons can mix, and their occupancy can vary. Diamond is a result of sp^3 hybridization of carbon. Other possibilities are e.g. sp^2 (graphene) and sp (carbyne) hybridization. sp^3 hybridised orbitals of carbon and the diamond fcc-cubic crystal lattice can be seen in Figure 1.2 (a) and (b), respectively.

Nanodiamonds (NDs) represent new building blocks at the nanoscale, where different properties from the bulk diamond could arise. Nowadays, NDs are commercially used in many areas including lubricants, nanocomposite materials, nanoelectronics components, optoelectronics, biosensors, biology and biomedical applications as biomarkers or for targeted drug delivery [14]. An example of usage of NDs for photovoltaic applications could be seen in Figure 1.1 showing a cross-sectional scheme of photodiode with embedded DNDs [28].

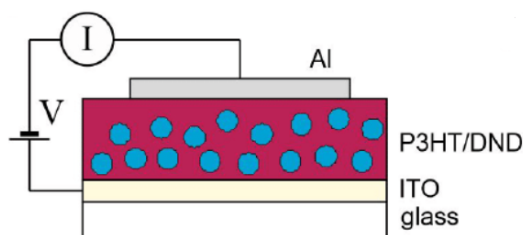


Figure 1.1: Cross-sectional scheme of photodiode with embedded DNDs. Reprinted from [28].

Diamond nanoparticles represent a new carbon nanostructure. NDs with the sizes at the microscale can be synthesised from graphite during high-pressure high-temperature synthesis, so called HPHT nanodiamonds [29]. Also, detonation-based synthesis of nanodiamonds giving rise to nanoscale detonation nanodiamonds (DND) has been developed [29]. In a closed chamber, explosives (a mixture of trinitrotoluene with hexogen) are detonated, and diamond crystals are formed from the carbon explosives.

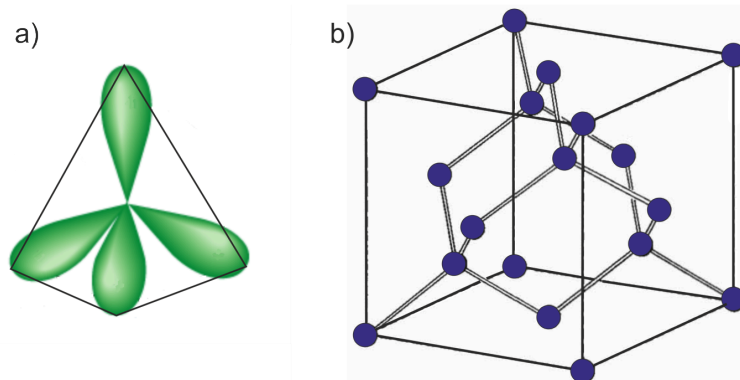


Figure 1.2: Schematic figure of sp^3 hybridized orbitals of carbon with valence angles $109^\circ 28'$ (a). Diamond crystal lattice (b).

DNDs, in contrast with HPHT NDs, contain larger variety of surface groups and also non-diamond carbon, which is further removed by purification processes. Both HPHT and DNDs are commercially available material produced on an industrial scale and applied in numerous fields.

As for any other nanomaterial, surface of NDs is important. In order to prevent dangling bonds, i.e. unsaturated valences on surface atoms, the surface has to be terminated. Depending on the manufacturing process, surface atoms are most often terminated with hydrogen or oxygen moieties (a consequence of using oxidizing reagents, e.g., concentrated mineral acids used for cleaning nanodiamonds). Schematic of truncated octahedral ND functionalized with various oxygen-containing groups and PPy is shown in Figure 1.3.

Experimentally, the most common surface chemical groups found on detonation nanodiamonds (DND) are related with oxygen, hydroxyls, carboxyls, and anhydrides owing to the production process, where newly formed detonation diamond crystallites react with a cooling medium, or arise from the purification process [30]. Hydrogen-terminated NDs, experimentally studied in [17, 31], can arise from a chemical vapor deposition (CVD) [32], from thermal annealing in pure hydrogen [33], or from a plasma-assisted hydrogenation process [34]. Hydrogen was identified as a prerequisite for further grafting of PPy molecules [35]. The size of DND can be controllably reduced down to 1.4 nm [36]. In Figure 1.4 can be seen a scanning transmission electron microscopy (STEM) image of DND [36]. Atomic force microscopy (AFM) image showing the topography of H- and O-terminated DNDs can be seen in Figure 1.5 (a) and (b), respectively [23].

Electronic and physical properties are significantly influenced by the chemical termination of NDs. In contrast with the negative electron affinity and surface conductivity of H-terminated ND, oxygen termination of ND provides positive electron affinity [37] and high electrical resistance [38]. Higher electronegativity of oxygen compared with carbon results in the polarization of the bond between oxygen and carbon with the negative charge δ^- on the oxygen and the positive charge δ^+ on the carbon. As a consequence of this surface C-O dipole layer, the vacuum level is above the conduction band minimum [39]. The opposite is true for C-H surface dipole.

The two most common low index diamond facets found on the surfaces of natural and synthetic diamonds are (111) and (100) facets [29, 40, 41]. These low-index surfaces dominate the polycrystalline CVD growth process, where they are the most

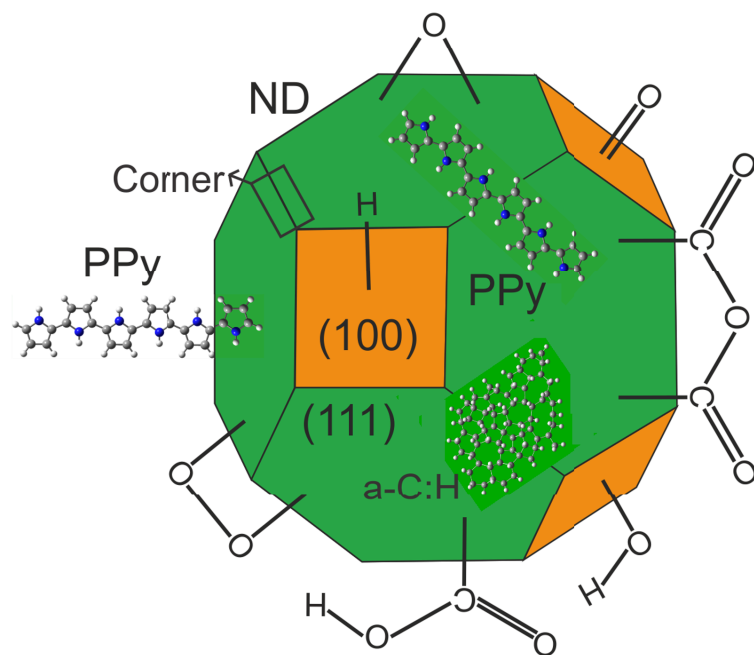


Figure 1.3: Schematic of truncated octahedral ND functionalized with various oxygen-containing groups, amorphous surface layer, and PPy oligomers adsorbed on the surface. (111) ND facets are in green, (100) ND facets are in orange, C atoms of PPy are in gray, H atoms of PPy are in white, and N atoms of PPy are in blue.

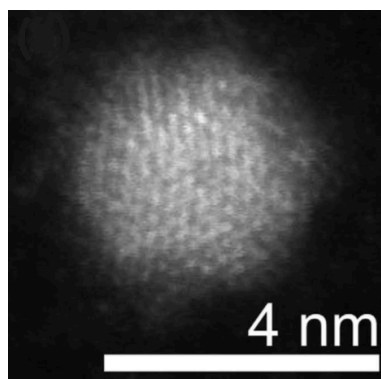


Figure 1.4: STEM image of as received H-terminated DND. Reprinted from [36].

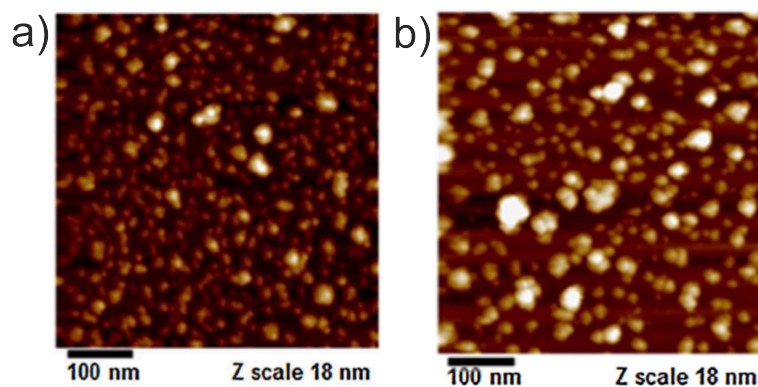


Figure 1.5: AFM topography images of as received H-terminated DNDs (a) and O-terminated DNDs (b). Reprinted from [23].

highly represented with a quota dependent on temperature and pressure [42]. The (100) surface represents the most defect-free surface obtained from experimental synthesis [43]. Moreover, surfaces of detonation NDs (DNDs), commercially available with sizes less than 4 nm in diameter [44] contain an amorphous layer of carbon on parts of their surfaces. Thermodynamic stability and surface reconstruction of NDs terminated with oxygen-containing groups under varying conditions, and different surface coverage of (111) and (100) facets was studied by both theoretical [12,37,42,43,45-59] and experimental [15,60-65] methods.

H-terminated (111) surfaces remains unreconstructed, i.e. in the 1×1 configuration, which was confirmed by both theoretical [37,40,42,66] and experimental [67,68] approaches. Although the (111) surface may be constructed as triradical with three dangling bonds per surface atom, it is much higher in energy [37], unstable and practically not observed [40]. H-terminated (100) surfaces occur in mono-hydride configuration on the 2×1 reconstructed surface, which was confirmed both by theoretical [37,40,45-47,69-71] and experimental [69,72,73] methods. Di-hydride configuration retaining the 1×1 structure surface is generally unstable, mostly due to steric interactions, unless the supersaturation of H is very high (such as in plasmas).

On the 1×1 (111) ND surface facet, oxygen in the on-top (i.e. ketone) position or with peroxide bridges is the most favorable [48]; the epoxide O-termination is unstable with respect to the on-top position here [42]. On the 2×1 (111) facet, oxygen adsorption in on-top and bridge positions were pointed out as the only plausible positions [42,60]. The epoxide configuration occurs preferably at 50% or lower oxygen coverage [48,51]; 100% O coverage leads to dimerization [42]. On the 1×1 (100) facet, the ether position is preferred at high surface coverage [29] [43,45]. Alternatively, etherized 1×1 (100) structures with a bridging ether may be convenient [47]. For oxygen surface coverage up to 50% on (100), the 2×1 reconstruction is preferred over the 1×1 reconstruction [29], and epoxy structure is more favorable than the ether structure [74]. The ether position is stable at high surface coverage [29,43,48]. For the both (111) and (100) facets, OH adsorption leads to destabilization of 2×1 reconstruction compared to the 1×1 reconstruction [54]. In the case of the OH-termination, there are two competing interadsorbate interactions, first hydrogen bonding, and second induced steric repulsions. The former one will stabilize the surface system while the latter will destabilize and thereby weaken the surface-adsorbate bonds [66]. For COOH species, it is energetically only possible to cover the surfaces up to 50% [75]. The adsorption of COOH is the most favorable on 2×1 (100) surface, being exothermic at all points on the surface [76]. Carboxylic and anhydride groups are supposed to be the most contributing to the spectral bands observed in the experimental FTIR spectra in the range of $1600\text{--}1950\text{ cm}^{-1}$ [59]. Anhydride bridges formed on ND surface were studied as one of the most probable groups on a heavily oxidized surface [59].

The hybrid semiconductor-organic ND-PPy interfacial system cannot be completely understood based purely on experimental techniques. With the exception of the author's publications, only one theoretical work studying PPy-ND systems have been published, particularly, investigating PPy chemisorbed on H-terminated NDs [77].

1.2 Theoretical approaches

Quantum theory was developed at the beginning of the 20th century. It is an adequate theory for a proper description of the atomistic structure of matter. To obtain properties, which depend on the electronic structure of matter, e.g., charge transfer or bonding parameters, we need to use the quantum theory. The description using classical approach is usually not appropriate, especially if we would like to consider the formation and breaking of chemical bonds. Although the quantum theory is in principle an exact theory, in practical applications we need to employ multiple approximations in quantum chemical protocols. Quantum theory was summarized in literature, e.g., [78,79].

1.2.1 Units

The unit of length used in this work is angström, Å, $1 \text{ Å} = 10^{-10} \text{ m}$.

In solid state physics, commonly used energy unit is electronvolt, eV. It is equal to $1.6022 \times 10^{-19} \text{ J}$, which is the energy acquired by a single electron moving through an electric potential difference of 1 volt.

The charge of an electron represents the elementary charge, $e = 1.6022 \cdot 10^{-19} \text{ C}$.

The equations in this section are presented in atomic units reducing the number of constants.

1.2.2 Basic principles

Quantum mechanics is based on a concept of wave function $\Psi(\mathbf{x}, t)$ that describes a state of a given system. The wave function $\Psi(\mathbf{x}, t)$ can be obtained as a solution of Schrödinger equation.

The time-dependent Schrödinger equation has the following form:

$$i\hbar \frac{d\Psi(\mathbf{x}, t)}{dt} = \hat{H}(\mathbf{x}, t)\Psi(\mathbf{x}, t), \quad (1.1)$$

where \hat{H} can generally be time-dependent Hamiltonian of the system, and \hbar is the reduced Planck's constant.

Its nonrelativistic and time independent form leading to stationary states is defined as follows:

$$\hat{H}(\mathbf{x})\psi(\mathbf{x}) = E\psi(\mathbf{x}). \quad (1.2)$$

In the time-independent case, the wave function can be divided into time and spatial part, $\Psi(\mathbf{x}, t) = \psi(\mathbf{x})\phi(t)$.

The Hamiltonian of a system is a sum of quantum operators describing kinetic energy of nuclei, kinetic energy of electrons, electron-nuclei attraction, electron-electron repulsion and nucleus-nucleus repulsion:

$$\hat{H} = -\frac{1}{2} \sum_{A=1}^{N_n} \frac{1}{m_A} \Delta_A - \frac{1}{2} \sum_{i=1}^{N_e} \Delta_i - \sum_{i=1}^{N_e} \sum_{A=1}^{N_n} \frac{Z_A}{r_{iA}} + \sum_{i=1}^{N_e-1} \sum_{j=i+1}^{N_e} \frac{1}{r_{ij}} + \sum_{A=1}^{N_n-1} \sum_{B=A+1}^{N_n} \frac{Z_A Z_B}{r_{AB}}, \quad (1.3)$$

where indexes A and B denote nuclei, i and j denote electrons, N is the number of respective particles, m and Z represent mass and charge of the corresponding particles, Δ is a Laplace operator.

1.2.3 Born-Oppenheimer approximations

Under certain assumptions, the wave function can be separated into a part depending on electron variables and into a part depending on nuclei variables. Considering the difference of at least three orders in the masses of electrons and nuclei, first, we can suppose that electrons move in an immobile field of nuclei due to their comparably negligible mass and high speed. Second, we can suppose that the nuclei move in an effective field created by fast moving electrons.

In the Born-Oppenheimer approximation solving the motion of electrons in the electrostatic field of fixed nuclei, the Hamiltonian has the following form:

$$\hat{H}_{BO} = -\frac{1}{2} \sum_{i=1}^{N_e} \Delta_i - \sum_{i=1}^{N_e} \sum_{A=1}^{N_n} \frac{Z_A}{r_{iA}} + \sum_{i=1}^{N_e-1} \sum_{j=i+1}^{N_e} \frac{1}{r_{ij}} + \sum_{A=1}^{N_n-1} \sum_{B=A+1}^{N_n} \frac{Z_A Z_B}{r_{AB}}, \quad (1.4)$$

where the last term is an electrostatic interaction of nuclei. It is constant because of the assumed fixed nuclei. The time-independent Schrödinger equation is solved without the last term, and the nuclei contribution to total energy is added afterward.

Another usual approximation is to solve the Schrödinger equation only for valence electrons after substituting nuclei and inner electrons with corresponding ions. Moreover, relativistic effects are often negligible for atoms with a low atomic number.

1.2.4 Basis set

It is convenient to solve the time independent Schrödinger equation with the wave function $\psi(x)$ represented with a suitable set of basis functions. For example, with a set of atomic orbitals $\phi_i(\mathbf{x})$ which are practical for molecular systems. The wave function $\psi(x)$ is expanded into a Linear Combination of Atomic Orbitals, LCAO:

$$\psi(\mathbf{x}) = \sum_{i=1}^K c_i \phi_i(\mathbf{x}), \quad (1.5)$$

where c_i are expansion coefficients. The problem of solving Schrödinger equation is transformed into search for the c_i coefficients. The atomic orbitals $\phi_i(\mathbf{x})$ can be approximated by Slater-type orbitals, STO, which are often expanded into series of Gaussian-type orbitals, GTO, with analytical atomic integrals.

1.2.5 Approximative methods in quantum theory

In practical applications, when solving Schrödinger equation, various variational and perturbation methods are used. They can be divided into three categories according to the level of the approximation. The most precise one are *ab initio* methods, where the Schrödinger equation is solved without any crucial approximation. Secondly, there are semiempirical methods, where the Schrödinger equation includes experimental parameters, the basis set has a lower number of atomic orbitals, and many electron integrals are neglected. And finally, very approximative empirical methods (e.g. Hückel method), where only the basic characteristics of molecules are taken into account.

1.2.6 Hartree-Fock method

The Hartree-Fock method is one-particle approximation to Schrödinger equation, where one electron is supposed to be in an effective field created by the other electrons. The antisymmetric condition to the wave function $\psi(\mathbf{x})$ is respected using Slater determinant:

$$\psi(\mathbf{x}) = \frac{1}{\sqrt{N_e!}} \sum_P (-1)^{\text{sgn}(P)} P[\chi_1(\mathbf{x}_1), \dots, \chi_n(\mathbf{x}_n)], \quad (1.6)$$

where χ_j is a set of one-electron functions and P is permutation of electrons \mathbf{x}_i and $\text{sgn}(P)$ is the signum function of P . The LCAO method is in this case applied on each molecular orbital instead of the total wave function.

Inserting the Slater determinant into the time-independent Schrödinger equation and after applying variational principle, we get the Hartree-Fock equations:

$$[\hat{H}_1^{\text{core}} + \sum_{j=1}^{N_e} \hat{J}_j - \hat{K}_j] \chi_i(\mathbf{x}_1) = \varepsilon_i \chi_i(\mathbf{x}_1), \quad (1.7)$$

where each index of each operator is related to the index of the electron on which the operator acts, \hat{H}_1^{core} is one-electron Hamiltonian, \hat{J}_j and \hat{K}_j are Coulombic and exchange operators and ε_i is one-electron energy. The expression in square brackets is called Fock operator.

The Coulombic and exchange operators are defined as follows:

$$\hat{J}_i = \int dx_2 \chi_i^*(\mathbf{x}_2) r_{12}^{-1} \chi_i(\mathbf{x}_2), \quad (1.8)$$

$$\hat{K}_i = \int dx_2 \chi_i^*(\mathbf{x}_2) r_{12}^{-1} P_{12} \chi_i(\mathbf{x}_2), \quad (1.9)$$

where P_{12} is permutation operator. Solution of the Hartree-Fock equations is a set of molecular orbitals $\chi(\mathbf{x})$ resulting in expression for total energy E :

$$E = \sum_i \varepsilon_i - \sum_{i < j} (J_{ij} - K_{ij}). \quad (1.10)$$

The sums run over all occupied orbitals. The total energy, E , can also be expressed by establishing one-electron integral H_{ii} :

$$E = \frac{1}{2} \sum_{i=1} (\varepsilon_i + H_{ii}), \quad (1.11)$$

where the sum run over all occupied orbitals and

$$H_{ii} = \int \chi_i^*(\mathbf{x}_1) \hat{H}_1^{\text{core}} \chi_i(\mathbf{x}_1) d\mathbf{x}_1. \quad (1.12)$$

The Hartree-Fock equations are nonlinear nonlocal integro-differential equations, usually solved iteratively or using numerical methods.

A disadvantage of the Hartree-Fock method is that the one-determinant representation of the wave function does not include dynamical correlation because each electron

is considered only in an average field of the rest of the electrons. We can define correlation energy, E_{corr} , as the difference between the energy in the Hartree-Fock limit E_{HF} and the exact nonrelativistic energy, E_{exact} :

$$E_{corr} = E_{exact} - E_{HF}. \quad (1.13)$$

Closed shells

For a closed shell system, the total spin of the system is equal to zero, and every one-electron level is occupied by two electrons with opposite spins. The spatial parts of the wave functions of both of the electrons at the same one-electron level are the same. In this case, the Hartree-Fock equations lead to Roothaan's equations with the following form:

$$\sum_{\nu} [H_{\mu\nu}^{core} + \sum_{\lambda} \sum_{\sigma} P_{\lambda\sigma} ((\mu\nu|\lambda\sigma) - \frac{1}{2}(\mu\sigma|\lambda\nu))] c_{\nu i} = \epsilon_i \sum_{\nu} S_{\mu\nu} c_{\nu i}, \quad (1.14)$$

where $c_{\nu i}$ are expansion coefficients of molecular orbitals $\psi_i(\mathbf{r})$ that are defined as linear combination of atomic orbitals $\phi_{\nu}(\mathbf{r})$. $H_{\mu\nu}^{core}$ is one-electron integral. $(\mu\nu|\lambda\sigma)$ and $(\mu\sigma|\lambda\nu)$ are two electron Coulombic and exchange integrals, transformed into the set of atomic orbitals in chemical notation. $P_{\lambda\sigma}$ is density matrix,

$$P_{\lambda\sigma} = 2 \sum_{i=1} c_{\sigma i}^* c_{\lambda i}, \quad (1.15)$$

where the sum of expansion coefficients run over all occupied orbitals and $S_{\mu\nu}$ is overlap matrix.

The total energy has the following form:

$$E = \frac{1}{2} \sum_{\mu} \sum_{\nu} P_{\nu\mu} (H_{\mu\nu}^{core} + F_{\mu\nu}), \quad (1.16)$$

where $F_{\mu\nu} = H_{\mu\nu}^{core} + \sum_{\lambda} \sum_{\sigma} P_{\lambda\sigma} [(\mu\nu|\sigma\lambda) - \frac{1}{2}(\mu\lambda|\sigma\nu)]$.

SCF method

The method employed for solving Hartree-Fock and Roothaan equations is called Self-Consistent Field method, SCF. It is an iterative method because of the nonlinear character of the task. It includes following steps:

1. Calculation of matrix elements of $H_{\mu\nu}^{core}$, $S_{\mu\nu}$ and $(\mu\nu|\lambda\sigma)$.
2. Obtain a guess of the density matrix using a computationally cheaper method.
3. Construct the Fock matrix.
4. Transformation of Fock matrix into a basis set where the overlap matrix $S_{\mu\nu}$ is the identity matrix.
5. Solving the eigenvalue problem and back transformation to obtain coefficients $c_{\mu i}$.

6. Construction of new density matrix $P_{\lambda\sigma}$.
7. Decision whether a convergence was reached, whether the new density matrix doesn't differ more from the old one according to a set criteria. If the condition is not satisfied, return to the step number 3 with the new density matrix.
8. If the procedure is converged, use the obtained solution to calculate required quantities.

Common criterion for establishing convergence in SCF method is to require convergence for elements of the density matrix by demanding the standard deviation of successive density matrix elements to be less than a small quantity δ .

Open shells

For an open shell system, two spin states of electron, marked α and β , have to be distinguished. This leads to Pople-Nesbet equations for two sets of molecular orbitals:

$$\sum_{\nu} [H_{\mu\nu}^{core} + \sum_{\lambda} \sum_{\sigma} P_{\lambda\sigma}^T (\mu\nu|\lambda\sigma) - P_{\lambda\sigma}^{\kappa} (\mu\sigma|\lambda\nu)] c_{\nu i}^{\kappa} = \epsilon_i^{\kappa} \sum_{\nu} S_{\mu\nu} c_{\nu i}^{\kappa}, \quad (1.17)$$

where $\kappa = \alpha, \beta$, $P^T = P^{\alpha} + P^{\beta}$ is total density matrix and $P_{\lambda\sigma}^{\kappa}$ is κ -spin density matrix,

$$P_{\lambda\sigma}^{\kappa} = \sum_i^{occ} c_{\sigma i}^{\kappa*} c_{\lambda i}^{\kappa}. \quad (1.18)$$

The total energy for open shell systems in Hartree-Fock approximation is expressed as follows:

$$E = \frac{1}{2} \sum_{\mu} \sum_{\nu} [P_{\nu\mu}^T H_{\mu\nu}^{core} + P_{\nu\mu}^{\alpha} F_{\mu\nu}^{\alpha} + P_{\nu\mu}^{\beta} F_{\mu\nu}^{\beta}], \quad (1.19)$$

where $F_{\mu\nu}^{\alpha} = H_{\mu\nu}^{core} + \sum_{\lambda} \sum_{\sigma} P_{\lambda\sigma}^T (\mu\nu|\sigma\lambda) - P_{\lambda\sigma}^{\alpha} (\mu\lambda|\sigma\nu)$ and $F_{\mu\nu}^{\beta} = H_{\mu\nu}^{core} + \sum_{\lambda} \sum_{\sigma} P_{\lambda\sigma}^T (\mu\nu|\sigma\lambda) - P_{\lambda\sigma}^{\beta} (\mu\lambda|\sigma\nu)$.

Beyond the Hartree-Fock approximation

The electron correlation can be described when Slater determinants corresponding to electron excitations are included in the wave function. The electron correlation is not included in the Hartree-Fock method, however, it is implemented, for example, in Configuration Interaction methods, CI. The more determinants are considered, the more exact but also more computationally demanding the calculation is.

Another approach for calculating the correlation energy is Perturbation Theory, PT. Hartree-Fock energy corresponds to the energy obtained from the zero order of PT. Møller-Plesset, MPn , methods (of different orders n), which originates from the perturbation theory are frequently used.

Another group of methods for the correlation energy calculations is based on Coupled Clusters method, CC, where higher number of Slater determinants of various electron excitations are considered.

1.2.7 Density functional theory

While the methods described in the previous section are based on the principle of many-particle wave function, the Density Functional Theory, DFT, works with electron density matrix functional instead. In comparison with the already mentioned computational methods, its computational costs are relatively low while preserving good quality, and the exchange and correlation functionals can be modeled properly.

Hohenberg–Kohn theorems

The DFT method is based on two Hohenberg-Kohn theorems. According to the first Hohenberg-Kohn theorem, the ground state density of a system determines its external potential.

Supposing the normalization of electron density $\rho(\mathbf{r})$ to number of electrons N :

$$\int \rho(\mathbf{r}) d\mathbf{r} = N. \quad (1.20)$$

The Hamiltonian of the whole system determined by the density is as follows:

$$\hat{H} = -\frac{1}{2} \sum_{i=1}^{N_e} \Delta_i + \sum_{i=1}^{N_e} v(\mathbf{r}_i) + \sum_{i=1}^{N_e-1} \sum_{j=i+1}^{N_e} \frac{1}{r_{ij}} \equiv \hat{T} + \hat{V}_{ext} + \hat{V}_{ee}, \quad (1.21)$$

where \hat{T} is the kinetic energy, \hat{V}_{ext} is the external potential, and \hat{V}_{ee} is the electron-electron repulsion.

The second Hohenberg-Kohn theorem states the relation between the exact energy of the ground state, E_0 , and energy determined by density, $\rho(\mathbf{r})$:

$$E_0 \leq E[\rho(\mathbf{r})]. \quad (1.22)$$

The wave function of non-degenerate ground state of many-electron system is unequivocal functional of one-electron density $\rho(\mathbf{r})$. However, the theorems give no information about the form of the functional.

Kohn–Sham method

The Kohn-Sham method was established in order to find the ground state electron density. It is based on treating non-interacting reference system of electrons representing the real system. Using the Hohenberg-Kohn theorems, there is a relationship between the density of the real and the reference system. Similarly, as in Hartree-Fock method, we can represent the densities by one-electron orbitals, which leads to canonical Kohn-Sham equations:

$$\left[-\frac{1}{2}\Delta + v_{eff}(\mathbf{r})\right]\psi_i(\mathbf{x}) = \varepsilon_i\psi_i(\mathbf{x}), \quad (1.23)$$

where $\psi_i(\mathbf{x})$ are one-electron functions from which is constructed the density $\rho(\mathbf{r})$:

$$\rho(\mathbf{r}) = \sum_{i=1}^{N_e} |\psi_i(\mathbf{x})|^2, \quad (1.24)$$

and $v_{eff}(\mathbf{r})$ is effective potential:

$$v_{eff}(\mathbf{r}) = v(\mathbf{r}) + \int \frac{\rho(\mathbf{r}')}{|\mathbf{r} - \mathbf{r}'|} d\mathbf{r}' + v_{xc}(\mathbf{r}). \quad (1.25)$$

In the latter equation, $v(\mathbf{r})$ is potential of nuclei and $v_{xc}(\mathbf{r})$ is exchange-correlation potential.

The resulting total energy of the system is:

$$E = \sum_{i=1}^{N_e} \varepsilon_i - \frac{1}{2} \int \frac{\rho(\mathbf{r})\rho(\mathbf{r}')}{|\mathbf{r} - \mathbf{r}'|} d\mathbf{r}d\mathbf{r}' + E_{xc}[\rho] - \int v_{xc}(\mathbf{r})\rho(\mathbf{r})d(\mathbf{r}). \quad (1.26)$$

The task in the Kohn-Sham theory is to derive approximations to the exchange-correlation energy functional $E_{xc}[\rho]$, while the kinetic energy, calculated under the assumption of non-interacting electrons, is almost correct.

The exchange-correlation energy E_{xc} can be separated into exchange, E_x , and correlation, E_c , part:

$$E_{xc}[\rho] = E_x[\rho] + E_c[\rho]. \quad (1.27)$$

The exchange energy can be expressed using Local Density Approximation, LDA, assuming that locally, the density can be treated as a uniform electron gas:

$$E_x^{LDA}[\rho] = -\frac{3}{4} \left(\frac{3}{\pi}\right)^{1/3} \int \rho^{4/3}(\mathbf{r})d(\mathbf{r}). \quad (1.28)$$

Often, in practical calculations, hybrid functionals are used. There, the exchange energy, e.g. from Becke's exchange functional, is combined with the exact energy from Hartree-Fock theory. For example, one of the most popular hybrid functional in calculations of organic molecules is B3LYP functional. B3LYP stands for Becke 3-parameter Lee-Yang-Parr. The parameters specify the amount of the exact exchange energy used.

2. Results

In this chapter, computational details are presented and selected representative results are summarized. These are composites of PPy with hydrogen-terminated NDs calculated with the B3LYP functional and composites of PPy with oxygen-terminated NDs calculated with the ω B97X-D functional. Using many non-equivalent starting conditions, the most probable structural configurations and electronic properties of the PPy-ND system are analyzed, showing high potential of the PPy-ND system for photovoltaic energy generation. An illustrative figure of the PPy-ND system can be seen in Figure 2.1.

Further details can be found in the enclosed reprints of journal publications written by the author of the thesis.

The first journal contribution of the author in *physica status solidi (a)* investigates PPy physisorbed and chemisorbed on reconstructed 1×1 (111) and 2×1 (100) H-terminated NDs [80]. Second, physisorbed interactions of PPy with NDs terminated with O atoms in different positions are included in Proceedings of the 8th International Conference Nanocon [81]. Third, results concerning PPy chemisorbed on NDs terminated with the different O-containing groups including ethers, ketones, peroxides, epoxides, hydroxyls, carboxyls, and anhydrides as well as NDs terminated with an amorphous surface layer saturated with H or O atoms are published in *physica status solidi (b)* journal [82]. These results include both ground state and excited state calculations. Fourth, simulations of PPy physisorbed and chemisorbed PPy on NDs terminated with different O-containing groups calculated with different methodology are presented in *Physical Chemistry Chemical Physics* journal [83].

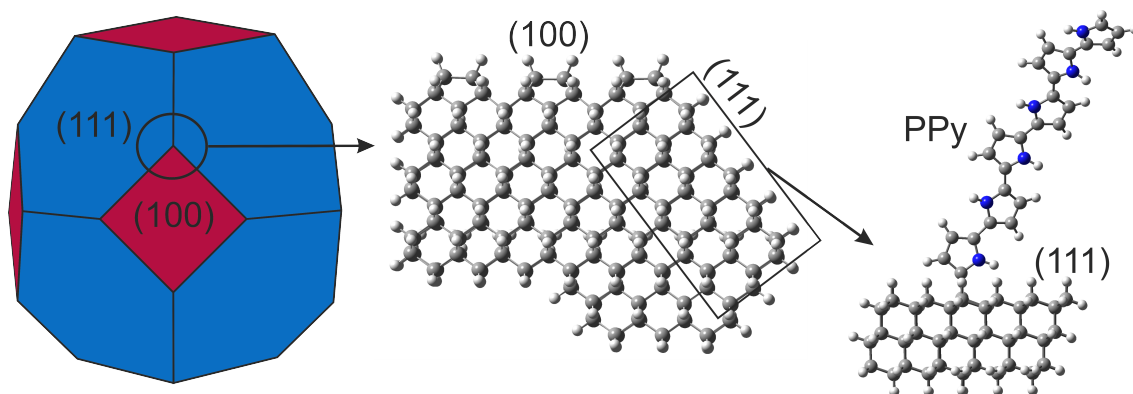


Figure 2.1: Truncated octahedral ND (left), (111) facets are in blue, (100) facets are in red. (111) - (100) - (111) corner of ND (middle), and (111) facet with chemisorbed PPy (right). C atoms are in gray, H atoms are in white, N atoms are in blue.

2.1 Computational details

The first-principles density functional theory (DFT) method implemented in Gaussian 09 electronic structure software [84] was used for optimizations of all the structures in order to obtain the ground state configurations. The computational resources were provided by the CESNET LM2015042 and the CERIT Scientific Cloud LM2015085, provided under the program "Projects of Large Research, Development, and Innovations Infrastructures".

First, the electron density was described with B3LYP hybrid functional [85, 86], one of the most widely used functionals in computations of organic molecules. The composites were preoptimized with a less complex but faster 3-21G basis set used for the description of molecular orbitals. Then, optimization using 6-31G(d) basis set was performed including polarization functions on non-hydrogen atoms. Second, for a comparison, long-range corrected hybrid density functional ω B97X-D [87] which includes empirical atom-atom dispersion and eliminates the self-interaction error was used. The ω B97X-D functional was found to be optimal, e.g., for calculations of π -conjugated oligomers [88]. Using this type of functional, the delocalization error is reduced [89]. Also, it is convenient for calculations of excited states properties, because the long-range correction brings the transition energies close to the experimental results [90].

Modeling the whole ND with typical experimentally accessible sizes from 4 nm [40] would be computationally unfeasible at this level of theory. Therefore, (111) and (100) non-periodic ND surface slabs consisting of 3 C double layers of 6×6 atoms, exceptionally 5×6 atoms if structurally needed, were used. The model size (about 1 nm ND) was chosen as a compromise with computational feasibility where the quantum confinement effects may be indeed possible. Nevertheless, the results show that the various surface terminations studied in this work have actually very pronounced effect while possible quantum confinement effect would be about the same for the same model size. Two additional H-terminated model sizes with double and triple size of the original ND slab consisted of 459 C atoms (7353 basis functions, i.e. about 2 nm), and 694 C atoms (11026 basis functions, i.e. about 3 nm), respectively were computed. Although the HOMO-LUMO gaps of such systems was close to the experimental bandgap of ND, the computational resources were enormous. The convergence criteria for all the optimizations in this work were 4.5×10^{-4} Ha/ a_0 for the maximum force remaining on an atom.

The (111) and (100) slabs represent an edge of ND, with one larger "top" surface aimed at PPy adsorption, one larger "side" surface and a small side surface closing the corner. These three "outer" surfaces of ND are functionalized with surface groups, and the remaining three "inner" surfaces representing the inner cut planes are saturated with H atoms in order to keep the sp^3 hybridization of neighboring carbon atoms, i.e. to avoid dangling bonds. These H atoms were fixed during further optimization. In this way, the inner C atom layers maintain plane shape yet retain certain flexibility to relax. If necessary to saturate two dangling bonds of C atoms, dimerized H atoms were placed symmetrically around the C atom. They were kept fixed during the optimizations to maintain the tetrahedral sp^3 character of the diamond structure, despite some steric tension arising between the hydrogen atoms [53, 69]. Few other authors suggest a canted configuration with increased distance between the hydrogen atoms, however, this problem merits more discussion [47, 53, 91].

Based on the literature and our preliminary calculations, we choose the most probable 1×1 and 2×1 surface reconstructions of both (111) and (100) surface fully passivated with hydrogens, fully passivated with oxygens in ether, epoxide, ketone, and peroxide positions, fully passivated with hydroxyls, 50% passivated with carboxyls, and from 26% to 36% passivated with anhydrides. The amorphous carbon layer was created by a random placement of the carbon atoms of the surface double layer and a consequent optimization on the slab. Next, surface terminating functional groups were added to saturate the free carbon valences. The amorphous surface was saturated by hydrogens (a-C:H structures) and a mixture of hydrogens and oxygens (a-C:O structures). For both reconstructions of both surface slabs and the amorphous surface layer, different surface functional groups were considered. The slabs with the lowest relative total energy after optimization were chosen for further optimizations with adsorbed PPy.

In the case of hydrogen-terminated NDs, always 100% termination with hydrogens was used. In the case of oxygen terminations, for the 1×1 (111) surface slab was chosen 100% termination with peroxides, for the π -bonded Pandey chain 2×1 (111) was chosen 50% of epoxides, for the 1×1 (100) 50% with ethers and for the 2×1 (100) 50% with epoxides. Note that in the case of ethers, epoxides, and anhydrides, the 50% surface coverage generates fully passivated forms. In the case of the OH- and COOH-terminated NDs, 100% and 50% surface coverage, respectively, was used for further calculations with adsorbed PPy. In the case of the anhydride-terminated NDs, surface coverages of 25.6%, 35.7% and 33.3% in the case of the 1×1 (111), 2×1 (111) and 2×1 (100) ND, respectively, turned out to be energetically the most favorable. The amorphous a-C:H slabs were 100% saturated with H atoms. The amorphous a-C:O slabs were from 48.7% saturated with O atoms (10.8% of peroxides, 18.9% of epoxides, 2.7% of ethers, and 13.5% of ketones) and from 51.3% with H atoms. Further, NDs terminated with hydroxyls, carboxyls, and anhydrides were calculated. These results can be found in the attached articles.

To study the contact formation, different non-equivalent initial configurations of adsorbed PPy on the slabs relaxed in the absence of PPy were optimized. The PPy is represented by oligomer with six pyrrole heterocycles, which was optimized separately and was proportionate to the modeled slabs. Non-equivalent positions of physisorbed and chemisorbed PPy, including one- and two- bond contacts, on the optimized slabs were considered as initial geometries. An example of the non-equivalent initial positions of PPy on the H-terminated 1×1 (111) ND slab is shown in Figure 2.2. The resulting optimized structures with the lowest relative total energies are shown further in the text in Figure 2.4. In some cases, different initial structures converged to almost identical structure. In other cases, we obtained different structures, which relative preferences were decided bases on comparison of their total energies. It was not possible to optimize a stable upright physisorbed position of PPy, which ended up in a horizontal position with respect to the ND facet. Therefore, the convergence of this type of calculations required high amounts of computational time.

The structure of each bonding type with the lowest binding energy was then taken for further analyses.

PPy and the top ND layer were allowed to relax during these further optimizations. PPy does not spontaneously chemisorb on the clean H-terminated diamond surface [77]. Hence, the one- and two-bond chemisorbed contacts, always mediated via C-C bonds, were allowed by a removal of one and two H atoms from PPy, respectively, and

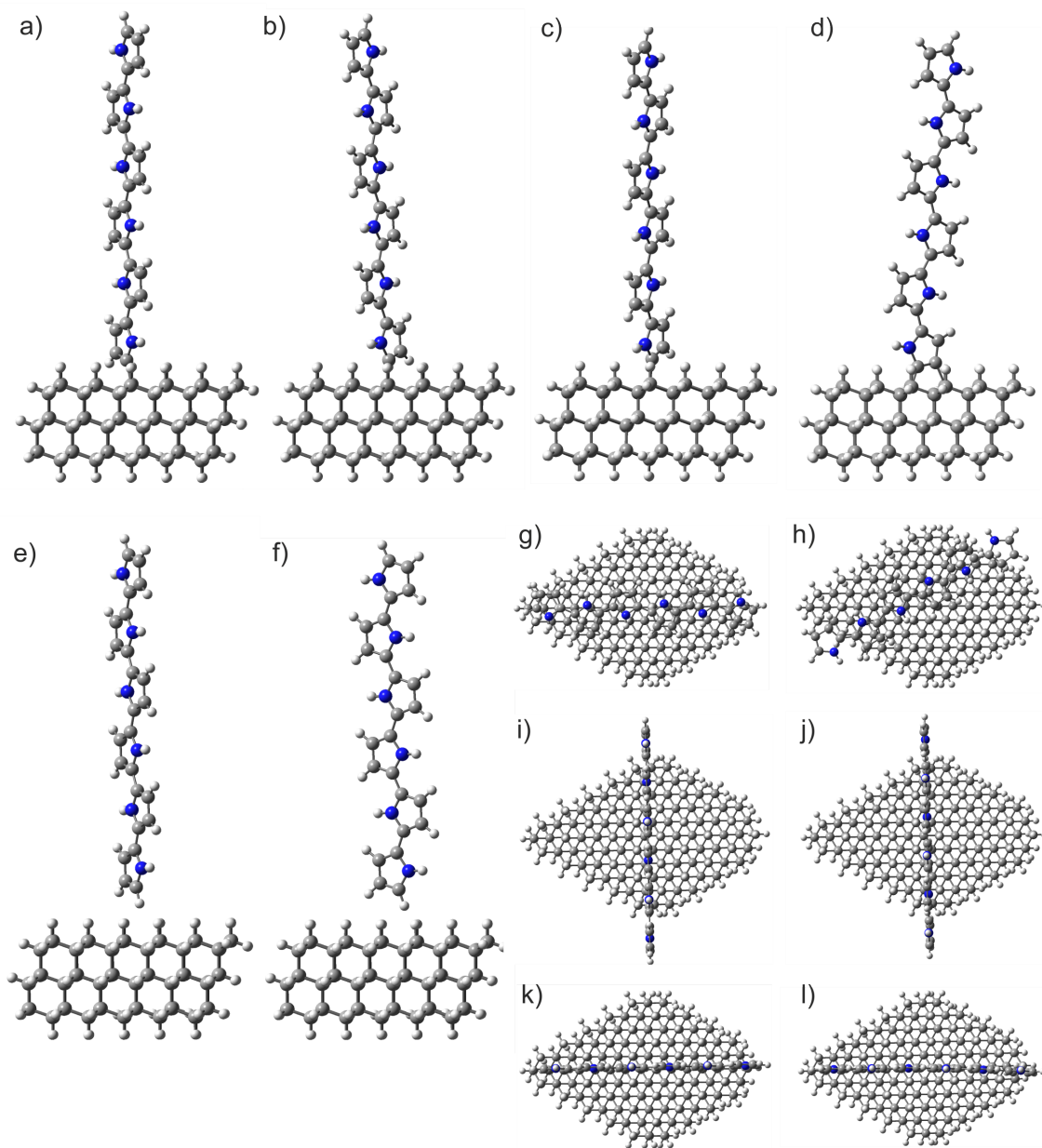


Figure 2.2: Non-equivalent initial positions of PPy in chemisorbed (side views (a) - (d)) and physisorbed (side views (e), (f), and top views (g) - (l)) on the H-terminated 1×1 (111) ND slab.

a corresponding number of atoms on the ND slabs. The transition processes itself is not studied here since the work is focused mainly on the nature of bonding between PPy and ND and resulting properties of the merged system. Experimentally, the H-termination of diamond is substituted by the PPy molecules during electrochemical synthesis process [31].

The energy barrier for replacing the O-containing surface functional groups by PPy is relatively high and makes the chemisorption of PPy difficult. However, the structures can exist if we consider chemisorption of PPy on H-terminated ND, where H atoms are likely to be substituted by PPy, and then replacing the remaining H-termination with the oxygen-related surface functional groups. Furthermore, surfaces of polyfunctional DNDs (the most common commercial nanodiamonds) contain a mixture of C-H and oxygen surface groups. PPy is thus likely to graft at the C-H bond with the oxide groups around. Hence, computing of PPy grafted on oxidized NDs corresponds to a quite realistic and possibly common situation. Note that due to steric reasons we didn't optimize PPy on hydroxyls-terminated 2×1 (100) ND slab, carboxyls-terminated 1×1 (100), and anhydrides-terminated 1×1 (100).

Geometry parameters, binding energy (E_b), interaction energy (E_{int}) HOMO-LUMO gap, and charge transfer (Δq) were analyzed on the selected most suitable structures. For selected representative structures, excited state properties were calculated using the time-dependent DFT (TDDFT), allowing to describe the electronic excitations in nanosystems [92].

2.2 Adsorption of PPy on H-terminated NDs

2.2.1 Structural analysis

Obtained structural parameters of optimized PPy structure displayed in Figure 2.3 (a) are in good agreement with prior theoretical studies [77,93].

HOMO and LUMO molecular orbitals shown in Figure 2.3 (b) and (c), respectively, are out-of-plane π molecular orbitals, slightly modified at both ends of PPy, gaining a character of σ -symmetry for the case of LUMO orbitals. Red and green colour indicated positive and negative value of the orbital surfaces, respectively. The molecular orbitals of the two middle PPy rings resemble the most the orbitals of an infinite PPy chain. The calculated HOMO-LUMO gap is 3.36 eV, which is in good agreement with theoretical [77] and experimental [15,17,93,94] results. Note that the relaxed morphologies of PPy-C:H structures differ due to the contact formation, as shown further below.

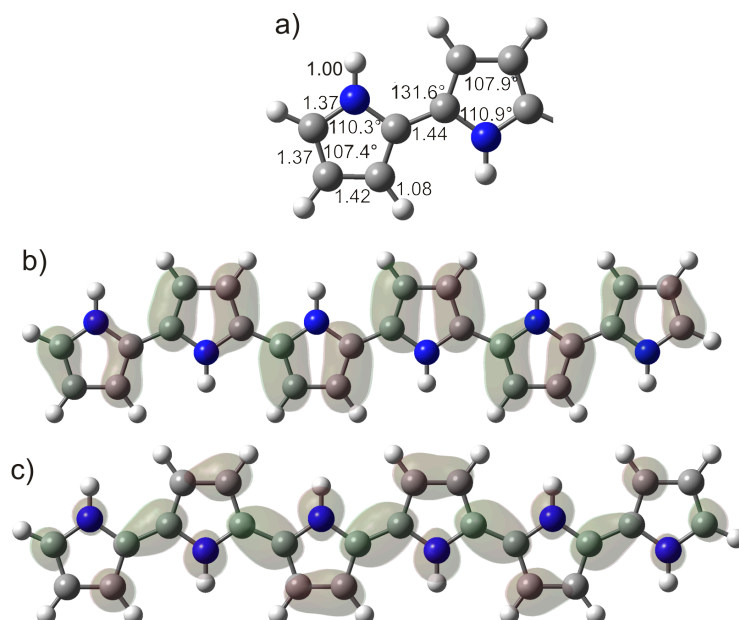


Figure 2.3: Main structural parameters of two terminal PPy heterocycles (a), HOMO (b), and LUMO (c) molecular orbitals of optimized PPy. Red and green colour indicate positive and negative value of the orbital surfaces, respectively, corresponding to the isovalue of $0.01e^{-\text{Å}^{-3}}$. The bond lengths are given in Å.

Figure 2.4 (a) – (d) and Figure 2.5 (a) – (d) show the optimized and energetically the lowest chemisorbed structures. Here, PPy is connected via C-C bonds and it stands under a tilt angle in the range between 68.6° and 83.9° . The lower angles correspond to the one-bond contacts. The main structural parameters including bond lengths between PPy and diamond slabs for the chemisorbed structures are displayed in Figure 2.6. For all the structures, the bond lengths of PPy are modified up to 0.4Å and the angles up to 2.7° . The bond lengths within the diamond slab are less significantly modified, up to 0.12Å in the closest area around the contact with PPy.

Figure 2.4 (e) and (f) and Figure 2.5 (e) and (f) show the optimized and energetically the lowest physisorbed structures. For the (111) facet, the optimizations converged to PPy lying along the surface diagonal, and for the (100) facet to PPy lying

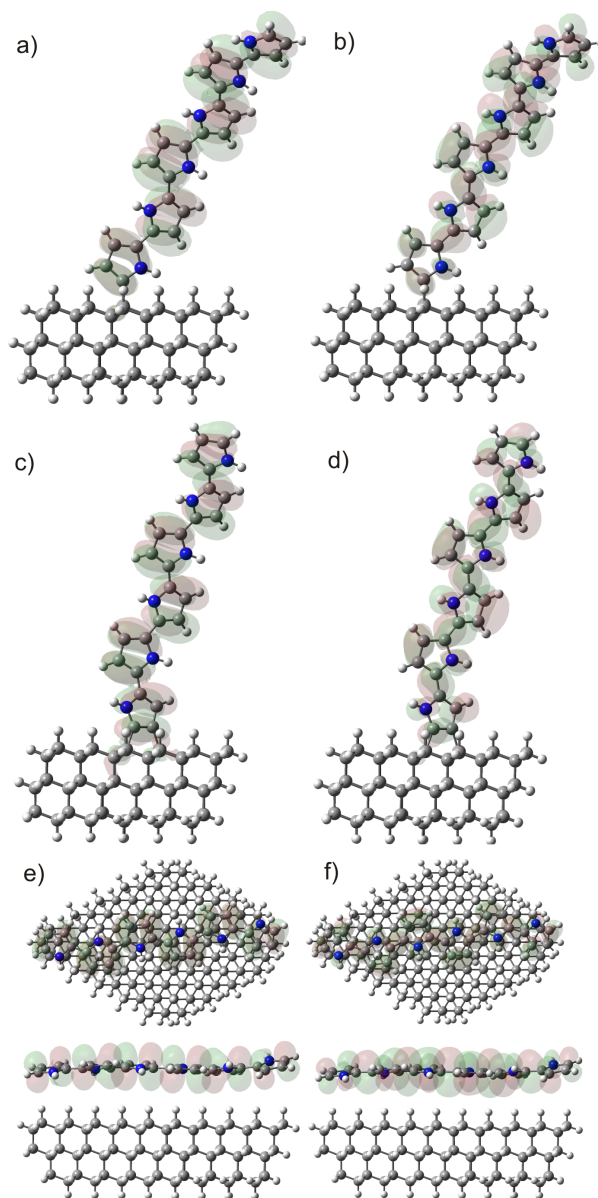


Figure 2.4: Resulting optimized structures of one-bond contact HOMO (a) and LUMO (b), two-bond contact HOMO (c) and LUMO (d), and physisorption HOMO (e) and LUMO (f) (top and side view) of PPy on 1×1 (111) H-terminated ND slab. Red and green colour indicate positive and negative value of the orbital surfaces, respectively, corresponding to the isovalue of $0.01e^{-\text{\AA}^{-3}}$

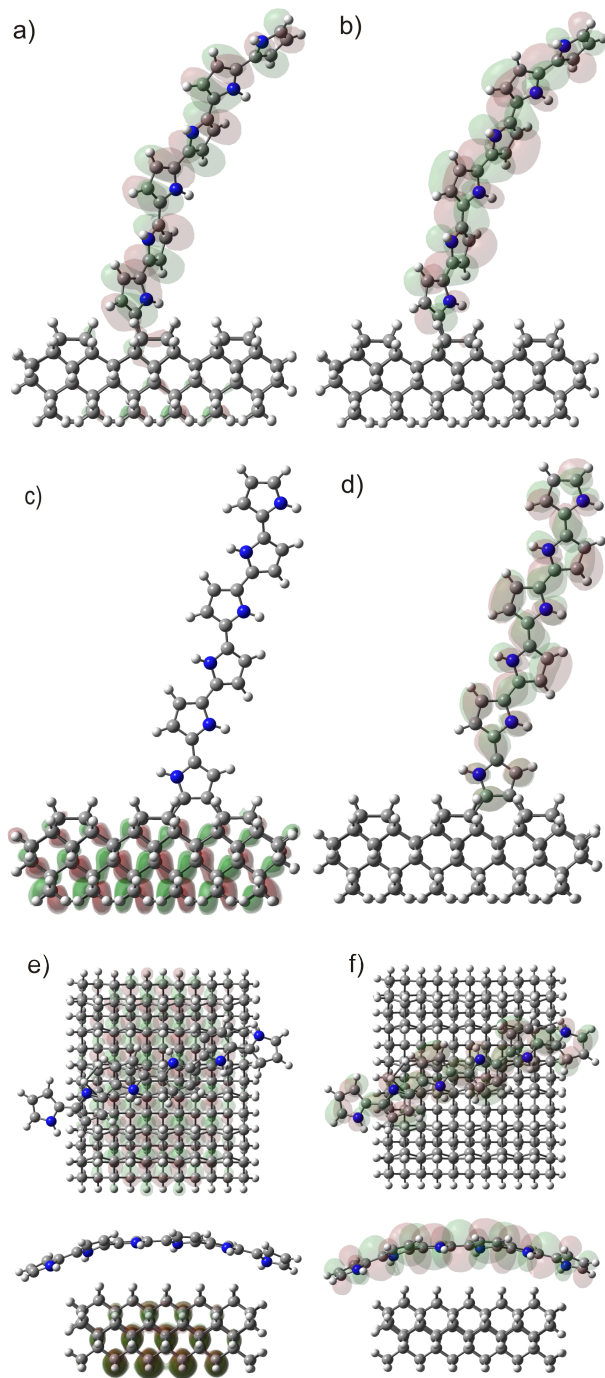


Figure 2.5: Resulting optimized structures of one-bond contact HOMO (a) and LUMO (b), two-bond contact HOMO (c) and LUMO (d), and physisorption HOMO (e) and LUMO (f) (top and side view) of PPy on 2×1 (111) H-terminated ND slab. Red and green colour indicate positive and negative value of the orbital surfaces, respectively, corresponding to the isovalue of $0.01 e^{-\text{\AA}^{-3}}$

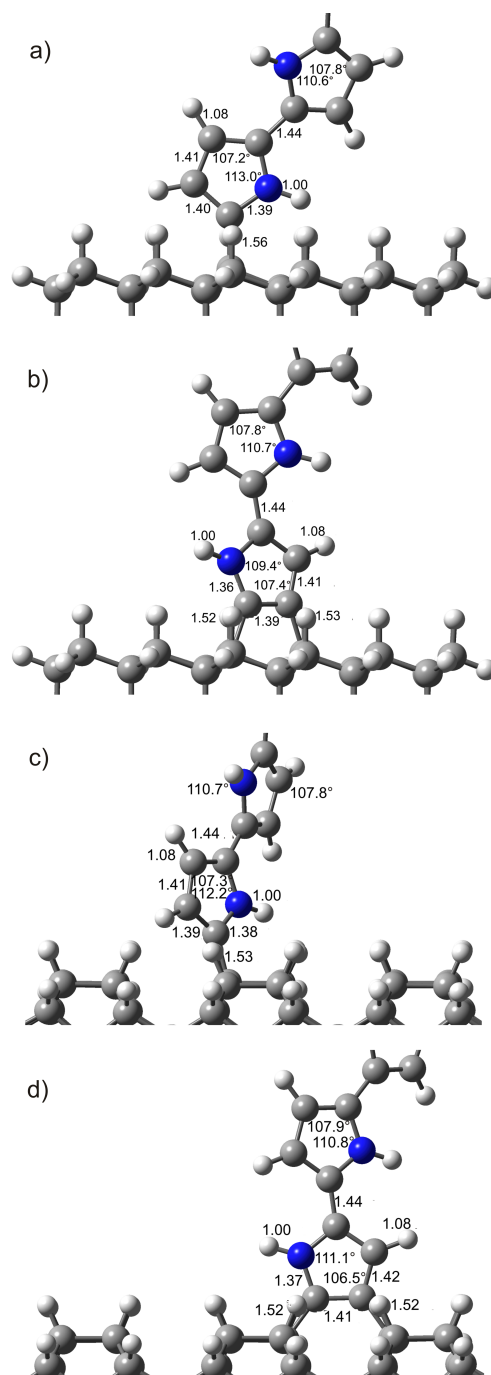


Figure 2.6: Main structural parameters of one-bond contact (a) and two-bond contact (b) of PPy on 1×1 (111) H-terminated ND slab, and one-bond contact (c) and two-bond contact (d) of PPy on 2×1 (100) H-terminated ND slab. The bond lengths are given in Å.

Table 2.1: Binding energy (E_b), interaction energy (E_{int}) and charge transfer (Δq) for the PPy-C:H interfaces.

PPy-C:H structure	E_b [eV]	E_{int} [eV]	Δq [e^-]
1×1 (111) 1-bond	-1,41	3,73	-0,11
1×1 (111) 2-bond	-2,23	9,01	-0,07
1×1 (111) physisorption	0,43	0,43	-0,06
2×1 (100) 1-bond	-1,11	4,23	-0,04
2×1 (100) 2-bond	-1,60	10,33	-0,08
2×1 (100) physisorption	0,62	0,62	-0,05

above the middle 2×1 reconstructed row. The geometry of the diamond remains unaffected, as well as the bond lengths and angles within the particular Py rings. However, PPy doesn't keep its planar character, dihedral angles between the Py rings are twisted up to 10.9° , where the most pronounced changes occur at the terminating Py rings. The $-NH$ groups within PPy are pointing slightly towards the H atoms of the diamond surface due to their partial charges arising from their polar character. The average distance between PPy and the diamond is 3.1 \AA .

2.2.2 Binding and Interaction energies

Binding energies E_b are related to the energy preference of the respective interactions. They were calculated as the difference in total energies of the relaxed structures before and after the contact formation. General formula including all the considered ND slabs in this work is as follows:

$$E_b = (E_{slab} + E_{PPy}) - (E_{con} + (n - 2 \cdot l) \cdot E_{H_2} + m \cdot E_{O_2} + l \cdot E_{CH_4}), \quad (2.1)$$

where E corresponds to total energies of C:H slab (E_{slab}), PPy molecule (E_{PPy}), PPy-C:H structure (E_{con}), molecules desorbed after the substitution (E_{H_2} , E_{O_2} , E_{CH_4}), n is the number of substituted pairs of H atoms, m is the number of substituted pairs of O atoms, and l is the number of substituted C atoms, depending on the type of the formed bond. Positive E_b corresponds to an exothermic process, i.e. thermodynamically favorable, whereas negative value corresponds to an endothermic process. Interaction energies E_{int} describing the character of the bonds between PPy and ND were calculated according to the formula:

$$E_{int} = (E_{slab-X} + E_{PPy-X}) - E_{con}, \quad (2.2)$$

where E_{slab-X} and E_{PPy-X} are total energies of ND slab and PPy calculated with the removed corresponding atoms from the contact region. Note that for the physisorbed structures, the formulas [2.1](#) and [2.2](#) coincide. The binding and interaction energies are summarized in Table [2.1](#).

Based on the binding energies, all the chemisorbed configurations correspond to endothermic processes with the values between -1.11 and -2.23 eV. The one-bond contact is more favorable than the two-bond contact for both types of the facets, especially for the (111) facet, where the two-bond contact requires additional energy of 0.82 eV. The most probable is the one-bond contact of PPy on the (100) facet. All the physisorbed processes are exothermic by about 0.5 eV.

Considering the interaction energies, all the calculated values for the chemisorbed structures correspond to covalent bonds ($E_{int} \sim 3.7$ eV for a typical C-C bond [95]) between PPy and diamond. The strongest bond with $E_{int} = 5.17$ eV per bond is obtained for the case of two-bond contact on (100). In the case of the physisorbed structures, the obtained values correspond to non-bonding interactions between the PPy and diamond ($E_{int} \sim 0.4$ eV for a typical non-bonding interaction).

For both the slabs, the binding energy results in one-bond contacts being more energetically favorable than the two-bond contacts, while the interaction energy indicates that the two bond-contacts are stronger. Less favorable (more negative) binding energy of two bond contacts can be caused by the fact that in the calculation of the interaction energy, there are two dangling bonds on the diamond slabs and two dangling bonds on the PPy chain, which is highly inconvenient and therefore the total energy of the contact formation is more significantly decreased.

2.2.3 Electronic properties and charge transfer

All the PPy-C:H structures are semiconducting, the original HOMO-LUMO gap of 6.31 eV and 5.70 eV for (111) and (100) slab, respectively, significantly decreased to values in range 3.42 – 3.55 eV and 3.39 – 3.53 eV, respectively, where the lowest values corresponds to the physisorbed structures. The original HOMO-LUMO gaps of ND slabs without PPy are higher in comparison with the gap of the bulk diamond (5.5 eV) due to quantum confinement and larger surface-to-volume ratio, which is in agreement with theoretical calculations in the literature [40,91] investigating fully passivated H-terminated NDs. In general, decreasing the particle size results in an increased HOMO-LUMO gap values in comparison with the bulk diamond.

Electron affinity, EA, based on Koopmans' theorem is for the case of PPy equal to 0.53 eV, which is in good agreement with other theoretical calculations [96]. EA of (111) and (100) ND slabs without absorbed PPy are negative, -1.81 and -1.70 respectively, which is in good agreement with other theoretical and experimental results [37]. After the absorption of PPy, the EA rises approximately to 0.58 and 0.50 for diamond (111) and (100) respectively.

In Figures 2.4 and Figure 2.5 are displayed HOMO and LUMO molecular orbital surfaces of the chosen optimized structures. The isosurfaces are visibly modified in the contact region for the chemisorbed (111) structures, where the effect is the most pronounced for the one-bond contact. For the (100) structures, only slight modification occurs in the contact region.

For the case of the physisorbed structures and the two-bond contact on (100), the HOMO orbitals are located on the ND slabs, while the LUMO orbitals are located on the PPy oligomer. Spatially separated HOMO and LUMO orbitals were already observed on the H-terminated 2×1 (100) diamond slab interacting upon adsorption of buckminsterfullerene (C60) modeled by DFT [97] as well as confirmed experimentally [98]. The spatial separation of the HOMO and LUMO is convenient for photovoltaic applications. It has a large influence on the separation of excitons and the consequent movement of charge carriers. Moreover, the chance of recombination process decreases, and thus the efficiency of a photovoltaic cell rises. However, relative energy positions of the frontier orbitals, which are shown in Figure 2.7, are also important to consider. There are several configurations that could lead to the transfer of holes or electrons between PPy and ND under illumination. In the case of two-bond

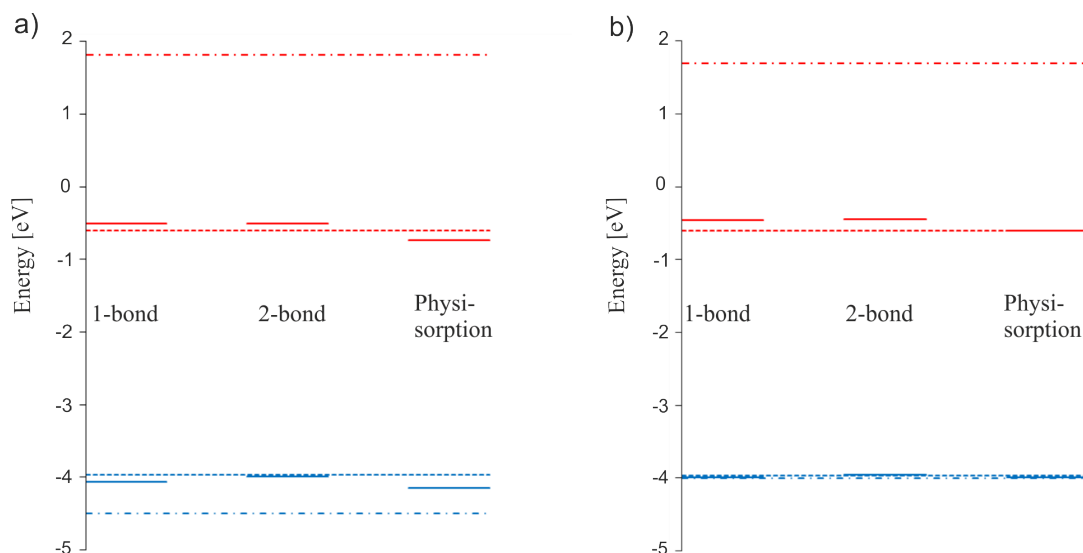


Figure 2.7: Relative energy positions of HOMO (in blue) and LUMO (in red) of one-bond, two-bond and physisorption of PPy on ND (111) (a) and (100) (b) surface slab. The dotted lines correspond to PPy and the dot-and-dash lines correspond to nanodiamond with H-terminated (111) (a) and (100) (b) surface.

contact on (100), holes are likely to transfer from PPy to ND, and the electrons are blocked. Therefore, this structure is promising not only due to the spatial separation of the frontier orbitals. Other configurations, namely the two-bond contact on (111) and the 1-bond contact on (100), where HOMO is also partially localized on ND near the interface with PPy, could work similarly. Opposite direction of charge separation may also be possible. According to the energy levels of the physisorbed PPy on (111), the holes are blocked, and the electrons could be transferred from PPy to ND. Yet note that HOMO and LUMO are not spatially separated in this case.

Charge transfer is another measure reflecting the mutual interaction of PPy and ND. PPy is a neutral molecule, however, when placed to a proximity of the semiconducting nanodiamond, charges are transferred between both the structures in order to achieve equilibrium. For the evaluation of the number of net transferred electrons between the PPy and diamond the charge transfer was calculated as the difference between the amount of donated electrons from ND to PPy and the amount of electrons back donated from PPy to ND based on summing up molecular orbitals redistributed to both of the fragments [99]. Natural bond analysis of the total density was performed in order to obtain coefficients and occupation numbers for natural orbitals. The positive charge transfer values (Δq) thus correspond to the net number of electrons transferred from ND to PPy and vice versa for negative Δq .

The charge transfer values are summarized in Table 2.1. They are negative values for all cases which implies that electrons are actually transferred from PPy to diamond after the contact formation. That can be seen on the modification of the HOMO and LUMO molecular orbitals discussed earlier.

The highest charge transfer of $-0.11 e^-$ is obtained for one-bond contact on (111) facet. In contrast, the lowest charge transfer of $-0.04 e^-$ is obtained for one-bond contact on (100) facet. Also, relatively high charge transfer is obtained even for the much weakly bound physisorbed structures, $\Delta q \sim -0.06 e^-$, most likely because the PPy chain lays on the structure. Therefore, all of its heterocycles contribute to the

charge transfer.

H-diamond can have a p-type conductive channel in the subsurface region. However, transfer doping of diamond by holes from PPy (in the dark) has not been evidenced so far. Here we found that interaction of diamond with PPy leads to significant decrease of LUMO level close to the energy of isolated PPy in all cases (see also Figure 2.7). Furthermore, this LUMO is located almost entirely on the PPy part of this hybrid system. Lowering of LUMO thus corresponds to additional positive charge on PPy, in agreement with calculated charge transfer in the dark.

In addition, one should consider that in the case of PPy grafting to diamond, hydrogen atoms are removed and thereby also diamond conductivity in the dark (if present initially) [31]. Only under illumination, measurements of photovoltages and photocurrents indicated that holes are transferred from PPy to diamond and that the interface provides efficient exciton dissociation [17, 31]. This is not in contradiction to the charge transfer we calculated based on summing-up all MOs in the dark, i.e. without illumination. Based on our calculations, LUMO of the combined PPy-diamond system is located on the PPy part. Under illumination, electrons would be thus excited to the PPy part.

2.3 Adsorption of PPy on O-terminated NDs

2.3.1 Structural analysis

All the initial PPy-ND structures were formed by design in multiple possible nonequivalent positions and consequently were allowed to relax into the energy minimum. All converged sooner or later to the structures that we present here. All energetically favorable structures of PPy adsorbed on (111), (100), and amorphous ND facets resulting from the optimization processes are shown in the Figures [2.8](#), [2.9](#), and [2.10](#). Geometrical parameters of the interactions are summarized in Table [2.2](#).

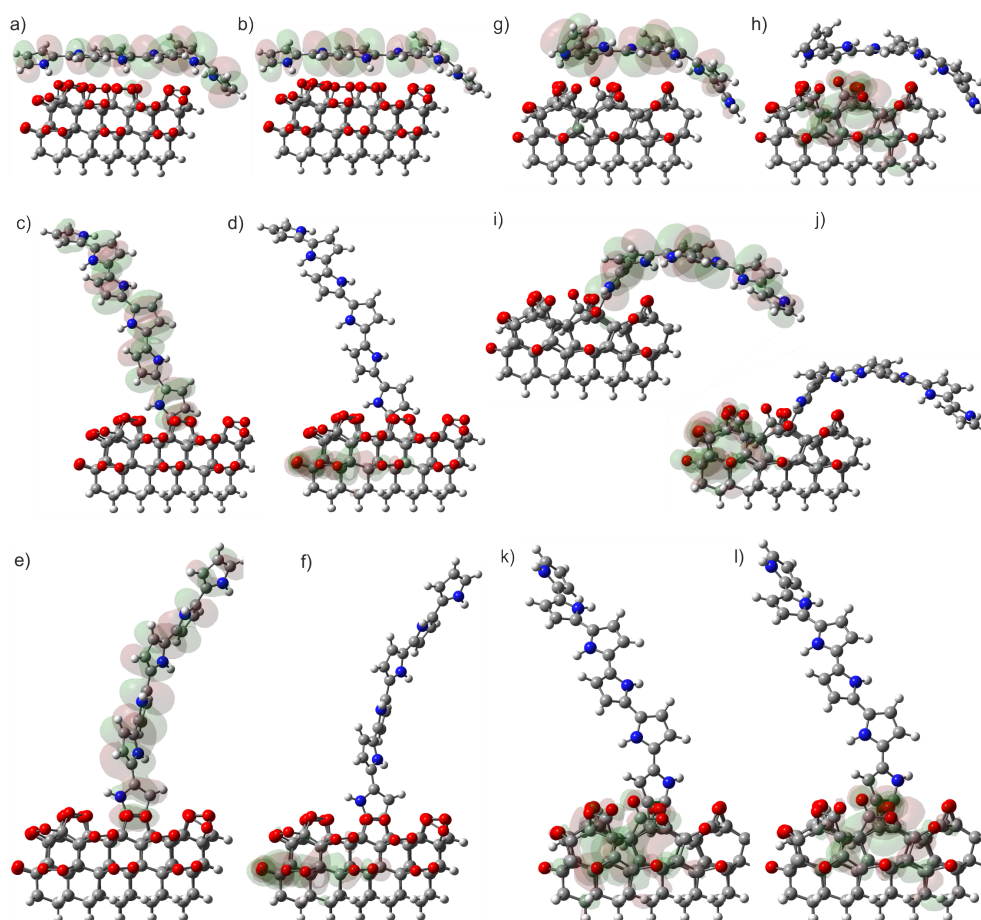


Figure 2.8: Optimized structures of PPy on O-terminated 1×1 (111) ND edge slab: physisorbed HOMO (a) and LUMO (b), one-bond contact HOMO (c) and LUMO (d), two-bond contact HOMO (e) and LUMO (f). Optimized structures of PPy on O-terminated 2×1 (111) ND edge slab: physisorbed HOMO (g) and LUMO (h), one-bond contact HOMO (i) and LUMO (j), two-bond contact HOMO (k) and LUMO (l). C atoms are grey, H atoms white, O atoms red, N atoms blue. Red and green clouds indicate positive and negative value of the orbital surfaces at the isovalue of $0.01e^{-\text{\AA}^{-3}}$.

In the case of physisorbed structures, the geometry of ND after the contact formation remained almost unchanged, individual atoms on the surface shift within 0.19 \AA . An exception is the peroxide-terminated 1×1 (111) structure, where two peroxide groups changed into two ketone groups and one bridging peroxide group.

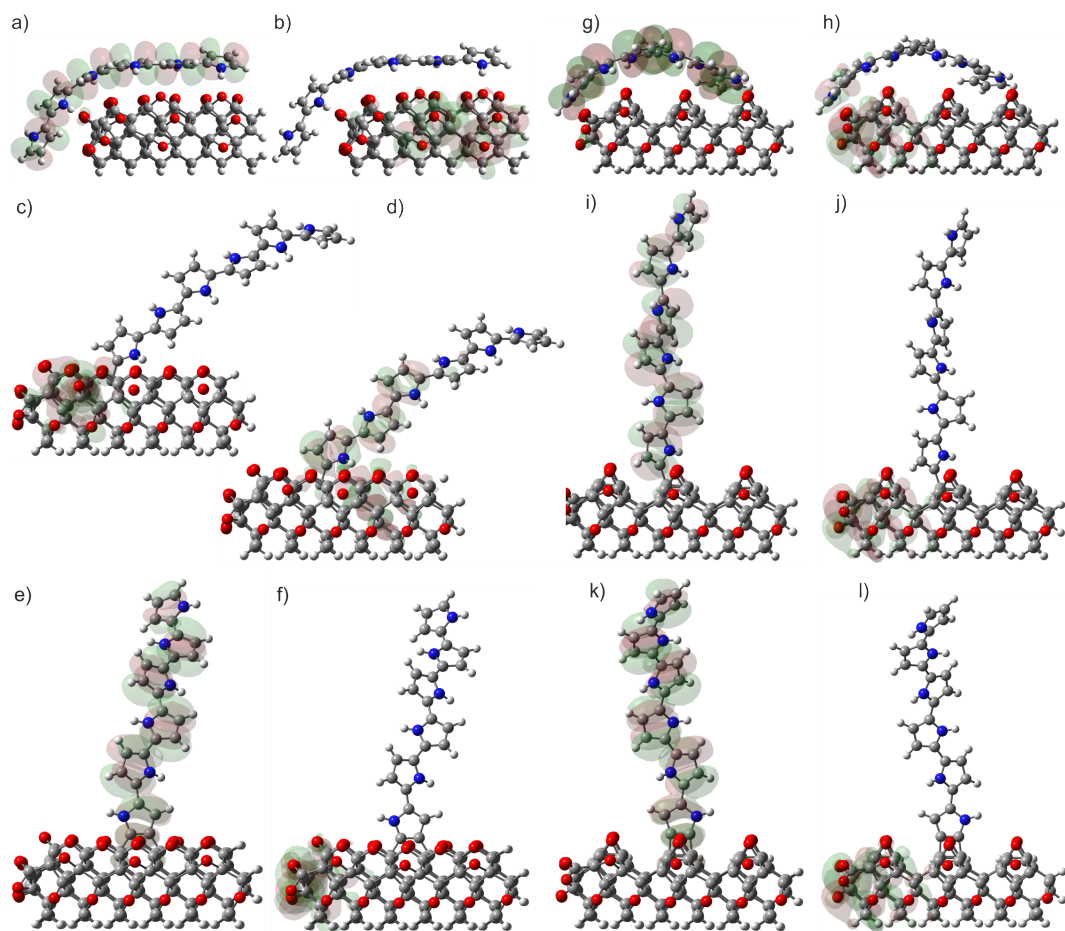


Figure 2.9: Optimized structures of PPy on O-terminated 1×1 (100) ND edge slab: physisorbed HOMO (a) and LUMO (b), one-bond contact HOMO (c) and LUMO (d), two-bond contact HOMO (e) and LUMO (f). Optimized structures of PPy on O-terminated 2×1 (100) ND edge slab: physisorbed HOMO (g) and LUMO (h), one-bond contact HOMO (i) and LUMO (j), two-bond contact HOMO (k) and LUMO (l). C atoms are grey, H atoms white, O atoms red, N atoms blue. Red and green clouds indicate positive and negative value of the orbital surfaces at the isovalue of $0.01e^{-\text{\AA}^{-3}}$.

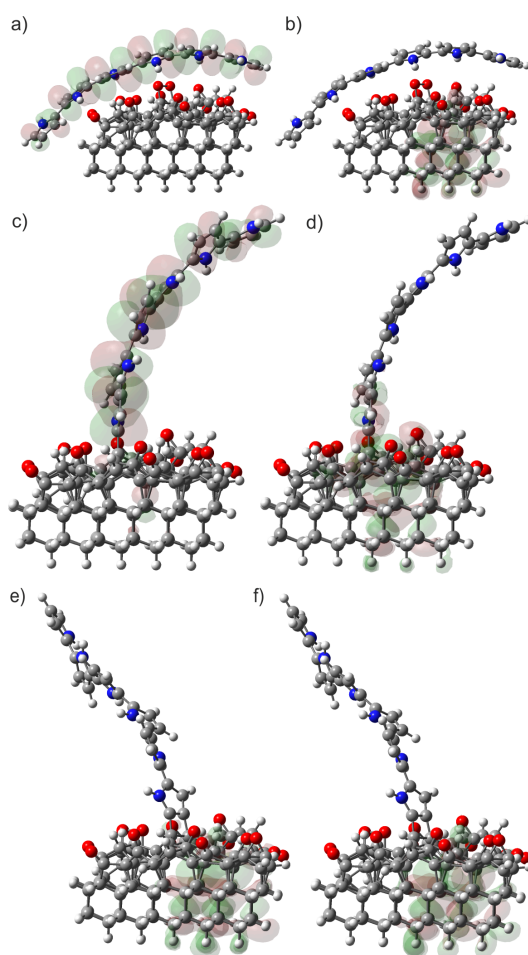


Figure 2.10: Optimized structures of PPy on a-C:O (111) ND edge slab: physisorbed HOMO (a) and LUMO (b), one-bond contact HOMO (c) and LUMO (d), two-bond contact HOMO (e) and LUMO (f). C atoms are grey, H atoms white, O atoms red, N atoms blue. Red and green clouds indicate positive and negative value of the orbital surfaces at the isovalue of $0.01e^{-\text{\AA}^{-3}}$.

Table 2.2: Summary of bond lengths between PPy and O-terminated ND: ND-PPy bond length [\AA], number of (n) and bond length [\AA] of hydrogen bonds formed between NH groups in PPy and O atoms on ND surface for various bonding configurations. Py heterocycles are numbered from the ND edge (physisorbed PPy) or from the bond with ND (chemisorbed PPy).

ND surface structure	PPy bonding	Bond length [\AA]	n	H-bond length [\AA]
1×1 (111), peroxides	physis.	-	3	3.73; 1.54 (Py 1), 1.85 (Py 3)
	1-bond	1.57	1	3.01 (Py 1)
	2-bond	1.51; 1.51	0	-
2×1 (111), epoxides	physis.	-	2	2.04 (Py 1), 2.10 (Py 5)
	1-bond	1.55	1	2.18 (Py 1)
	2-bond	1.52; 1.53	0	-
1×1 (100), ethers	physis.	-	2	1.62 (Py 2), 2.99 (Py 4)
	1-bond	1.50	1	2.68 (Py 1)
	2-bond	1.46; 1.56	0	-
2×1 (100), epoxides	physis.	-	1	3.12 (Py 4)
	1-bond	1.51	0	-
	2-bond	1.51; 1.52	0	-
a-C:O, mix	physis.	-	3	2.02 (Py 2), 2.14; 2.77 (Py 4)
	1-bond	1.49	1	1.90 (Py 1)
	2-bond	1.49; 1.53	0	-

Consequently, a strong hydrogen bond was created between PPy and both ketone groups. Another exception is a rearrangement of one ether group on the ether-terminated 1×1 (100) structure into one ketone group forming a strong hydrogen bond to PPy and leaving one dangling bond on C atom of the ND surface.

The physisorbed structures converged into PPy lying over the ND surface and having nonzero dihedral angles between individual Py heterocycles and thus maximizing the electrostatic interactions at the interface with ND. Note also typical bending of PPy molecule over the edge of the slab, i.e. over the edge of nanodiamond particle (see, e.g. Figure 2.8 a, b, i, j). Chemisorbed (grafted) PPy is inclined relative to the ND surface, deviating from an initially set perpendicular position, which is observed for all the structures in this work. In the case of one-bond contact of PPy on epoxide-terminated 2×1 (111) ND, the PPy even bends over the ND edge, as a result of strong electrostatic interactions. Next, in the case of the chemisorbed structures, ND bond lengths are modified up to 0.5\AA but only in the contact region.

Generally, the bond lengths are shorter for most of the two-bond contacts in comparison with the one-bond contacts. This trend was also observed in the case of the H-terminated NDs. It could be a result of less steric repulsions in the case of the two bond contacts, where two spacious oxygen groups are missing.

Owing to hydrogen bonds, a strong interaction is established even for the non-bonding physisorbed structures. The strongest hydrogen bonds occur between the polar amino groups of PPy and the terminating O-containing groups of ND. For the physisorbed structures, in average, there are 2.2 hydrogen bonds per PPy-ND system. Considering the chemisorbed structures, the one-bond contacts are more likely to cre-

ate the hydrogen bonds than two-bond contacts, owing to a feasible rotation around the one-bond in order to accommodate the electrostatic interactions.

The significance of hydrogen bonds was noted in the literature [100–102], where diamond with hydrophilic oxygen-containing surface groups is prone to adsorb polar molecules by hydrogen bonding and other polar interactions. In the case of H-terminated surfaces, the physisorbed bonding appears to be mediated primarily via van-der-Waals interactions. Therefore, H-terminated surfaces seem to be less likely to physisorb organic compounds, due to this lack of possible polar interactions. That is in agreement with the fact that the highest binding energies are obtained for the structures terminated with O-containing groups.

The optimized structures with amorphous carbon inter-layer exhibit the same structural characteristics as the corresponding PPy-ND structures without the interlayer. The features are mainly the following: Establishment of hydrogen bonds between PPy and surface oxygens for the PPy-a-C:O structures, especially for the physisorbed and one-bond contact chemisorbed structures. The latter is relatively flexible towards a rotation around the C-C bond one-bond contact in contrast with the two-bond contact.

2.3.2 HOMO and LUMO distribution and energies

In addition to the computed structural configurations, Figures 2.8, 2.9, and 2.10 also shows HOMO and LUMO surfaces on several representative structures of the PPy-ND systems. It is noteworthy that highly pronounced spatial separation of HOMO and LUMO between PPy and ND is obtained for a predominant number of the structures. The HOMO-LUMO spatial separation was not observed only on the following structures: PPy physisorbed on peroxide-terminated 1×1 (111), 2-bond contact of PPy on epoxide-terminated 2×1 (111), and 2-bond contact on a-C:O ND. For most of the structures with the pronounced spatial separation, the HOMO is placed along the whole PPy chain. LUMO is placed below the surface of ND in the location with the strongest interaction with PPy or at ND edge enclosed by the oxygen-containing groups. The spatial separation of HOMO and LUMO influences the separation of excitons and the consequent movement of charge carriers. It contributes to the decrease of the probability of recombination processes and to the increase of the efficiency of a solar cell. Therefore, it is highly interesting for photovoltaic applications.

The values of HOMO-LUMO energy gaps of the discussed structures are listed in Table 2.3. The calculated HOMO-LUMO gap of the standalone PPy oligomer calculated with the ω B97X-D functional is 6.95 eV, which is about twice as much in comparison with prior experimental [15, 17, 93, 94] and theoretical [56, 77] studies, as well as our results with B3LYP functional (section 2.2.1). Such large HOMO-LUMO gap corresponds rather to the transport gap (E_t) than to the optical gap (E_g). Similar effect was previously reported in the case of π -conjugated oligomers where E_t exceeded E_g by 2.8 eV [88].

The HOMO-LUMO gap of the standalone NDs with different surface reconstruction and facets terminated with oxygen in different positions is highly variable. The band gap values are between 5.21 eV and 8.07 eV. Some of the surface terminations were studied previously by means of DFT [12, 56, 103]. For most of the structures, the HOMO-LUMO gaps are higher mostly due to the quantum confinement effects and larger surface-to-volume ratio, resulting in the increase of the gap with decreasing size of ND below 2 nm [40, 69]. However, for example, the epoxide-terminated $2 \times$

Table 2.3: Summary of binding energy (E_b), interaction energy (E_{int}), charge transfer (Δq), and HOMO-LUMO gap of PPy on O-terminated NDs. ND structure without PPy bonding (“none”) corresponds to a standalone ND.

ND surface structure	PPy bonding	E_b [eV]	E_{int} [eV]	Δq [e^-]	HOMO-LUMO gap
1×1 (111), peroxides	physis.	3.66	3.66	0.31	4.36
	1-bond	-2.00	5.52	-0.03	4.10
	2-bond	-0.57	10.34	-0.05	4.31
	none	-	-	-	8.07
2×1 (111), epoxides	physis.	2.54	2.54	0.04	3.12
	1-bond	-0.88	5.86	-0.02	5.86
	2-bond	-4.41	5.71	-0.13	3.61
	none	-	-	-	5.21
1×1 (100), ethers	physis.	3.42	3.42	0.03	5.13
	1-bond	-6.93	4.98	0.02	2.90
	2-bond	-2.12	9.11	0.03	5.36
	none	-	-	-	7.56
2×1 (100), epoxides	physis.	2.13	2.13	0.02	4.34
	1-bond	-0.79	4.72	-0.06	4.44
	2-bond	-0.42	7.73	-0.04	4.45
	none	-	-	-	6.34
a-C:O, mix	physis.	2.03	2.03	0.01	3.00
	1-bond	0.48	5.05	-0.12	4.76
	2-bond	-1.66	6.31	-0.03	3.18
	none	-	-	-	3.17

1 (111) ND, the HOMO-LUMO gap of 5.21 eV is in a good agreement with the band gap of bulk diamond, with the experimentally obtained value of 5.48 eV [104]. It is assumed that the trends in relative energy positions of the frontier molecular orbitals as compared between different surface configurations remain the same regardless the possible shifts in the absolute values due to quantum confinement effects.

After the PPy physisorption or chemisorption, the calculated values of HOMO-LUMO gap are in the range between 2.90 and 5.86 eV, resulting from different surface orientation, termination, and type of the bonding between PPy and ND. The reduced band gap is mostly a result of a shift of the HOMO towards less negative energies compared with standalone NDs. As follows from all results covering also less probable surface configurations (see author's article [83]), the HOMO-LUMO gaps of different PPy-ND structures are the most variable with respect to the different surface functional groups, as obtained also for the standalone NDs, while the HOMO-LUMO gaps of the PPy-ND systems within the same functional group, but with different surface reconstruction differ only up to 2.74 eV. Generally, the highly variable HOMO-LUMO gap depending on particular PPy-ND structures points out to possible tunability of the devices based on the PPy-ND system.

Energy levels of HOMO and LUMO of the PPy-ND systems compared with separately calculated energy levels of PPy and NDs are included in Figures 2.11 and 2.12. For most of the structures (except the amorphous NDs), the HOMO of standalone ND is below the HOMO of standalone PPy. Moreover, for all the structures the LUMO of standalone NDs is below the LUMO of standalone PPy. This represents favorable arrangement for transport of photo-generated electrons from PPy to ND; for holes in opposite direction. The situation at the PPy-ND junction is varying depending on surface termination, facet orientation, and type of bonding. Note that zero energy does not correspond to the vacuum energy in our calculations. The vacuum energy could be obtained by summing the HOMO energy and the ionization potential. In a notable number of cases, a favorable energy alignment promoting charge dissociation and one directional transport is observed.

The order of the frontier molecular orbitals suggests several options for the transfer of the charge carriers between PPy and ND. The results indicate great flexibility and tunability of the PPy-ND system since the movement of the charge carriers depends on the ND surface properties and the type of interaction with PPy. In order to elucidate the pronounced effect of PPy-ND system on HOMO-LUMO energy levels and their spatial separation, we performed detailed analysis of mutual PPy and ND interaction in terms of binding energy, interaction energy, and related charge transfer in the PPy-ND systems.

2.3.3 Binding and interaction energies

Values of binding and interaction energies for all the PPy-NDs structures are listed in Table 2.3. For all the physisorbed and chemisorbed structures, the binding energies are exothermic (positive) and endothermic (negative), respectively. This suggests that the physisorbed structures are energetically favorable and more likely to be spontaneously formed in real systems. The bond formation in chemisorbed structures requires extra energy. The only exception is an exothermic one-bond contact of PPy on a-C:O ($E_b = 0.48$ eV). This highest E_b among the chemisorbed structures correlates with one of the shortest bond lengths between ND and PPy in this study. The positive E_b also indicates

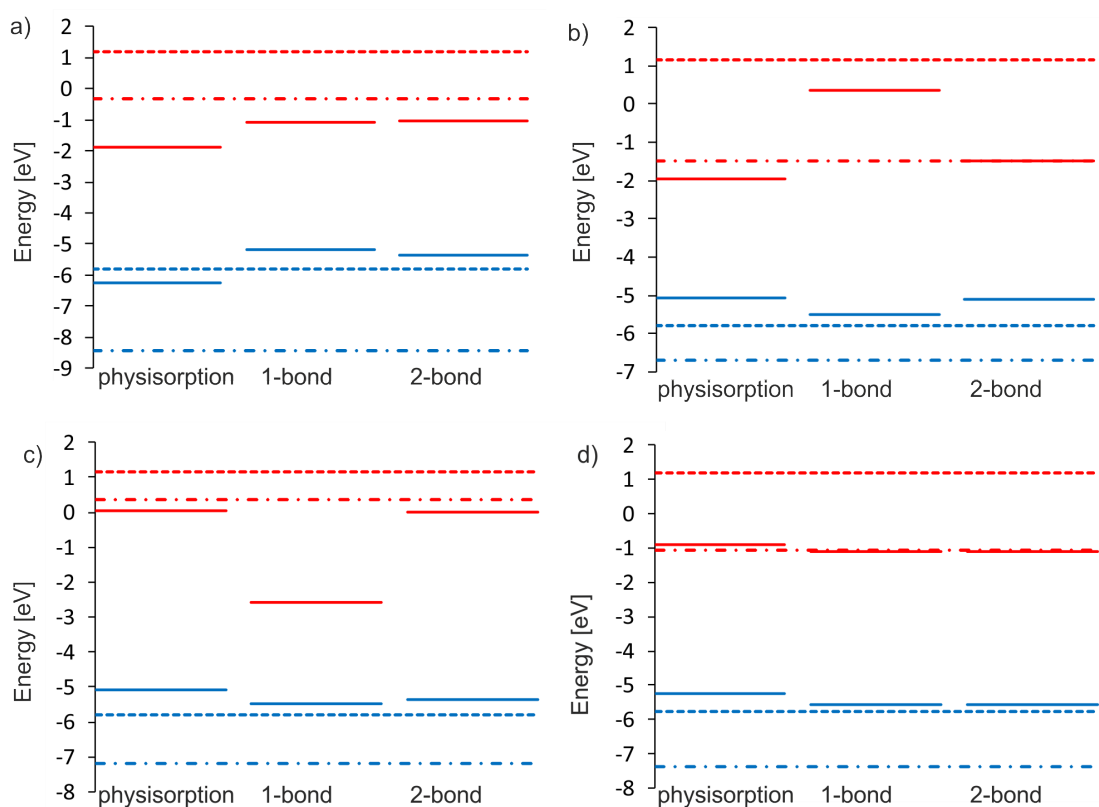


Figure 2.11: HOMO (blue) and LUMO (red) energy levels of i) standalone PPY (dashed lines), ii) standalone O-terminated ND slabs (dot-and-dashed lines), and iii) PPY physisorbed or chemisorbed (1-bond, 2-bond) on O-terminated ND (full lines) in the case of 1×1 (111) (a), 2×1 (111) (b), 1×1 (100) (c), and 2×1 (100) (d) ND slabs.

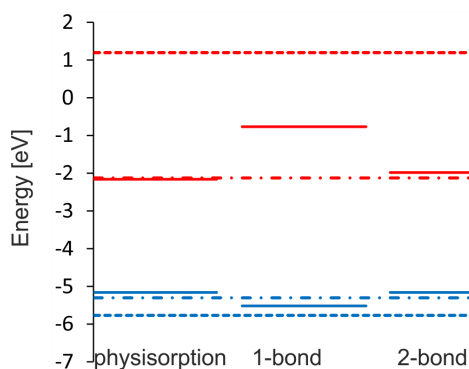


Figure 2.12: HOMO (blue) and LUMO (red) energy levels of i) standalone PPY (dashed lines), ii) standalone ND slabs with amorphous surface layer (dot-and-dashed lines), and iii) PPY physisorbed or chemisorbed (1-bond, 2-bond) on a-C:O slabs (full lines).

that grafting of PPy could happen spontaneously especially on the oxidized NDs with the amorphous surface. Nevertheless, an energy barrier corresponding to the transition state on the reaction coordinate could slow down the process significantly.

The binding energies of the physisorbed PPy on NDs are in the range of 2.03 and 3.66 eV. That are relatively high values in comparison with the H-terminated NDs. The most exothermic is the 1×1 (111) physisorbed structure of PPy on the peroxide-terminated NDs. The binding energy is very dependent on the surface orientation and reconstruction. This is natural considering the preferential formation of ethers, peroxides, epoxides, or ketones on the particular surface, as discussed in the Computational details section. These different O-terminations then lead to different strength of polar attractions and tendency of hydrogen bond formation.

The most negative binding energies, $E_b = -6.93$ eV, (thus the most endothermic and the least probable to occur) are obtained for the one-bond contact of PPy on the epoxide-terminated 2×1 (111) ND. This is consistent with a slightly longer bond length and a result of saturating only one of the two dangling bonds left after removal of one epoxide group.

For most of the reconstructed NDs, the two-bond contacts of PPy on NDs have less negative values of the binding energies compared to the one-bond contacts (thus they are more likely to form). On the O-terminated NDs, the oxygen functional groups saturate two bonds of C atoms, therefore, if the groups are not present, it is more favorable to saturate both of the C atoms via the two-bond contact to PPy.

For most the chemisorbed structures, magnitudes of the interaction energies correspond to relatively strong covalent bonds as the typical value for a C-C bond is $E_{int} \sim 3.7$ eV [95]. After relating the interaction energy to one bond, the highest interaction energy, $E_{int} = 5.86$ eV, is obtained for 1-bond contact on epoxide-terminated 2×1 (111) ND. In this case, the PPy is slightly bended towards the ND surface and one hydrogen bond contribute to the high E_{int} .

Regarding the physisorbed structures, the interaction energies indicate strong interactions for all the studied cases owing to the non-bonding electrostatic and van der Waals interactions.

2.3.4 Charge transfer

The values of charge transfer for all studied structures are listed in Table 2.3. For most of the structures, predominantly for the physisorbed contacts, the electrons are transferred from ND to PPy and the situation is opposite for the chemisorbed contacts with an exception of the chemisorbed PPy on the 1×1 (100) ND. The highest negative charge transfer, $\Delta q = -0.13 e^-$, is obtained for the two-bond contact of PPy on the 2×1 (111) epoxide-terminated ND, where electrons effectively transfer from PPy to ND. The highest positive charge transfer, $\Delta q = 0.31 e^-$, is obtained for PPy physisorbed on 1×1 (111) peroxide-terminated ND, where electrons effectively transfer from ND to PPy. Nevertheless, in general, both directions of charge transfer are possible.

For the amorphous NDs, values of Δq are obtained in range between -0.12 and $0.02 e^-$). The absolute value for the 1-bond contact is the highest of all studied 1-bond-structures.

2.3.5 Excited states

TDDFT was used for the excited state analysis. The excited states are lined up according to their increasing energy and different molecular orbitals may contribute to different excited state. Excited state analysis resulting from the calculations of the O-terminated complexes, as the most interesting ones for photovoltaic applications, is summarized in Table 2.4. For a representative structure of the two-bond contact of PPy on epoxide-terminated 2×1 (100) ND, the charge density difference between the first excited state and ground state, and third excited state and ground state is visualized in Figure 2.13 together with the most contributing molecular orbitals to the transitions.

Table 2.4: Summary of oscillator strength (f), excitation energy (E_{ex}), the most contributing pair of orbitals (MO pair) and its contribution to the transition (Contrib.) for the first three excited states.

ND surface structure	PPy bonding	Ex. state	f	E_{ex} [eV]	MO pair	Contrib. [%]
1×1 (111), peroxides	physis.	1st	0.650	1.92	H \rightarrow L	60
		2nd	0.519	2.03	H-1 \rightarrow L	65
		3rd	0.034	2.22	H-2 \rightarrow L	93
1×1 (111), peroxides	1-bond	1st	0.000	2.06	H-53 \rightarrow L	11
		2nd	0.031	2.13	H \rightarrow L+2	50
		3rd	0.000	2.29	H-43 \rightarrow L+1	14
1×1 (111), peroxides	2-bond	1st	0.000	3.11	H-53 \rightarrow L	23
		2nd	0.000	3.34	H \rightarrow L	89
		3rd	0.003	3.39	H-1 \rightarrow L+10	7
2×1 (111), epoxides	physis.	1st	0.019	0.64	H \rightarrow L	60
		2nd	0.014	0.69	H-1 \rightarrow L	68
		3rd	0.002	1.85	H-2 \rightarrow L	82
2×1 (111), epoxides	1-bond	1st	0.000	2.15	H-9 \rightarrow L+2	18
		2nd	0.000	2.72	H-18 \rightarrow L+1	16
		3rd	0.000	2.75	H \rightarrow L+7	28
2×1 (111), epoxides	2-bond	1st	0.051	0.75	H \rightarrow L	57
		2nd	0.005	1.83	H-1 \rightarrow L	66
		3rd	0.015	2.64	H \rightarrow L+1	45
1×1 (100), ethers	physis.	1st	0.000	-1.03	H-2 \rightarrow L+2	28
		2nd	0.460	1.07	H \rightarrow L	92
		3rd	0.013	2.11	H-1 \rightarrow L	77
1×1 (100), ethers	1-bond	1st	0.002	2.13	H \rightarrow L+3	70
		2nd	0.011	2.46	H-1 \rightarrow L+3	69
		3rd	0.027	3.00	H-3 \rightarrow L+3	96
1×1 (100), ethers	2-bond	1st	0.000	-1.03	H-3 \rightarrow L+3	42
		2nd	0.003	1.16	H-6 \rightarrow L	41
		3rd	0.0002	1.79	H-6 \rightarrow L+1	19
2×1 (100), epoxides	physis.	1st	0.083	2.01	H \rightarrow L	42
		2nd	0.016	2.62	H-5 \rightarrow L	32
		3rd	0.001	2.94	H \rightarrow L+1	75
2×1 (100), epoxides	1-bond	1st	0.000	-1.15	H-7 \rightarrow L	26
		2nd	0.043	2.49	H-7 \rightarrow L	30

		3rd	0.004	2.53	H → L+1	45
2 × 1 (100), epoxides	2-bond	1st	0.041	2.49	H-7 → L	50
		2nd	0.000	3.30	H → L	91
		3rd	2.673	3.87	H → L + 8	77
a-C:O	physis.	1st	0.014	0.37	H-1 → L	95
		2nd	0.000	1.37	H → L	98
		3rd	0.0001	2.31	H-2 → L	93
a-C:O	1-bond	1st	0.000	2.06	H-8 → L+1	27
		2nd	0.054	2.54	H-2 → L	39
		3rd	0.016	2.65	H → L+8	20
a-C:O	2-bond	1st	0.014	0.37	H → L	88
		2nd	0.0004	2.12	H-1 → L	62
		3rd	0.004	2.40	H-6 → L	34

For the two-bond contact of PPy on epoxide-terminated 2 × 1 (100) ND, the charge density difference corresponding to the first and third excited state is placed on ND and PPy, respectively, pointing out the local excitation type of the transition for both of the cases. Based on the oscillator strengths, the electron excitation from the ground to the third excited state is the most likely for this structure. The most contributing pairs of molecular orbitals to this transition are: HOMO → LUMO + 8, and with about three times lower coefficient HOMO - 1 → LUMO + 12 (not shown in [2.4](#)). In agreement with the position of the charge density difference, the localization of all the mentioned orbitals is on the PPy part, as visualized in Figure [2.13](#) (e - h). That is consistent with the dipole moments which are mostly aligned to the PPy axis, with the total value of 43.0 D. Excitation energy is equal to 3.9 eV, thus, the most pronounced transitions are in the near UV region.

The first excited state of the two-bond contact of PPy on epoxide-terminated 2 × 1 (100) ND occurs with much smaller oscillator strength. However, it corresponds to smaller excitation energy possibly applicable for longer wave lengths (497.5 nm) in the VIS region of the spectrum. Moreover, the first excitation of the structure with epoxides is always from an orbital below HOMO to LUMO. According to Kasha's rule, the fluorescence is from the lowest excited state. Therefore, vibrational relaxation of the excited electron from the third excited state (LUMO + 8 and LUMO + 12) on PPy to the first excited state (LUMO) on ND is expected before the recombination. This process could be slowed down owing to the different localization of the discussed orbitals.

Considering the excited state with the highest oscillator strength, the transition exactly from HOMO to LUMO is the most probable for six following structures: PPy physisorbed on 1 × 1 (111), PPy physisorbed and two-bond contact of PPy on 2 × 1 (111), PPy physisorbed on 1 × 1 (100), PPy physisorbed on 2 × 1 (100), and two-bond contact of PPy on a-C:O. For four of these six structures (except for the PPy physisorbed on 1 × 1 (111) and two-bond contact of PPy on 2 × 1 (111)), the HOMO and LUMO are spatially separated between PPy and ND. This demonstrates, that for some cases, the excitation from HOMO to LUMO indeed leads to spatially separated excitons.

The computed excitation energies are in the range from near IR to near UV energies, covering the whole visible spectrum, depending on the type of the contact between PPy and ND and the surface termination of ND.

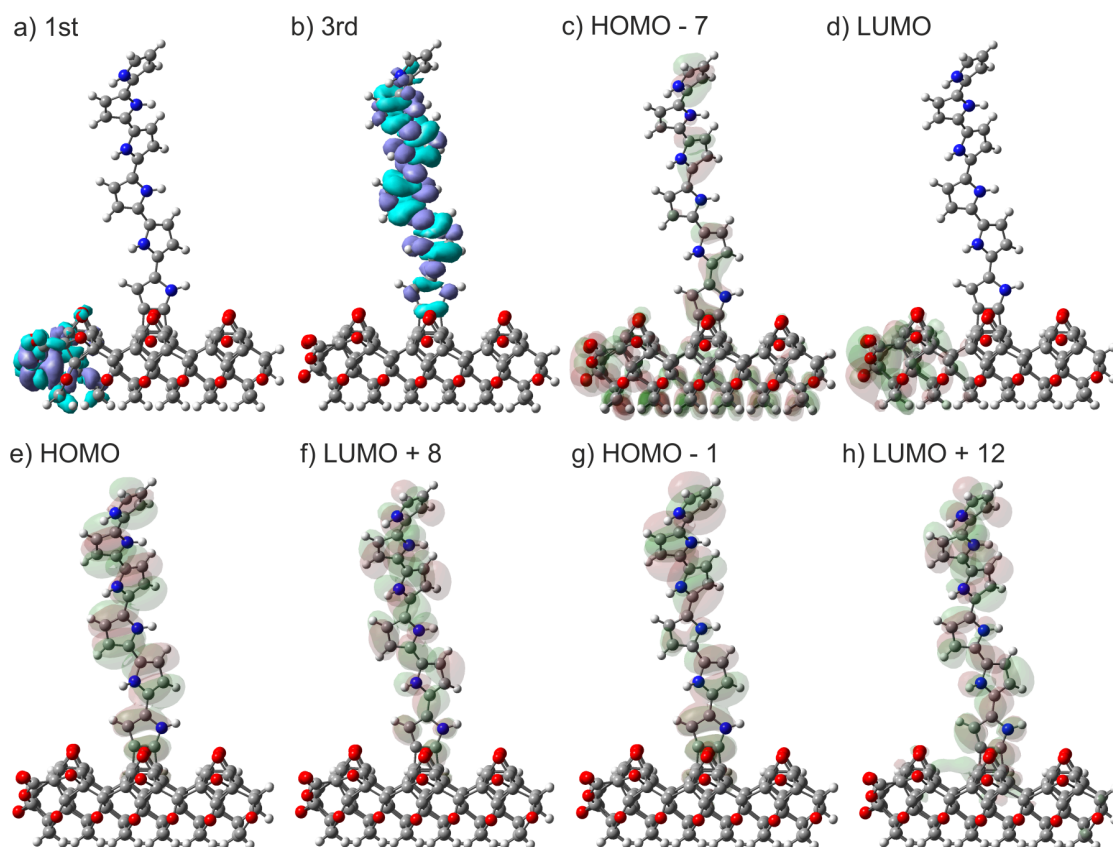


Figure 2.13: Charge density difference between the first (a) and third (b) excited and ground state and for two-bond contact of PPY on epoxide-terminated 2×1 (100) ND. Blue and purple represents the decrease and increase, respectively, of the electron density after the excitation. The density corresponds to the isovalue of $0.4 \times 10^{-3} e^{-\text{\AA}^{-3}}$. Molecular orbitals contributing the most to the first excited state (c, d) and to the third excited state (e - h). C atoms are in grey, H atoms are in white, O atoms are in red, and N atoms are in blue.

3. Conclusion

First-principles electronic structure DFT calculations were employed in order to understand the interactions between PPy and ND, a promising organic-semiconductor functional system. Different chemisorbed (covalently grafted) and physisorbed (non-covalent) positions of PPy on 1×1 (111) and 2×1 (100) as well as amorphous surface slabs of ND were geometrically and energetically optimized to obtain ground state structures and these were further analyzed. Different most frequently occurring surface functional groups of ND were explored, particularly, hydrogens and oxygens in peroxide, epoxide, ether and keton positions. Two different levels of theory were applied to study the PPy-ND composite systems. First, the most straightforward B3LYP functional was used, and second, the dispersion-corrected wB97XD functional was selected.

According to the binding energies, E_b , most of the chemisorption interactions are endothermic, the only positive value is obtained for the one-bond contact of PPy on amorphous oxygen-terminated ND. This interaction represents the most likely chemisorbed binding. Overall, the one-bond contact is more favorable than two-bond contact. In the case of the physisorbed structures, all the interactions are exothermic (and therefore energetically more favorable processes). Furthermore, considering the H-terminated NDs, all the structures of PPy on (100) facet were energetically more favorable than the corresponding structures on (111) facet. Comparing the H- and O-terminated NDs, the physisorbed structures are energetically more convenient on the O-terminated NDs, where the key role plays the hydrogen bonds present between the surface oxygens and PPy.

The interaction energies, E_{int} , indicate a covalent nature of all the chemisorbed structures and non-bonding interaction for the physisorbed structures.

Relatively strong charge transfer, Δq , is calculated especially for PPy on NDs terminated with oxygen surface functional groups. For the H-terminated NDs with surface reconstruction, the covalent bonds facilitates mostly more pronounced charge transfer.

Under both physisorbed and chemisorbed PPy configurations, the computed results revealed that HOMO and LUMO are spatially separated between PPy and ND for most of the PPy-ND composites. The (100) ND facets turns out to be more efficient in this regard. For most of the structures, HOMO is positioned on PPy and LUMO on ND. This is the predominant effect on all the oxidized NDs. The diamond would thus act as an electron acceptor. Interestingly, the separation does not occur on H-terminated NDs (with two exceptions). The spatial separation persists even on NDs with the amorphous carbon interlayer, the closest structure to the real ND materials. Analysis of energy levels showed that HOMO and LUMO energy levels are favourably aligned for exciton dissociation in PPy-ND composite.

Under illumination, the HOMO-LUMO spatial separation may promote dissociation of excitons. Analysis of excited states calculated with the time-dependent DFT theory showed that for some cases with spatially separated HOMO and LUMO, the

direct HOMO-LUMO transition is the most probable based on the calculated oscillator strength of the excited state and molecular orbital contribution to the transition. Moreover, the energetic levels alignment favors the transfer of electrons from excited LUMO states in PPy to ground state LUMO in nanodiamond. In addition, excitation to different states is still possible with correspondingly lower excitation energy (albeit with lower oscillator strength). This may lead to optical absorption in a broader spectral range as also observed experimentally. Therefore, the organic-inorganic composite of PPy covalently adsorbed to oxygen-terminated diamond nanoparticles provide promising features for photovoltaic applications.

To sum up, detailed analysis revealed a strong mutual interaction (in terms of binding energy, interaction energy, charge transfer) not only for covalently grafted PPy to ND but even larger between PPy and ND in the physisorbed configurations due to the formation of multiple hydrogen bonds (H...O bridges). Also, we conclude that oxygens may be more efficient in comparison with hydrogens for PPy adsorption and photovoltaic applications of the hybrid PPy-ND system. Simulations taking into account the amorphous surface layer present on DNDs evidence similar trends as the NDs with reconstructed surfaces. The observed effects can most likely be generalized also for interactions with other organic molecules (dyes, donor molecules, acceptor molecules, proteins, etc.).

For a better understanding of the observed phenomena and further improvement of the models, simultaneous experimental work is also being done as a part of another Ph.D. thesis. For instance, structural character of PPy-ND systems is corroborated by atomic force microscopy and Fourier-transform infrared spectroscopy. Photovoltaic effects are characterized by measuring local photovoltages using Kelvin probe.

Bibliography

- [1] M. A. Green, K. Emery, Y. Hishikawa, W. Warta, E. D. Dunlop, D. H. Levi, and A. W. Y. Ho-Baillie. Solar cell efficiency tables (version 49): Solar cell efficiency tables (version 49). *Progress in Photovoltaics: Research and Applications*, 25(1):3–13, January 2017.
- [2] V. Švrček, D. Mariotti, T. Nagai, Y. Shibata, I. Turkevych, and M. Kondo. Photovoltaic Applications of Silicon Nanocrystal Based Nanostructures Induced by Nanosecond Laser Fragmentation in Liquid Media. *The Journal of Physical Chemistry C*, 115(12):5084–5093, March 2011.
- [3] C. Liu, Z. C. Holman, and U. R. Kortshagen. Hybrid Solar Cells from P3ht and Silicon Nanocrystals. *Nano Letters*, 9(1):449–452, January 2009.
- [4] S. Mori, H. Oh-oka, H. Nakao, T. Gotanda, Y. Nakano, H. Jung, A. Iida, R. Hayase, N. Shida, M. Saito, K. Todor, T. Asakura, A. Matsui, and M. Hosoya. Organic photovoltaic module development with inverted device structure. *MRS Online Proceedings Library Archive*, 1737, January 2015.
- [5] P. Roy and Thao P. Nguyen. Ab initio calculation of pentacene–PbSe hybrid interface for photovoltaic applications. *Physical Chemistry Chemical Physics*, 18(27):18209–18218, 2016.
- [6] O. V. Kontkanen, M. Niskanen, T. I. Hukka, and T. T. Rantala. Electronic structure of p-type perylene monoimide-based donor–acceptor dyes on the nickel oxide (100) surface: a DFT approach. *Physical Chemistry Chemical Physics*, 18(21):14382–14389, 2016.
- [7] J. S. Shaikh, N. S. Shaikh, S. S. Mali, J. V. Patil, K. K. Pawar, P. Kanjanaboos, C. K. Hong, J. H. Kim, and P. S. Patil. Nanoarchitectures in dye-sensitized solar cells: metal oxides, oxide perovskites and carbon-based materials. *Nanoscale*, 10(11):4987–5034, March 2018.
- [8] M. Anafcheh, R. Ghafouri, and N. L. Hadipour. A computational proof toward correlation between the theoretical chemical concept of electrophilicity index for the acceptors of C60 and C70 fullerene derivatives with the open-circuit voltage of polymer–fullerene solar cells. *Solar Energy Materials and Solar Cells*, 105:125–131, October 2012.
- [9] H. Zhu, J. Wei, K. Wang, and D. Wu. Applications of carbon materials in photovoltaic solar cells. *Solar Energy Materials and Solar Cells*, 93(9):1461–1470, September 2009.

- [10] S. Collavini and J. L. Delgado. Carbon Nanoforms in Perovskite-Based Solar Cells. *Advanced Energy Materials*, 7(10):1601000, May 2017.
- [11] M. Grätzel. Photoelectrochemical cells. *Nature*, 414(6861):338–344, November 2001.
- [12] N. Brown and O. Hod. Controlling the Electronic Properties of Nanodiamonds via Surface Chemical Functionalization: A DFT Study. *The Journal of Physical Chemistry C*, 118(10):5530–5537, March 2014.
- [13] T. V. Vernitskaya and O. N. Efimov. Polypyrrole: a conducting polymer; its synthesis, properties and applications. *Russian Chemical Reviews*, 66(5):443–457, 1997.
- [14] A. Krueger. Diamond Nanoparticles: Jewels for Chemistry and Physics. *Advanced Materials*, 20(12):2445–2449, June 2008.
- [15] R. K. John and D. S. Kumar. Structural, electrical, and optical studies of plasma-polymerized and iodine-doped poly pyrrole. *Journal of Applied Polymer Science*, 83(9):1856–1859, February 2002.
- [16] J. Čermák, B. Rezek, P. Hubík, J. J. Mareš, A. Kromka, and A. Fejfar. Photoconductivity and Hall mobility of holes at polypyrrole–diamond interface. *Diamond and Related Materials*, 19(2–3):174–177, February 2010.
- [17] B. Rezek, J. Čermák, A. Kromka, M. Ledinský, and J. Kočka. Photovoltage effects in polypyrrole–diamond nanosystem. *Diamond and Related Materials*, 18(2–3):249–252, February 2009.
- [18] P. Galář, J. Čermák, P. Malý, A. Kromka, and B. Rezek. Electrochemically grafted polypyrrole changes photoluminescence of electronic states inside nanocrystalline diamond. *Journal of Applied Physics*, 116(22):223103, December 2014.
- [19] B. Rezek, J. Čermák, A. Kromka, M. Ledinský, P. Hubík, J. J. Mareš, A. Purkrt, V. Cimrová, A. Fejfar, and J. Kočka. Synthesis, structure, and opto-electronic properties of organic-based nanoscale heterojunctions. *Nanoscale research letters*, 6(1):1–12, 2011.
- [20] Y. L. Zhong, A. Midya, Z. Ng, Z. Chen, M. Daenen, M. Nesladek, and K. P. Loh. Diamond-based molecular platform for photoelectrochemistry. *Journal of the American Chemical Society*, 130(51):17218–17219, December 2008.
- [21] S. Günes, H. Neugebauer, and N. S. Sariciftci. Conjugated Polymer-Based Organic Solar Cells. *Chemical Reviews*, 107(4):1324–1338, April 2007.
- [22] M. Yun, N. V. Myung, R. P. Vasquez, C. Lee, E. Menke, and R. M. Penner. Electrochemically Grown Wires for Individually Addressable Sensor Arrays. *Nano Letters*, 4(3):419–422, March 2004.
- [23] D. Miliarova, S. Stehlik, P. Stenclova, and B. Rezek. Synthesis of polypyrrole on nanodiamonds with hydrogenated and oxidized surfaces: Synthesis of polypyrrole on nanodiamonds. *physica status solidi (a)*, September 2016.

- [24] S. Honda, H. Ohkita, H. Benten, and S. Ito. Selective Dye Loading at the Heterojunction in Polymer/Fullerene Solar Cells. *Advanced Energy Materials*, 1(4):588–598, July 2011.
- [25] S. V. Kesava, Z. Fei, A. D. Rimshaw, C. Wang, A. Hexemer, J. B. Asbury, M. Heeney, and E. D. Gomez. Domain Compositions and Fullerene Aggregation Govern Charge Photogeneration in Polymer/Fullerene Solar Cells. *Advanced Energy Materials*, 4(11):1400116, August 2014.
- [26] A. Vul' and O. Shenderova. *Detonation Nanodiamonds: Science and Applications*. CRC Press, Singapore, February 2014. Google-Books-ID: J97MBQAAQBAJ.
- [27] J. Arnault. *Nanodiamonds: advanced material analysis, properties and applications*. Elsevier, Boston, MA, 2017.
- [28] B. Rezek, S. Stehlik, A. Kromka, J. Arnault, M. Weis, and J. Jakabovic. Visible Light Photodiodes and Photovoltages from Detonation Nanodiamonds. *MRS Advances*, 1(14):971–975, 2016.
- [29] O. A. Shenderova and G. E. McGuire. Science and engineering of nanodiamond particle surfaces for biological applications (Review). *Biointerphases*, 10(3):030802, September 2015.
- [30] A. Krueger. The structure and reactivity of nanoscale diamond. *Journal of Materials Chemistry*, 18(13):1485, 2008.
- [31] J. Čermák, B. Rezek, A. Kromka, M. Ledinský, and J. Kočka. Electrochemical synthesis and electronic properties of polypyrrole on intrinsic diamond. *Diamond and Related Materials*, 18(9):1098–1101, September 2009.
- [32] M. Frenklach, R. Kematich, D. Huang, W. Howard, K.E. Spear, A.W. Phelps, and R. Koba. Homogeneous nucleation of diamond powder in the gas phase. *Journal of Applied Physics*, 66(1):395–399, 1989.
- [33] S. Stehlik, M. Varga, P. Stenclova, L. Ondic, M. Ledinsky, J. Pangrac, O. Vanek, J. Lipov, A. Kromka, and B. Rezek. Ultrathin Nanocrystalline Diamond Films with Silicon Vacancy Color Centers via Seeding by 2 nm Detonation Nanodiamonds. *ACS Applied Materials & Interfaces*, 9(44):38842–38853, November 2017.
- [34] A. Kromka, J. Čech, H. Kozak, A. Artemenko, T. Ižák, J. Čermák, B. Rezek, and M. Černák. Low-Temperature hydrogenation of diamond nanoparticles using diffuse coplanar surface barrier discharge at atmospheric pressure: Low-temperature hydrogenation of diamond nanoparticles. *physica status solidi (b)*, 252(11):2602–2607, November 2015.
- [35] E. Ukraintsev, A. Kromka, W. Janssen, K. Haenen, and B. Rezek. Controlling physical and chemical bonding of polypyrrole to boron doped diamond by surface termination. *Int. J. Electrochem. Sci*, 8:17–26, 2013.

- [36] S. Stehlik, M. Varga, M. Ledinsky, D. Miliaieva, H. Kozak, V. Skakalova, C. Mangler, T. J. Pennycook, J. C. Meyer, A. Kromka, and B. Rezek. High-yield fabrication and properties of 1.4 nm nanodiamonds with narrow size distribution. *Scientific Reports*, 6(1), December 2016.
- [37] A. K. Tiwari, J. P. Goss, P. R. Briddon, N. G. Wright, A. B. Horsfall, R. Jones, H. Pinto, and M. J. Rayson. Calculated electron affinity and stability of halogen-terminated diamond. *Physical Review B*, 84(24), December 2011.
- [38] T. Kondo, I. Neitzel, V. N. Mochalin, J. Urai, M. Yuasa, and Y. Gogotsi. Electrical conductivity of thermally hydrogenated nanodiamond powders. *Journal of Applied Physics*, 113(21):214307, June 2013.
- [39] F. Maier, J. Ristein, and L. Ley. Electron affinity of plasma-hydrogenated and chemically oxidized diamond (100) surfaces. *Physical Review B*, 64(16), October 2001.
- [40] A. S. Barnard. Modeling polydispersive ensembles of diamond nanoparticles. *Nanotechnology*, 24(8):085703, March 2013.
- [41] A. Datta, m. Kirca, Y. Fu, and A. C. To. Surface structure and properties of functionalized nanodiamonds: a first-principles study. *Nanotechnology*, 22(6):065706, February 2011.
- [42] D. Petrini and K. Larsson. Theoretical Study of the Thermodynamic and Kinetic Aspects of Terminated (111) Diamond Surfaces. *Journal of Physical Chemistry C*, 112(8):3018–3026, February 2008.
- [43] D. Petrini and K. Larsson. A theoretical study of the energetic stability and geometry of hydrogen-and oxygen-terminated diamond (100) surfaces. *The Journal of Physical Chemistry C*, 111(2):795–801, 2007.
- [44] S. L. Y. Chang, A. S. Barnard, C. Dwyer, C. B. Boothroyd, R. K. Hocking, E. Ōsawa, and R. J. Nicholls. Counting vacancies and nitrogen-vacancy centers in detonation nanodiamond. *Nanoscale*, 8(20):10548–10552, 2016.
- [45] S. Skokov, B. Weiner, and M. Frenklach. Theoretical study of oxygenated (100) diamond surfaces in the presence of hydrogen. *Physical Review B*, 55(3):1895, 1997.
- [46] Z. G. Wang, X. T. Zu, J. L. Nie, and H. Y. Xiao. Chemisorptions of Atomic Oxygen and its Replacement by Hydrogen on the Diamond (100) Surface Studied by First Principles. *Surface Review and Letters*, 13(01):45–49, 2006.
- [47] H. Tamura, H. Zhou, K. Sugisako, Y. Yokoi, S. Takami, M. Kubo, K. Teraishi, A. Miyamoto, A. Imamura, N. Mikka, and A. Toshihiro. Periodic density-functional study on oxidation of diamond (100) surfaces. *Physical Review B*, 61(16):11025, 2000.
- [48] X. M. Zheng and P. V. Smith. The stable configurations for oxygen chemisorption on the diamond (100) and (111) surfaces. *Surface Science*, 262(1–2):219–234, February 1992.

- [49] L. Lai and A. S. Barnard. Modeling the thermostability of surface functionalisation by oxygen, hydroxyl, and water on nanodiamonds. *Nanoscale*, 3(6):2566, 2011.
- [50] L. Lai and A. S. Barnard. Surface phase diagram and thermodynamic stability of functionalisation of nanodiamonds. *Journal of Materials Chemistry*, 22(33):16774, 2012.
- [51] G. S. Sriram and C. T. v. D. Adri. Direction dependent etching of diamond surfaces by hyperthermal atomic oxygen: A ReaxFF based molecular dynamics study. *Carbon*, 82:314–326, February 2015.
- [52] S. Moustafa, N. Tokuda, and T. Inokuma. Density functional studies of surface potentials for hydrogen and oxygen atoms on diamond (111) surfaces. *Japanese Journal of Applied Physics*, 53(2S):02BD01, February 2014.
- [53] M. J. Rutter and J. Robertson. Ab initio calculation of electron affinities of diamond surfaces. *Physical Review B*, 57(15):9241, 1998.
- [54] C. Stampfl, T. E. Derry, and N. W. Makau. Interaction of diamond (111) - (1 × 1) and (2 × 1) surfaces with OH: a first principles study. *Journal of Physics: Condensed Matter*, 22(47):475005, December 2010.
- [55] H. Yang, L. Xu, C. Gu, and S. B. Zhang. First-principles study of oxygenated diamond (001) surfaces with and without hydrogen. *Applied Surface Science*, 253(9):4260–4266, February 2007.
- [56] R. Long, Y. Dai, and M. Guo. Characterization of diamond (100) surface with oxygen termination. *Applied Surface Science*, 254(9):2851–2855, February 2008.
- [57] T. E. Derry, N. W. Makau, and C. Stampfl. Oxygen adsorption on the (1 × 1) and (2 × 1) reconstructed C(111) surfaces: a density functional theory study. *Journal of Physics: Condensed Matter*, 22(26):265007, July 2010.
- [58] J. L. Whitten, P. Cremaschi, R. E. Thomas, R. A. Rudder, and R. J. Markunas. Effects of oxygen on surface reconstruction of carbon. *Applied Surface Science*, 75(1–4):45–50, January 1994.
- [59] V. Jirásek, H. Kozak, and Z. Remeš. DFT Calculations of Vibrational Spectra of Oxidized (111) Diamond Surface. *Advanced Science, Engineering and Medicine*, 7(4):275–278, April 2015.
- [60] K. Bobrov, H. Shechter, A. Hoffman, and M. Folman. Molecular oxygen adsorption and desorption from single crystal diamond (1 1 1) and (1 1 0) surfaces. *Applied Surface Science*, 196(1–4):173–180, August 2002.
- [61] F. K. de Theije, M. F. Reedijk, J. Arsic, W. J. P. van Enckevort, and E. Vlieg. Atomic structure of diamond {111} surfaces etched in oxygen water vapor. *Physical Review B*, 64(8), August 2001.

- [62] F. K. de Theije, N. J. van der Laag, M. Plomp, and W. J. P. van Enckevort. A surface topographic investigation of {001} diamond surfaces etched in oxygen. *Philosophical Magazine A*, 80(3):725–745, March 2000.
- [63] P. E. Pehrsson, T. W. Mercer, and J. A. Chaney. Thermal oxidation of the hydrogenated diamond (100) surface. *Surface Science*, 497(1–3):13–28, January 2002.
- [64] X. Wang, A. R. Ruslinda, Y. Ishiyama, Y. Ishii, and H. Kawarada. Higher coverage of carboxylic acid groups on oxidized single crystal diamond (001). *Diamond and Related Materials*, 20(10):1319–1324, November 2011.
- [65] B. Dzurňák, F. Trojánek, J. Preclíková, A. Kromka, B. Rezek, and P. Malý. Ultrafast photoluminescence spectroscopy of H- and O-terminated nanocrystalline diamond films. *Diamond and Related Materials*, 20(8):1155–1159, August 2011.
- [66] S. Zhao and K. Larsson. Theoretical Study of the Energetic Stability and Geometry of Terminated and B-Doped Diamond (111) Surfaces. *The Journal of Physical Chemistry C*, 118(4):1944–1957, January 2014.
- [67] H. Busmann, S. Lauer, I. V. Hertel, W. Zimmermann-Edling, H. Güntherodt, T. Frauenheim, P. Blaudeck, and D. Porezag. Observation of $(3 \times 3)R30^\circ$ diamond (111) on vapour-grown polycrystalline films. *Surface Science*, 295(3):340–346, October 1993.
- [68] R. Klauser, J. Chen, T. J. Chuang, L. M. Chen, M. C. Shih, and J. Lin. The interaction of oxygen and hydrogen on a diamond C(111) surface: a synchrotron radiation photoemission, LEED and AES study. *Surface Science*, 356(1–3):L410–L416, June 1996.
- [69] T. Frauenheim, T. Köhler, M. Sternberg, D. Porezag, and M. R. Pederson. Vibrational and electronic signatures of diamond surfaces. *Thin Solid Films*, 272(2):314–330, January 1996.
- [70] J.Y. Raty and G. Galli. Optical properties and structure of nanodiamonds. *Journal of Electroanalytical Chemistry*, 584(1):9–12, October 2005.
- [71] J. Raty and G. Galli. Ultradispersity of diamond at the nanoscale. *Nature Materials*, 2(12):792–795, December 2003.
- [72] R. E. Thomas, R. A. Rudder, and R. J. Markunas. Thermal desorption from hydrogenated and oxygenated diamond (100) surfaces. *Journal of Vacuum Science & Technology A*, 10(4):2451–2457, July 1992.
- [73] Y. Yu, C. Z. Gu, L. F. Xu, and S. B. Zhang. *Ab initio* structural characterization of a hydrogen-covered diamond (001) surface. *Physical Review B*, 70(12), September 2004.
- [74] H. Tamura, H. Zhou, Kiyoshi S., Y. Yokoi, S. Takami, M. Kubo, K. Teraishi, A. Miyamoto, A. Imamura, N. Mikka, and A. Toshihiro. Periodic density-functional study on oxidation of diamond (100) surfaces. *Physical Review B*, 61(16):11025, 2000.

- [75] Y. Tian and K. Larsson. Process of Diamond Surface Termination by Carboxylic and Amino groups – A Quantum Mechanics Approach. <http://www.diva-portal.org/smash/record.jsf?pid=diva2:765999>, 2014 (accessed January 18, 2017).
- [76] L. Lai and A. S. Barnard. Anisotropic adsorption and distribution of immobilized carboxyl on nanodiamond. *Nanoscale*, 6(23):14185–14189, October 2014.
- [77] W. Kamiński, V. Rozsival, and P. Jelínek. Theoretical study of electronic and transport properties of PPy–Pt(111) and PPy–C(111):H interfaces. *Journal of Physics: Condensed Matter*, 22(4):045003, February 2010.
- [78] A. Szabo and N. S. Ostlund. *Modern Quantum Chemistry: Introduction to Advanced Electronic Structure Theory*. Dover Publications, Mineola, N.Y, revised ed. edition edition, July 1996.
- [79] F. Jensen. *Introduction to computational chemistry*. John Wiley & Sons, Chichester, England ; Hoboken, NJ, 2nd ed edition, 2007. OCLC: ocm70707839.
- [80] P. Matunová, V. Jirásek, and B. Rezek. Computational study of physisorption and chemisorption of polypyrrole on H-terminated (111) and (100) nanodiamond facets: Physisorption and chemisorption of polypyrrole on nanodiamond facets. *physica status solidi (a)*, 213(10):2672–2679, October 2016.
- [81] P. Matunová, V. Jirásek, and B. Rezek. Spatially separated HOMO/LUMO at the interface of polypyrrole physisorbed on oxidized nanodiamond facets. *Proceedings of the 8th International Conference Nanocon*, pages 15–19, 2017.
- [82] P. Matunová, V. Jirásek, and B. Rezek. Structural and electronic properties of oxidized and amorphous nanodiamond surfaces with covalently grafted polypyrrole. *physica status solidi (b)*, pages 1900176–1900183, 2019.
- [83] P. Matunová, V. Jirásek, and B. Rezek. DFT calculations reveal pronounced homo-lumo spatial separation in polypyrrole-nanodiamond system. *Physical Chemistry Chemical Physics*, 21:11033–11042, 2019.
- [84] M. J. Frisch et al. Gaussian 09, Revision E.01, 2009. Gaussian, Inc., Wallingford CT.
- [85] A. D. Becke. Density-functional thermochemistry. III. The role of exact exchange. *The Journal of Chemical Physics*, 98(7):5648–5652, April 1993.
- [86] P. J. Stephens, F. J. Devlin, C. F. Chabalowski, and M. J. Frisch. Ab Initio Calculation of Vibrational Absorption and Circular Dichroism Spectra Using Density Functional Force Fields. *The Journal of Physical Chemistry*, 98(45):11623–11627, November 1994.
- [87] J. Chai and M. Head-Gordon. Long-range corrected hybrid density functionals with damped atom–atom dispersion corrections. *Physical Chemistry Chemical Physics*, 10(44):6615, 2008.
- [88] U. Salzner and A. Aydin. *Journal of Chemical Theory and Computation*, 7(8):2568–2583, August 2011.

- [89] L. Pandey, C. Doiron, J. S. Sears, and J. Brédas. Lowest excited states and optical absorption spectra of donor–acceptor copolymers for organic photovoltaics: a new picture emerging from tuned long-range corrected density functionals. *Physical Chemistry Chemical Physics*, 14(41):14243, 2012.
- [90] I. T. Lima, A. d. S. Prado, J. B. L. Martins, Pedro H. de Oliveira N., A. M. Ceschin, W. F. da Cunha, and Demétrio A. da Silva F. Improving the Description of the Optical Properties of Carotenoids by Tuning the Long-Range Corrected Functionals. *The Journal of Physical Chemistry A*, 120(27):4944–4950, July 2016.
- [91] T. Yuan and K. Larsson. Theoretical Study of Size Effects on Surface Chemical Properties for Nanoscale Diamond Particles. *The Journal of Physical Chemistry C*, 118(45):26061–26069, November 2014.
- [92] R. J. Magyar and S. Tretiak. Dependence of Spurious Charge-Transfer Excited States on Orbital Exchange in TDDFT: Large Molecules and Clusters. *Journal of Chemical Theory and Computation*, 3(3):976–987, May 2007.
- [93] J. L. Brédas, B. Thémans, J. G. Fripiat, J. M. André, and R. R. Chance. Highly conducting polyparaphenylene, polypyrrole, and polythiophene chains: An *ab initio* study of the geometry and electronic-structure modifications upon doping. *Physical Review B*, 29(12):6761–6773, June 1984.
- [94] L. Micaroni, F. Nart, and I. Hümmelgen. Considerations about the electrochemical estimation of the ionization potential of conducting polymers. *Journal of Solid State Electrochemistry*, 7(1):55–59, December 2002.
- [95] J. M. Berg, J. L. Tymoczko, L. Stryer, J. M. Berg, J. L. Tymoczko, and L. Stryer. *Biochemistry*. W H Freeman, New York, 5th edition, 2002.
- [96] H. Kuzmany, M. Mehring, and Siegmund Roth. *Electronic Properties of Polymers and Related Compounds: Proceedings of an International Winter School, Kirchberg, Tirol, February 23 – March 1, 1985*. Springer Science & Business Media, December 2012.
- [97] S. J. Sque, R. Jones, S. Öberg, and P. R. Briddon. Transfer doping of diamond: Buckminsterfullerene on hydrogenated, hydroxylated, and oxygenated diamond surfaces. *Journal of Materials Science: Materials in Electronics*, 17(6):459–465, June 2006.
- [98] M. Nimmrich, M. Kittelmann, P. Rahe, W. Harneit, A. J. Mayne, G. Dujardin, and A. Kühnle. Influence of charge transfer doping on the morphologies of C 60 islands on hydrogenated diamond C(100)-(2×1). *Physical Review B*, 85(3), January 2012.
- [99] M. Xiao and L. Tian. Generalized Charge Decomposition Analysis (GCDA) Method. *Journal of Advances in Physical Chemistry*, 04(04):111–124, 2015.
- [100] D. Steinmullernethl, F. Kloss, M. Najamulhaq, M. Rainer, K. Larsson, C. Linsmeier, G. Kohler, C. Fehrer, G. Lepperdinger, and X. Liu. Strong binding of bioactive BMP-2 to nanocrystalline diamond by physisorption. *Biomaterials*, 27(26):4547–4556, September 2006.

- [101] B. Rezek, D. Shin, T. Nakamura, and C. E. Nebel. Geometric Properties of Covalently Bonded DNA on Single-Crystalline Diamond. *Journal of the American Chemical Society*, 128(12):3884–3885, March 2006.
- [102] G. P. Bogatyreva, M. A. Marinich, E. V. Ishchenko, V. L. Gvyazdovskaya, and G. A. Bazalij. Adsorption and catalysis processes on the surface of nanodisperse diamonds. *Sverkhtverdye Materialy*, (6):10–15, 2002.
- [103] S. J. Sque, R. Jones, and P. R. Briddon. Structure, electronics, and interaction of hydrogen and oxygen on diamond surfaces. *Physical Review B*, 73(8), February 2006.
- [104] D. Bimberg. *Physics of Group IV Elements and III-V Compounds*. Springer-Verlag Berlin Heidelberg, 1982.

List of Abbreviations

AFM	Atomic force microscopy
B3LYP	Becke 3-parameter Lee-Yang-Parr hybrid exchange correlation functional
CC	Coupled Clusters
CI	Configuration Interaction method
CVD	Chemical vapor deposition
DFT	Density functional theory
DND	Detonation diamond nanoparticles
HOMO	Highest occupied molecular orbital
LCAO	Linear Combination of Atomic Orbitals
LDA	Local Density Approximation
LUMO	Lowest unoccupied molecular orbital
MP	Møller-Plesset
ND	Diamond nanoparticles (Nanodiamond)
PPy	Polypyrrole
PT	Perturbation theory
Py	Pyrrole
SCF	Self Consistent Field method
STEM	Scanning transmission electron microscopy
TDDFT	Time-dependent density functional theory

List of Publications

Own contribution of the author

In the publications related to the thesis, the author performed all the DFT calculations presented in the publications as well as the further calculations of the analyzed properties related to the theoretical calculations. The author created all the figures and tables related to the theoretical results presented in the publications and supplementary information. The author wrote all the texts in all the publications where she is the first author. These texts were further reshaped by the co-authors. In the manuscript with D. Miliaieva as the first author, the theoretical results were written based on the thesis author's simulations.

Publications related to the thesis

Publications in impacted journals

1. P. Matunová, V. Jirásek, B. Rezek. Computational study of physisorption and chemisorption of polypyrrole on H-terminated (111) and (100) nanodiamond facets. *physica status solidi (a)*, 213, 2672–2679, October 2016.
Co-authorship of P. Matunová: 70%
Current number of citations: 4.
2. P. Matunová, V. Jirásek, B. Rezek. DFT Calculations Reveal Pronounced HOMO-LUMO Spatial Separation in Polypyrrole-Nanodiamond System. *Physical Chemistry Chemical Physics*, 21, 11033-11042, May 2019.
Co-authorship of P. Matunová: 70%
3. P. Matunová, V. Jirásek, B. Rezek. Structural and Electronic Properties of Oxidized and Amorphous Nanodiamond Surfaces with Covalently Grafted Polypyrrole. *physica status solidi (b)*, 1900176-1900183, June 2019.
Co-authorship of P. Matunová: 80%
4. D. Miliaieva, P. Matunová, J. Čermák, Š. Stehlík, A. Cernescu, Z. Remeš, P. Štenclová, B. Rezek. Nanodiamond surface chemistry controls assembly of organic dye and photovoltage. Submitted in *ACS Applied Materials & Interfaces*, June 2019.
Co-authorship of P. Matunová: 10%

Publications in conference proceedings

1. P. Matunová, V. Jirásek, B. Rezek. Spatially separated HOMO/LUMO at interface of polypyrrole physisorbed on oxidized nanodiamond facets. Proceeding of the 8th International Conference Nanocon, 2017, pp. 15–19, ISBN 978-80-87294-71-0.

Co-authorship of P. Matunová: 70%

Publications not related to the thesis

1. P. Matunová, W. Kaiser, A. Garliardi, U. Wurstbauer, A. Holleitner. Cross-plane transport properties of 2D materials. To be submitted in 2D Materials.

Co-authorship of P. Matunová: 50%

List of Activities

Conference presentations

Oral presentations

1. 8th International Conference on Nanomaterials - Research & Application (NANOCON, October 2016), Brno, Czech Republic. Title of the presentation: Spatially separated HOMO/LUMO at interface of polypyrrole physisorbed on oxidized nanodiamond facets.
2. 10th International Symposium on Flexible Organic Electronics (ISFOE17, July 2017), Thessaloniki, Greece. Title of the presentation: Computational study of interfacial properties of polypyrrole on diamond nanoparticles for photovoltaic applications.

Poster presentations

1. 21st Hasselt Diamond Workshop (March 2016), Hasselt, Belgium. Title of the presentation: Computational Study of Physisorption and Chemisorption of Polypyrrole on H-terminated (111) and (100) Nanodiamond Facets.
2. International Workshop on Computational Nanotechnology (ICWN, June 2017), Windermere, United Kingdom. Title of the presentation: Computing interfacial properties of polypyrrole on diamond nanoparticles for photovoltaic applications.
3. Cena Nadace ČEZ 2017 (June 2017), Prague, Czech Republic. Title of the presentation: Computing interfacial properties of polypyrrole on diamond nanoparticles for photovoltaic applications.
4. 20th International Winterschool on New Developments in Solid State Physics (IWTPV, February 2018), Mauterndorf, Austria. Title of the presentation: Computing interfacial properties of polypyrrole on diamond nanoparticles for photovoltaic applications.
5. 10th International Conference on Hybrid and Organic Photovoltaics (HOPV18, May 2018), Benidorm, Spain. Title of the presentation: Different effects of nanodiamond surfaces on HOMO/LUMO separation in complexes with polypyrrole - DFT study.
6. NIM Conference "The Future of Nanoscience" (September 2018), Tutzing, Germany. Title of the presentation: Cross-plane transport properties of 2D materials.

Awards

1. Poster presentation of P. Matunová was selected as one of the five best student posters at the conference International Workshop on Computational Nanotechnology (IWCN 2017, Windermere, U.K., June 2017). Title of the presentation: Computing interfacial properties of polypyrrole on diamond nanoparticles for photovoltaic applications.
2. Awarded in competition 'Cena Nadace ČEZ 2017' for the 3rd place in a category called 'Obnovitelné zdroje energie a životní prostředí' for a project called 'Computing interfacial properties of polypyrrole on diamond nanoparticles for photovoltaic applications'.
3. Obtained Bayhost scholarship for one-year exchange study for the academic year 2017/2018 at the Technical University of Munich, Germany.
4. Second place in a national round of 'Present around the World competition' organized by the Czech center of EIT (Institution of Engineering and Technology), May 2019.

Attached Publications

Computational study of physisorption and chemisorption of polypyrrole on H-terminated (111) and (100) nanodiamond facets

Petra Matunová^{*1,2}, Vít Jirásek¹, and Bohuslav Rezek^{1,2}

¹Institute of Physics ASCR, Cukrovarnická 10, 162 00 Prague 6, Czech Republic

²Faculty of Electrical Engineering, Czech Technical University, Technická 2, 160 00 Prague 6, Czech Republic

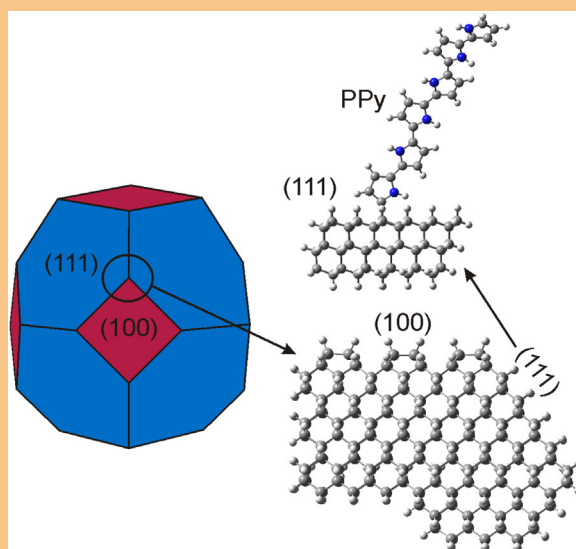
Received 4 April 2016, revised 18 May 2016, accepted 23 May 2016

Published online 8 June 2016

Keywords charge transfer, density functional theory, diamond, nanomaterials, nanoparticles, polypyrrole

*Corresponding author: e-mail matunova@fzu.cz, Phone: +420 774 811 654, Fax: +420 233 343 184

Interaction of diamond with molecules is important for various applications. For instance, experimentally observed charge transfer between bulk diamond and polypyrrole (PPy) is promising for photovoltaics. Here we explore the interactions of PPy with surfaces of nanodiamonds (NDs) by density functional theory (DFT) calculations at the B3LYP/6-31G(d) level of theory. The most probable H-terminated 1×1 (111) and 2×1 (100) diamond surface facets are considered. Geometrical arrangement, binding energy (E_b), interaction energy (E_{int}), charge transfer (Δq), and HOMO-LUMO gap are calculated on geometrically relaxed structures of PPy on the ND facets in physisorbed or chemisorbed configuration. Energetically, the most favorable is physisorption of PPy on NDs. For chemisorption, one-bond contact is more favorable than two-bond contact, with the most probable binding on (100) facet. Charge transfer of electrons (up to $\Delta q = -0.11 e^-$) from PPy to diamond is observed for all the configurations in the dark. In some cases, the calculations reveal spatial separation of the HOMO and LUMO, which may be useful for photovoltaic applications.



Truncated octahedral ND (left), (111) facets are in blue, (100) facets are in red. (111)–(100)–(111) corner of ND (bottom), and (111) facet with chemisorbed PPy (top). C atoms are in gray, H atoms are in white, N atoms are in blue.

© 2016 WILEY-VCH Verlag GmbH & Co. KGaA, Weinheim

1 Introduction In the 21st century, diamond is investigated owing to its unique semiconducting and chemical properties, e.g., superb hardness, chemical inertness, non-toxicity, biocompatibility, high carrier mobility, efficient heat dissipation, and luminescence.

Diamond has an indirect band structure with the band gap width of 5.5 eV [1]. The applications of diamond are numerous, e.g., in electronics, optoelectronic devices, biosensors, and in photovoltaics. Photovoltaics and the related energy generation from a renewable source, e.g.,

light-to-energy conversion is an attractive idea [2]. From more than half a century ago, when the first solar cells were manufactured, up till now bulk silicon wafers have been the most commonly used material for solar cells. Despite the efficiency of silicon in photovoltaic conversions constantly improving, it has not exceeded 24% for monocrystalline silicon. Silicon nanoparticles are considered as an alternative to the traditional bulk silicon material [3, 4] owing to charge carrier multiplication, low toxicity, and possibility to rely on well-established silicon industry. However, the synthesis and stabilization of Si nanocrystal surfaces is complicated. Diamond nanoparticles, denoted as NDs, possess many unique properties that could be beneficial alternative to silicon and other traditional photovoltaic materials, e.g., TiO₂, GaAs, and CdS [3–5]. Yet, the potential of NDs for energy conversion remains virtually unexplored.

The main goal of this work is to explore the interactions of polypyrrole (PPy) with surfaces of NDs for photovoltaic applications. PPy is one of the most chemically stable conjugated polymers [6], its conductivity can be controlled, contains an amino group within its heterocycle, and it can be a linker to biomolecules [7]. In this respect, NDs modified with PPy could be used as a sensor. Furthermore, PPy is a visible light sensitive polymer (organic dye actually). Its experimental HOMO–LUMO gap is 1.3–3.2 eV, depending on the method of preparation [8]. There has been an experimental evidence of charge transfer between the bulk diamond and PPy on its surface observed by Kelvin force microscopy [1] and optical spectroscopy [9].

These results showed that merging diamond and organics provides an efficient interface for exciton dissociation and electron transfer [10, 11]. Such hybrid organic–inorganic interfaces are considered perspective for novel photovoltaic systems [12, 13]. For these purposes, chemical modification and investigation of interaction of diamond surface with molecules is important. NDs are capable to bind a wide array of surface groups, which can stabilize their surfaces. Functionalization of NDs changes the electrical properties of the structures [14]. That cannot be fully understood based purely on experimental techniques. Therefore, computational approach involving first-principles calculations is essential. Interaction of PPy with semiconducting H-terminated diamond has already been studied experimentally [15, 16]. However, only one computational study of PPy chemisorbed to hydrogen terminated diamond (111) surface has been published yet. Covalent one- and two-bond contact of PPy on H-terminated diamond 1×1 (111) surface facet with the charge transfer of $-0.11 e^-$ and $-0.20 e^-$, respectively, from the ND to the PPy was calculated [8].

In this work, we have investigated physisorption and chemisorption of PPy with H-terminated (111) and (100) surfaces of NDs. Hydrogen was identified as a prerequisite for further grafting of PPy molecules [17]. NDs are usually dominated by (111) and (100) facets [18–20]. These low-index surfaces dominate the polycrystalline CVD growth

process, where they are the most highly represented with a quota dependent on temperature and pressure [20]. Moreover, the (100) surface represents the most defect-free surface obtained from experimental synthesis [21].

H-terminated (111) surfaces remains unreconstructed, i.e., in the 1×1 configuration, which was confirmed by both theoretical [18–20, 22, 23] and experimental [24, 25] approaches. Although the (111) surface may be constructed as triradical with three dangling bonds per surface atom, it is much higher in energy [23], unstable, and practically not observed [18].

H-terminated (100) surfaces occur in mono-hydride configuration on the 2×1 reconstructed surface, which was confirmed both by theoretical [18, 23, 26–31] and experimental [28, 32, 33] methods. Di-hydride configuration retaining the 1×1 structure surface is generally unstable, mostly due to steric interactions, unless the supersaturation of H is very high (such as in plasmas).

2 Computational details The first-principles DFT calculations implemented in Gaussian 09 electronic structure software [34] were employed. B3LYP hybrid functional [35, 36], one of the most widely used functionals in computations of organic molecules, with the 6-31G(d) basis set was used for optimizations, i.e., structural relaxation for obtaining the energetically lowest structures.

Modeling whole ND with experimentally accessible size starting at 4 nm [18] would be computationally unfeasible at this level of theory. Therefore, first, surface slabs bordering on a corner of ND were modeled and optimized. These are 1×1 (111) and 2×1 (100) fully H-terminated surface slabs of NDs consisting of 3C layers of 6×6 surface units. The atoms were allowed to relax during the optimizations with the exception of three “surfaces,” representing inner cut planes where the particle continues further into the bulk, were treated differently. C atoms on these planes were saturated by H atoms in order to keep their sp^3 hybridization. These H atoms were fixed during further optimization. In this way, the inner atom layers maintain plane shape yet retain certain flexibility to relax.

For the need to saturate two dangling bonds of carbon atoms, the dimerized hydrogen atoms were placed symmetrically around the carbon atom. They were kept fixed during the optimizations in order to maintain the tetrahedral sp^3 character of diamond structure, despite some steric tension arising between the hydrogen atoms [28, 37]. Few other authors suggest a canted configuration with increased distance between the hydrogen atoms, however, this problem merits more discussion [30, 37, 38].

To study the contact formation, different initial configurations of PPy on the relaxed slabs were optimized. The PPy was represented by six Py heterocycles, which were optimized separately and were proportionate to the modeled slabs. Non-equivalent positions of physisorbed and chemisorbed PPy, including one- and two-bond contacts, on

the optimized slabs were considered as initial geometries. PPy and the top C-H layer were allowed to relax during these further optimizations.

PPy does not spontaneously chemisorb on the clean H-terminated diamond surface [8]. Therefore, the one- and two-bond chemisorbed contacts were allowed by a removal of one and two H atoms, respectively, both from the slab and PPy. Experimentally, the H-termination of diamond is substituted by the PPy molecules during electrochemical synthesis process [16]. The dehydrogenation process itself was not studied here since the work is focused mainly on the nature of the PPy-C:H bonding.

For each bonding situation, structure with the lowest relative energy with respect to the optimized (111) or (100) ND slabs was taken for further analyses. Geometrical arrangement, calculations of binding energy (E_b), interaction energy (E_{int}), HOMO-LUMO gap, and charge transfer (Δq) were analyzed on the chosen optimized structures.

3 Results and discussion

3.1 Structural analysis Obtained structural parameters of optimized PPy structure displayed in Fig. 1(a) are in good agreement with prior theoretical studies [8, 39].

HOMO and LUMO molecular orbitals shown in Fig. 1(b) and (c), respectively, are out-of-plane π molecular orbitals, slightly modified at both ends of PPy, gaining a character of σ -symmetry for the case of LUMO orbitals. The molecular orbitals of the two middle PPy rings resemble the most the orbitals of infinite PPy chain. The calculated HOMO-LUMO gap is 3.36 eV, which is in a good agreement with theoretical [8] and experimental [15, 39–41] results. Note that the relaxed morphologies of

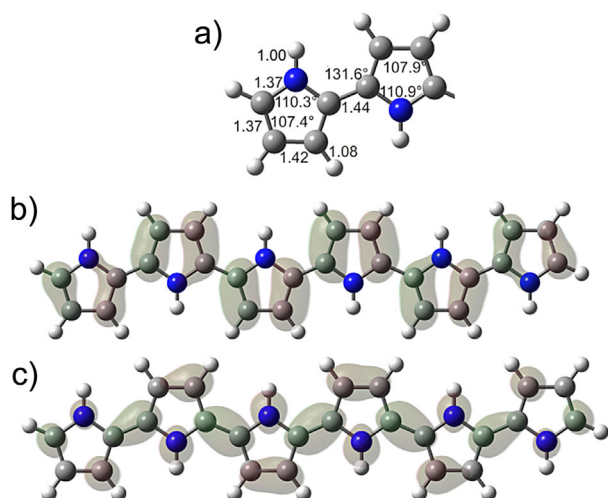


Figure 1 Main structural parameters of two terminal PPy heterocycles (a), HOMO (b), and LUMO (c) molecular orbitals of optimized PPy. Red and green color indicated positive and negative values of the orbital surfaces, respectively, corresponding to the isovalue of $0.01 \text{ e}^- \text{ \AA}^{-3}$. The bond lengths are given in Å.

PPy-C:H structures differ due to the contact formation, as shown further below.

Figures 2(a)–(d) and 3(a)–(d) show the optimized and energetically lowest chemisorbed structures. Here, PPy is connected via C–C bonds and it stands under a tilt angle in the range between 68.6° and 83.9° . The lower angles correspond to the one-bond contacts. The main structural parameters including bond lengths between PPy and diamond slabs for the chemisorbed structures are displayed in Fig. 4. For all the structures, the bond lengths of PPy are

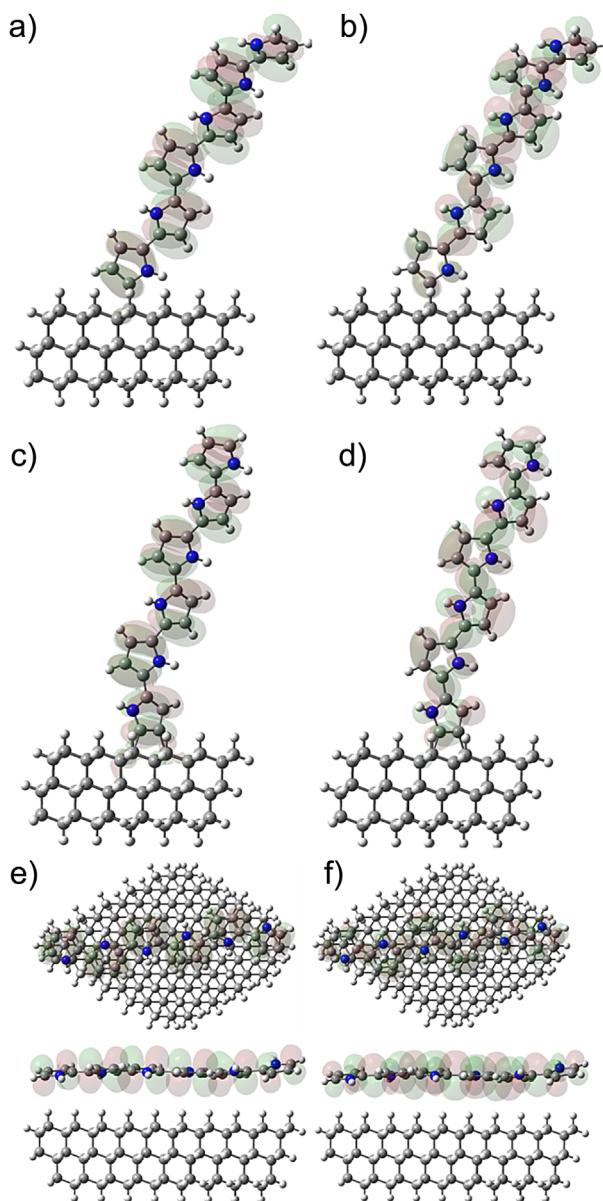


Figure 2 Resulting optimized structures of one-bond contact HOMO (a) and LUMO (b), two-bond contact HOMO (c) and LUMO (d), and physisorption HOMO (e) and LUMO (f) (top and side views) of PPy on 1×1 (111) diamond slab. Red and green color indicated positive and negative values of the orbital surfaces, respectively, corresponding to the isovalue of $0.01 \text{ e}^- \text{ \AA}^{-3}$.

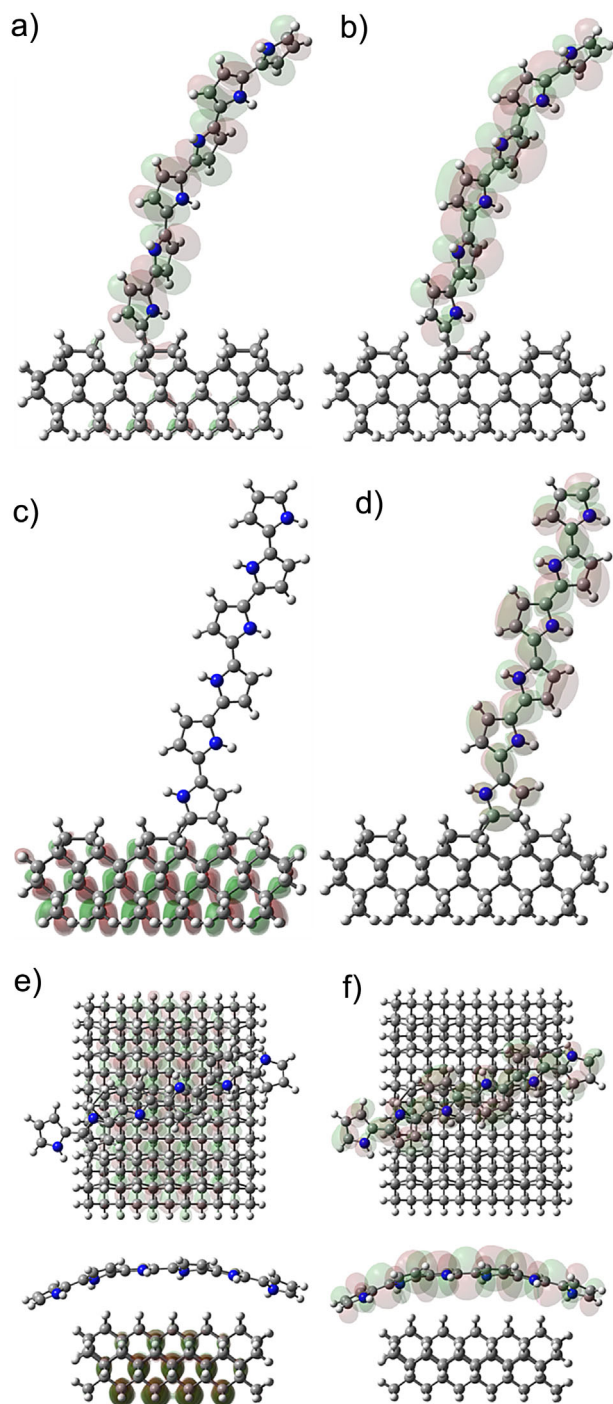


Figure 3 Resulting optimized structures of one-bond contact HOMO (a) and LUMO (b), two-bond contact HOMO (c) and LUMO (d), and physisorption HOMO (e) and LUMO (f) (top and side views) of PPy on 2×1 (100) diamond slab. Red and green color indicated positive and negative values of the orbital surfaces, respectively, corresponding to the isovalue of $0.01 \text{ e}^- \text{ \AA}^{-3}$.

modified up to 0.4 \AA and the angles up to 2.7° . The bond lengths within the diamond slab are less significantly modified, up to 0.12 \AA in the closest area around the contact with PPy.

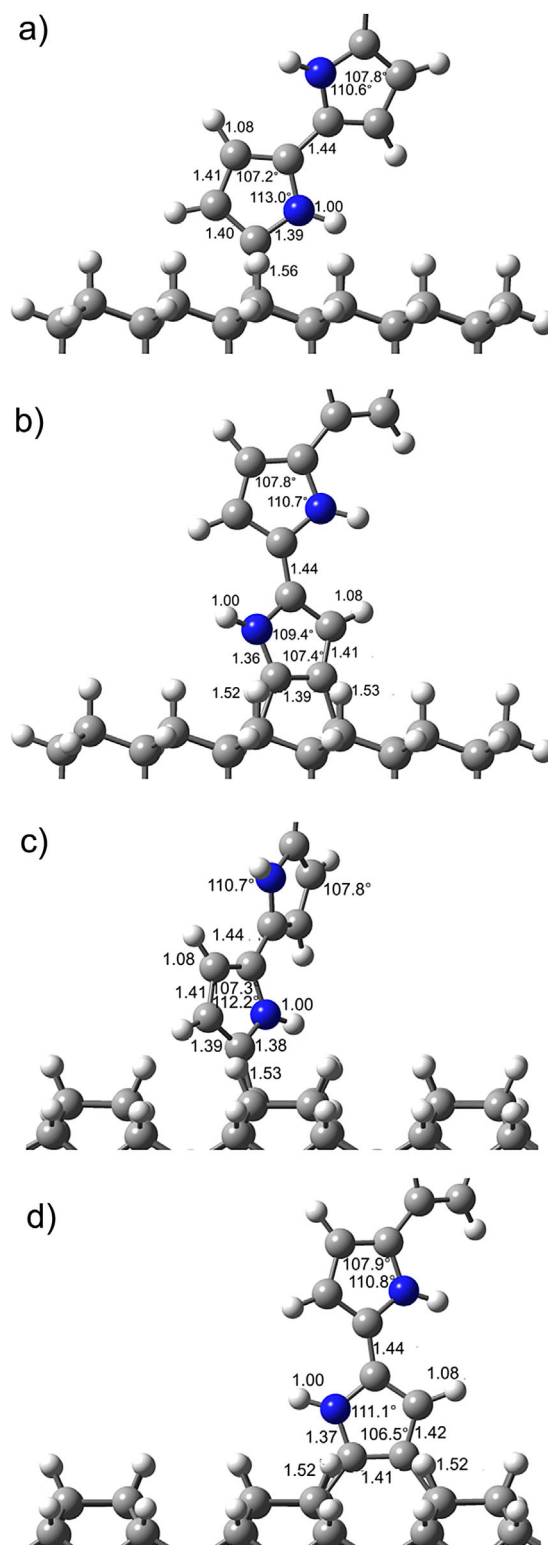


Figure 4 Main structural parameters of one-bond contact (a) and two-bond contact (b) of PPy on 1×1 (111) diamond slab, and one-bond contact (c) and two-bond contact (d) of PPy on 2×1 (100) diamond slab. The bond lengths are given in \AA .

Figures 2(e) and (f) and 3(e) and (f) show the optimized and energetically lowest physisorbed structures. For the (111) facet, the optimizations converged to PPy lying along the surface diagonal, and for the (100) facet to PPy lying above the middle 2×1 reconstructed row.

The geometry of the diamond remains unaffected, as well as the bond lengths and angles within the particular Py rings. However, PPy does not keep its planar character, dihedral angles between the Py rings are twisted up to 10.9° , where the most pronounced changes occurs at the terminating Py rings. The $-NH$ groups within PPy are pointing slightly toward the H atoms of the diamond surface due to their partial charges arising from their polar character. The average distance between PPy and the diamond is 3.1 Å.

3.2 Binding energy Energetic preferences of the interactions were characterized by the binding energies E_b , which are summarized in Table 1. The binding energies were calculated as the difference of total energies of the relaxed structures before and after the contact formation according to the following formula:

$$E_b = (E_{\text{slab}} + E_{\text{PPy}}) - (E_{\text{con}} + n E_{\text{H}_2}), \quad (1)$$

where E correspond to total energies of C:H slab (E_{slab}), PPy molecule (E_{PPy}), PPy-C:H structure (E_{con}), H_2 molecule (E_{H_2}), and $n = 0; 1; 2$ is the number of substituted H atoms on diamond depending on the type of the formed bond. Positive E_b corresponds to an exothermic process, i.e., thermodynamically favorable, whereas negative value correspond to an endothermic process. All the chemisorbed configurations correspond to endothermic processes with the values between -1.11 and -2.23 eV. The one-bond contact is more favorable than the two-bond contact for both types of the facets, especially for the (111) facet, where the two-bond contact requires additional energy of 0.82 eV. The most probable is the one-bond contact of PPy on the (100) facet.

All the physisorbed processes are exothermic by about 0.5 eV.

3.3 Interaction energy Interaction energies E_{int} describing the character of the bonds between PPy and diamond are summarized in Table 1. They were calculated

according to the following formula:

$$E_{\text{int}} = (E_{\text{slab-H}} + E_{\text{PPy-H}}) - E_{\text{con}}, \quad (2)$$

where $E_{\text{slab-H}}$ and $E_{\text{PPy-H}}$ are total energies of C:H slab and PPy calculated with the removed corresponding number of hydrogens from the contact region. All the calculated values for the chemisorbed structures correspond to covalent bonds ($E_{\text{int}} \sim 3.7$ eV for typical C–C bond [42]) between PPy and diamond. The strongest bond $E_{\text{int}} = 5.17$ eV per bond was obtained for the case of two-bond contact on (100). In the case of the physisorbed structures, the obtained values correspond to non-bonding interactions between the PPy and diamond ($E_{\text{int}} \sim 0.4$ eV for a typical non-bonding interaction).

For both of the slabs, the binding energy results in one-bond contacts being more energetically favorable than the two-bond contacts, while the interaction energy indicates that the two bond-contacts are stronger. Less favorable (more negative) binding energy of two bond contacts can be caused by the fact that in the calculation of the interaction energy, there are two dangling bonds on the diamond slabs and two dangling bonds on the PPy chain, which is highly inconvenient and therefore the total energy of the contact formation is more significantly decreased.

3.4 Electronic properties and charge transfer

All the PPy-C:H structures are semiconducting, the original HOMO–LUMO gap of 6.31 and 5.70 eV for (111) and (100) slab, respectively, significantly decreased to values in range 3.42–3.55 and 3.39–3.53 eV, respectively, where the lowest values corresponds to the physisorbed structures. The original HOMO–LUMO gaps are higher in comparison with the gap of the bulk diamond (5.5 eV) due to quantum confinement and larger surface-to-volume ratio, which is in agreement with theoretical calculations in the literature [18, 38] investigating fully passivated H-terminated NDs. In general, decreasing the particle size results in an increased HOMO–LUMO gap values in comparison with the bulk diamond.

Electron affinity, EA, based on Koopmans' theorem is for the case of PPy equal to 0.53 eV, which is in good agreement with other theoretical calculations [43]. EA of (111) and (100) ND slabs without absorbed PPy are negative, -1.81 and -1.70 , respectively, which is in good agreement with other theoretical and experimental results [23]. After the absorption of PPy, the EA rises approximately to 0.58 and 0.50 for diamond (111) and (100), respectively.

In Figs. 2 and 3 are displayed HOMO and LUMO molecular orbital surfaces of the chosen optimized structures. The isosurfaces are visibly modified in the contact region for the chemisorbed (111) structures, where the effect is the most pronounced for the one-bond contact. For the (100) structures, only slight modification occurs in the contact region.

Table 1 Binding energy (E_b), interaction energy (E_{int}), and charge transfer (Δq) for the PPy-C:H interfaces.

PPy-C:H structure	E_b (eV)	E_{int} (eV)	Δq (e^-)
1×1 (111) 1-bond	-1.41	3.73	-0.11
1×1 (111) 2-bond	-2.23	9.1	-0.07
1×1 (111) physisorption	0.43	0.43	-0.06
2×1 (100) 1-bond	-1.11	4.23	-0.04
2×1 (100) 2-bond	-1.60	10.33	-0.08
2×1 (100) physisorption	0.62	0.62	-0.05

For the case of the physisorbed structures and the two-bond contact on (100), the HOMO orbitals are located on the diamond slabs. Spatially separated HOMO and LUMO orbitals were already observed on the H-terminated 2×1 (100) diamond slab interacting upon adsorption of buckminsterfullerene (C_{60}) modeled by DFT [44] as well as confirmed experimentally [45]. The spatial separation of the HOMO and LUMO is convenient for photovoltaic applications. It has a large influence on the separation of the exciton and the consequent movement of charge carriers. Moreover, the chance of recombination process decreases, and thus efficiency of a photovoltaic cell rises. However, relative energy positions of the frontier orbitals, which are shown in Fig. 5, are also important to consider. There are several configurations that could lead to the transfer of holes or electrons between PPy and ND under illumination. In the case of two-bond contact on (100), holes are likely to transfer from PPy to ND and the electrons are blocked. Therefore, this structure is promising not only due to the spatial separation of the frontier orbitals. Other configurations, namely the two-bond contact on (111) and the one-bond contact on (100), where HOMO is also partially localized on ND near the interface with PPy, could work similarly. Opposite direction of charge separation may also be possible. According to the energy levels of the physisorbed PPy on (111), the holes are blocked and the electrons could be transferred from PPy to ND. Yet note that HOMO and LUMO are not spatially separated in this case.

PPy is a neutral molecule, however, when placed to a proximity of the semiconducting nanodiamond, charges are transferred between both of the structures in order to achieve equilibrium. For the evaluation of the number of net

transferred electrons between the PPy and diamond, the charge transfer was calculated as the difference between the amount of donated electrons from ND to PPy and the amount of electrons back donated from PPy to ND based on summing up molecular orbitals redistributed to both of the fragments [46]. Consequently, the charge transfer values Δq , summarized in Table 1, correspond to the number of net transferred electrons from diamond to PPy. The charge transfer values are negative values for all cases which implies that electrons are actually transferred from PPy to diamond after the contact formation. That can be seen on the modification of the HOMO and LUMO molecular orbitals discussed earlier.

The highest charge transfer of $-0.11 e^-$ is obtained for one-bond contact on (111) facet. In contrast, the lowest charge transfer of $-0.04 e^-$ is obtained for one-bond contact on (100) facet. Also, relatively high charge transfer is obtained even for the much weakly bound physisorbed structures, $\Delta q \sim -0.06 e^-$, most likely because the PPy chain lays on the structure and therefore all of its rings contribute to the charge transfer.

H-diamond can have a p-type conductive channel in the subsurface region. However, transfer doping of diamond by holes from PPy (in dark) has not been evidenced so far. Here, we found that interaction of diamond with PPy leads to significant decrease of LUMO level close to the energy of isolated PPy in all cases (see also the new Fig. 5). Furthermore, this LUMO is located almost entirely on PPy part of this hybrid system. Lowering of LUMO thus corresponds to additional positive charge on PPy, in agreement with calculated charge transfer in dark.

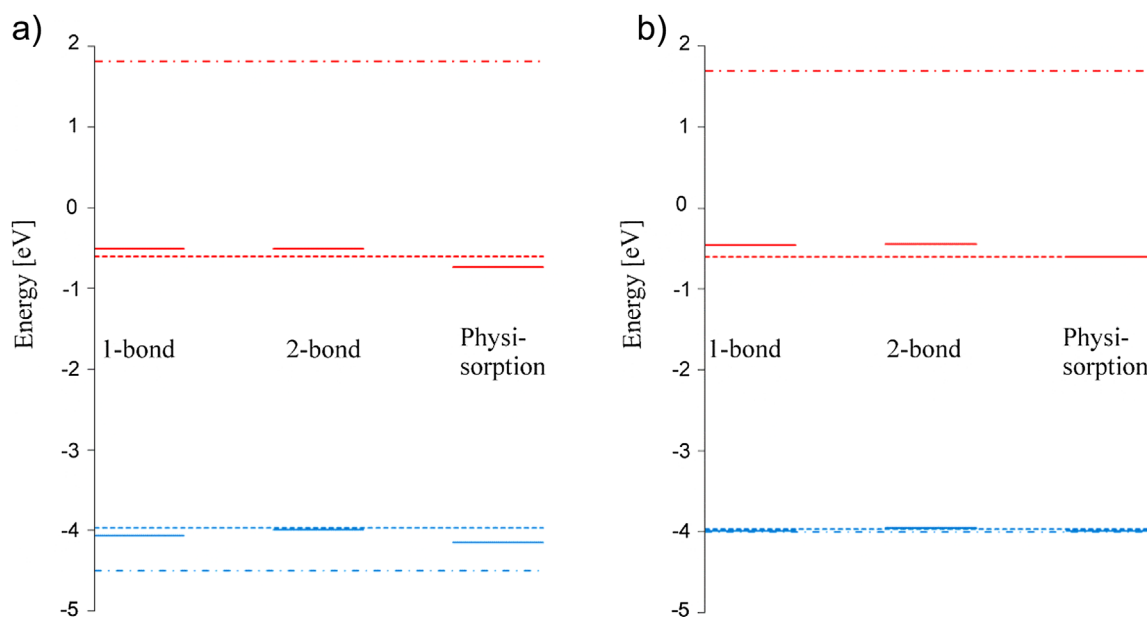


Figure 5 Relative energy positions of HOMO (in blue) and LUMO (in red) of one-bond, two-bond and physisorption of PPy on ND (111) (a) and (100) (b) surface slab. The dotted lines correspond to PPy and the dot-and-dashed lines correspond to nanodiamond with H-terminated (111) (a) and (100) (b) surfaces.

In addition, one should consider that in the case of PPy grafting to diamond, hydrogen atoms are removed and thereby also diamond conductivity in the dark (if present initially) [16]. Only under illumination, measurements of photovoltages and photocurrents indicated that holes are transferred from PPy to diamond and that the interface provides efficient exciton dissociation [15, 16]. This is not in contradiction to the charge transfer we calculated based on summing-up all MOs in the dark, i.e., without illumination. Based on our calculations, LUMO of the combined PPy-diamond system is located on the PPy part. Under illumination, electrons would be thus excited to the PPy part.

4 Conclusions First-principles electronic structure DFT calculations were employed in order to understand the interactions between PPy and ND, a promising organic-semiconductor functional system. Different chemisorbed and physisorbed structures of PPy on 1×1 (111) and 2×1 (100) H-terminated surface slab of ND were geometrically optimized.

According to the binding energy, E_b , all chemisorption processes are endothermic, the least negative value of -1.05 eV (i.e., the most likely binding) is obtained for one-bond contact of PPy on the (100) facet. For both facets, the one-bond contact is more favorable than two-bond contact. In the case of physisorption, the reactions are exothermic (and therefore energetically more favorable processes). Furthermore, all the structures of PPy on (100) facet were energetically more favorable than the corresponding structures on (111) facet.

The interaction energy, E_{int} , indicates the covalent nature of all the chemisorbed structures and non-covalent interaction for the case of physisorbed structures. Formation of the covalent bond is allowed by removal of the terminating hydrogen atoms. This facilitates more pronounced charge transfer, Δq .

We observe the charge transfer from PPy to diamond for all the considered cases. The highest charge transfer is found for PPy chemisorbed on (111) facet via one bond.

For practical applications, it may be important to consider that the chemisorption is more efficient on (100) facets, while the charge transfer is more pronounced on (111) facets.

Acknowledgements We acknowledge the projects GACR 15-01809S and SGS ČVUT SGS16/222/OHK4/3T/13. Computational resources were provided by the CESNET LM2015042 and the CERIT Scientific Cloud LM2015085, provided under the programme “Projects of Large Research, Development, and Innovations Infrastructures.”

References

- [1] M. Kozák, F. Trojánek, and P. Malý, *Phys. Status Solidi A* **211**, 2244 (2014).
- [2] S. Elfimchev, S. Michaelson, R. Akhvediani, M. Chandran, H. Kaslasi, and A. Hoffman, *Phys. Status Solidi A* **211**, 2238 (2014).
- [3] V. Švrček, D. Mariotti, T. Nagai, Y. Shibata, I. Turkevych, and M. Kondo, *J. Phys. Chem. C* **115**, 5084 (2011).
- [4] C.-Y. Liu, Z. C. Holman, and U. R. Kortshagen, *Nano Lett.* **9**, 449 (2009).
- [5] M. Grätzel, *Nature* **414**, 338 (2001).
- [6] G. B. Street, *Handbook of Conducting Polymers* (Marcel Dekker, New York, 1989), pp. 265–291.
- [7] J. Čermák, B. Rezek, P. Hubík, J. J. Mareš, A. Kromka, and A. Fejfar, *Diam. Relat. Mater.* **19**, 174 (2010).
- [8] W. Kamiński, V. Rozsívál, and P. Jelínek, *J. Phys.: Condens. Matter* **22**, 45003 (2010).
- [9] P. Galář, B. Dzurňák, P. Malý, J. Čermák, A. Kromka, M. Omastová, and B. Rezek, *Int. J. Electrochem. Sci.* **8**, 57 (2013).
- [10] B. Rezek, J. Čermák, A. Kromka, M. Ledinský, P. Hubík, J. J. Mareš, A. Purkrt, V. Cimrová, A. Fejfar, and J. Kočka, *Nanoscale Res. Lett.* **6**, 1 (2011).
- [11] Y. L. Zhong, A. Midya, Z. Ng, Z.-K. Chen, M. Daenen, M. Nesladek, and K. P. Loh, *J. Am. Chem. Soc.* **130**, 17218 (2008).
- [12] S. Günes, H. Neugebauer, and N. S. Sariciftci, *Chem. Rev.* **107**, 1324 (2007).
- [13] M. Yun, N. V. Myung, R. P. Vasquez, C. Lee, E. Menke, and R. M. Penner, *Nano Lett.* **4**, 419 (2004).
- [14] N. Brown and O. Hod, *J. Phys. Chem. C* **118**, 5530 (2014).
- [15] B. Rezek, J. Čermák, A. Kromka, M. Ledinský, and J. Kočka, *Diam. Relat. Mater.* **18**, 249 (2009).
- [16] J. Čermák, B. Rezek, A. Kromka, M. Ledinský, and J. Kočka, *Diam. Relat. Mater.* **18**, 1098 (2009).
- [17] E. Ukraintsev, A. Kromka, W. Janssen, K. Haenen, and B. Rezek, *Int. J. Electrochem. Sci.* **8**, 17 (2013).
- [18] A. S. Barnard, *Nanotechnology* **24**, 85703 (2013).
- [19] O. A. Shenderova and G. E. McGuire, *Biointerphases* **10**, 30802 (2015).
- [20] D. Petrini and K. Larsson, *J. Phys. Chem. C* **112**, 3018 (2008).
- [21] D. Petrini and K. Larsson, *J. Phys. Chem. C* **111**, 795 (2007).
- [22] S. Zhao and K. Larsson, *J. Phys. Chem. C* **118**, 1944 (2014).
- [23] A. K. Tiwari, J. P. Goss, P. R. Briddon, N. G. Wright, A. B. Horsfall, R. Jones, H. Pinto, and M. J. Rayson, *Phys. Rev. B* **84**, (2011).
- [24] H.-G. Busmann, S. Lauer, I. V. Hertel, W. Zimmermann-Edling, H.-J. Güntherodt, T. Frauenheim, P. Blaudeck, and D. Porezag, *Surf. Sci.* **295**, 340 (1993).
- [25] R. Klauser, J.-M. Chen, T. J. Chuang, L. M. Chen, M. C. Shih, and J.-C. Lin, *Surf. Sci.* **356**, L410 (1996).
- [26] Z. G. Wang, X. T. Zu, J. L. Nie, and H. Y. Xiao, *Surf. Rev. Lett.* **13**, 45 (2006).
- [27] S. Skokov, B. Weiner, and M. Frenklach, *Phys. Rev. B* **55**, 1895 (1997).
- [28] T. Frauenheim, T. Köhler, M. Sternberg, D. Porezag, and M. R. Pederson, *Thin Solid Films* **272**, 314 (1996).
- [29] J. Y. Raty and G. Galli, *J. Electroanal. Chem.* **584**, 9 (2005).
- [30] H. Tamura, H. Zhou, K. Sugisako, Y. Yokoi, S. Takami, M. Kubo, K. Teraishi, A. Miyamoto, A. Imamura, M. N. Gamo, and T. Ando, *Phys. Rev. B* **61**, 11025 (2000).
- [31] J.-Y. Raty and G. Galli, *Nature Mater.* **2**, 792 (2003).
- [32] R. E. Thomas, R. A. Rudder, and R. J. Markunas, *J. Vac. Sci. Technol. A* **10**, 2451 (1992).
- [33] Y. Yu, C. Z. Gu, L. F. Xu, and S. B. Zhang, *Phys. Rev. B* **70**, (2004).

- [34] M. J. Frisch, G. W. Trucks, H. B. Schlegel, G. E. Scuseria, M. A. Robb, J. R. Cheeseman, G. Scalmani, V. Barone, B. Mennucci, G. A. Petersson, H. Nakatsuji, M. Caricato, X. Li, H. P. Hratchian, A. F. Izmaylov, J. Bloino, G. Zheng, J. L. Sonnenberg, M. Hada, M. Ehara, K. Toyota, R. Fukuda, J. Hasegawa, M. Ishida, T. Nakajima, Y. Honda, O. Kitao, H. Nakai, T. Vreven, J. A. Montgomery, Jr., J. E. Peralta, F. Ogliaro, M. Bearpark, J. J. Heyd, E. Brothers, K. N. Kudin, V. N. Staroverov, R. Kobayashi, J. Normand, K. Raghavachari, A. Rendell, J. C. Burant, S. S. Iyengar, J. Tomasi, M. Cossi, N. Rega, J. M. Millam, M. Klene, J. E. Knox, J. B. Cross, V. Bakken, C. Adamo, J. Jaramillo, R. Gomperts, R. E. Stratmann, O. Yazyev, A. J. Austin, R. Cammi, C. Pomelli, J. W. Ochterski, R. L. Martin, K. Morokuma, V. G. Zakrzewski, G. A. Voth, P. Salvador, J. J. Dannenberg, S. Dapprich, A. D. Daniels, Ö. Farkas, J. B. Foresman, J. V. Ortiz, J. Cioslowski, and D. J. Fox, Gaussian 09, Revision E.01, Wallingford CT: Gaussian, Inc., Gaussian (2009).
- [35] A. D. Becke, *J. Chem. Phys.* **98**, 5648 (1993).
- [36] P. J. Stephens, F. J. Devlin, C. F. Chabalowski, and M. J. Frisch, *J. Phys. Chem.* **98**, 11623 (1994).
- [37] M. J. Rutter and J. Robertson, *Phys. Rev. B* **57**, 9241 (1998).
- [38] T. Yuan and K. Larsson, *J. Phys. Chem. C* **118**, 26061 (2014).
- [39] J. L. Brédas, B. Thémans, J. G. Fripiat, J. M. André, and R. R. Chance, *Phys. Rev. B* **29**, 6761 (1984).
- [40] R. K. John and D. S. Kumar, *J. Appl. Polym. Sci.* **83**, 1856 (2002).
- [41] L. Micaroni, F. Nart, and I. Hümmelgen, *J. Solid State Electrochem.* **7**, 55 (2002).
- [42] J. M. Berg, J. L. Tymoczko, L. Stryer, J. M. Berg, J. L. Tymoczko, and L. Stryer, *Biochemistry*, 5th ed. (W. H. Freeman, New York, 2002).
- [43] H. Kuzmany, M. Mehring, and S. Roth, *Electronic Properties of Polymers and Related Compounds*, in: Proc. International Winter School, Kirchberg, Tirol, February 23–March 1, 1985 (Springer Science & Business Media, Berlin, Heidelberg, 2012).
- [44] S. J. Sque, R. Jones, S. Öberg, and P. R. Briddon, *J. Mater. Sci. Mater. Electron.* **17**, 459 (2006).
- [45] M. Nimmrich, M. Kittelmann, P. Rahe, W. Harneit, A. J. Mayne, G. Dujardin, and A. Kühnle, *Phys. Rev. B* **85**, (2012).
- [46] M. Xiao and L. Tian, *J. Adv. Phys. Chem.* **4**, 111 (2015).

SPATIALLY SEPARATED HOMO/LUMO AT INTERFACE OF POLYPYRROLE PHYSISORBED ON OXIDIZED NANODIAMOND FACETS

MATUNOVÁ Petra^{1,2}, JIRÁSEK Vít¹, REZEK Bohuslav^{1,2}

¹*Institute of Physics, Czech Academy of Sciences, Prague, Czech Republic, EU*

²*Faculty of Electrical Engineering, Czech Technical University, Prague, Czech Republic, EU*

Abstract

Nanodiamond particles (NDs) have recently risen in popularity owing to their unique and perspective properties. Merging NDs with organic molecules, such as polypyrrole (PPy), into hybrid organic-semiconductor functional systems gives rise to potential applications in photovoltaics, which is supported by prior experimentally observed charge transfer between bulk diamond and PPy. This work focuses on the most relevant (111) and (100) O-terminated ND facets with different coverage of surface terminating oxygens in ether, epoxide, ketone, and peroxide positions. We use density functional theory computations employing B3LYP functional and 6-31G(d) basis set. Energetically the most favorable oxidized ND facets were further optimized with PPy in physisorbed configurations. Analysis of geometry, binding energy, HOMO-LUMO gap, and charge transfer was done on the relaxed PPy-ND structures. Multiple hydrogen bonds are formed between PPy amino groups and O atoms on ND surface. PPy on 1×1 reconstructions is energetically favorable with exothermic binding energy (2.7 eV) and high charge transfer (up to $0.26 e^-$) in the dark. The HOMO-LUMO at the PPy-ND interface becomes spatially separated and significantly closer in energy (down to about 1 eV). These features may be beneficial for photovoltaic applications of nanodiamond.

Keywords: diamond, nanoparticles, polypyrrole, density functional theory, charge transfer

1. INTRODUCTION

Recent progress in nanotechnology and the increasing ability to characterize matter at the atomic-scale leads to the discovery of intriguing properties and obtaining novel materials with a vast potential for applications. Nanodiamond particles (NDs) have been a focus of nowadays research owing to their unique semiconducting, chemical, and optical properties, as well as tunable surface structure. The applications cover a large range of fields from biomedicine to optoelectronics including renewable energy. Combining NDs with organic molecules into joint organic-inorganic functional systems may result in novel functional devices. An example of a suitable organic material is polypyrrole (PPy), which is one of the most chemically stable conjugated polymers [1] with controllable conductivity. Its HOMO-LUMO gap is 1.3 - 3.2 eV, depending on the method of preparation [2]. Combining PPy with ND has potential use in photovoltaic (PV) applications based on an experimentally measured charge transfer between the bulk diamond and PPy [2]. We have recently reported a computational study of physisorption and chemisorption of PPy on ND facets passivated by hydrogen, which indicated energetic level alignment promising for PV applications [3]. Oxidized nanodiamonds represent an interesting complementary system as the surface dipole of the terminating C-O bonds of diamond is opposite with respect to the dipole of the C-H bonds and relatively stronger.

The most representative surface facets on NDs are (111) and (100) facets [4], [5]. Thermodynamic stability and surface reconstruction of O-terminated NDs under varying conditions and surface coverage of (111) and (100) facets were studied both theoretically [5]–[8] and experimentally [9]. On the 1×1 (111) ND surface facet, oxygen in the on-top (i.e. ketone) position with peroxide bridges is the most favorable [8]. On the 2×1 (111) facet, oxygen adsorption in on-top and bridge positions were pointed out as the only plausible positions

[5]. The bridge configuration occurs preferably at 50% or lower oxygen coverage [4], [8]; 100% O coverage leads to dimerization [5]. On the 1×1 (100) facet, the bridge position is preferred at high surface coverage [4]. Alternatively, etherized 1×1 (100) structures with a bridging ether may be convenient [7]. For oxygen surface coverage up to 50% on (100), the 2×1 reconstruction is preferred over the 1×1 reconstruction [4] and epoxy structure is more favorable than the bridge structure [6]. The bridge position is stable at high surface coverage [6], [8].

In this study, we investigate a physisorption of PPy on the most stable, fully oxygen passivated 1×1 and 2×1 reconstructed (111) and (100) ND surface facets.

2. COMPUTATIONAL METHODS

The first-principles density functional theory (DFT) method implemented in Gaussian 09 electronic structure software [10] was used for the optimization of all of the structures employing B3LYP functional with the 6-31G(d) basis set. We used (111) and (100) ND surface slabs consisting of 3 C layers of 6×6 pattern and surface terminating layer of O atoms. The slabs represented a corner of ND, hence always three “outer” surfaces of ND were functionalized with oxygens and the remaining three “inner” surfaces representing inner cut planes were saturated with hydrogen atoms, which were fixed during the optimizations. More details on the computational setup are provided in our prior work [3].

Based on the literature and our preliminary calculations, we choose the most probable 1×1 and 2×1 surface reconstructions of both (111) and (100) surface with fully passivated oxygens in ether, epoxide, ketone, and peroxide positions. For both reconstructions of both surface slabs, the oxygen structure with the lowest relative total energy after optimization was chosen for further simulations with absorbed PPy. For the 1×1 (111) surface slab was chosen 100% termination with peroxides, for the 2×1 (111) 50% of epoxides, for the 1×1 (100) 50% with ethers and for the 2×1 (100) 50% with epoxides. Note that in the case of ethers and epoxides, the 50% surface coverage generates fully passivated forms.

To study the contact formation, different non-equivalent positions of physisorbed PPy (represented by six Py units) on the relaxed slabs were optimized. Chemisorbed PPy was not calculated due to the high activation barrier for oxygen to be replaced with PPy. The top C layer with the terminating O atoms and PPy were allowed to relax during these further optimizations. For each of the four ND slabs, several initial PPy-ND configurations were tried. The structure with the lowest relative energy with respect to the optimized 1×1 (111) or 2×1 (100) O-terminated ND slabs was then taken for analysis of geometry, binding energy (E_b), HOMO-LUMO gap, and charge transfer (Δq).

3. RESULTS AND DISCUSSION

Figures 1 and 2 show the relaxed structures of PPy on ND slabs. The geometry of ND remained almost unchanged. The originally planar character of PPy modifies into an out-of-plane structure as a result of electrostatic interactions between PPy and ND. Multiple H-bonds are created between amino groups of PPy and surface O atoms of ND.

The binding energies E_b , related to the energetic preferences of the interactions are summarized in Table 1. The binding energies were calculated as the difference of total energies of the relaxed structures before and after the contact formation according to the formula:

$$E_b = (E_{slab} + E_{PPy}) - E_{con}, \quad (1)$$

where E corresponds to total energies of C:H slab (E_{slab}), PPy molecule (E_{PPy}), and PPy-C:H structure (E_{con}). Positive E_b corresponds to an exothermic process, i.e. thermodynamically favorable, whereas negative value corresponds to an endothermic process.

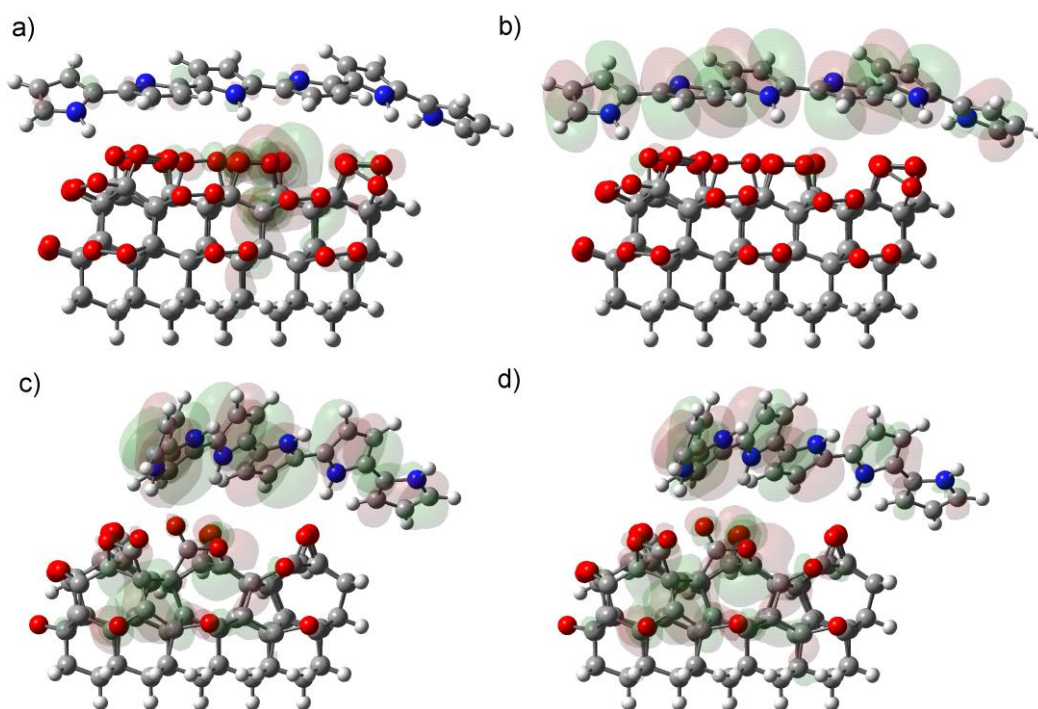


Figure 1 PPy physisorbed on peroxide-terminated 1×1 (111) ND slab, side view of HOMO (a) and LUMO (b). PPy physisorbed on epoxide-terminated 2×1 (111) ND slab, side view of HOMO (c) and LUMO (d). C atoms are in gray, H atoms are in white, O atoms are in red, and N atoms are in blue.

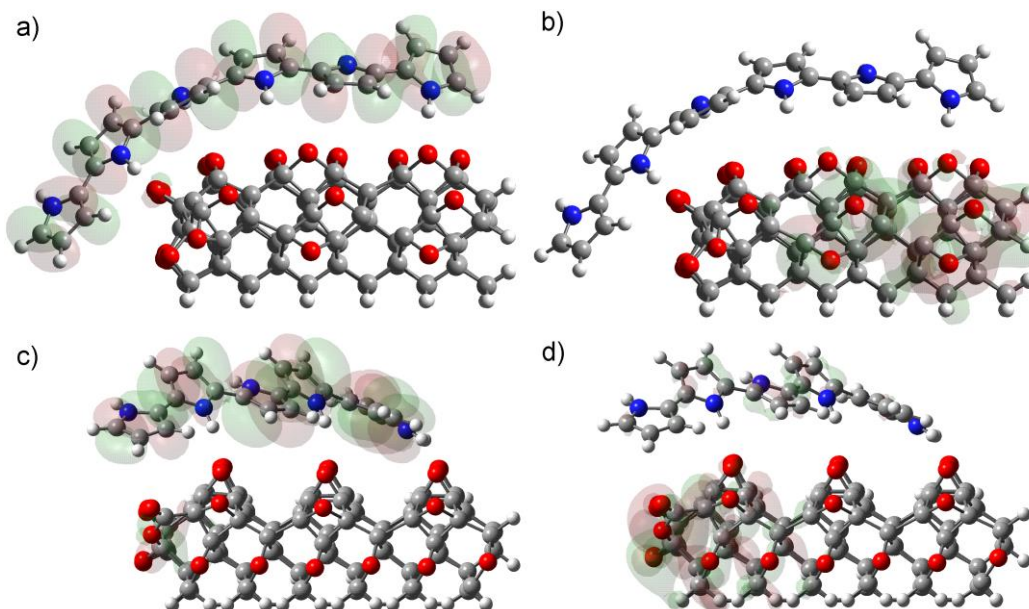


Figure 2 PPy physisorbed on ether-terminated 1×1 (100) ND slab, side view of HOMO (a) and LUMO (b). PPy physisorbed on epoxide-terminated 2×1 (100) ND slab, side view of HOMO (c) and LUMO (d). C atoms are in gray, H atoms are in white, O atoms are in red, and N atoms are in blue.

Formation of all of the calculated structures is exothermic, the highest binding energy of around 2.7 eV is obtained for the case of PPy on 1×1 reconstructed facets. The values for the 1×1 reconstructed facets are 1.68 – 1.84 eV higher than the values obtained for the 2×1 reconstructed facets.

Table 1 Binding energy (E_b), charge transfer (Δq), HOMO-LUMO gap, HOMO and LUMO values.

Structure	E_b [eV]	Δq [e^-]	HOMO-LUMO gap [eV]	HOMO [eV]	LUMO [eV]
1 × 1 (111)	-	-	3.32	-6.35	-3.03
2 × 1 (111)	-	-	3.09	-4.41	-1.32
1 × 1 (100)	-	-	3.29	-5.22	-1.93
2 × 1 (100)	-	-	2.50	-5.42	-2.92
PPy - 1 × 1 (111)	2.76	0.26	1.09	-4.39	-3.30
PPy - 2 × 1 (111)	1.08	0.12	0.40	-3.52	-3.12
PPy - 1 × 1 (100)	2.71	0.19	1.71	-3.53	-1.83
PPy - 2 × 1 (100)	0.87	0.08	0.35	-3.22	-2.87

The calculated HOMO-LUMO gap of PPy is 3.36 eV, agreeing well with theoretical [11] and experimental [2] values. Band gap of bulk diamond is 5.48 eV. The calculated HOMO-LUMO gaps of the O-terminated NDs are in the range of 3.09 – 3.32 eV except for the HOMO-LUMO gap of 2.50 eV for the 2 × 1 (100) slab. Similar results of HOMO-LUMO gaps, equal to 2.76 and 3.72 eV, were obtained for fully passivated O-terminated diamond nanocrystals (with small enough size below 2 nm) by DFT [12]. Band gap in the range of 2.0 and 2.6 eV was also obtained for the O-terminated (100) bulk diamond surface by DFT [13]. After the physisorption of PPy, the HOMO-LUMO gaps significantly decreased by 1.6 – 2.7 eV. Upon the PPy adsorption, the HOMO energy of the ND is increased in the PPy-ND complex in all cases. The LUMO energy decreases in the case of PPy on (111) but increases in the case of PPy on (100) facets.

There is also a considerable spatial separation of HOMO and LUMO at the PPy-ND interface in all cases except the 2 × 1 (111) ND where it is only moderate. HOMO is located mostly on PPy and LUMO is located mostly on ND for all the cases except for PPy on the 1 × 1 (111) ND slab, for which the separation is opposite. Generally, the HOMO and LUMO are found in areas with a significant interaction between PPy and ND, where the most pronounced modification with respect to the separate components happens. This is mostly in the ND corner enclosed by oxygens. Thus the nanoparticle form of diamond may be important for such strong interaction.

The spatial separation of HOMO and LUMO is convenient for photovoltaic applications. It was calculated by DFT for the case of H-terminated NDs interacting with PPy [3] or diamond with adsorbed buckminsterfullerene (C₆₀) [14], for which it was also observed experimentally [15]. Under illumination, the HOMO-LUMO spatial separation can promote dissociation of excitons and thereby lead to a generation of free charge carriers. Moreover, it increases the efficiency of a photovoltaic cell by decreasing the probability of recombination processes.

Charge transfer was calculated as the difference between the number of donated electrons from ND to PPy, and the number of electrons back donated from PPy to ND based on summing up molecular orbitals redistributed to both of the fragments [16]. The positive values of charge transfer, shown in Table 1, thus correspond to the net transfer of electrons from ND to PPy. After the absorption, the formerly electrically neutral PPy and the intrinsic O-terminated ND thus become oppositely charged. This may again facilitate the exciton dissociation under illumination. The highest charge transfer of 0.26 e^- is observed for PPy on the 1 × 1 (111) structure. The values of the charge transfer are consistent with the binding energy. The higher the binding energy, the greater is the charge transfer. Generally, the values of charge transfer were relatively high comparing with the values obtained for physisorption of PPy on the H-terminated NDs without any H-bonds [3]. The calculated charge transfer mirrors the changes in the frontier molecular orbitals.

4. CONCLUSION

We showed in our calculations that even without chemisorption there is a considerably strong interaction between PPy and O-NDs in terms of PPy structural changes, high exothermic binding energy, high charge transfer and pronounced changes of HOMO-LUMO energy levels at the PPy-ND interface. Formation of hydrogen bonds plays probably an important role in these phenomena. The results also showed that the complex of PPy with O-terminated ND might be suitable for photovoltaic applications since spatially separated HOMO-LUMO orbitals may promote separation of photogenerated charge carriers.

ACKNOWLEDGEMENTS

We acknowledge the projects GACR 15-01809S and SGS ČVUT SGS16/222/OHK4/3T/13.

Computational resources were provided by the CESNET LM2015042 and the CERIT Scientific Cloud LM2015085, provided under the programme "Projects of Large Research, Development, and Innovations Infrastructures."

REFERENCES

- [1] STREET, G. B. Handbook of Conducting Polymers. New York: Marcel Dekker, 1989. 265–291 pp.
- [2] REZEK, B., ČERMÁK, J., KROMKA, A., LEDINSKÝ, M., KOČKA, J. Photovoltage effects in polypyrrole–diamond nanosystem. *Diamond and Related Materials*, 2009, vol. 18, no. 2–3, pp. 249–252.
- [3] MATUNOVÁ, P., JIRÁSEK, V., REZEK, B. Computational study of physisorption and chemisorption of polypyrrole on H-terminated (111) and (100) nanodiamond facets. *Physica Status Solidi A*, 2016, vol. 213, no. 10, pp 2672–2679
- [4] SHENDEROVA O. A., MCGUIRE, G. E. Science and engineering of nanodiamond particle surfaces for biological applications (Review). *Biointerphases*, 2015, vol. 10, no. 3, pp. 30802.
- [5] PETRINI, D., LARSSON, K. Theoretical Study of the Thermodynamic and Kinetic Aspects of Terminated (111) Diamond Surfaces. *Journal of Physical Chemistry C*, 2008, vol. 112, no. 8, pp. 3018–3026.
- [6] PETRINI D., LARSSON, K. A theoretical study of the energetic stability and geometry of hydrogen-and oxygen-terminated diamond (100) surfaces. *The Journal of Physical Chemistry C*, 2007, vol. 111, no. 2, pp. 795–801.
- [7] TAMURA, H., ZHOU, H., SUGISAKO, K., YOKOI, Y., TAKAMI, S., KUBO, M., TERAISHI, K., MIYAMOTO, A., IMAMURA, A., MIKKA, N., IMAMURA, A., N.-GAMO, M., ANDO, T. Periodic density-functional study on oxidation of diamond (100) surfaces. *Physical Review B*, 2000, vol. 61, no. 16, pp. 11025.
- [8] ZHENG X. M., SMITH, P. V. The stable configurations for oxygen chemisorption on the diamond (100) and (111) surfaces. *Surface Science*, 1992, vol. 262, no. 1–2, pp. 219–234.
- [9] PEHRSSON, P. E., MERCER, T. W., CHANEY, J. A. Thermal oxidation of the hydrogenated diamond (1 0 0) surface. *Surface Science*, 2002, vol. 497, no. 1–3, pp. 13–28.
- [10] FRISCH, M. J. et al., Gaussian 09, Revision E.01, Wallingford CT: Gaussian, Inc., Gaussian, 2009.
- [11] KAMIŃSKI, W., ROZSÍVAL, V., JELÍNEK, P. Theoretical study of electronic and transport properties of PPy–Pt(111) and PPy–C(111):H interfaces. *Journal of Physics: Condensed Matter*, 2010, vol. 22, no. 4, pp. 45003.
- [12] BROWN, N., HOD, O. Controlling the Electronic Properties of Nanodiamonds via Surface Chemical Functionalization: A DFT Study. *The Journal of Physical Chemistry C*, 2014, vol. 118, no. 10, pp. 5530–5537.
- [13] LONG, R., DAI, Y., GUO, M. Characterization of diamond (100) surface with oxygen termination. *Applied Surface Science*, 2008, vol. 254, no. 9, pp. 2851–2855.
- [14] SQUE, S. J., JONES, R., ÖBERG, S., BRIDDON, P. R. Transfer doping of diamond: Buckminsterfullerene on hydrogenated, hydroxylated, and oxygenated diamond surfaces. *Journal of Materials Science: Materials in Electronics*, 2006, vol. 17, no. 6, pp. 459–465.
- [15] NIMMIRICH, M., KITTELMANN, M., RAHE, P., HARNEIT, W., MAYNE, A. J., DUJARDIN, G., KÜHNLE, A. Influence of charge transfer doping on the morphologies of C 60 islands on hydrogenated diamond C(100)-(2 × 1). *Physical Review B*, 2012, vol. 85, no. 3, pp. 035420.
- [16] XIAO M., TIAN, L. Generalized Charge Decomposition Analysis (GCDA) Method. *Journal of Advances in Physical Chemistry*, 2015, vol. 4, no. 4, pp. 111–124.

Structural and Electronic Properties of Oxidized and Amorphous Nanodiamond Surfaces with Covalently Grafted Polypyrrole

Petra Matunová,* Vít Jirásek, and Bohuslav Rezek

Diamond nanoparticles denoted as nanodiamonds (NDs) possess numerous beneficial material properties and are envisioned for a wide range of applications. In this work, complexes of polypyrrole (PPy) organic dye covalently grafted to ND surfaces are investigated by atomic scale density functional theory (DFT) computations with a view to their structural and electronic properties. NDs terminated with oxygen, hydroxyl, carboxyl, anhydride, as well as amorphous carbon (a-C:H, a-C:O) have been considered. Thereby the theoretical model is brought close to real nanodiamonds. Spatially separated highest occupied molecular orbitals (HOMO) and lowest unoccupied molecular orbitals (LUMO) and a favorable energetic level alignment at the ND–PPy interface are observed for the majority of the oxidized NDs. This feature is also retained for NDs with amorphous surface layer. Excited states are computed by time-dependent DFT to analyze how the electronic configuration can promote dissociation of excitons, for instance in photovoltaic applications.

For this purpose, we investigate diamond nanoparticles mostly denoted as nanodiamonds (NDs) in combination with a suitable organic material, polypyrrole (PPy). Diamond nanoparticles represent a novel type of carbon nanomaterial with a range of unique properties including non-toxicity, semiconducting properties, visible light absorption, and their carbon-based surface chemistry is rich and highly adjustable for achieving desired properties and functions.^[5]

Detonation NDs (DNDs) are commercially available with sizes less than 4 nm in diameter.^[6] Resulting from the production process, DNDs contain an amorphous layer of carbon on their surfaces. The most frequent functional groups found on surfaces of NDs are hydrogens, oxygens, hydroxyls, carboxyls, and anhydrides.^[7,8]

The bonds between oxygen and carbon or hydrogen are polarized, and consequently, a surface dipole layer is established. Moreover, NDs can be sensitized by organic dyes. Properties and functions of nanodiamonds can be modified by complexes with organic molecules. For instance, encapsulation of individual NDs with phenol-ionic complexes leads to enhanced photoluminescence from the ND defects.^[9] Our prior studies with polypyrrole (PPy) organic dye showed experimentally that composites of hydrogenated and oxidized detonation nanodiamonds (DNDs) with PPy were successfully fabricated and evince promising properties for photovoltaic applications.^[10] Suitability of PPy for photovoltaic applications was also supported by an observed transfer of photogenerated charge between the bulk diamond and PPy observed by Kelvin force microscopy and optical spectroscopy.^[11,12]

The most typical ND facets, present both on the synthetic and natural diamonds, are (111) and (100) facets.^[13,14] The preference for the different surface functional group and the extent of its coverage on a particular surface reconstruction of a ND facet was studied by both computational^[14–17] and experimental^[18–21] methods. Due to the steric reasons, carboxyl and anhydride surface functional groups saturate 50% and about 30% of the dangling bonds of the surface carbon atoms, respectively.


This work builds upon prior theoretical works investigating electronic and energetic characteristics of the most simplified PPy-ND system where all surface dangling bonds, and internal

1. Introduction

Organic photovoltaics is a recently rapidly developing field^[1] with many advantages such as lower requirements on the light conditions, simplified manufacturing process and increased flexibility regarding its installation and usage. However, certain disadvantages such as relatively low efficiency and stability are still present. Organic–inorganic hybrid solar cells have thus gained a lot of attention.^[2–4] The systems consist of conjugated polymers and inorganic semiconductor nanocrystals and could serve as an efficient light harvesting and charge transporting materials.

P. Matunová, Prof. B. Rezek
Faculty of Electrical Engineering
Czech Technical University
Technická 2, Prague 6, 166 27, Czech Republic
E-mail: matunova@fzu.cz

P. Matunová, Dr. V. Jirásek, Prof. B. Rezek
Institute of Physics
Czech Academy of Sciences
Cukrovarnická 10, Prague 6, 162 00, Czech Republic

 The ORCID identification number(s) for the author(s) of this article can be found under <https://doi.org/10.1002/pssb.201900176>.

DOI: 10.1002/pssb.201900176

surfaces of ND were passivated merely by hydrogen^[22,23] and system of PPy merely physisorbed on oxidized NDs.^[24] Here, we concentrate on the system of PPy chemisorbed (covalently bonded) on oxidized NDs. The obtained results are considerably different to merely hydrogenated nanodiamonds. We also include amorphous carbon on ND surface to resemble the real DNDs closely. We show that even with amorphous carbon the PPy-ND system retains its qualities. The results thus complement the recent experimental work on the PPy-DND composites,^[10] corroborating their potential as an opto-electronically active medium in solar cells.

2. Computational Details

For geometry optimization of all the structures, we employed the first-principles density functional theory (DFT) method implemented in Gaussian 09 electronic structure software^[25] and B3LYP functional^[26,27] and 6-31G(d) basis set, where the inclusion of the polarization functions turned out to be particularly important. Due to the computational unfeasibility of the theory to model the whole ND particle with the typical sizes from 1.4 nm,^[28] we used (111), (100), and amorphous carbon surface slabs consisting of three double layers of 6×6 carbon atoms. Two additional H-terminated model sizes with the double and triple size of the original ND slab consisted of 459C atoms (7353 basis functions, i.e., about 2 nm), and 694C atoms (11026 basis functions, i.e., about 3 nm), respectively were computed. Although the gaps between highest occupied molecular orbital (HOMO) and lowest unoccupied molecular orbital (LUMO) of such systems were close to the experimental bandgap of ND, the computational resources were enormous, and it was not possible to perform, e.g., the frequency analysis. Thus, the original model size (about 1 nm ND) was retained as a compromise between computational feasibility and possible quantum confinement effects. Nevertheless, the results show that the various surface terminations studied in our work have actually very different effects while possible quantum confinement effect would be about the same for the same model size.

Various terminating surface functional groups were used. These include oxygens in different positions (peroxides, epoxides, ethers, ketones), hydroxyls, carboxyls, and anhydrides. We choose energetically the most probable functional group for 1×1 and 2×1 surface reconstructions of both the (111) and (100) ND slabs based on published theoretical^[14,15,29–34] and experimental^[18,19,21,35–37] works and our preliminary calculations. The amorphous carbon layer was saturated by hydrogens (a-C:H) or by a mixture of hydrogens and oxygens (a-C:O), resembling the polyfunctional detonation NDs used in practical experiments. The slabs represent a corner of ND, hence always three “outer” surfaces of ND were terminated with oxygen surface groups, and the remaining three “inner” surfaces representing inner cut planes were saturated with hydrogen atoms, which were fixed during the optimizations. More details on the computational setup are provided in our prior work.^[23]

To study the contact formation, different non-equivalent positions of one-bond and two-bond covalent contacts of PPy (represented by six Py units) on the relaxed ND slabs were optimized. During this optimization, the outermost C atoms,

and terminating O and H atoms were allowed to relax, while the rest of the particle was kept fixed. On the PPy-ND structures with different bond type and the lowest relative energy with respect to the optimized ND slab without PPy were then performed analyses of geometry parameters, HOMO and LUMO molecular orbitals, binding energies (E_b), interaction energies (E_{int}), and charge transfer (Δq).

PPy does not spontaneously chemisorb on the clean H-terminated diamond surface.^[17] Therefore, the one- and two-bond chemisorbed contacts were allowed by removal of one and two H atoms, respectively, both, from the slab and PPy. In the case of the O-containing groups, the energy barrier for their replacement with PPy is relatively high, and it would avert the chemisorption of PPy. However, the structures could exist if we consider chemisorption of PPy on at least partially H-terminated ND. Such typical polyfunctional detonation nanodiamonds arise from a usual manufacturing and purification process,^[5] where H atoms are likely to be substituted with PPy oxygen groups, and further, the oxidized surfaces arise from competitive oxidation during the PPy synthesis process or from oxidation in the surrounding air. Note that due to steric reasons we did not optimize PPy on hydroxyl-terminated 2×1 (100) ND slab, carboxyl-terminated 1×1 (100), and anhydride-terminated 1×1 (100).

For selected representative structures, excited state properties were calculated using the time-dependent DFT (TDDFT), allowing to describe the electronic excitations in nanosystems.^[38] Long-range corrected hybrid density functional ω B97X-D^[39] with the 6-31G(d) basis set was used for the optimization of the structures. Using this type of functional, the delocalization error is reduced,^[40] and the long-range correction brings the transition energies close to the experimental results.^[41]

3. Results and Discussion

3.1. Structural Properties

Different nonequivalent positions of one-bond contact and two-bond contact of PPy on ND with varying surface termination were optimized, and the lowest energy systems were further analyzed. Selected representative structures are presented in **Figure 1**. All computed structures are shown in Figure S1–S9, Supporting Information. Geometrical parameters of the structures are summarized in Table S1–S5, Supporting Information. On the relaxed structures, the surfaces of the NDs remain almost unchanged. The only observed modification is as a reorganization of the surface functional groups near the PPy-ND bond. For instance, the OH groups of the hydroxylated NDs in close proximity to the PPy chain are often rotated in order to include the amino group of PPy into the system of hydrogen bonds established over the whole ND surface.

Standalone PPy is a planar structure, however, after its chemisorption on ND, it is slightly tilted with respect to the ND surface, and individual Py heterocycles rotate relative to each other to accommodate the electrostatic interactions with ND.

Consistently with the hydrogenated NDs^[23] the C-C bond lengths between PPy and ND are mostly shorter for the two-bond contacts than for the one-bond contacts. This is owing to the less

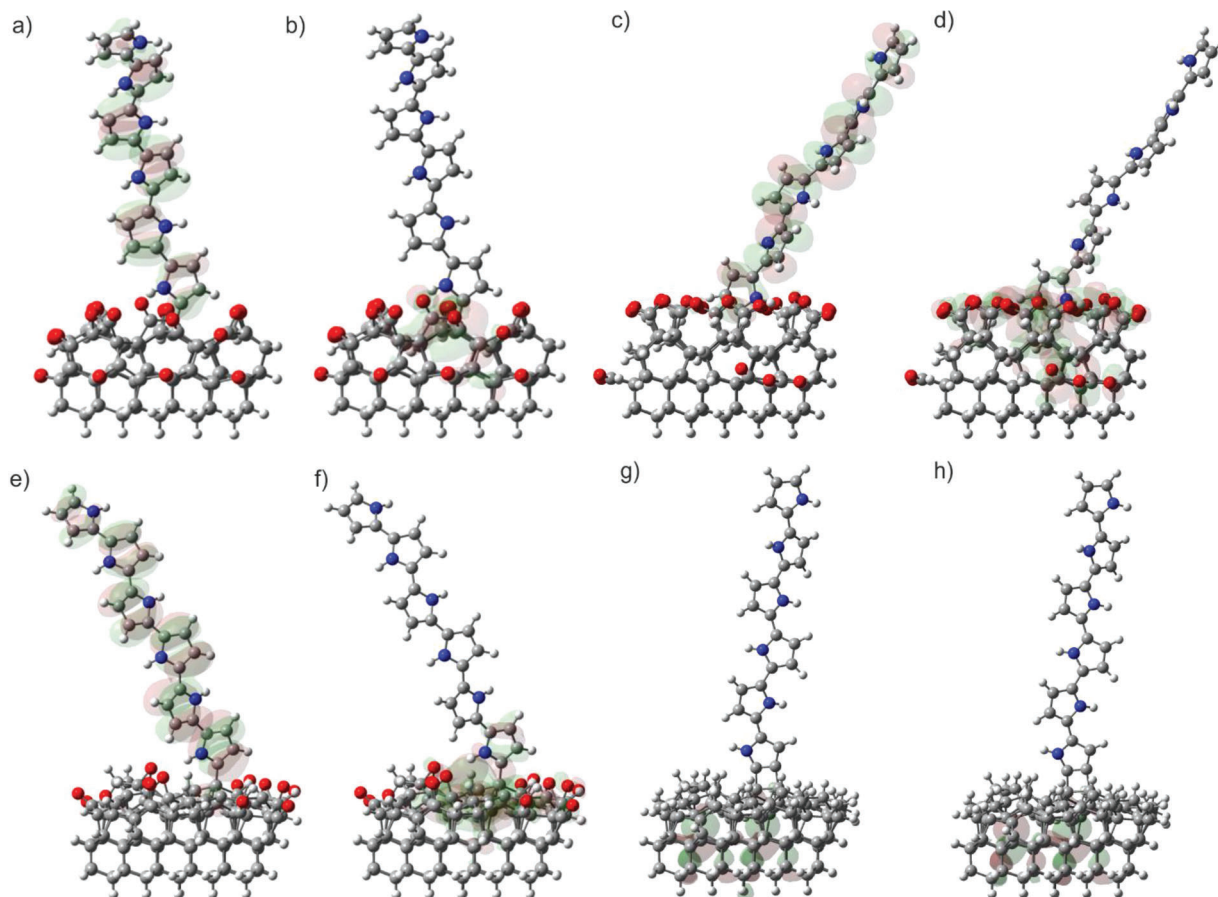


Figure 1. Optimized structures of one-bond contact of PPy on epoxide-terminated 2×1 (111) – HOMO (a) and LUMO (b); one-bond contact of PPy on anhydride-terminated 2×1 (111) – HOMO (c) and LUMO (d); one-bond contact of PPy on a-C:O – HOMO (e) and LUMO (f); two-bond contact of PPy on a-C:H – HOMO (g) and LUMO (h). C atoms are in gray, H atoms are in white, O atoms are in red, and N atoms are in blue. Red and green colors indicate positive and negative values of the orbital surfaces, respectively, corresponding to the isovalue of $0.01 \text{ e}^{-\text{Å}^{-3}}$.

steric repulsion from the removal of the two surface functional groups instead of one for the former case, especially for the carboxylated and hydroxylated NDs. In extreme case, for one-bond contacts on the hydroxylated (111) surface, the originally set covalent bonds diminish since the optimized lengths of the bonds are up to 1.96 Å. For the oxidized surfaces and in contrast to the hydrogenated surfaces, the one-bond contacts are more likely to establish the directional hydrogen bonds with the ND surface thanks to their higher flexibility to rotate around the C-C bond between PPy and ND. The described structural trends are valid for both the reconstructed and amorphous nanodiamond surfaces.

3.2. HOMO LUMO Distribution and Energies

The positions of the frontier molecular orbitals, HOMO and LUMO, are also displayed in Figure 1 and Figure S1–S9, Supporting Information. We observe that for most of the oxidized PPy-ND, HOMO and LUMO are spatially separated. HOMO is located on the whole PPy oligomer and LUMO on the surface of ND. The spatial separation of the frontier molecular

orbitals is a desirable effect for the solar cell applications, contributing to more efficient separation of excitons and their consequent movement toward electrodes while avoiding recombination processes at the same time. However, the separation is not observed in the PPy-ND composites with hydrogenated and hydroxylated NDs. Instead, both frontier orbitals are located on PPy (see Figure S4, Supporting Information).

The calculated HOMO–LUMO gap of the standalone PPy oligomer is 3.36 eV, which agrees well with prior experimental^[11,42–44] and theoretical^[22] studies.

The obtained values of the HOMO–LUMO energy gaps of NDs without PPy (2.50–4.77 eV for the reconstructed NDs, and about 0.6 eV for the amorphous NDs) are highly variable, mostly with regard to the different surface functional groups. For most of the O-terminated NDs, the obtained band gap of about 3.1 eV is in a good agreement with other DFT studies.^[32,33,45] The values of the band gaps of the separate NDs are in agreement also for the H- and COOH-terminations, however, there is a lack of studies concerning the anhydride surface termination. Generally, the band gaps from DFT studies are somewhat lower compared to the band gap of bulk diamond, 5.48 eV.^[46] This feature must be related with the surface termination since

size-dependent studies on very small nanodiamonds with the same theory predict increasing energy band gap (above the bulk diamond value) with decreasing cluster size.^[47] These quantum confinement effects are present for ND with sizes up to 2 nm.^[48] Also, the dependence of the HOMO-LUMO gap on the ND size was computationally observed.^[49] Our preliminary calculations with the larger models of 2 and 3 nm H-terminated NDs yielded the HOMO-LUMO gap values of 5.45 and 5.83 eV, respectively, which is in a good agreement with the experimental value of bulk diamond. Due to the quantum confinement effects and the related higher surface to volume ratio, the HOMO-LUMO gaps could differ quantitatively, but the trends related to surface termination will remain.

After the chemisorption of PPy, the PPy-ND gap is in the range from 0.33 to 3.52 eV. The lower values in comparison with the separate NDs are primarily due to the upshift of HOMO energies. Generally, the variability of the gap is increased suggesting the tunability of the PPy-ND composites. HOMO-LUMO energy gaps of all the composites are summarized in Table S6–S10, Supporting Information.

Figure S10–S14, Supporting Information visualize the HOMO and LUMO energy levels of the PPy-ND structures along with standalone PPy and corresponding NDs. A typical arrangement of HOMO and LUMO of the standalone NDs and PPy with increasing energy is following: HOMO of ND, HOMO of PPy, LUMO of ND, and LUMO of PPy. This energy arrangement leads to the transfer of photo-generated electrons from PPy to ND and the other way around for holes. The HOMO-LUMO alignment of the PPy-ND composites is dependent on the particular surface reconstruction, the type of the functional groups, and the type of the interaction between PPy and ND. In this sense, the PPy-ND composites exhibit the possibility of high tunability. Often, a convenient arrangement for the photo-generated charge dissociation and transport is obtained.

Figure 2 displays a representative result of relative energy positions of HOMO and LUMO for the case of the COOH- and anhydride-terminated 1×1 (111) ND. The order of the frontier molecular orbitals suggests several options for the transfer of the charge carriers between PPy and ND. For the 1-bond contact on COOH-terminated ND, the energy levels are favorable. After

exciton generation at the interface, electrons are likely to go to ND, and at the same time, they are blocked to go to PPy. Holes are likely to transfer to PPy and are blocked to transfer to ND. The same is valid for the 1-bond contact on the anhydride-terminated ND. To provide a better insight into the observed phenomena, sections with detailed energetic analysis and quantification of the redistribution of charges follow.

3.3. Binding and Interaction Energies

Binding energies, E_b , related to the energy preferences of the interactions, were calculated as the difference in total energies of the ground state structures before and after the chemisorption of PPy. Equation (1) is a general formula including all the computed ND slabs in this work

$$E_b = [E_{\text{slab}} + E_{\text{PPy}}] - [E_{\text{con}} + (n - 2 \cdot l) \cdot E_{\text{H}_2} + m \cdot E_{\text{O}_2} + l \cdot E_{\text{C}_2\text{H}_4}] \quad (1)$$

where E corresponds to total energies of C:H slab (E_{slab}), PPy molecule (E_{PPy}), PPy-C:H structure (E_{con}), molecules desorbed after the substitution (E_{H_2} , E_{O_2} , $E_{\text{C}_2\text{H}_4}$), n is the number of substituted pairs of H atoms, m is the number of substituted pairs of O atoms, and l is the number of substituted C atoms, depending on the type of the formed bond. Positive E_b corresponds to an exothermic process, i.e., thermodynamically favorable, whereas negative value corresponds to an endothermic process. Equation (1) allows to calculate the interaction energies, E_{int} , which are related to the strength of the bonds between PPy and ND

$$E_{\text{int}} = (E_{\text{slab-X}} + E_{\text{PPy-H}}) - E_{\text{con}} \quad (2)$$

where $E_{\text{slab-X}}$ and $E_{\text{PPy-H}}$ are total energies of ND slab and PPy calculated with the removed corresponding atoms from the contact region.

The binding energies are displayed in Figure 3 along the horizontal axis. Values of the binding, as well as interaction energies, are summarized in Table S6–S10, Supporting

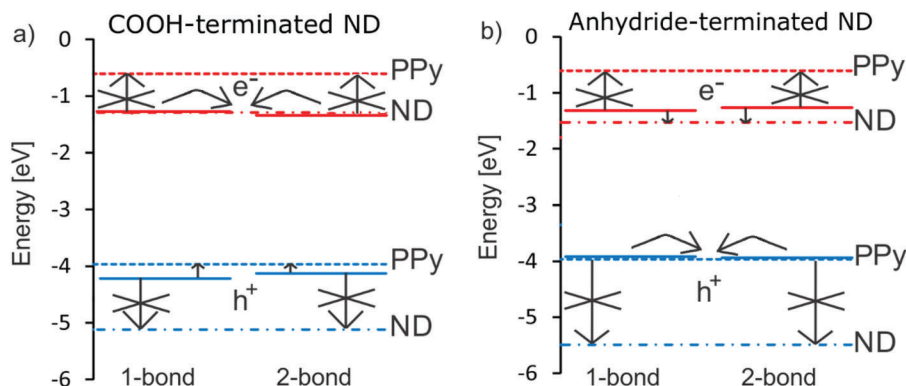


Figure 2. Relative energy positions of HOMO (in blue) and LUMO (in red) of PPy (dashed lines), 1×1 (111) ND slabs (dot-dashed lines), and PPy chemisorbed (1-bond, 2-bond) on carboxylated (a) and anhydride-terminated (b) surfaces. The arrows indicate possible and blocked transport of electrons and holes in LUMO and HOMO, respectively.

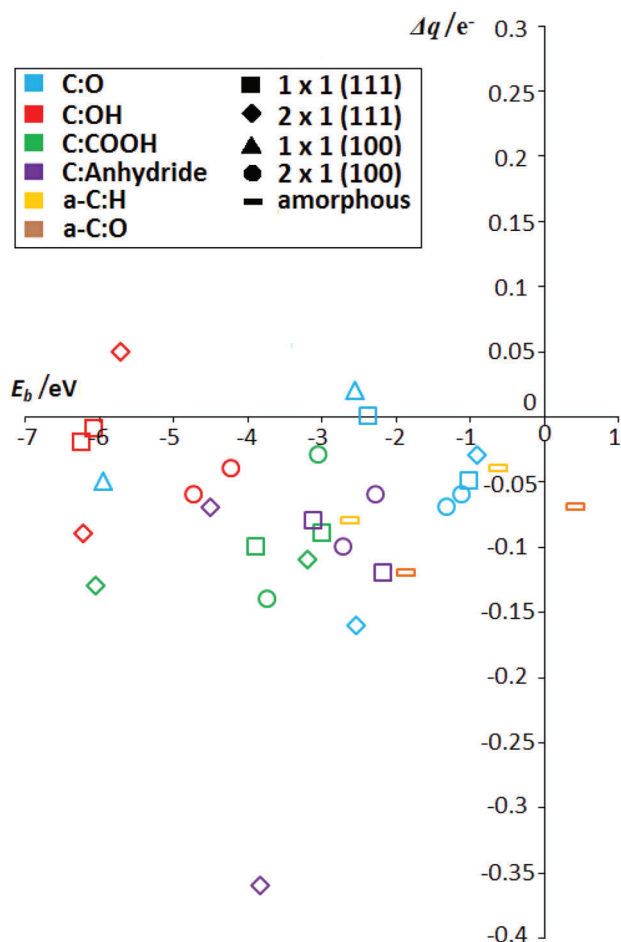


Figure 3. Charge transfer (Δq) versus binding energy (E_b) for the PPY-ND structures. Surface chemistry is coded by color; surface reconstruction is coded by symbol shape (see the legend in the inset).

Information. All the binding energies are negative, i.e., endothermic reactions requiring a supply of energy in order to create the bonding contacts. An exception is the one-bond contact of PPy on a-C:O, where $E_b = 0.30$ eV. This is in agreement with a very short bond length between ND and PPy of 1.50 Å obtained for this composite. Therefore, not considering a possible energetic barrier of the interaction, PPy could spontaneously covalently bound the oxidized amorphous NDs.

According to the binding energies, the least likely is the PPy chemisorption on the hydroxylated NDs with the most positive value of $E_b = -4.22$ eV. This assertion is supported by the longest bond lengths obtained in this case and by low interaction energies indicating the diminishing covalent character of the one-bond contacts here.

The binding energies suggest that PPy is more likely to bind via one covalent bond on hydrogenated, hydroxylated, and carboxylated NDs, in contrast with peroxide, epoxide, and ether-terminated NDs, where two covalent bonds are preferred. That is a consequence of the fact that the former functional groups each saturate one valence of a surface carbon of ND, while the latter saturate two and no dangling bond remains in this case. In addition, for the latter case, the dominance of the two-bond

contacts is confirmed by high interaction energies indicating strong covalent bonds. The only exception is the epoxide-terminated 2×1 (111) structure, which also represents the highest value of all the composited of non-amorphous NDs, $E_b = -0.90$ eV. In this case, the unfavorable two-bond contact may be caused by too high steric repulsions resulting in a nonplanar character of the formed bonds.

The binding energies also indicate more favorable interactions for the amorphous a-C:O in comparison with the a-C:H structures due to the more pronounced electrostatics interactions for the a-C:O structures.

High interaction energies (up to 4.94 eV per bond for two-bond contact on anhydride-terminated 2×1 (100) ND, see Table S10, Supporting Information) are obtained for most of the composites. They correspond to relatively strong covalent bonds as the typical value for a C–C bond is $E_{\text{int}} \approx 3.7$ eV.^[50] The interaction energies thus confirm a highly covalent bond, among others, in the case of the one-bond contact on a-C:O, $E_{\text{int}} = 4.34$ eV. It should be emphasized that in all cases the bonds between PPy and ND are via the C surface atoms. The observed differences between various surface termination types are thus arising solely due to the different surface chemical groups in the PPy-ND contact neighborhood.

3.4. Charge Transfer

To evaluate the charge redistribution after the contact formation in formerly electroneutral complexes we evaluated the charge transfer, Δq . It was calculated as the difference between the number of donated electrons from ND to PPy and the number of electrons donated from PPy to ND based on summing up molecular orbitals redistributed to both components under equilibrium conditions.^[51] Analysis of the total density was performed in order to obtain coefficients and occupation numbers for natural bond orbitals. Consequently, positive Δq correspond to the net number of electrons transferred from ND to PPy and vice versa for negative Δq .

Charge transfer values are mostly negative. They are summarized in Table S6–S10, Supporting Information and displayed in Figure 3 along the Y-axis. The highest absolute value of charge transfer, $\Delta q = 0.36 e^-$, corresponding to the transfer of electrons from PPy to ND is obtained for the one-bond contact of PPy on the 2×1 (111) anhydride-terminated ND. Consistently with the energetic preferences, for the hydroxylated NDs were calculated the lowest values of $\Delta q \approx 0.09 e^-$. Generally, the PPy composites with the hydroxylated NDs show the least promising features. That is in agreement with the literature, where the limitation of the hydroxylated NDs in relation to an adsorbate molecule was reported.^[45]

Overall, significant values of charge transfer are obtained for most of the structures, including the nanodiamonds with an amorphous surface layer, which are included in Table S10, Supporting Information. The charge transfer values for the a-C:H structures are consistent with the values obtained for the reconstructed hydrogenated NDs.^[23] Moreover, higher charge transfer is obtained for the a-C:O structures than for the a-C:H structures. This is the same trend as for the reconstructed diamond surfaces.

3.5. Excited States

For three representative structures, two-bond contact of PPy on epoxide-terminated 2×1 (100), one-bond contact of PPy on hydroxyl-terminated 2×1 (100), and one-bond contact of PPy on carboxyl-terminated 2×1 (100) ND, the excited state analysis is included. **Figure 4** shows the electron density difference between the excited state and the ground state. It is placed on PPy for all the composites, pointing out the local excitation type of the transition.

Based on the oscillator strengths, the electron excitation from the ground to the first excited state is the most likely for the structures with hydroxyls and carboxyls. For the epoxide-terminated composite, the highest transition probability is for the third excited state. Therefore, it is visualized in **Figure 4** instead of the first excited state.

For the epoxide-terminated composite, the most contributing pairs of molecular orbitals to the transition are: HOMO \rightarrow LUMO + 8, and with about three times lower coefficient HOMO $-1 \rightarrow$ LUMO + 12. For the hydroxylated case, the orbitals are: HOMO \rightarrow LUMO and with about three times lower coefficient HOMO $-1 \rightarrow$ LUMO + 1. For the structure with anhydrides, the orbitals are: HOMO \rightarrow LUMO + 2 and with about three times lower coefficient HOMO $-2 \rightarrow$ LUMO + 6. In agreement with the position of the charge density difference, the localization of all the mentioned orbitals is on the PPy part, as visualized in **Figure S15**, Supporting Information. That is consistent with the dipole moments which are mostly aligned to the PPy axis, with the total value of 43.0 D, 25.3 D, and 24.1 D for the epoxide, OH, and anhydride-terminated ND, respectively. Excitation energies are equal to 3.9, 3.9, and 3.6 eV for the epoxide, OH, and COOH-terminated ND, respectively. Thus, the most pronounced transitions are in the near UV region.

The first excited state of the structure with epoxides occurs with much smaller oscillator strength. However, it corresponds to smaller excitation energy possibly applicable for longer wave

lengths (497.5 nm) in the VIS region of the spectrum. Moreover, the first excitation of the structure with epoxides is always from an orbital below HOMO to LUMO. According to Kasha's rule, the fluorescence is from the lowest excited state. Therefore, vibrational relaxation of the excited electron from the third excited state (LUMO + 8 and LUMO + 12) on PPy to the first excited state (LUMO) on ND is expected before the recombination. This process could be slowed down owing to the different localization of the discussed orbitals.

4. Conclusion

Chemisorbed interactions between PPy molecule and ND with different surface terminations, surface reconstructions as well as amorphous surface layer were investigated by employing atomic scale DFT simulations. Based on the analysis of the binding energies, the most favorable NDs for the chemisorption of PPy are the reconstructed peroxide, epoxide, and ether-terminated as well as amorphous oxidized and hydrogenated NDs. Also, relatively high values of charge transfer and variable energy band gap of various chemisorbed PPy-ND structures were observed. Spatial separation of HOMO and LUMO arises for most of the structures. This includes the structures with amorphous carbon surface layer that are the closest approximation to the real detonation nanodiamonds. Under illumination, the HOMO-LUMO spatial separation may promote dissociation of excitons. However, analysis of excited states showed that direct HOMO-LUMO transition has smaller oscillator strength in that case than higher excited states that are localized on PPy molecule. Nevertheless, the energetic levels alignment favors the transfer of electrons from excited LUMO states in PPy to ground state LUMO in nanodiamond. In addition, excitation to lower states is still possible with correspondingly lower excitation energy (albeit with lower oscillator strength). This may lead to optical absorption in a broader spectral range. Therefore, the organic-inorganic composite of PPy covalently adsorbed to

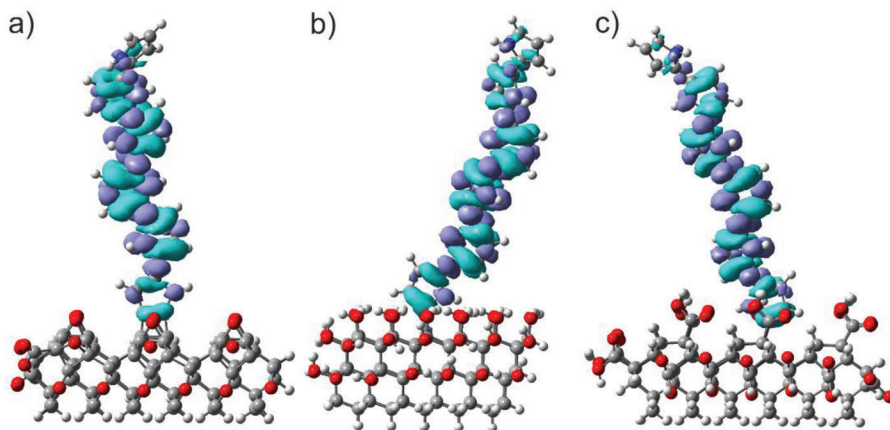


Figure 4. Charge density difference between the third excited and ground state for two-bond contact of PPy on epoxide-terminated 2×1 (100) ND (a) and charge density difference between the first excited and ground state for one-bond contact of PPy on hydroxyl-terminated 2×1 (100) ND (b) and one-bond contact of PPy on carboxyl-terminated 2×1 (100) ND (c). C atoms are in gray, H atoms are in white, O atoms are in red, and N atoms are in blue. Blue and purple represent the decrease and increase, respectively, of the electron density after the excitation. The density corresponds to the isovalue of $0.4 \times 10^{-3} \text{ e}^{-} \text{ \AA}^{-3}$.

oxygen-terminated diamond nanoparticles provide promising features for photovoltaic applications.

Supporting Information

Supporting Information is available from the Wiley Online Library or from the author.

Acknowledgments

The authors would like to thank Dr. Diego López Carballeira for fruitful discussions. The authors acknowledge financial support from the Czech Science Foundation project GACR 15-01809S, CVUT student project SGS18/179/OHK4/3T/13, European Regional Development Fund project CZ.02.1.01/0.0/0.0/15_003/0000464, and COST Action MP1307 Stable-NextSol. Computational resources were provided by the CESNET LM2015042 and the CERIT Scientific Cloud LM2015085 under the program "Projects of Large Research, Development, and Innovations Infrastructures."

Conflict of Interest

The authors declare no conflict of interest.

Keywords

density functional theory, nanodiamonds, photovoltaics, polypyrrole

Received: March 26, 2019

Revised: May 16, 2019

Published online:

- [1] Y. Masuda, G. Giorgi, K. Yamashita, *Phys. Status Solidi B* **2014**, *251*, 1471.
- [2] A. Jaros, S. Bley, K. Zimmermann, L. Krieg, A. Castro-Carranza, J. Gutowski, F. Meierhofer, T. Voss, *Phys. Status Solidi B* **2019**, *256*, 1800463.
- [3] L. Kavan, J.-H. Yum, M. Graetzel, *Phys. Status Solidi B* **2013**, *250*, 2643.
- [4] M. Braik, C. Dridi, A. Rybak, J. Davenas, D. Cornu, *Phys. Status Solidi A* **2014**, *211*, 670.
- [5] O. A. Shenderova, G. E. McGuire, *Biointerphases* **2015**, *10*, 030802.
- [6] S. L. Y. Chang, A. S. Barnard, C. Dwyer, C. B. Boothroyd, R. K. Hocking, E. Ōsawa, R. J. Nicholls, *Nanoscale* **2016**, *8*, 10548.
- [7] Z. Shpilman, I. Gouzman, E. Grossman, L. Shen, T. K. Minton, J. T. Paci, G. C. Schatz, R. Akhvediani, A. Hoffman, *J. Phys. Chem. C* **2010**, *114*, 18996.
- [8] A. Krueger, *Adv. Mater.* **2008**, *20*, 2445.
- [9] K. Bray, R. Previdi, B. C. Gibson, O. Shimoni, I. Aharonovich, *Nanoscale* **2015**, *7*, 4869.
- [10] D. Miliáieva, S. Stehlik, P. Stenclova, B. Rezek, *Phys. Status Solidi A* **2016**, *213*, 2687.
- [11] B. Rezek, J. Čermák, A. Kromka, M. Ledinský, J. Kočka, *Diam. Relat. Mater.* **2009**, *18*, 249.
- [12] J. Čermák, B. Rezek, A. Kromka, M. Ledinský, J. Kočka, *Diam. Relat. Mater.* **2009**, *18*, 1098.
- [13] A. S. Barnard, *Nanotechnology* **2013**, *24*, 085703.
- [14] D. Petrini, K. Larsson, *J. Phys. Chem. C* **2008**, *112*, 3018.
- [15] D. Petrini, K. Larsson, *J. Phys. Chem. C* **2007**, *111*, 795.
- [16] H. Tamura, H. Zhou, K. Sugisako, Y. Yokoi, S. Takami, M. Kubo, K. Teraishi, A. Miyamoto, A. Imamura, N. Mikka, T. Ando, *Phys. Rev. B* **2000**, *61*, 11025.
- [17] X. M. Zheng, P. V. Smith, *Surf. Sci.* **1992**, *262*, 219.
- [18] P. E. Pehrsson, T. W. Mercer, J. A. Chaney, *Surf. Sci.* **2002**, *497*, 13.
- [19] P. John, N. Polwart, C. E. Troupe, J. I. B. Wilson, *Diam. Relat. Mater.* **2002**, *11*, 861.
- [20] K. P. Loh, X. N. Xie, Y. H. Lim, E. J. Teo, J. C. Zheng, T. Ando, *Surf. Sci.* **2002**, *505*, 93.
- [21] X. Wang, A. R. Ruslinda, Y. Ishiyama, Y. Ishii, H. Kawarada, *Diam. Relat. Mater.* **2011**, *20*, 1319.
- [22] W. Kamiński, V. Rozsival, P. Jelínek, *J. Phys.: Condens. Matter* **2010**, *22*, 045003.
- [23] P. Matunová, V. Jirásek, B. Rezek, *Phys. Status Solidi A* **2016**, *213*, 2672.
- [24] P. Matunová, V. Jirásek, B. Rezek, in *NANOCON 2016, Conference Proceedings: 8th International Conference on Nanomaterials – Research & Application*, October 2016, Brno, Czech Republic, Tanger Ltd., Ostrava **2017**, pp. 15–19.
- [25] M. J. Frisch, G. W. Trucks, H. B. Schlegel, G. E. Scuseria, M. A. Robb, J. R. Cheeseman, G. Scalmani, V. Barone, G. A. Petersson, H. Nakatsuji, X. Li, M. Caricato, A. V. Marenich, J. Bloino, B. G. Janesko, R. Gomperts, B. Mennucci, H. P. Hratchian, J. V. Ortiz, A. F. Izmaylov, J. L. Sonnenberg, D. Williams-Young, F. Ding, F. Lipparini, F. Egidi, J. Goings, B. Peng, A. Petrone, T. Henderson, D. Ranasinghe, V. G. Zakrzewski, J. Gao, N. Rega, G. Zheng, W. Liang, M. Hada, M. Ehara, K. Toyota, R. Fukuda, J. Hasegawa, M. Ishida, T. Nakajima, Y. Honda, O. Kitao, H. Nakai, T. Vreven, K. Throssell, J. A. Montgomery, Jr. J. E. Peralta, F. Ogliaro, M. J. Bearpark, J. J. Heyd, E. N. Brothers, K. N. Kudin, V. N. Staroverov, T. A. Keith, R. Kobayashi, J. Normand, K. Raghavachari, A. P. Rendell, J. C. Burant, S. S. Iyengar, J. Tomasi, M. Cossi, J. M. Millam, M. Klene, C. Adamo, R. Cammi, J. W. Ochterski, R. L. Martin, K. Morokuma, O. Farkas, J. B. Foresman, D. J. Fox, *Gaussian 09 (Revision E.01)*, Gaussian Inc., Wallingford, CT **2016**.
- [26] A. D. Becke, *J. Chem. Phys.* **1993**, *98*, 5648.
- [27] P. J. Stephens, F. J. Devlin, C. F. Chabalowski, M. J. Frisch, *J. Phys. Chem.* **1994**, *98*, 11623.
- [28] S. Stehlik, M. Varga, M. Ledinsky, D. Miliáieva, H. Kozak, V. Skakalova, C. Mangler, T. J. Pennycook, J. C. Meyer, A. Kromka, B. Rezek, *Sci. Rep.* **2016**, *6*, 38419.
- [29] A. K. Tiwari, J. P. Goss, P. R. Briddon, N. G. Wright, A. B. Horsfall, R. Jones, H. Pinto, M. J. Rayson, *Phys. Rev. B* **2011**, *84*, 245305.
- [30] L. Lai, A. S. Barnard, *J. Mater. Chem.* **2012**, *22*, 16774.
- [31] S. Goverapet Srinivasan, A. C. T. van Duin, *Carbon* **2015**, *82*, 314.
- [32] T. E. Derry, N. W. Makau, C. Stampfl, *J. Phys.: Condens. Matter* **2010**, *22*, 265007.
- [33] N. Brown, O. Hod, *J. Phys. Chem. C* **2014**, *118*, 5530.
- [34] V. Jirásek, H. Kozak, Z. Remeš, *Adv. Sci. Eng. Med.* **2015**, *7*, 275.
- [35] F. Maier, J. Ristein, L. Ley, *Phys. Rev. B* **2001**, *64*, 165411.
- [36] K. Bobrov, H. Shechter, A. Hoffman, M. Folman, *Appl. Surf. Sci.* **2002**, *196*, 173.
- [37] F. K. de Theije, N. J. van der Laag, M. Plomp, W. J. P. van Enckevort, *Philos. Mag. A* **2000**, *80*, 725.
- [38] R. J. Magyar, S. Tretiak, *J. Chem. Theory Comput.* **2007**, *3*, 976.
- [39] J.-D. Chai, M. Head-Gordon, *Phys. Chem. Chem. Phys.* **2008**, *10*, 6615.
- [40] L. Pandey, C. Doiron, J. S. Sears, J.-L. Brédas, *Phys. Chem. Chem. Phys.* **2012**, *14*, 14243.
- [41] I. T. Lima, A. da S. Prado, J. B. L. Martins, P. H. de Oliveira Neto, A. M. Ceschin, W. F. da Cunha, D. A. da Silva Filho, *J. Phys. Chem. A* **2016**, *120*, 4944.
- [42] R. K. John, D. S. Kumar, *J. Appl. Polym. Sci.* **2002**, *83*, 1856.

- [43] J. L. Brédas, B. Thémans, J. G. Fripiat, J. M. André, R. R. Chance, *Phys. Rev. B* **1984**, 29, 6761.
- [44] L. Micaroni, F. Nart, I. Hümmelgen, *J. Solid State Electrochem.* **2002**, 7, 55.
- [45] S. J. Sque, R. Jones, P. R. Briddon, *Phys. Rev. B* **2006**, 73, 085313.
- [46] D. Bimberg, *Physics of Group IV Elements and III-V Compounds*. Springer, Berlin **1982**.
- [47] A. A. Fokin, P. R. Schreiner, *Mol. Phys.* **2009**, 107, 823.
- [48] T. Yuan, K. Larsson, *J. Phys. Chem. C* **2014**, 118, 26061.
- [49] A. S. Barnard, *Cryst. Growth Des.* **2009**, 9, 4860.
- [50] J. M. Berg, J. L. Tymoczko, L. Stryer, J. M. Berg, J. L. Tymoczko, L. Stryer, *Biochemistry*. W. H. Freeman, New York **2002**.
- [51] S. Dapprich, G. Frenking, *J. Phys. Chem.* **1995**, 99, 9352.

Supporting Information

Structural and Electronic Properties of Oxidized and Amorphous Nanodiamond Surfaces with Covalently Grafted Polypyrrole*Petra Matunová*, Vít Jirásek, and Bohuslav Rezek*

Figure S1. Optimized structures of **PPy on O-terminated 1 × 1 (111) ND edge slab**: one-bond contact HOMO (a) and LUMO (b), two-bond contact HOMO (c) and LUMO (d). Optimized structures of **PPy on O-terminated 2 × 1 (111) ND edge slab**: one-bond contact HOMO (e) and LUMO (f), two-bond contact HOMO (g) and LUMO (h). C atoms are grey, H atoms white, O atoms red, N atoms blue. Red and green clouds indicate positive and negative value of the orbital surfaces at the isovalue of $0.01e^{-\text{Å}^{-3}}$.

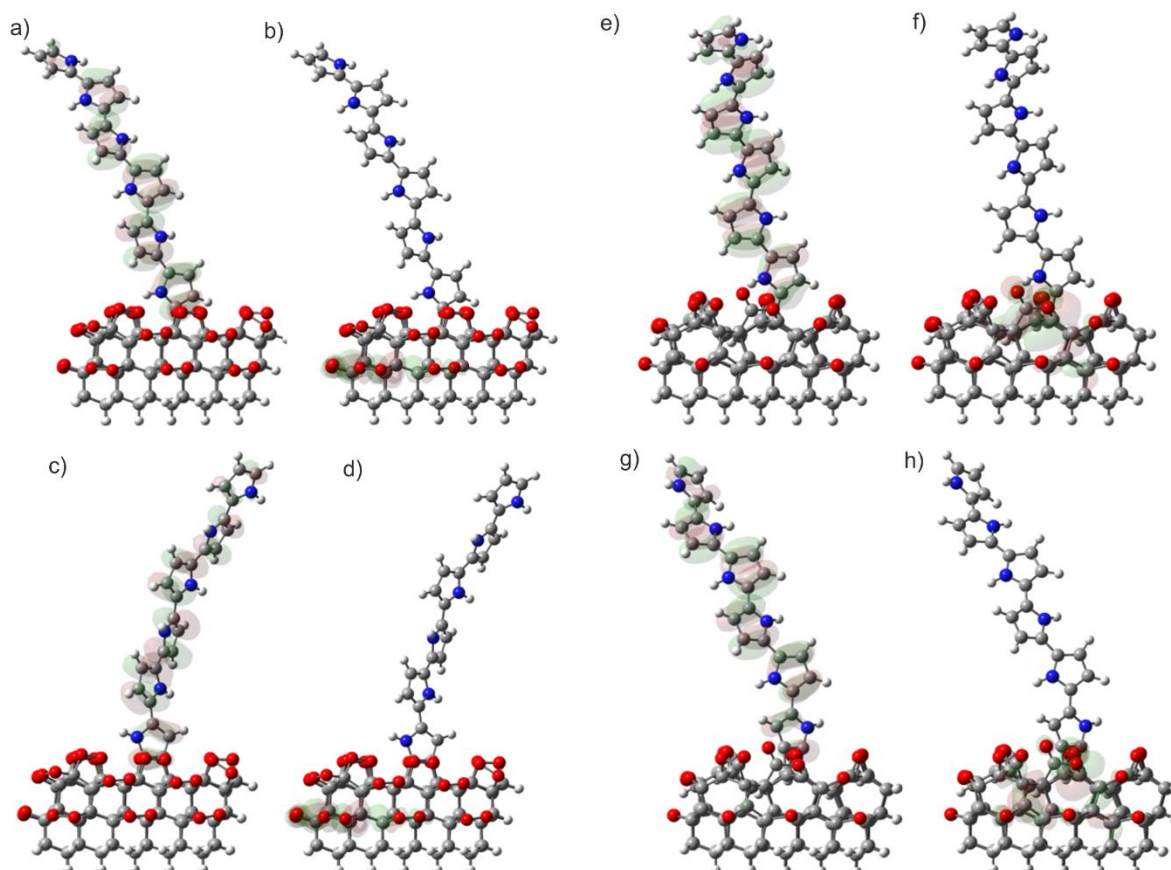


Figure S2. Optimized structures of **PPy on O-terminated 1×1 (100) ND edge slab**: one-bond contact HOMO (a) and LUMO (b), two-bond contact HOMO (c) and LUMO (d). Optimized structures of **PPy on O-terminated 2×1 (100) ND edge slab**: one-bond contact HOMO (e) and LUMO (f), two-bond contact HOMO (g) and LUMO (h). C atoms are grey, H atoms white, O atoms red, N atoms blue. Red and green clouds indicate positive and negative value of the orbital surfaces at the isovalue of $0.01e^{-\text{\AA}^{-3}}$.

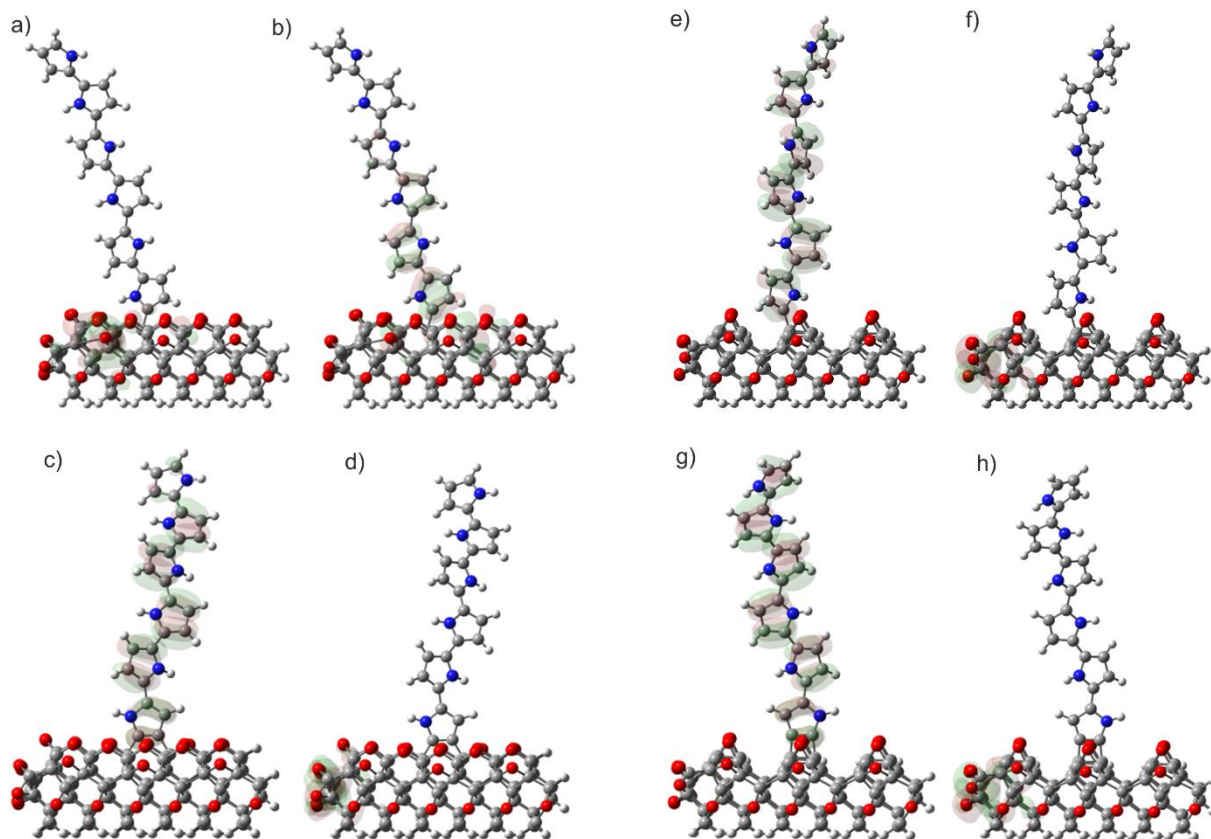


Figure S3. Optimized structures of **PPy on OH-terminated 1×1 (111) ND edge slab**: one-bond contact HOMO (a) and LUMO (b), two-bond contact HOMO (c) and LUMO (d). Optimized structures of **PPy on OH-terminated 2×1 (111) ND edge slab**: one-bond contact HOMO (e) and LUMO (f), two-bond contact HOMO (g) and LUMO (h). C atoms are grey, H atoms white, O atoms red, N atoms blue. Red and green clouds indicate positive and negative value of the orbital surfaces at the isovalue of $0.01e^{-\text{\AA}^{-3}}$.

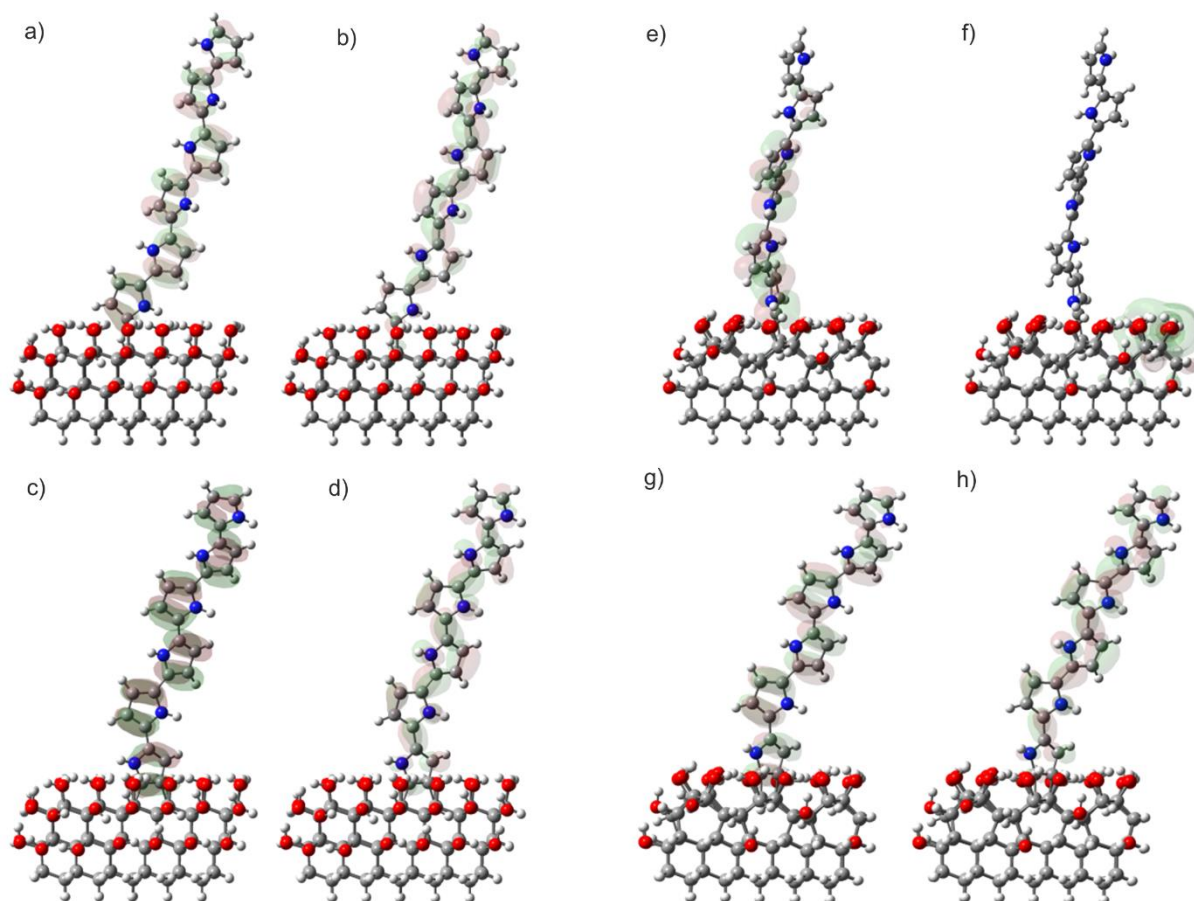


Figure S4. Optimized structures of **PPy on OH-terminated 2×1 (100) ND edge slab**: one-bond contact HOMO (a) and LUMO (b), two-bond contact HOMO (c) and LUMO (d). C atoms are grey, H atoms white, O atoms red, N atoms blue. Red and green clouds indicate positive and negative value of the orbital surfaces at the isovalue of $0.01e^{-\text{\AA}^{-3}}$.

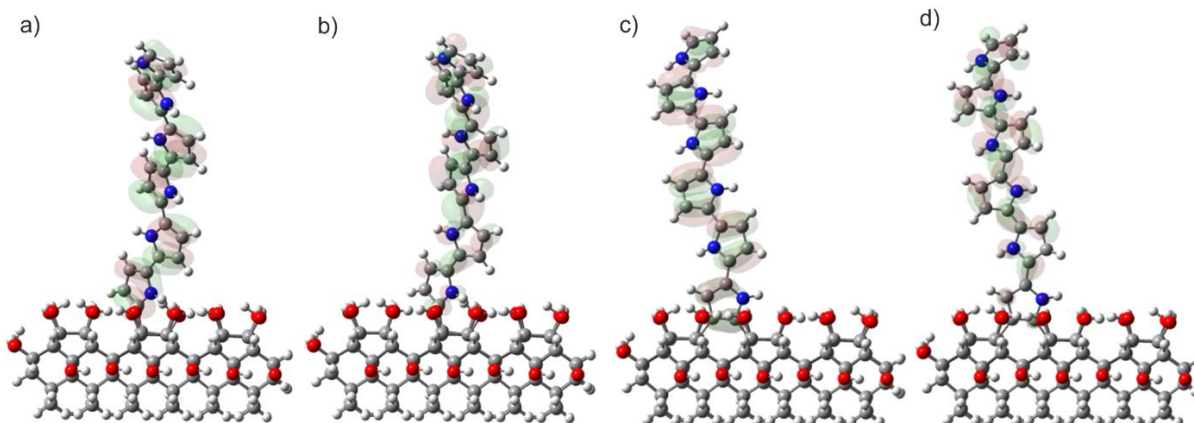


Figure S5. Optimized structures of PPy on COOH-terminated 1×1 (111) ND edge slab: one-bond contact HOMO (a) and LUMO (b), two-bond contact HOMO (c) and LUMO (d). Optimized structures of PPy on COOH-terminated 2×1 (111) ND edge slab: one-bond contact HOMO (e) and LUMO (f), two-bond contact HOMO (g) and LUMO (h). C atoms are grey, H atoms white, O atoms red, N atoms blue. Red and green clouds indicate positive and negative value of the orbital surfaces at the isovalue of $0.01e^- \text{\AA}^{-3}$.

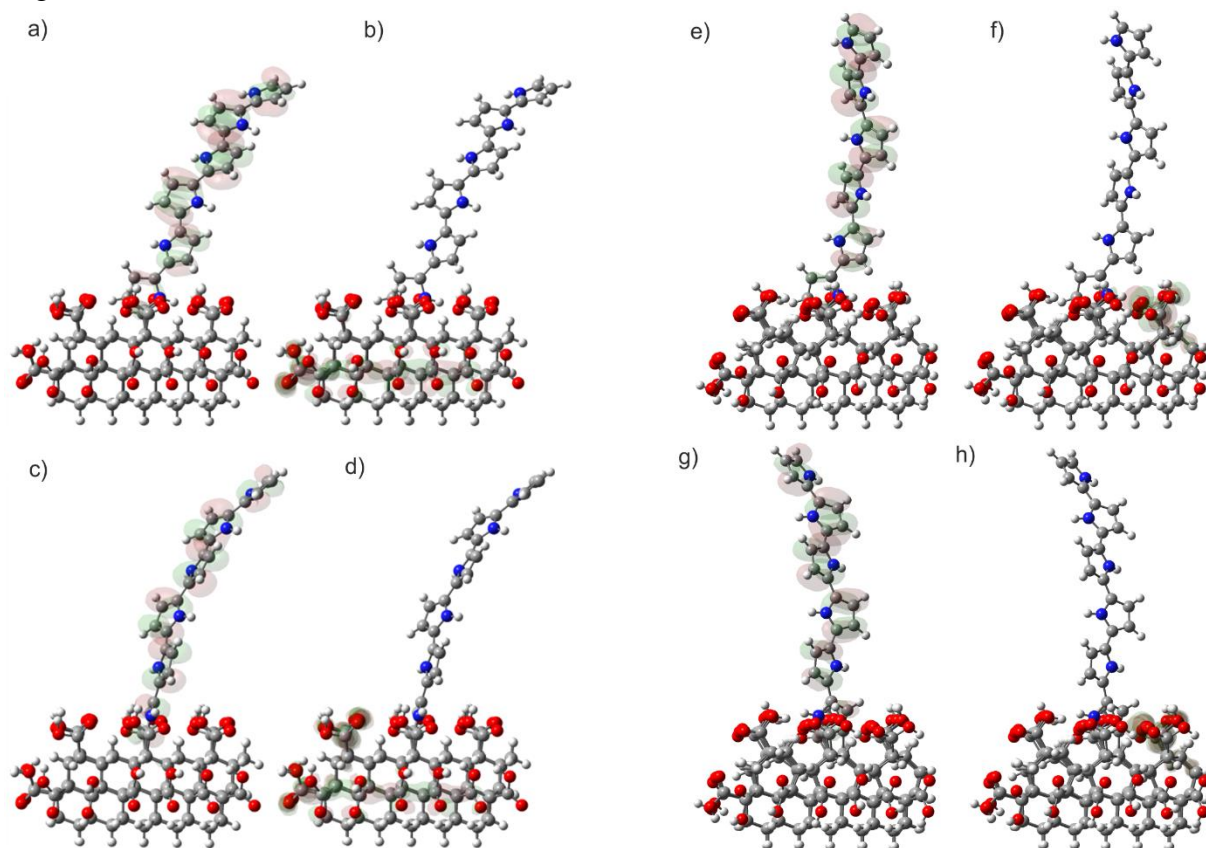


Figure S6. Optimized structures of PPy on COOH-terminated 2×1 (100) ND edge slab: one-bond contact HOMO (a) and LUMO (b), two-bond contact HOMO (c) and LUMO (d). C atoms are grey, H atoms white, O atoms red, N atoms blue. Red and green clouds indicate positive and negative value of the orbital surfaces at the isovalue of $0.01e^- \text{\AA}^{-3}$.

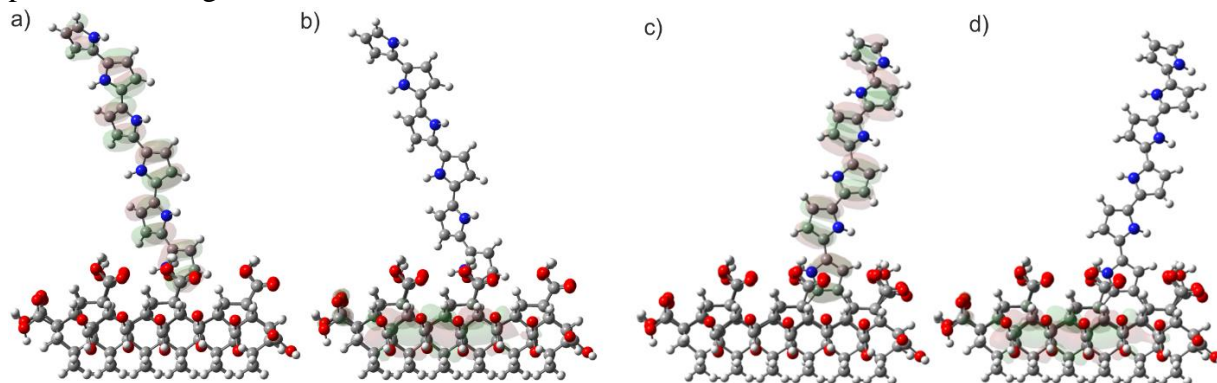


Figure S7. Optimized structures of **PPy** on **anhydride-terminated 1×1 (111) ND edge slab**: one-bond contact HOMO (a) and LUMO (b), two-bond contact HOMO (c) and LUMO (d). Optimized structures of **PPy** on **anhydride-terminated 2×1 (111) ND edge slab**: one-bond contact HOMO (e) and LUMO (f), two-bond contact HOMO (g) and LUMO (h). C atoms are grey, H atoms white, O atoms red, N atoms blue. Red and green clouds indicate positive and negative value of the orbital surfaces at the isovalue of $0.01e^{-\text{\AA}^{-3}}$.

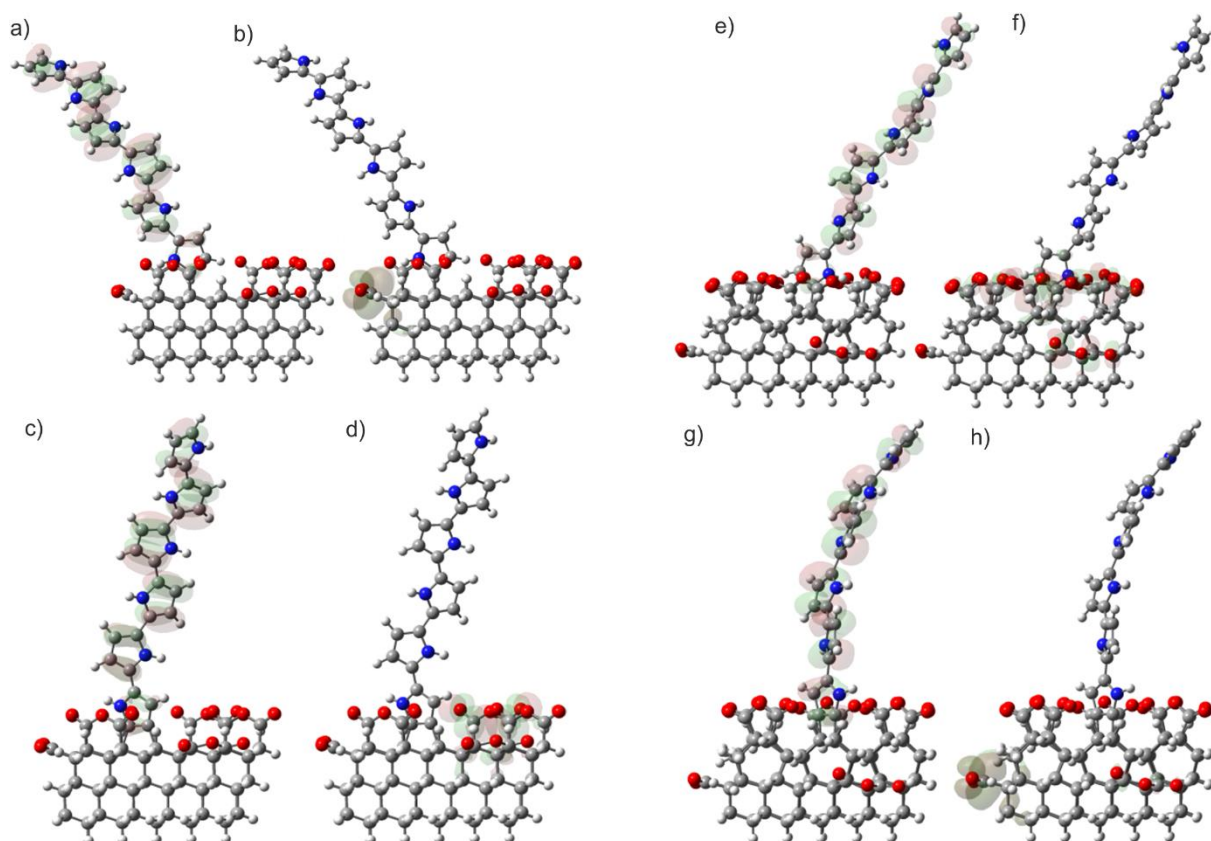


Figure S8. Optimized structures of **PPy** on **anhydride-terminated 2×1 (100) ND edge slab**: one-bond contact HOMO (a) and LUMO (b), two-bond contact HOMO (c) and LUMO (d). C atoms are grey, H atoms white, O atoms red, N atoms blue. Red and green clouds indicate positive and negative value of the orbital surfaces at the isovalue of $0.01e^{-\text{\AA}^{-3}}$.

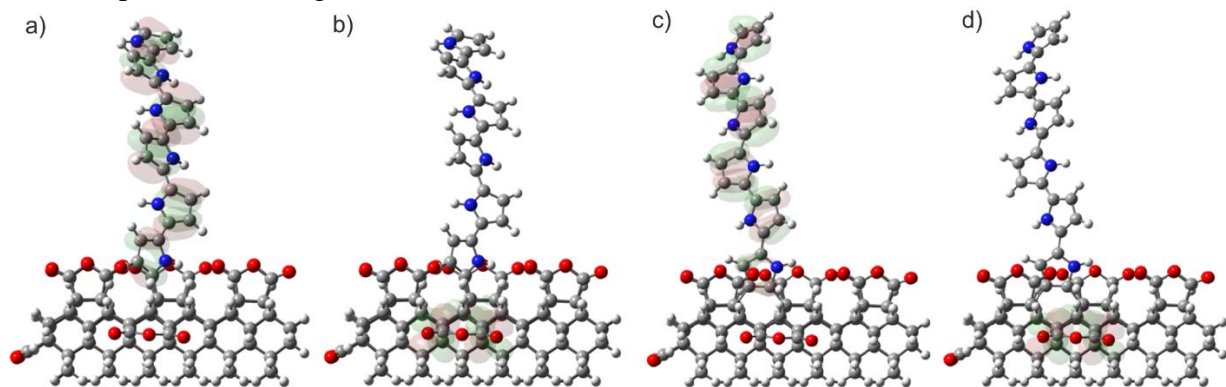


Figure S9. Optimized structures of **PPy on a-C:H ND edge slab**: one-bond contact HOMO (a) and LUMO (b), two-bond contact HOMO (c) and LUMO (d). Optimized structures of **PPy on a-C:O ND edge slab**: one-bond contact HOMO (e) and LUMO (f), two-bond contact HOMO (g) and LUMO (h). C atoms are grey, H atoms white, O atoms red, N atoms blue. Red and green clouds indicate positive and negative value of the orbital surfaces at the isovalue of $0.01\text{e}\text{-}\text{\AA}^{-3}$.

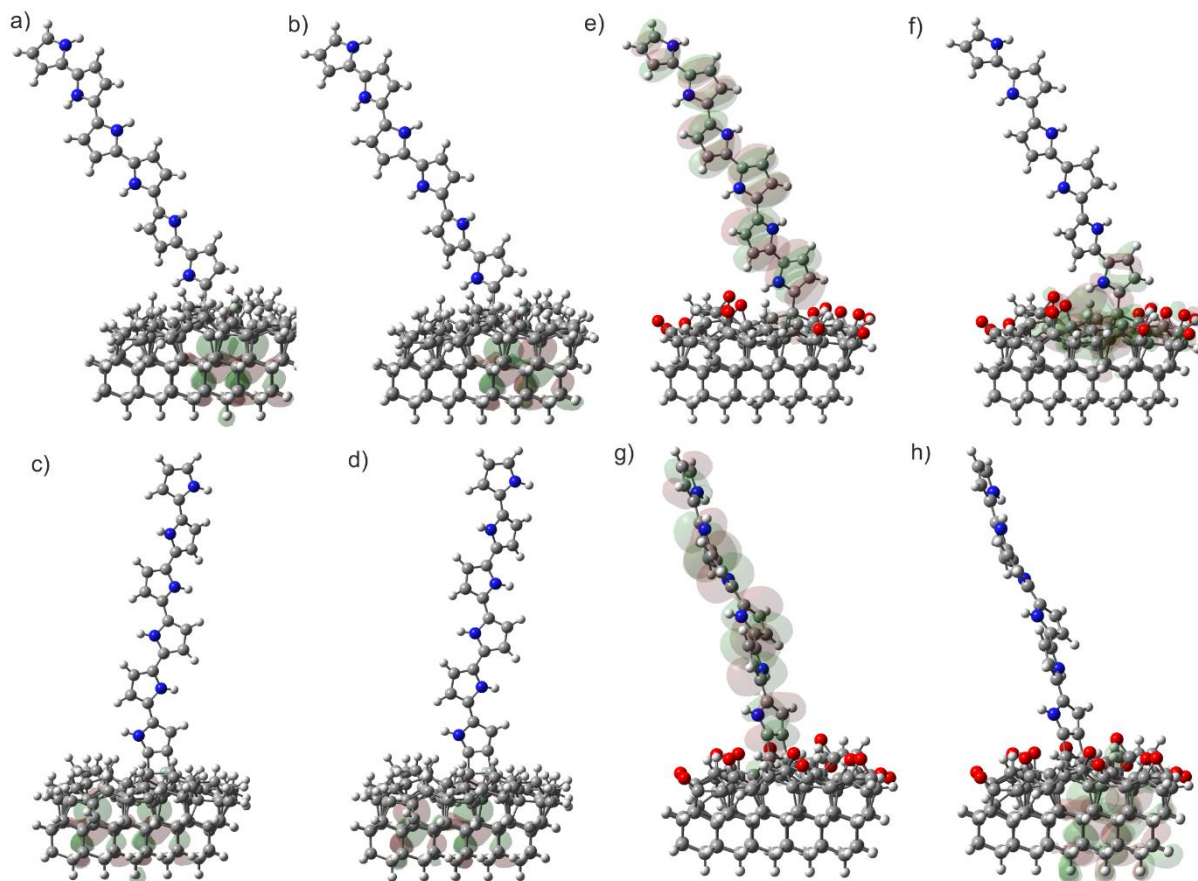


Figure S10. Graphs of HOMO (blue) and LUMO (red) energy levels of i) standalone PPy (dashed lines), ii) standalone **O-terminated** ND slabs (dot-and-dashed lines), and iii) PPy chemisorbed (1-bond, 2-bond) on O-terminated ND (full lines) in the case of 1×1 (111) (a), 2×1 (111) (b), 1×1 (100) (c), and 2×1 (100) (d) ND slabs.

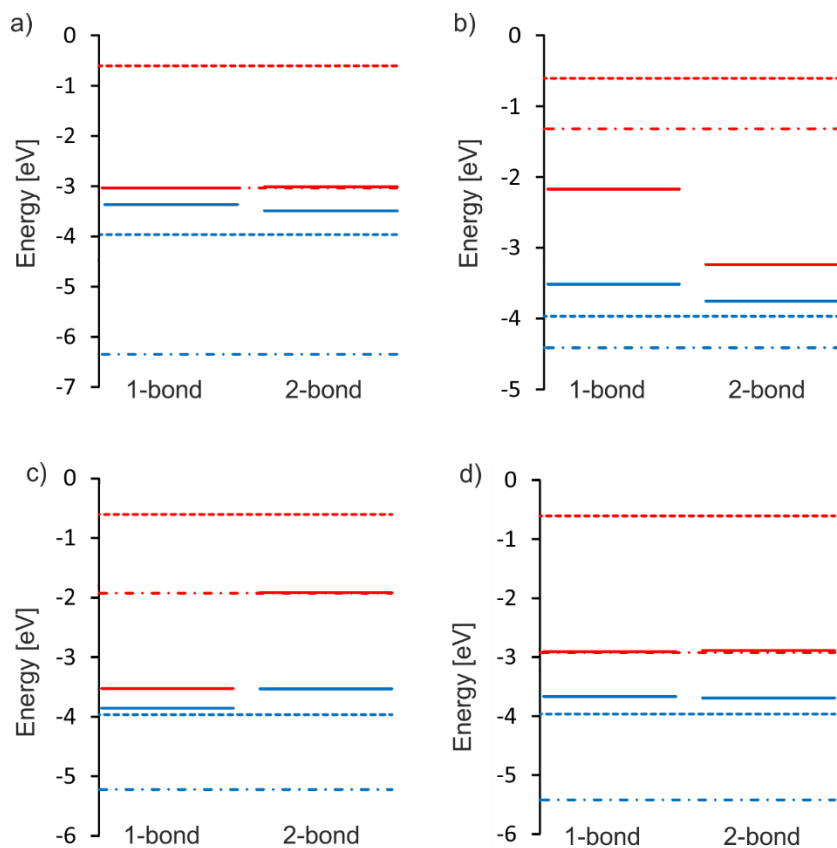


Figure S11. Graphs of HOMO (blue) and LUMO (red) energy levels of i) standalone PPy (dashed lines), ii) standalone **OH-terminated** ND slabs (dot-and-dashed lines), and iii) PPy chemisorbed (1-bond, 2-bond) on OH-terminated ND (full lines) in the case of 1×1 (111) (a), 2×1 (111) (b), and 2×1 (100) (c) ND slabs.

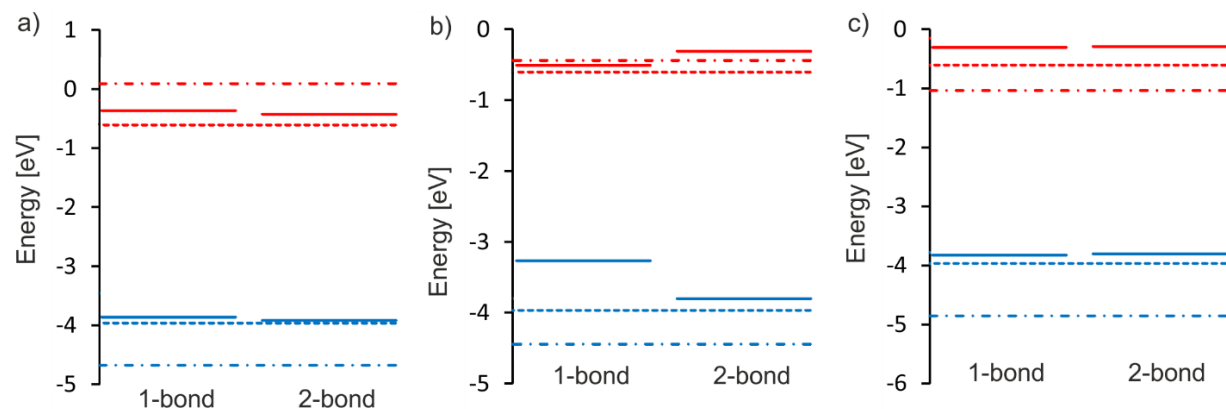


Figure S12. Graphs of HOMO (blue) and LUMO (red) energy levels of i) standalone PPy (dashed lines), ii) standalone **COOH-terminated** ND slabs (dot-and-dashed lines), and iii) PPy chemisorbed (1-bond, 2-bond) on COOH-terminated ND (full lines) in the case of 1×1 (111) (a), 2×1 (111) (b), and 2×1 (100) (c) ND slabs.

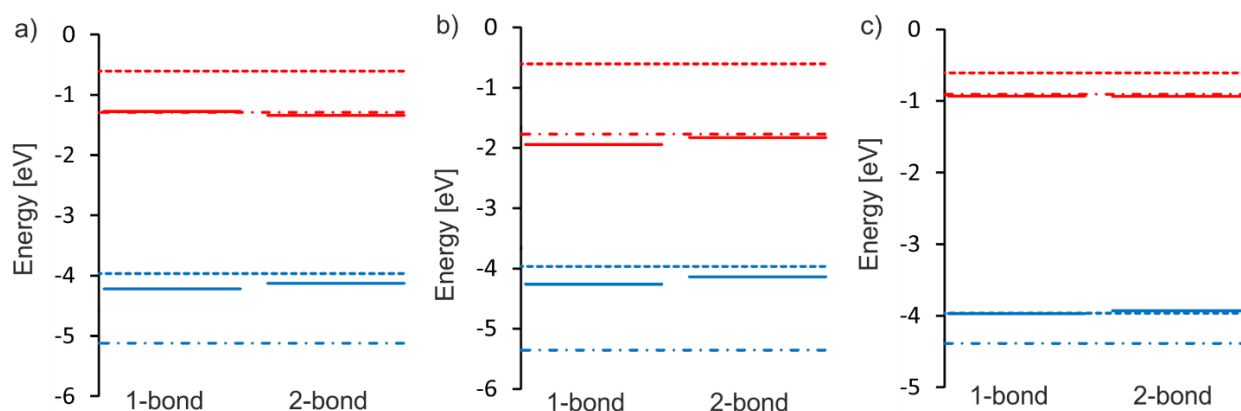


Figure S13. Graphs of HOMO (blue) and LUMO (red) energy levels of i) standalone PPy (dashed lines), ii) standalone **anhydride-terminated** ND slabs (dot-and-dashed lines), and iii) PPy chemisorbed (1-bond, 2-bond) on anhydride-terminated ND (full lines) in the case of 1×1 (111) (a), 2×1 (111) (b), and 2×1 (100) (c) ND slabs.

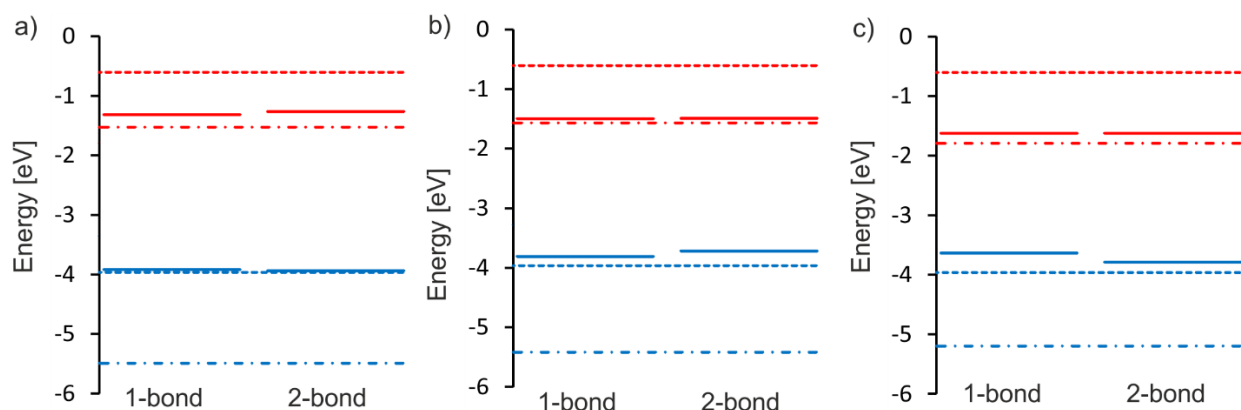


Figure S14. Relative energy positions of HOMO (in blue) and LUMO (in red) of PPy (dashed lines), ND slabs with **amorphous surface layer** (dot-and-dashed lines), and PPy chemisorbed (1-bond, 2-bond) on **a-C:H** (a) and **a-C:O** slabs (b) (full lines).

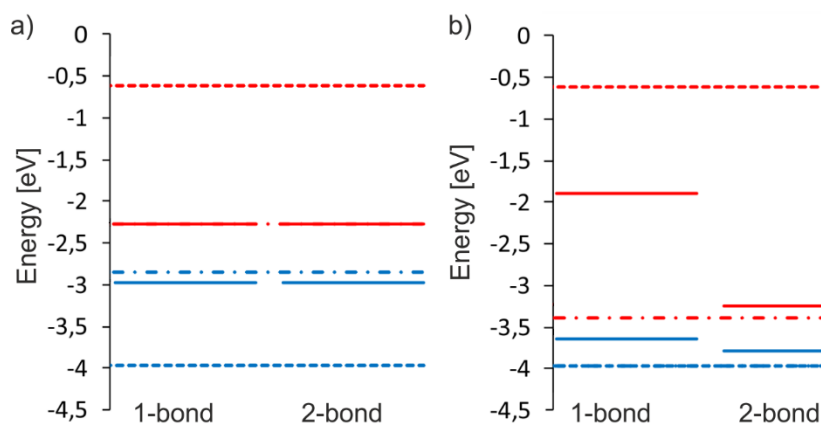


Figure S15. Molecular orbitals contributing to the third excited state of the two-bond contact of PPy on epoxide-terminated 2×1 (100) ND (a - d) and its LUMO (e). Molecular orbitals contributing to the first excited state of the one-bond contact of PPy on hydroxyl-terminated 2×1 (100) ND (f - i) and carboxyl-terminated 2×1 (100) ND (j - m) and its LUMO (n).

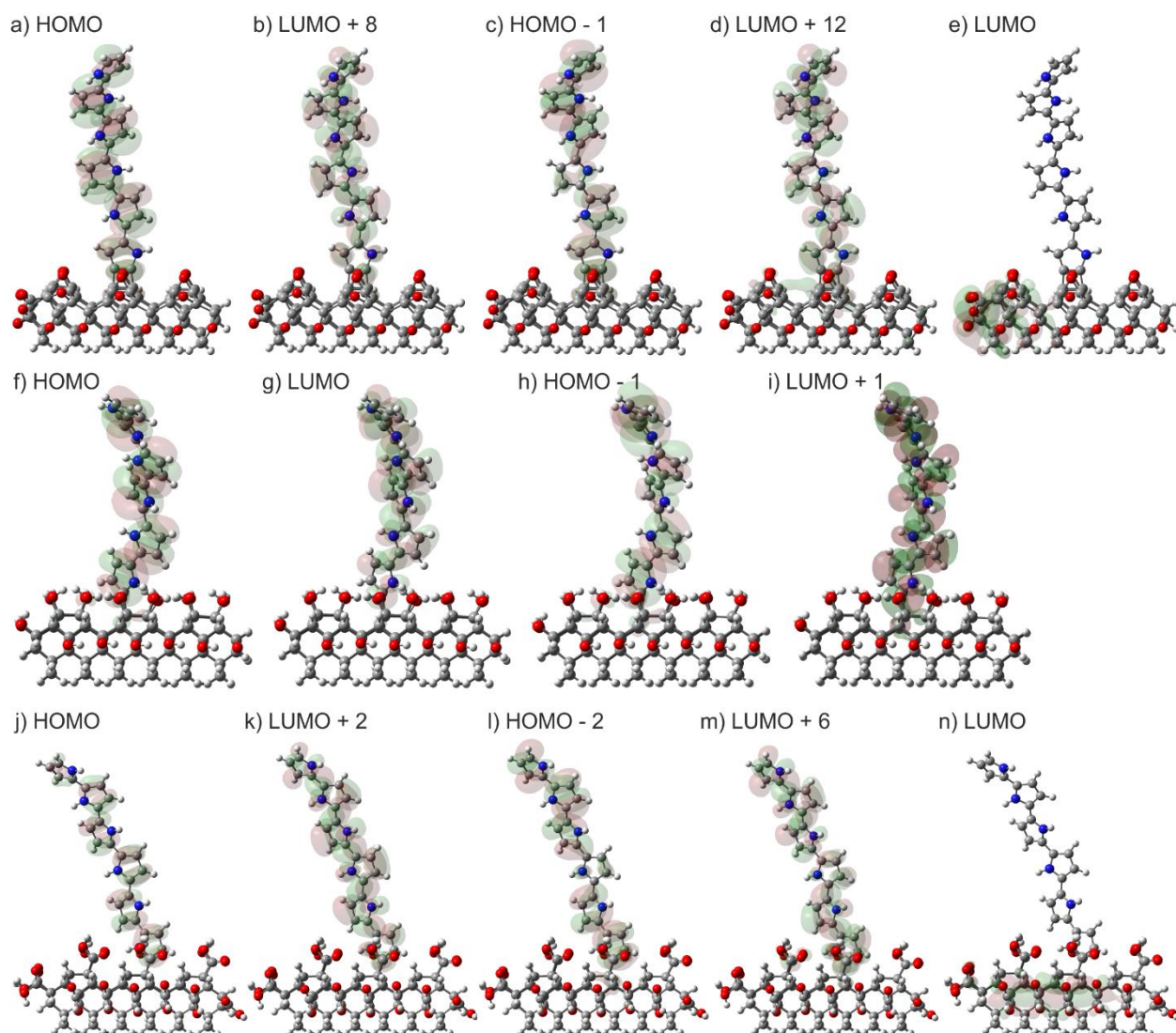


Table S1. Summary of bond lengths between PPy and O-terminated ND: ND-PPy bond length [\AA], number of (n) and bond length [\AA] of hydrogen bonds formed between NH groups in PPy and O atoms on ND surface. Py heterocycles are numbered from the ND edge (physisorbed PPy) or from the bond with ND (chemisorbed PPy).

PPy-ND structure	Type of bond	Bond length [\AA]	n	Py 1	Py 2	Py 3	Py 4	Py 5	Py 6
1×1 (111), peroxides	1-bond	1,58	2	2.68; 3.04	-	-	-	-	-
1×1 (111), peroxides	2-bond	1,52; 1,52	0	-	-	-	-	-	-
2×1 (111), epoxides	1-bond	1,54	0	-	-	-	-	-	-
2×1 (111), epoxides	2-bond	1,54; 1,54	0	-	-	-	-	-	-
1×1 (100), ethers	1-bond	1,52	1	2,76	-	-	-	-	-
1×1 (100), ethers	2-bond	1,47; 1,48	0	-	-	-	-	-	-
2×1 (100), epoxides	1-bond	1,52	0	-	-	-	-	-	-
2×1 (100), epoxides	2-bond	1,52; 1,53	0	-	-	-	-	-	-

Table S2. Summary of bond lengths between **PPy and OH-terminated ND**: ND-PPy bond length [\AA], number of (n) and bond length [\AA] of hydrogen bonds formed between NH groups in PPy and O atoms on ND surface. Py heterocycles are numbered from the ND edge (physisorbed PPy) or from the bond with ND (chemisorbed PPy).

PPy-ND structure	Type of bond	Bond length [\AA]	n	Py 1	Py 2	Py 3	Py 4	Py 5	Py 6
1 \times 1 (111)	1-bond	1,96	2	3.36; 2.78	-	-	-	-	-
1 \times 1 (111)	2-bond	1,52; 1,55	0	-	-	-	-	-	-
2 \times 1 (111)	1-bond	1,78	0	-	-	-	-	-	-
2 \times 1 (111)	2-bond	1,53; 1,55	0	-	-	-	-	-	-
2 \times 1 (100)	1-bond	1,63	2	1.68; 3.04	-	-	-	-	-
2 \times 1 (100)	2-bond	1,52	0	-	-	-	-	-	-

Table S3. Summary of bond lengths between **PPy and COOH-terminated ND**: ND-PPy bond length [\AA], number of (n) and bond length [\AA] of hydrogen bonds formed between NH groups in PPy and O atoms on ND surface. Py heterocycles are numbered from the ND edge (physisorbed PPy) or from the bond with ND (chemisorbed PPy).

PPy-ND structure	Type of bond	Bond length [\AA]	n	Py 1	Py 2	Py 3	Py 4	Py 5	Py 6
1 \times 1 (111)	1-bond	1.58	1	1.65	-	-	-	-	-
1 \times 1 (111)	2-bond	1.53; 1.56	1	2.06	-	-	-	-	-
2 \times 1 (111)	1-bond	1.59	1	1.61	-	-	-	-	-
2 \times 1 (111)	2-bond	1.52; 1.61	1	2.23	-	-	-	-	-
2 \times 1 (100)	1-bond	1.53	1	2.61	-	-	-	-	-
2 \times 1 (100)	2-bond	1.52; 1.54	0	-	-	-	-	-	-

Table S4. Summary of bond lengths between **PPy and anhydride-terminated ND**: ND-PPy bond length [\AA], number of (n) and bond length [\AA] of hydrogen bonds formed between NH groups in PPy and O atoms on ND surface. Py heterocycles are numbered from the ND edge (physisorbed PPy) or from the bond with ND (chemisorbed PPy).

PPy-ND structure	Type of bond	Bond length [\AA]	n	Py 1	Py 2	Py 3	Py 4	Py 5	Py 6
1 \times 1 (111)	1-bond	1.57	0	-	-	-	-	-	-
1 \times 1 (111)	2-bond	1.53; 1.54	0	-	-	-	-	-	-
2 \times 1 (111)	1-bond	1.57	0	-	-	-	-	-	-
2 \times 1 (111)	2-bond	1.55; 1.55	0	-	-	-	-	-	-
2 \times 1 (100)	1-bond	1.53	1	2.64	-	-	-	-	-
2 \times 1 (100)	2-bond	1.53	0	-	-	-	-	-	-

Table S5. Summary of bond lengths between **PPy and NDs with an amorphous surface layer**: ND-PPy bond length [\AA], number of (n) and bond length [\AA] of hydrogen bonds formed between NH groups in PPy and O atoms on ND surface. Py heterocycles are numbered from the bond with ND.

PPy-ND structure	Type of bond	Bond length [\AA]	n	Py 1	Py 2	Py 3	Py 4	Py 5	Py 6
a-C:H	1-bond	1.53	0	-	-	-	-	-	-
a-C:H	2-bond	1.52; 1.53	0	-	-	-	-	-	-
a-C:O	1-bond	1.50	1	2.14	-	-	-	-	-
a-C:O	2-bond	1.51; 1.54	0	-	-	-	-	-	-

Table S6. Summary of binding energy (E_b), interaction energy (E_{int}), charge transfer (Δq), and HOMO-LUMO gap of **PPy on O-terminated NDs**. ND structure without PPy bonding (“none”) corresponds to a standalone ND.

ND surface structure	PPy bonding	E_b [eV]	E_{int} [eV]	Δq [e^-]	HOMO-LUMO gap [eV]
1 × 1 (111), peroxides	1-bond	-2.36	4.25	0.00(1)	0.33
1 × 1 (111), peroxides	2-bond	-1.01	8.78	-0.05	0.48
1 × 1 (111), peroxides	none	-	-	-	3.31
2 × 1 (111), epoxides	1-bond	-0.90	3.18	-0.03	1.35
2 × 1 (111), epoxides	2-bond	-2.54	4.71	-0.16	0.52
2 × 1 (111), epoxides	none	-	-	-	3.10
1 × 1 (100), ethers	1-bond	-5.94	4.90	-0.05	0.33
1 × 1 (100), ethers	2-bond	-2.55	7.78	0.02	1.61
1 × 1 (100), ethers	none	-	-	-	3.29
2 × 1 (100), epoxides	1-bond	-1.31	3.70	-0.06	0.76
2 × 1 (100), epoxides	2-bond	-1.10	6.67	-0.07	0.81
2 × 1 (100), epoxides	none	-	-	-	2.50

Table S7. Summary of binding energy (E_b), interaction energy (E_{int}), charge transfer (Δq), and HOMO-LUMO gap of **PPy on OH-terminated NDs**. ND structure without PPy bonding (“none”) corresponds to a standalone ND.

ND surface structure	Type of bond	E_b [eV]	E_{int} [eV]	Δq [e^-]	HOMO-LUMO gap [eV]
1 × 1 (111)	1-bond	-6.23	0.24	-0.02	3.50
1 × 1 (111)	2-bond	-6.06	7.52	-0.01	3.49
1 × 1 (111)	none	-	-	-	4.77
2 × 1 (111)	1-bond	-5.71	0.06	0.05	2.76
2 × 1 (111)	2-bond	-6.22	3.93	-0.09	3.49
2 × 1 (111)	none	-	-	-	4.01
2 × 1 (100)	1-bond	-4.22	2.41	-0.04	3.52
2 × 1 (100)	2-bond	-4.71	9.87	-0.06	3.51
2 × 1 (100)	none	-	-	-	3.82

Table S8. Summary of binding energy (E_b), interaction energy (E_{int}), charge transfer (Δq), and HOMO-LUMO gap of **PPy on COOH-terminated NDs**. ND structure without PPy bonding (“none”) corresponds to a standalone ND.

ND surface structure	Type of bond	E_b [eV]	E_{int} [eV]	Δq [e^-]	HOMO-LUMO gap [eV]
1 × 1 (111)	1-bond	-2.99	3.02	-0.09	2.95
1 × 1 (111)	2-bond	-3.87	7.93	-0.10	2.79
1 × 1 (111)	none	-	-	-	3.83
2 × 1 (111)	1-bond	-3.19	2.59	-0.11	2.32
2 × 1 (111)	2-bond	-6.04	4.54	-0.13	2.31
2 × 1 (111)	none	-	-	-	3.59
2 × 1 (100)	1-bond	-3.03	4.08	-0.03	3.04
2 × 1 (100)	2-bond	-3.73	8.71	-0.14	3.00
2 × 1 (100)	none	-	-	-	3.48

Table S9. Summary of binding energy (E_b), interaction energy (E_{int}), charge transfer (Δq), and HOMO-LUMO gap of **PPy on anhydride-terminated NDs**. ND structure without PPy bonding (“none”) corresponds to a standalone ND.

ND surface structure	Type of bond	E_b [eV]	E_{int} [eV]	Δq [e ⁻]	HOMO-LUMO gap [eV]
1 × 1 (111)	1-bond	-2.16	4.29	-0.12	2.60
1 × 1 (111)	2-bond	-3.10	8.97	-0.08	2.68
1 × 1 (111)	none	-	-	-	3.97
2 × 1 (111)	1-bond	-3.82	3.21	-0.36	2.31
2 × 1 (111)	2-bond	-4.49	4.31	-0.07	2.23
2 × 1 (111)	none	-	-	-	3.85
2 × 1 (100)	1-bond	-2.26	4.46	-0.06	2.01
2 × 1 (100)	2-bond	-2.7	8.14	-0.10	2.17
2 × 1 (100)	none	-	-	-	3.41

Table S10. Summary of binding energy (E_b), interaction energy (E_{int}), charge transfer (Δq), and HOMO-LUMO gap of **PPy on NDs with an amorphous surface layer**. ND structure without PPy bonding (“none”) corresponds to a standalone ND.

ND surface structure	Type of bond	E_b [eV]	E_{int} [eV]	Δq [e ⁻]	HOMO-LUMO gap [eV]
a-C:H	1-bond	-0.74	2.48	-0.04	0.70
a-C:H	2-bond	-2.74	4.98	-0.08	0.71
a-C:H	none	-	-	-	0.57
a-C:O	1-bond	0.30	4.34	-0.07	1.76
a-C:O	2-bond	-1.98	5.23	-0.12	0.55
a-C:O	none	-	-	-	0.58



Cite this: *Phys. Chem. Chem. Phys.*,
2019, 21, 11033

DFT calculations reveal pronounced HOMO–LUMO spatial separation in polypyrrole–nanodiamond systems†

Petra Matunová,^a Vít Jirásek^b and Bohuslav Rezek^{a,b}

The low-cost efficient generation of renewable energy and its blending with societal lifestyle is becoming increasingly pervasive. Diamond-based inorganic–organic hybrid systems may have an immense, yet still mostly unexplored, potential in photovoltaic solar cells applications. In this work, we study the interactions of polypyrrole (PPy) with diamond nanoparticles (so-called nanodiamonds, NDs) by computational density functional theory (DFT) methods. We compute the structural and electronic properties of such hybrid organic–inorganic systems. During modeling, PPy is chemisorbed and physisorbed on (111) and (100) ND edge-like surface slabs terminated with oxygen, hydroxyl, carboxyl, and anhydride functional groups, *i.e.*, in the arrangements most commonly found in real NDs. Moreover, NDs terminated with an amorphous surface layer (a-C:H, a-C:O) are considered to approach realistic conditions even further. In a predominant number of cases, we obtain the spatial separation of HOMO and LUMO at the interface, facilitating exciton dissociation. Further, there is a favorable energy level alignment for charge transport. The theoretical results, therefore, show the promising potential of PPy–ND composites in photovoltaic applications.

Received 13th December 2018,
Accepted 26th April 2019

DOI: 10.1039/c8cp07622g

rsc.li/pccp

Introduction

Solar energy production, particularly photovoltaics (PV), has become one of the key elements to support the energy transition from fossil fuel to renewable energy sources, thereby directly contributing toward resolving the climate change problem. In the last ten years, PV has seen exponential growth, with an installed capacity of over 100 GW in Europe alone. Mass realization and further exponential growth are expected when integrated PV becomes common, *i.e.*, in roofs, facades, windows, and other objects. However, current silicon-based PV devices have certain limitations that obstruct their ubiquitous applications. Although they can reach efficiency of up to 26.7% in a single junction cell,¹ the efficiency-to-cost ratio remains unsatisfactory as higher efficiencies are reached only for multiple-junction cells. They can also facilitate the realization of their full potential (energy conversion efficiency) only under high and direct solar irradiation, which does not coincide

with areas of the highest energy consumption in developed countries.

Organic PV (OPV) is a promising alternative, particularly owing to its ability to cover large surface areas and better performance under low-light conditions. The development of high-performance organic semiconductors has enabled OPVs to become an important source of alternative energy over the past few years. The newly developed active materials used in OPVs are nontoxic and enable cost-effective and eco-friendly roll-to-roll manufacturing with orders of magnitude lower energy consumption as compared to the manufacturing process for classic PV. However, current OPV technology still suffers from fundamental issues. Some examples are degradation, higher cost of certain key components, and relatively low efficiency of only up to 11%.²

Worldwide research and development efforts have, therefore, been directed toward investigating newly combined inorganic and organic materials,^{3,4} which would provide a breakthrough for OPV-type solar cell performance and wider applications. One of the main challenges is to increase the efficiency while decreasing the production and installation costs. Diamond nanoparticles–nanodiamonds (NDs)—represent an inexpensive (~1 EUR per g) carbon nanomaterial, possessing a unique set of material, chemical, and electronic properties. Nowadays, they are commercially used in many areas from lubricants to electronic, chemical, and biomedical applications.⁵ Various carbon nanostructures have already been studied as charge-transporting materials and

^a Faculty of Electrical Engineering, Czech Technical University, Technická 2,
166 27 Prague 6, Czech Republic. E-mail: matunpet@fel.cvut.cz

^b Institute of Physics, Czech Academy of Sciences, Cukrovarnická 10,
162 00 Prague 6, Czech Republic

^c Walter Schottky Institut and Physik-Department, Technische Universität München,
Am Coulombwall 4a, D-85748 Garching, Germany

† Electronic supplementary information (ESI) available: Fig. S1–S20 and Tables S1–S10.
See DOI: 10.1039/c8cp07622g

additives within a light-harvesting material.^{6–8} However, the potential of NDs in PV and the connected light-to-energy conversion remains mostly unexplored.

The possible functionalization of NDs is diverse, and their combination with organic materials can lead to novel semiconductor–organic functional systems. Polypyrrole (PPy) is a typical representative of organic semiconductors. PPy is a chemically stable conjugated polymer⁹ that can effectively absorb visible light (hence, it is called an organic dye); its conductivity and energy bandgap (typically within 1.3–3.2 eV) can be controlled by the preparation method.^{10,11} Combining PPy with NDs has potential applications in PV applications based on an experimentally measured transfer of photogenerated charge between bulk diamond and PPy observed by Kelvin force microscopy and optical spectroscopy.^{10,12,13} Earlier experimental studies have revealed various configurations of PPy binding with NDs.¹⁴ Moreover, carbon allotropes in conjunction with polymers have revealed promising materials for solar cells.^{15–17}

The most common surface chemical groups found on detonation nanodiamonds (DNDs) are related to oxygen (*e.g.*, peroxides and ethers were found on chemical vapor deposition (CVD)-treated diamond films after exposure to atomic oxygen),¹⁸ hydroxyls, carboxyls, and anhydrides owing to the production process, where newly formed detonation diamond crystallites react with a cooling medium or arise from the purification process.¹⁹ Hydrogen-terminated NDs can be fabricated using a CVD process²⁰ or from thermal annealing in pure hydrogen.²¹ Electronic and physical properties are significantly influenced by the chemical termination of NDs. In contrast with the negative electron affinity and surface conductivity of H-terminated diamonds, the oxygen termination of diamonds yields positive electron affinity²² and higher electrical resistance.²³ The higher electronegativity of oxygen when compared with that of carbon yields the polarization of the bond between oxygen and carbon with a negative charge (δ^-) on oxygen and positive charge (δ^+) on carbon. As a consequence of this surface C–O dipole layer, the vacuum level is above the conduction band minimum.²⁴ The opposite occurs for the C–H surface dipole.

With regard to the surface structure, the two most common low-index diamond facets found on the surfaces of natural and synthetic diamonds are (111) and (100) facets^{25–27} depending on the temperature and pressure.²⁸ The (100) surface represents the most defect-free surface obtained from experimental syntheses.²⁹ Moreover, the surfaces of DNDs, commercially available with diameters less than 4 nm,³⁰ contain an amorphous layer of carbon on parts of their surfaces. The thermodynamic stability and surface reconstruction of NDs terminated with oxygen-containing groups under varying conditions and different surface coverage values of (111) and (100) facets were studied by both theoretical^{22,28,29,31–46} and experimental^{24,47–54} methods. On the 1×1 (111) ND surface facet, oxygen in the on-top (*i.e.*, ketone) position or with peroxide bridges is the most favorable;³⁴ the epoxide O-termination is unstable with respect to the on-top position in this case.²⁸ On the 2×1 (111) facet, oxygen adsorption in the on-top and epoxide positions were pointed out as the only plausible positions.^{28,49} The epoxide

configuration occurs preferably at 50% or lower oxygen coverage;^{27,34,37} 100% oxygen coverage leads to dimerization.²⁸ On the 1×1 (100) facet, the ether position is preferred at higher surface coverage.^{27,29,31} Alternatively, etherized 1×1 (100) structures with a bridging ether may be convenient.³³ For oxygen surface coverage up to 50% on (100), the 2×1 reconstruction is preferred over the 1×1 reconstruction,²⁷ and the epoxy structure is more favorable than the ether structure.³² The ether position is stable at high surface coverage.^{27,29,34} For the (111) and (100) facets, OH adsorption leads to the destabilization of the 2×1 reconstruction as compared to the 1×1 reconstruction.⁴⁰ In the case of OH termination, there are two competing interactions: hydrogen bonding and steric repulsions. The former one can stabilize the surface system, while the latter can destabilize, and therefore, weaken the surface–adsorbate bonds.⁵⁵ For the COOH species, it is only energetically possible to cover the surfaces up to 50%.⁵⁶ The adsorption of COOH is the most favorable on the 2×1 (100) surface, which is exothermic at all the points on the surface.⁵⁷ Carboxylic and anhydride groups are supposed to contribute the most to the spectral bands observed in the experimental FTIR spectra in the range of 1600–1950 cm^{-1} .⁴⁶ Anhydride bridges formed on the ND surface were studied as one of the most probable groups on a heavily oxidized surface.⁴⁶

The hybrid semiconductor–organic PPy–ND interfacial system cannot be completely understood only based on experimental techniques. Only a few theoretical works involving PPy–ND systems have been published, particularly investigating PPy that is chemisorbed⁵⁸ and physisorbed⁵⁹ on H-terminated NDs; PPy that is physisorbed on O-terminated NDs⁶⁰ exhibits considerable charge transfer and promising electronic properties.

In this work, we present a comprehensive theoretical study of chemisorbed (grafted) and physisorbed (merely adsorbed) PPy on oxidized ND surfaces and on NDs with additional hydrogenated or oxidized amorphous carbon layers. We include commonly occurring surface functional groups: hydroxyls, carboxyls, and anhydrides.^{19,61} Using many nonequivalent starting conditions, we analyze the most probable structural configurations and electronic properties of the PPy–ND system, showing promising potential of PPy–ND systems in PV energy generation applications.

Computational details

The first-principles density functional theory (DFT) method implemented in Gaussian 09 electronic structure software⁶² was used for optimizing all the structures in order to obtain stable ground-state configurations. Electron density was described with a long-range corrected hybrid density functional ω B97X-D,⁶³ which includes empirical atom–atom dispersion and eliminates the self-interaction error. Moreover, ω B97X-D was found to be optimal for calculations of π -conjugated oligomers.⁶⁴ Molecular orbitals were described with the 6-31G(d) basis set including polarization functions on non-hydrogen atoms.

Modeling the entire ND particle with experimentally accessible size starting at 1.4 nm⁶⁵ would be computationally unfeasible at this level of theory. Therefore, we use the (111), (100), and

amorphous ND surface slabs consisting of 3 C double layers of 6×6 atoms, particularly 5×6 atoms if structurally needed. The slabs represent an edge of ND, with one larger “top” surface aimed at PPy adsorption, one larger “side” surface, and a small side surface closing the corner. These three “outer” surfaces of ND are functionalized with surface groups, and the remaining three “inner” surfaces that represent the inner cut planes are saturated with H atoms in order to maintain the sp^3 hybridization of neighboring carbon atoms. These H atoms were fixed during further optimization. In this way, the inner carbon atom layers maintain the planar shape, yet retaining a certain amount of flexibility to relax.

If necessary to saturate two dangling bonds of C atoms, dimerized H atoms were symmetrically placed around the C atom. They were kept fixed during optimizations to maintain the tetrahedral sp^3 characteristic of the diamond structure, despite certain steric tension arising between the hydrogen atoms.^{39,66} Few other authors have suggested a canted configuration with increased distance between the hydrogen atoms; however, this problem merits further discussions.^{33,39,67}

Based on the literature and our preliminary calculations, we choose the most probable 1×1 and 2×1 surface reconstructions of both (111) and (100) surfaces fully passivated with oxygens in the ether, epoxide, ketone, and peroxide positions (these configurations are referred to as O-terminated NDs), fully passivated with hydroxyls, 50% passivated with carboxyls, and passivated with anhydrides from 26% to 36%. The amorphous carbon layer was created by a random placement of the carbon atoms of the surface double layer and subsequent optimization on the slab. Next, surface-terminating functional groups were added to saturate the free carbon valences. The amorphous surface was saturated by hydrogens (a-C:H structures) and a mixture of hydrogens and oxygens (a-C:O structures). For the reconstructions of the surface slabs as well as the amorphous surface layer, different surface functional groups were considered. The slabs with the lowest relative total energy after optimization were chosen for further optimizations with adsorbed PPy. In the case of oxygen terminations, for the 1×1 (111) surface slab, we chose 100% termination with peroxides; for the π -bonded 2×1 (111) Pandey chain, we chose 50% epoxides; for the 1×1 (100), we chose 50% ethers; and for the 2×1 (100), we chose 50% epoxides. It should be noted that in the case of ethers, epoxides, and anhydrides, 50% surface coverage yielded a fully passivated surface. In the case of the OH- and COOH-terminated NDs, 100% and 50% surface coverage percentages, respectively, were used for further calculations with adsorbed PPy. In the case of anhydride-terminated NDs, surface coverage percentages of 25.6%, 35.7%, and 33.3% in the case of the 1×1 (111), 2×1 (111), and 2×1 (100) NDs, respectively, turned out to be energetically the most favorable. The amorphous a-C:H slabs were 100% saturated with H atoms. The amorphous a-C:O slabs were 48.7% saturated with O atoms (10.8% peroxides, 18.9% epoxides, 2.7% ethers, and 13.5% ketones) and 51.3% with H atoms. To study the contact formation, different nonequivalent initial configurations of the adsorbed PPy on the relaxed slabs were employed for computations. The PPy was represented by oligomer with six

PPy heterocycles, which were separately optimized and were proportionate to the modeled slabs. Nonequivalent positions of the physisorbed and chemisorbed PPy, including one- and two-bond contacts, on the optimized slabs were considered as the initial geometries. The structure with the lowest relative energy with respect to its corresponding and optimized 1×1 (111), 2×1 (100), or amorphous O- and H-terminated ND slabs was then considered for further analysis.

PPy and the top ND layer were allowed to relax during these further computations. PPy does not spontaneously chemisorb on the diamond surface. Hence, the one- and two-bonded chemisorbed contacts *via* C–C bonds were formed because of the removal of one or two H atoms from PPy, respectively, and a corresponding number of surface atoms on the ND slabs. The transition process itself is not studied in this case since the work is focused mainly on the nature of the bonding between PPy and ND and the resulting properties of the merged system. The energy barrier for replacing the oxygen surface groups by PPy is relatively high and complicates the direct chemisorption of PPy. However, the structures can exist if we consider the chemisorption of PPy on H-terminated NDs, where H atoms are likely to be substituted by PPy, and then replacing the remaining H-terminations with oxygen-related surface functional groups. Furthermore, the surfaces of polyfunctional DNDs (the most common commercially available NDs) contain a mixture of C–H and oxygen surface groups. PPy is, therefore, likely to graft at the C–H bond surrounded by oxide groups. Hence, determining PPy grafted on oxidized NDs can yield a fairly realistic and possibly common situation.

It should be noted that due to steric reasons, we did not optimize PPy on hydroxyl-terminated 2×1 (100) ND slabs, carboxyl-terminated 1×1 (100), and anhydrides-terminated 1×1 (100).

Geometrical parameters, binding energy (E_b), interaction energy (E_{int}), HOMO–LUMO gap, and charge transfer (Δq) were analyzed for a few select and the most suitable structures.

Results and discussion

Structural properties

All the initial PPy–ND structures were formed by design in all the possible nonequivalent positions and were consequently allowed to relax to the energy minimum. All of them converged sooner or later into the structures that were presented in this study. Only the OH-terminated 1×1 (100) ND turned out to be unstable during the optimization process; it converged into the 2×1 surface reconstruction; therefore, it was not included. All the energetically favorable structures of PPy adsorbed on (111), (100), and amorphous ND facets resulting from the optimization processes are shown in Fig. S1–S9 (ESI†). The geometrical parameters of the interactions are summarized in Tables S1–S5 (ESI†). The selected representative structures are shown in Fig. 1.

In the case of the physisorbed structures, the geometry of ND after contact formation remained almost unchanged; individual atoms on the surface shift within 0.19 Å. An exception

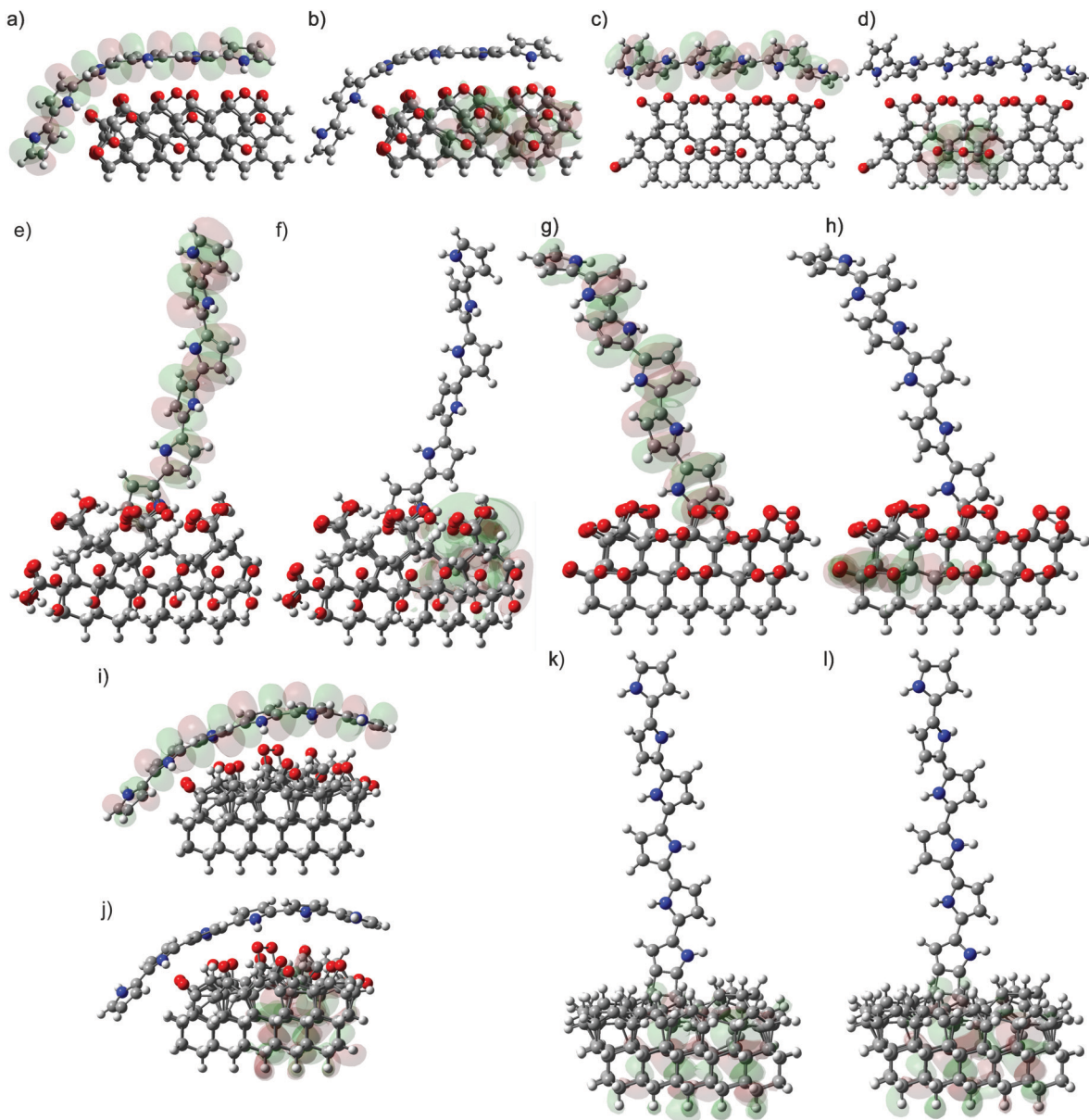


Fig. 1 Optimized structures of PPy physisorbed on epoxide-terminated 1×1 (100): HOMO (a) and LUMO (b); PPy physisorbed on anhydride-terminated 2×1 (100): HOMO (c) and LUMO (d); one-bond contact on carboxyl-terminated 2×1 (111): HOMO (e) and LUMO (f); two-bond contact of PPy on peroxide-terminated 1×1 (111): HOMO (g) and LUMO (h); PPy physisorbed on a-C:C:O: HOMO (i) and LUMO (j); two-bond contact of PPy on a-C:C:H: HOMO (k) and LUMO (l). C atoms are represented in grey; H atoms, white; O atoms, red; and N atoms, blue. Red and green colors indicate the positive and negative values of the orbital surfaces, respectively, corresponding to an isovalue of $0.01 \text{ e}^- \text{ \AA}^{-3}$.

is the peroxide-terminated 1×1 (111) structure, where two peroxide groups changed into two ketone groups and one bridging peroxide group. Consequently, a strong hydrogen bond was created between PPy and both the ketone groups. Another exception is the rearrangement of one ether group on the ether-terminated 1×1 (100) structure into one ketone group, forming a strong hydrogen bond with PPy and leaving one dangling bond on the C atom of the ND surface. For the hydroxylated NDs, the H atoms of several OH groups near the contact formation, mostly within the chemisorbed systems, were rotated up to 130° around the C–H bond (in the case of

the one-bond contact of PPy on 1×1 (100) ND), which led to the creation of two hydrogen bonds between two nearby OH groups and the amino group of PPy.

The physisorbed structures converged into PPy lying over the ND surface and having nonzero dihedral angles between the individual PPy heterocycles, thereby maximizing the electrostatic interactions at the ND interface. Exceptions are hydroxylated NDs, where two configurations with PPy in vertical positions, but higher in its total energy, are also obtained after optimization. Moreover, one structure in the horizontal position is obtained in the case of the carboxyl and anhydride groups.

Further, it should be noted that there is typical bending of the PPy molecule over the edge of the slab, *i.e.*, over the edge of the ND particle (Fig. 1a, b, i and j).

Chemisorbed (grafted) PPy is inclined relative to the ND surface, deviating from an initially set perpendicular position, which is observed for all the structures in this work. In the case of one-bond contact of PPy on epoxide-terminated 2×1 (111) ND, carboxyl-terminated 1×1 (111), 2×1 (100) ND, and anhydride-terminated 2×1 (100) ND, PPy even bends over the ND edge because of strong electrostatic interactions. Next, in the case of chemisorbed structures, ND is modified up to 0.5 Å only in the contact region. For carboxylated (anhydride-terminated) NDs, the only change in the ND geometry, up to 1.8 (1.6) Å, is in the positions of the carboxyl (anhydride) groups in the case of the two-bond contact on the 2×1 (100) (one-bond contact on the 2×1 (111)) ND facet, where the groups tilt to create space for PPy.

Generally, the bond lengths are shorter for most of the two-bond contacts in comparison with the one-bond contacts. This trend was also observed in the case of the H-terminated NDs.⁵⁹ For the carboxylated structures, this could be the result of less steric repulsion in the case of two-bond contacts, where two spacious carboxyl groups are missing.

Owing to the hydrogen bonds, a strong interaction is established even for the nonbonding physisorbed structures. The strongest hydrogen bonds occur between the polar amino groups of PPy and the terminating O-containing groups of ND. For the physisorbed structures, on an average, there are 2.2 hydrogen bonds per PPy–ND system. The highest number of hydrogen bonds is present in the carboxyl-terminated NDs. Considering the chemisorbed structures, the one-bond contacts are more likely to create the hydrogen bonds, owing to the feasible rotation around the one-bond structure in order to accommodate the electrostatic interactions.

The significance of hydrogen bonds was noted in the literature,^{68–70} where diamonds with hydrophilic oxygen-containing surface groups are prone to adsorb polar molecules *via* hydrogen bonding and other polar interactions. In the case of H-terminated surfaces, physisorbed bonding appears to be primarily mediated *via* van der Waals interactions. Therefore, H-terminated surfaces seem to be less likely to physisorb organic compounds due to the lack of possible polar interactions. This is in agreement with the fact that the highest binding energies are obtained for the structures terminated with O-containing groups.

For hydroxylated NDs, due to the 100% saturation of the ND surface with OH groups, the chemisorption of PPy leads to steric repulsions, resulting in the elongation of the bond lengths of the one-bond contacts. In the case of the one-bond contacts on the (111) surfaces, the covalent bonds seem to fade out. In the case of two-bond contacts, owing to the additional removal of OH groups, PPy adsorption does not cause as much steric repulsion as that in the case of one-bond contacts. Further, for two-bond contacts, the OH groups prefer to form hydrogen bonds between each other than to interact with PPy. This is also in contrast to the one-bond contacts. Otherwise, the

bond lengths of all the chemisorbed structures correspond to covalent bonds.

The optimized structures with amorphous carbon interlayers exhibit the same structural characteristics as the corresponding PPy–ND structures without the interlayer (for more details, see Fig. S9 and Table S10, ESI†). The following features are present. The establishment of hydrogen bonds between PPy and surface oxygens for the PPy–a-C:O structures, particularly for the physisorbed and one-bond-contact chemisorbed structures. The latter is relatively flexible toward rotation around the C–C bond one-bond contact in contrast with the two-bond contact. The a-C:H slabs, similar to H-terminated NDs,⁵⁹ do not participate in hydrogen bonds; therefore, the distance of PPy from a-C:H is larger than that from a-C:O.

HOMO and LUMO distribution and energies

In addition to the computed structural configurations, Fig. 1 also shows the HOMO and LUMO surfaces on several representative structures of the PPy–ND systems. All the structures are shown in Fig. S1–S9 (ESI†). It is noteworthy that highly pronounced spatial separation of the HOMO and LUMO between PPy and ND can be obtained for a predominant number of structures. The HOMO–LUMO spatial separation was not observed only on the following structures: all the OH-terminated ND structures, except for the one-bond contact on hydroxyl-terminated 2×1 (111); PPy physisorbed on peroxide-terminated 1×1 (111); two-bond contact of PPy on epoxide-terminated 2×1 (111); PPy physisorbed on carboxyl-terminated 1×1 and 2×1 (111); one-bond contact of PPy on 2×1 (100) COOH-terminated ND; two-bond contact on a-C:O ND; and all the composites of PPy with a-C:H. Regardless of the presence of the amorphous surface layer, the spatial separation between HOMO and LUMO is found mostly on NDs terminated with O-containing groups, which is in contrast to H-terminated NDs.

For most of the structures with pronounced spatial separation, the HOMO is placed along the entire PPy chain. LUMO is placed below the surface of ND at the location with the strongest interaction with PPy or at the ND edge enclosed by the oxygen-containing groups. The spatial separation of the HOMO and LUMO influences the separation of excitons and the consequent movement of charge carriers. This contributes toward the decreased probability of recombination processes and increases the efficiency of the solar cell. Therefore, this is highly interesting for PV applications.

The values of the HOMO–LUMO energy gaps of all the structures are listed in Tables S6–S10 (ESI†). The calculated HOMO–LUMO gap of the standalone PPy oligomer is 6.95 eV, which is about twice that when compared with earlier experimental^{10,11,71,72} and theoretical^{42,58} studies. Such a large HOMO–LUMO gap corresponds rather to the transport gap (E_t) than to the optical gap (E_g). A similar effect has been reported earlier in the case of π -conjugated oligomers, where E_t exceeded E_g by 2.8 eV.⁶⁴

The HOMO–LUMO gap of standalone NDs with various oxygen-containing surface groups and reconstructions is highly

variable with respect to the different surface functional groups. The bandgap values are between 3.17 and 9.81 eV. Some of the surface terminations were studied earlier by means of DFT.^{42,44,73} For most of such structures, the HOMO–LUMO gaps increase mostly due to the quantum confinement effects and larger surface-to-volume ratios, resulting in an increase in the gap with decreasing size of the ND below 2 nm.^{25,66} However, for example, the epoxide-terminated 2×1 (111) ND, the HOMO–LUMO gap of 5.21 eV is in good agreement with the bandgap of bulk diamond, with an experimentally determined value of 5.48 eV.⁷⁴ Moreover, the relative energy positions of the frontier molecular orbitals, which are of interest here, remain comparable.

After the physisorption or chemisorption of PPy, the calculated values of the HOMO–LUMO gap are in the range between 2.90 and 7.29 eV, resulting from different surface orientations, terminations, and types of bonding between PPy and ND. The reduced bandgap is mostly a result of a shift in the HOMO toward less negative energies when compared with standalone NDs. Generally, the highly variable HOMO–LUMO gap depending on particular PPy–ND structures indicates its possible tunability in devices based on PPy–ND systems.

The energy levels of HOMO and LUMO of PPy–ND systems when compared with separately calculated energy levels of PPy and NDs are shown in Fig. S10–S14 (ESI[†]).

The HOMO–LUMO gaps of different PPy–ND structures are the most variable with respect to the different surface functional groups, as also obtained for standalone NDs, while the HOMO–LUMO gaps of the PPy–ND systems within the same functional group, but with different surface reconstructions, differ only up to 2.74 eV.

For most of the structures (except amorphous NDs), the HOMO of standalone NDs is below the HOMO of standalone PPy. Moreover, for most of the structures (except OH-terminated NDs), the LUMO of standalone NDs is below the LUMO of standalone PPy. This represents a favorable arrangement for the transport of photogenerated electrons from PPy to ND; for holes, the transport is in the opposite direction. The situation at the PPy–ND junction varies depending on surface termination, facet orientation, and type of bonding. Since on a real ND, there is typically a mixture of surface functional groups, Fig. 2 shows a summary of all the calculated HOMO and LUMO energy levels of standalone PPy and NDs and those of the PPy–ND system. It should be noted that zero energy does not correspond to the vacuum energy in our calculations. The vacuum energy could be obtained by summing up the HOMO energy and ionization potential. In a notable number of cases, a favorable energy alignment promoting charge dissociation and one-directional transport is observed.

Fig. 3 shows a representative result of the relative energy positions of HOMO and LUMO in the case of COOH- and anhydride-terminated 1×1 (111) NDs. The order of the frontier molecular orbitals suggests several options for the transfer of charge carriers between PPy and ND. For all the chemisorbed structures (as shown in Fig. 3), the energy levels are favorable. After exciton generation at the interface, electrons are likely to

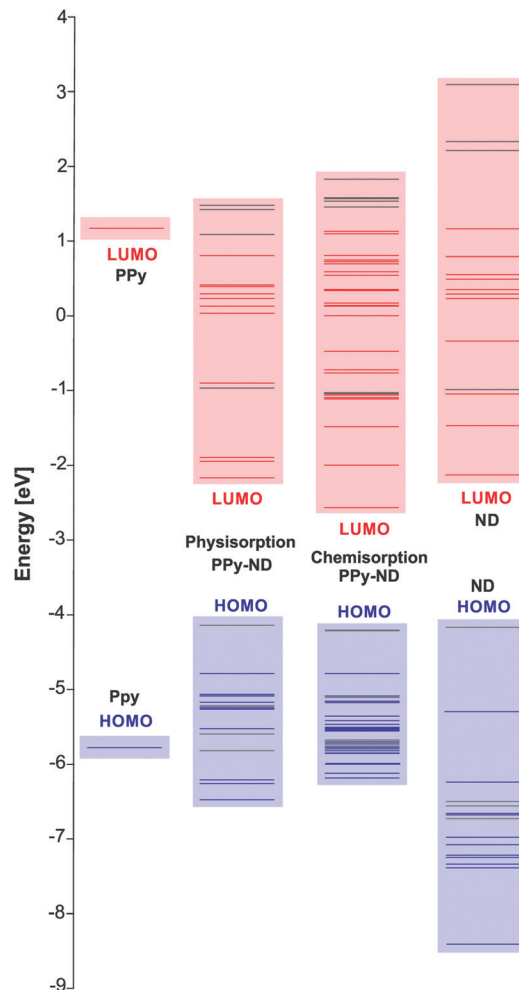


Fig. 2 Relative energy positions of HOMO (red) and LUMO (blue) energy levels for standalone PPy, physisorbed and chemisorbed PPy–ND structures, and standalone NDs. The individual energy levels in the middle and on the right correspond to the HOMO and LUMO of all the investigated structures, *i.e.*, NDs terminated with O, OH, COOH, and anhydride, as well as a-C:H and a-C:O. Energy levels in grey correspond to hydroxylated and hydrogenated NDs, where the spatial separation of HOMO and LUMO is mostly not observed.

migrate toward ND; at the same time, their migration toward PPy is blocked. Holes are likely to transfer to PPy and are blocked to transfer to ND. Such a favorable arrangement is not observed for physisorbed structures (Fig. 3). These results indicate the considerable flexibility and tunability of PPy–ND systems since the movement of charge carriers depends on the ND surface properties and the type of interaction with PPy.

In order to elucidate the pronounced effect of the PPy–ND system on the HOMO–LUMO energy levels and their spatial separations, we performed a detailed analysis of the mutual PPy and ND interaction in terms of binding energy, interaction energy, and related charge transfer in PPy–ND systems.

Binding and interaction energies

Binding energies (E_b) are related to the energy preference of the respective interactions. They can be calculated as the difference

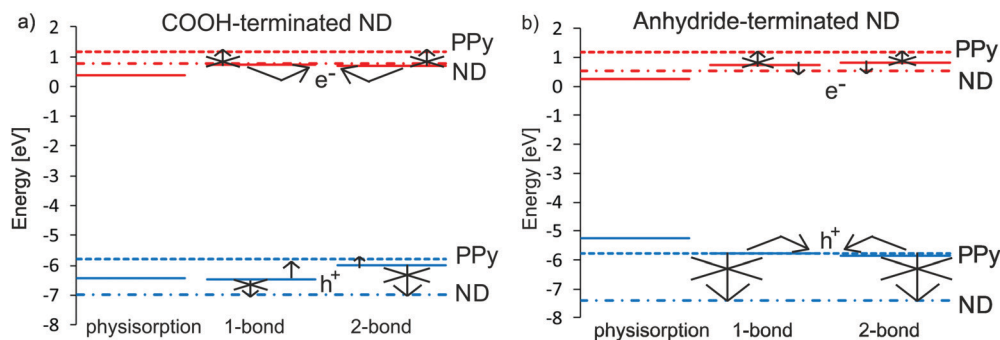


Fig. 3 Relative energy positions of HOMO (in blue) and LUMO (in red) of PPy (dashed lines), 1×1 (111) ND slabs (dot-dashed lines), and PPy physisorbed and chemisorbed (1-bond, 2-bond) on carboxylated (a) and anhydride-terminated (b) surfaces. The arrows indicate possible and blocked transport of electrons and holes in LUMO and HOMO, respectively.

in the total energies of the relaxed structures before and after contact formation. Their general formula, including all the considered ND slabs in this work, can be expressed as follows:

$$E_b = [E_{\text{slab}} + E_{\text{PPy}}] - [E_{\text{con}} + (n - 2 \cdot l) \cdot E_{\text{H}_2} + m \cdot E_{\text{O}_2} + l \cdot E_{\text{CH}_4}] \quad (1)$$

where the variable E corresponds to the total energies of the C:H slab (E_{slab}), PPy molecule (E_{PPy}), PPy-C:H structure (E_{con}), and the molecules desorbed after substitution (E_{H_2} , E_{O_2} , and E_{CH_4}); n is the number of substituted pairs of H atoms, m is the number of substituted pairs of O atoms, and l is the number of substituted C atoms, depending on the type of formed bond. Positive E_b corresponds to an exothermic process, *i.e.*, thermodynamically favorable, whereas negative value corresponds to an endothermic process.

Interaction energies (E_{int}) describing the characteristics of the bonds between PPy and ND can be calculated according to the following formula:

$$E_{\text{int}} = (E_{\text{slab-X}} + E_{\text{PPy-H}}) - E_{\text{con}} \quad (2)$$

where $E_{\text{slab-X}}$ and $E_{\text{PPy-H}}$ are the total energies of the ND slab and PPy calculated by removing the corresponding atoms from the contact region. It should be noted that for physisorbed structures, formulas (1) and (2) are coincidental.

The binding and interaction energy values for all the PPy-NDs structures are listed in Tables S6–S12 (ESI[†]). For an overview, the binding energies are graphically shown in Fig. 4 along the horizontal axis. For physisorbed and chemisorbed structures, binding energies are exothermic (positive) and endothermic (negative), respectively. This suggests that physisorbed structures are energetically favorable and more likely to be spontaneously formed in real systems. Bond formation in chemisorbed structures requires additional energy. The only exception is the exothermic one-bond contact of PPy on a-C:O ($E_b = 0.48$ eV). This highest E_b value among the chemisorbed structures correlates with one of the shortest bond lengths between ND and PPy in this study. A positive E_b value indicates that the grafting of PPy could occur spontaneously, particularly on oxidized NDs with an amorphous surface. Nevertheless, an energy barrier

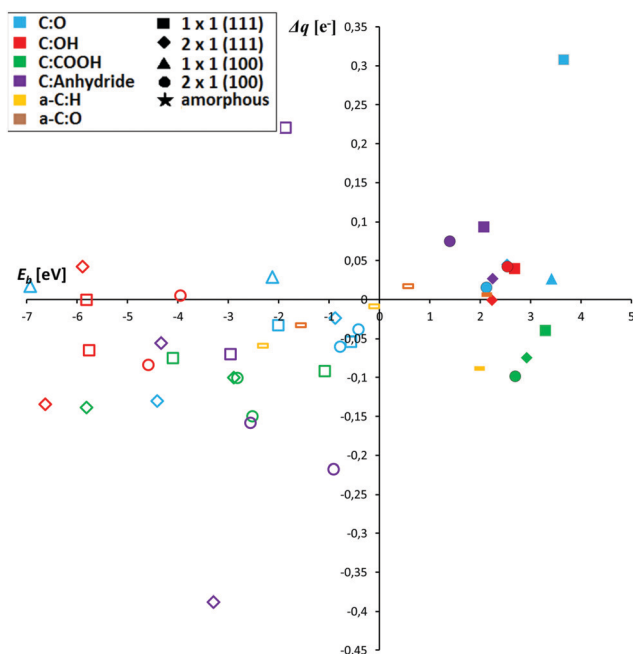


Fig. 4 Charge transfer (Δq) vs. binding energy (E_b) for PPy-ND structures. Surface chemistry is color coded; surface reconstruction is coded by symbol shapes (see the legend in the inset). Full and empty symbols correspond to physisorbed and chemisorbed structures, respectively.

corresponding to the transition state on the reaction coordinate could significantly slow down the process.

The binding energies of physisorbed PPy on NDs are in the range of 1.40 and 3.66 eV, with an average value of 2.54 eV. These are relatively high values in comparison to those of H-terminated NDs.⁵⁹ The most exothermic is the 1×1 (111) physisorbed structure of PPy on O-terminated NDs. On the other hand, when compared with the remaining O-containing ND surfaces, the lowest binding energies of the physisorbed structures are on anhydride-terminated NDs. This could be due to steric reasons: anhydride groups saturate only up to 35.7% of the ND surface. In the case of C:O surfaces, the binding energy is very dependent on the surface orientation and reconstruction. This is natural considering the preferential formation of ethers,

peroxides, epoxides, or ketones on the particular surface, as discussed in the Introduction. These different O-terminations then lead to different strengths of polar attractions and tendencies of hydrogen bond formation.

The most negative binding energies (and therefore the most endothermic and the least probable to occur) are obtained from the chemisorption of PPy on hydroxylated NDs. The most positive value of E_b for this surface termination is -3.96 eV. This is consistent with the relatively long bond lengths. The interaction energies confirm the diminishing covalent character of the one-bond contacts for these structures.

The one-bond contacts of PPy on NDs have less negative values of binding energies as compared to those of two-bond contacts (and therefore, they are more likely to form) on most of the hydroxylated, carboxylated, and H-terminated⁵⁹ NDs; however, on O-terminated NDs, the situation is the opposite. Analogous to H atoms, COOH and OH groups saturate one valence of the C atom of ND. Therefore, no dangling bond is left in the case of one-bond contacts, which is in contrast to the one-bond contacts on O-terminated NDs that leave one dangling C bond on the surface. On the O-terminated NDs, the oxygen functional groups saturate two bonds of C atoms; therefore, if these groups are not present, it is more favorable to saturate both the C atoms *via* a two-bond contact to PPy.

Considering amorphous surfaces, the binding energies are more favorable toward a-C:O in comparison with a-C:H structures for every bonding case. Again, this results from the more pronounced electrostatic interactions in a-C:O structures. Comparing hydrogenated NDs, the preference of one-bond contacts over two-bond contacts⁵⁹ is also maintained for a-C:H structures.

For most chemisorbed structures, the magnitudes of the interaction energies (Table S10, ESI†) correspond to relatively strong covalent bonds as the typical value for a C–C bond is $E_{\text{int}} = \sim 3.7$ eV.⁷⁵ The only exceptions are the one-bond contacts on hydroxylated 1×1 and 2×1 (111) NDs, where low interaction energies confirm the diminishing covalent bond indicated in the bond length analysis. After relating the interaction energy to one bond, the highest interaction energy, $E_{\text{int}} = 6.27$ eV, is obtained for one-bond contact on anhydride-terminated 2×1 (100) NDs. In this case, PPy is bent over the corner of ND and two additional strong hydrogen bonds contribute to the high E_{int} value.

With regard to physisorbed structures, the interaction energies indicate strong interactions for all the studied cases owing to the nonbonding electrostatic and van der Waals interactions.

Charge transfer

Charge transfer is another measure that reflects the mutual interaction of PPy and ND. Charge transfer can be calculated as the difference between the number of donated electrons from ND to PPy and the number of electrons donated from PPy to ND based on summing up the molecular orbitals redistributed to both these components under equilibrium.⁷⁶ Natural bond analysis of the total density was performed in order to yield coefficients and occupation numbers for the natural orbitals.

Positive charge transfer values (Δq), therefore, correspond to the net number of electrons transferred from ND to PPy and *vice versa* for negative Δq .

The values of charge transfer for all the studied structures are listed in Tables S6–S10 (ESI†). For an overview, Δq is graphically summarized along the Y-axis (Fig. 4). For H- and COOH-terminated NDs, the electrons are transferred from PPy to ND. For the remaining structures, predominantly for the physisorbed and one-bond contacts, electrons are transferred from ND to PPy and the situation is mostly opposite for two-bond contacts. The highest negative charge transfer, $\Delta q = -0.39 e^-$, is obtained for the one-bond contact of PPy on the 2×1 (111) anhydride-terminated ND, where electrons effectively transfer from PPy to ND. The highest positive charge transfer, $\Delta q = 0.31 e^-$, is obtained for PPy physisorbed on 1×1 (111) O-terminated ND, where electrons effectively transfer from ND to PPy. Nevertheless, in general, both directions of charge transfer are possible for both chemisorbed and physisorbed structures. Fig. 4 shows that charge transfer is independent of binding energy. However, for physisorbed structures, Δq appears to be divided according to the surface functional groups. The dependencies of various binding and electronic parameters are shown in Fig. S15–S20 (ESI†). There are no significant correlations observed.

One of the smallest absolute values of charge transfer is obtained for amorphous and OH-terminated NDs (within 0.04 and $0.05 e^-$, respectively). In comparison with the remaining structures, OH-terminated NDs, therefore, show the least favorable characteristics. Further, their binding energies are the least favorable, particularly considering the chemisorbed structures. The drawback of the OH-terminated NDs was already pointed out in the literature. It has small negative electron affinity and a lack of surface-related unoccupied electronic states and could be successfully transfer-doped only with an adsorbate molecule with very high electron affinity.⁷³

Table S10 (ESI†) lists the values of the charge transfer for NDs with an amorphous surface layer. The highest value ($-0.12 e^-$) is obtained for the one-bond contact on a-C:O. On average, similar values of charge transfer are obtained for the a-C:H structures as those for H-terminated NDs,⁵⁹ both of which indicate electron transfer from PPy to ND. Furthermore, the values of charge transfer are lower for a-C:H NDs than the corresponding a-C:O NDs, which is consistent with the trend observed in NDs without an amorphous surface interlayer.

Conclusions

DFT calculations were employed to describe the interactions between PPy and NDs terminated with various oxygen surface functional groups or terminated with oxidized or hydrogenated amorphous carbon surface layers. We investigated the PPy interaction under both physisorbed (noncovalent) and chemisorbed (covalently grafted) conditions. All the different nonequivalent initial PPy–ND configurations geometrically relaxed to the structures that are presented in this work, and therefore, correspond to the global energy minima. The bonding characteristic

between PPy and ND was confirmed by the analysis of the interaction energies. A detailed analysis revealed a strong mutual interaction (in terms of binding energy, interaction energy, and charge transfer) not only for covalently grafted PPy to ND, but even larger between PPy and ND in the physisorbed configurations due to the formation of multiple hydrogen bonds (H ··· O bridges).

Under both physisorbed and chemisorbed PPy configurations, the computed results revealed that HOMO and LUMO are highly spatially separated in all the PPy–ND systems. For most of the structures, HOMO is positioned on PPy and LUMO on ND. This is the predominant effect on all the oxidized NDs. Diamond would, therefore, act as an electron acceptor. Interestingly, separation does not occur on H- and OH-terminated NDs (with one exception). The spatial separation persists even on NDs with an amorphous carbon interlayer, the closest structure to real ND materials. The analysis involving energy levels showed that HOMO and LUMO energy levels are favorably aligned for exciton dissociation in PPy–ND composites. The spatial separation and energy alignment may be beneficial for PV applications of PPy–ND systems. The observed effects can most likely be generalized also for interactions with other organic molecules (dyes, donor–acceptor molecules, proteins, etc.).

Conflicts of interest

There are no conflicts to declare.

Acknowledgements

We acknowledge financial support from the Czech Science Foundation project GACR 15-01809S, CVUT student project SGS18/179/OHK4/3T/13, European Regional Development Fund project CZ.02.1.01/0.0/0.0/15_003/0000464, and COST Action MP1307 StableNextSol. Computational resources were provided by the CESNET LM2015042 and the CERIT Scientific Cloud LM2015085 under the program “Projects of Large Research, Development, and Innovations Infrastructures.” A kind support of Prof. A. Holleitner is also gratefully appreciated.

Notes and references

- M. A. Green, K. Emery, Y. Hishikawa, W. Warta, E. D. Dunlop, D. H. Levi and A. W. Y. Ho-Baillie, *Prog. Photovoltaics*, 2017, **25**, 3–13.
- S. Mori, H. Oh-oka, H. Nakao, T. Gotanda, Y. Nakano, H. Jung, A. Iida, R. Hayase, N. Shida, M. Saito, K. Todorii, T. Asakura, A. Matsui and M. Hosoya, *MRS Online Proc. Libr. Arch.*, 2015, 1737.
- P. Roy and P. T. Nguyen, *Phys. Chem. Chem. Phys.*, 2016, **18**, 18209–18218.
- O. V. Kontkanen, M. Niskanen, T. I. Hukka and T. T. Rantala, *Phys. Chem. Chem. Phys.*, 2016, **18**, 14382–14389.
- A. Krueger, *Adv. Mater.*, 2008, **20**, 2445–2449.
- M. Anafcheh, R. Ghafouri and N. L. Hadipour, *Sol. Energy Mater. Sol. Cells*, 2012, **105**, 125–131.
- H. Zhu, J. Wei, K. Wang and D. Wu, *Sol. Energy Mater. Sol. Cells*, 2009, **93**, 1461–1470.
- S. Collavini and J. L. Delgado, *Adv. Energy Mater.*, 2017, **7**, 1601000.
- T. V. Vernitskaya and O. N. Efimov, *Russ. Chem. Rev.*, 1997, **66**, 443–457.
- B. Rezek, J. Čermák, A. Kromka, M. Ledinský and J. Kočka, *Diamond Relat. Mater.*, 2009, **18**, 249–252.
- R. K. John and D. S. Kumar, *J. Appl. Polym. Sci.*, 2002, **83**, 1856–1859.
- P. Galář, J. Čermák, P. Malý, A. Kromka and B. Rezek, *J. Appl. Phys.*, 2014, **116**, 223103.
- B. Rezek, J. Čermák, A. Kromka, M. Ledinský, P. Hubík, J. J. Mareš, A. Purkrt, V. Cimrová, A. Fejfar and J. Kočka, *Nanoscale Res. Lett.*, 2011, **6**, 1–12.
- D. Miliáieva, S. Stehlik, P. Stenclova and B. Rezek, *Phys. Status Solidi A*, 2016, **213**, 2687–2692.
- J. S. Shaikh, N. S. Shaikh, S. S. Mali, J. V. Patil, K. K. Pawar, P. Kanjanaboos, C. K. Hong, J. H. Kim and P. S. Patil, *Nanoscale*, 2018, **10**, 4987–5034.
- S. Honda, H. Ohkita, H. Benten and S. Ito, *Adv. Energy Mater.*, 2011, **1**, 588–598.
- S. V. Kesava, Z. Fei, A. D. Rimshaw, C. Wang, A. Hexemer, J. B. Asbury, M. Heeney and E. D. Gomez, *Adv. Energy Mater.*, 2014, **4**, 1400116.
- Z. Shpilman, I. Gouzman, E. Grossman, L. Shen, T. K. Minton, J. T. Paci, G. C. Schatz, R. Akhvediani and A. Hoffman, *J. Phys. Chem. C*, 2010, **114**, 18996–19003.
- A. Krueger, *J. Mater. Chem.*, 2008, **18**, 1485.
- M. Frenklach, R. Kematick, D. Huang, W. Howard, K. E. Spear, A. W. Phelps and R. Koba, *J. Appl. Phys.*, 1989, **66**, 395–399.
- S. Stehlik, M. Varga, P. Stenclova, L. Ondic, M. Ledinsky, J. Pangrac, O. Vanek, J. Lipov, A. Kromka and B. Rezek, *ACS Appl. Mater. Interfaces*, 2017, **9**, 38842–38853.
- A. K. Tiwari, J. P. Goss, P. R. Briddon, N. G. Wright, A. B. Horsfall, R. Jones, H. Pinto and M. J. Rayson, *Phys. Rev. B: Condens. Matter Mater. Phys.*, 2011, 84.
- T. Kondo, I. Neitzel, V. N. Mochalin, J. Urai, M. Yuasa and Y. Gogotsi, *J. Appl. Phys.*, 2013, **113**, 214307.
- F. Maier, J. Ristein and L. Ley, *Phys. Rev. B: Condens. Matter Mater. Phys.*, 2001, 64.
- A. S. Barnard, *Nanotechnology*, 2013, **24**, 085703.
- A. Datta, M. Kirca, Y. Fu and A. C. To, *Nanotechnology*, 2011, **22**, 065706.
- O. A. Shenderova and G. E. McGuire, *Biointerphases*, 2015, **10**, 030802.
- D. Petrini and K. Larsson, *J. Phys. Chem. C*, 2008, **112**, 3018–3026.
- D. Petrini and K. Larsson, *J. Phys. Chem. C*, 2007, **111**, 795–801.
- S. L. Y. Chang, A. S. Barnard, C. Dwyer, C. B. Boothroyd, R. K. Hocking, E. Osawa and R. J. Nicholls, *Nanoscale*, 2016, **8**, 10548–10552.

- 31 S. Skokov, B. Weiner and M. Frenklach, *Phys. Rev. B: Condens. Matter Mater. Phys.*, 1997, **55**, 1895.
- 32 Z. G. Wang, X. T. Zu, J. L. Nie and H. Y. Xiao, *Surf. Rev. Lett.*, 2006, **13**, 45–49.
- 33 H. Tamura, H. Zhou, K. Sugisako, Y. Yokoi, S. Takami, M. Kubo, K. Teraishi, A. Miyamoto, A. Imamura and N. Mikka, *et al.*, *Phys. Rev. B: Condens. Matter Mater. Phys.*, 2000, **61**, 11025.
- 34 X. M. Zheng and P. V. Smith, *Surf. Sci.*, 1992, **262**, 219–234.
- 35 L. Lai and A. S. Barnard, *Nanoscale*, 2011, **3**, 2566.
- 36 L. Lai and A. S. Barnard, *J. Mater. Chem.*, 2012, **22**, 16774.
- 37 S. Goverapet Srinivasan and A. C. T. van Duin, *Carbon*, 2015, **82**, 314–326.
- 38 S. Moustafa, N. Tokuda and T. Inokuma, *Jpn. J. Appl. Phys.*, 2014, **53**, 02BD01.
- 39 M. J. Rutter and J. Robertson, *Phys. Rev. B: Condens. Matter Mater. Phys.*, 1998, **57**, 9241.
- 40 C. Stampfl, T. E. Derry and N. W. Makau, *J. Phys.: Condens. Matter*, 2010, **22**, 475005.
- 41 H. Yang, L. Xu, C. Gu and S. B. Zhang, *Appl. Surf. Sci.*, 2007, **253**, 4260–4266.
- 42 R. Long, Y. Dai and M. Guo, *Appl. Surf. Sci.*, 2008, **254**, 2851–2855.
- 43 T. E. Derry, N. W. Makau and C. Stampfl, *J. Phys.: Condens. Matter*, 2010, **22**, 265007.
- 44 N. Brown and O. Hod, *J. Phys. Chem. C*, 2014, **118**, 5530–5537.
- 45 J. L. Whitten, P. Cremaschi, R. E. Thomas, R. A. Rudder and R. J. Markunas, *Appl. Surf. Sci.*, 1994, **75**, 45–50.
- 46 V. Jirásek, H. Kozak and Z. Remeš, *Adv. Sci., Eng. Med.*, 2015, **7**, 275–278.
- 47 P. John, N. Polwart, C. E. Troupe and J. I. B. Wilson, *Diamond Relat. Mater.*, 2002, **11**, 861–866.
- 48 K. P. Loh, X. N. Xie, Y. H. Lim, E. J. Teo, J. C. Zheng and T. Ando, *Surf. Sci.*, 2002, **505**, 93–114.
- 49 K. Bobrov, H. Shechter, A. Hoffman and M. Folman, *Appl. Surf. Sci.*, 2002, **196**, 173–180.
- 50 F. K. de Theije, M. F. Reedijk, J. Arsic, W. J. P. van Enkevort and E. Vlieg, *Phys. Rev. B: Condens. Matter Mater. Phys.*, 2001, **64**.
- 51 F. K. de Theije, N. J. van der Laag, M. Plomp and W. J. P. van Enkevort, *Philos. Mag. A*, 2000, **80**, 725–745.
- 52 P. E. Pehrsson, T. W. Mercer and J. A. Chaney, *Surf. Sci.*, 2002, **497**, 13–28.
- 53 X. Wang, A. R. Ruslinda, Y. Ishiyama, Y. Ishii and H. Kawarada, *Diamond Relat. Mater.*, 2011, **20**, 1319–1324.
- 54 B. Dzurňák, F. Trojánek, J. Preclíková, A. Kromka, B. Rezek and P. Malý, *Diamond Relat. Mater.*, 2011, **20**, 1155–1159.
- 55 S. Zhao and K. Larsson, *J. Phys. Chem. C*, 2014, **118**, 1944–1957.
- 56 Y. Tian and K. Larsson, Process of Diamond Surface Termination by Carboxylic and Amino groups – A Quantum Mechanics Approach. <http://www.diva-portal.org/smash/record.jsf?pid=diva2:765999>, 2014 (accessed January 18, 2017).
- 57 L. Lai and A. S. Barnard, *Nanoscale*, 2014, **6**, 14185–14189.
- 58 W. Kamiński, V. Rozsival and P. Jelínek, *J. Phys.: Condens. Matter*, 2010, **22**, 045003.
- 59 P. Matunová, V. Jirásek and B. Rezek, *Phys. Status Solidi A*, 2016, **213**, 2672–2679.
- 60 P. Matunová, V. Jirásek and B. Rezek, Proc. 8th Int. Conf. Nanocon, 2017, pp. 15–19.
- 61 T. Ando, K. Yamamoto, M. Ishii and Y. Sato, *J. Chem. Soc., Faraday Trans.*, 1993, **89**, 3635–3640.
- 62 M. J. Frisch, G. W. Trucks, H. B. Schlegel, G. E. Scuseria, M. A. Robb, J. R. Cheeseman, G. Scalmani, V. Barone, G. A. Petersson, H. Nakatsuji, X. Li, M. Caricato, A. V. Marenich, J. Bloino, B. G. Janesko, R. Gomperts, B. Mennucci, H. P. Hratchian, J. V. Ortiz, A. F. Izmaylov, J. L. Sonnenberg, D. Williams-Young, F. Ding, F. Lipparini, F. Egidi, J. Goings, B. Peng, A. Petrone, T. Henderson, D. Ranasinghe, V. G. Zakrzewski, J. Gao, N. Rega, G. Zheng, W. Liang, M. Hada, M. Ehara, K. Toyota, R. Fukuda, J. Hasegawa, M. Ishida, T. Nakajima, Y. Honda, O. Kitao, H. Nakai, T. Vreven, K. Throssell, J. A. Montgomery Jr., J. E. Peralta, F. Ogliaro, M. J. Bearpark, J. J. Heyd, E. N. Brothers, K. N. Kudin, V. N. Staroverov, T. A. Keith, R. Kobayashi, J. Normand, K. Raghavachari, A. P. Rendell, J. C. Burant, S. S. Iyengar, J. Tomasi, M. Cossi, J. M. Millam, M. Klene, C. Adamo, R. Cammi, J. W. Ochterski, R. L. Martin, K. Morokuma, O. Farkas, J. B. Foresman and D. J. Fox, *Gaussian 09 (Revision E.01)*, Gaussian Inc., Wallingford CT, 2016.
- 63 J.-D. Chai and M. Head-Gordon, *Phys. Chem. Chem. Phys.*, 2008, **10**, 6615–6620.
- 64 U. Salzner and A. Aydin, *J. Chem. Theory Comput.*, 2011, **7**, 2568–2583.
- 65 S. Stehlik, M. Varga, M. Ledinsky, D. Miliaieva, H. Kozak, V. Skakalova, C. Mangler, T. J. Pencycook, J. C. Meyer, A. Kromka and B. Rezek, *Sci. Rep.*, 2016, **6**.
- 66 T. Frauenheim, T. Köhler, M. Sternberg, D. Porezag and M. R. Pederson, *Thin Solid Films*, 1996, **272**, 314–330.
- 67 T. Yuan and K. Larsson, *J. Phys. Chem. C*, 2014, **118**, 26061–26069.
- 68 D. Steinmullernethl, F. Kloss, M. Najamulhaq, M. Rainer, K. Larsson, C. Linsmeier, G. Kohler, C. Fehrer, G. Lepperdinger and X. Liu, *Biomaterials*, 2006, **27**, 4547–4556.
- 69 B. Rezek, D. Shin, T. Nakamura and C. E. Nebel, *J. Am. Chem. Soc.*, 2006, **128**, 3884–3885.
- 70 G. P. Bogatyreva, M. A. Marinich, E. V. Ishchenko, V. L. Gvyazdovskaya and G. A. Bazalij, *Sverkhverd. Mater.*, 2002, **10–15**.
- 71 J. L. Brédas, B. Thémans, J. G. Fripiat, J. M. André and R. R. Chance, *Phys. Rev. B: Condens. Matter Mater. Phys.*, 1984, **29**, 6761–6773.
- 72 L. Micaroni, F. Nart and I. Hümmelgen, *J. Solid State Electrochem.*, 2002, **7**, 55–59.
- 73 S. J. Sque, R. Jones and P. R. Briddon, *Phys. Rev. B: Condens. Matter Mater. Phys.*, 2006, **73**.
- 74 D. Bimberg, *Physics of Group IV Elements and III-V Compounds*, Springer, 1982.
- 75 J. M. Berg, J. L. Tymoczko, L. Stryer, J. M. Berg, J. L. Tymoczko and L. Stryer, *Biochemistry*, W. H. Freeman, New York, 5th edn, 2002.
- 76 S. Dapprich and G. Frenking, *J. Phys. Chem.*, 1995, **99**, 9352–9362.

Supplementary Information

DFT Calculations Reveal Pronounced HOMO-LUMO Spatial Separation in Polypyrrole-Nanodiamond System

Petra Matunová*, Vít Jirásek, Bohuslav Rezek

Figure S1: Optimized structures of PPy on O-terminated 1×1 (111) ND edge slab: physisorbed HOMO (a) and LUMO (b), one-bond contact HOMO (c) and LUMO (d), two-bond contact HOMO (e) and LUMO (f). Optimized structures of PPy on O-terminated 2×1 (111) ND edge slab: physisorbed HOMO (g) and LUMO (h), one-bond contact HOMO (i) and LUMO (j), two-bond contact HOMO (k) and LUMO (l). C atoms are grey, H atoms white, O atoms red, N atoms blue. Red and green clouds indicate positive and negative value of the orbital surfaces at the isovalue of $0.01e^{-\text{Å}^{-3}}$.

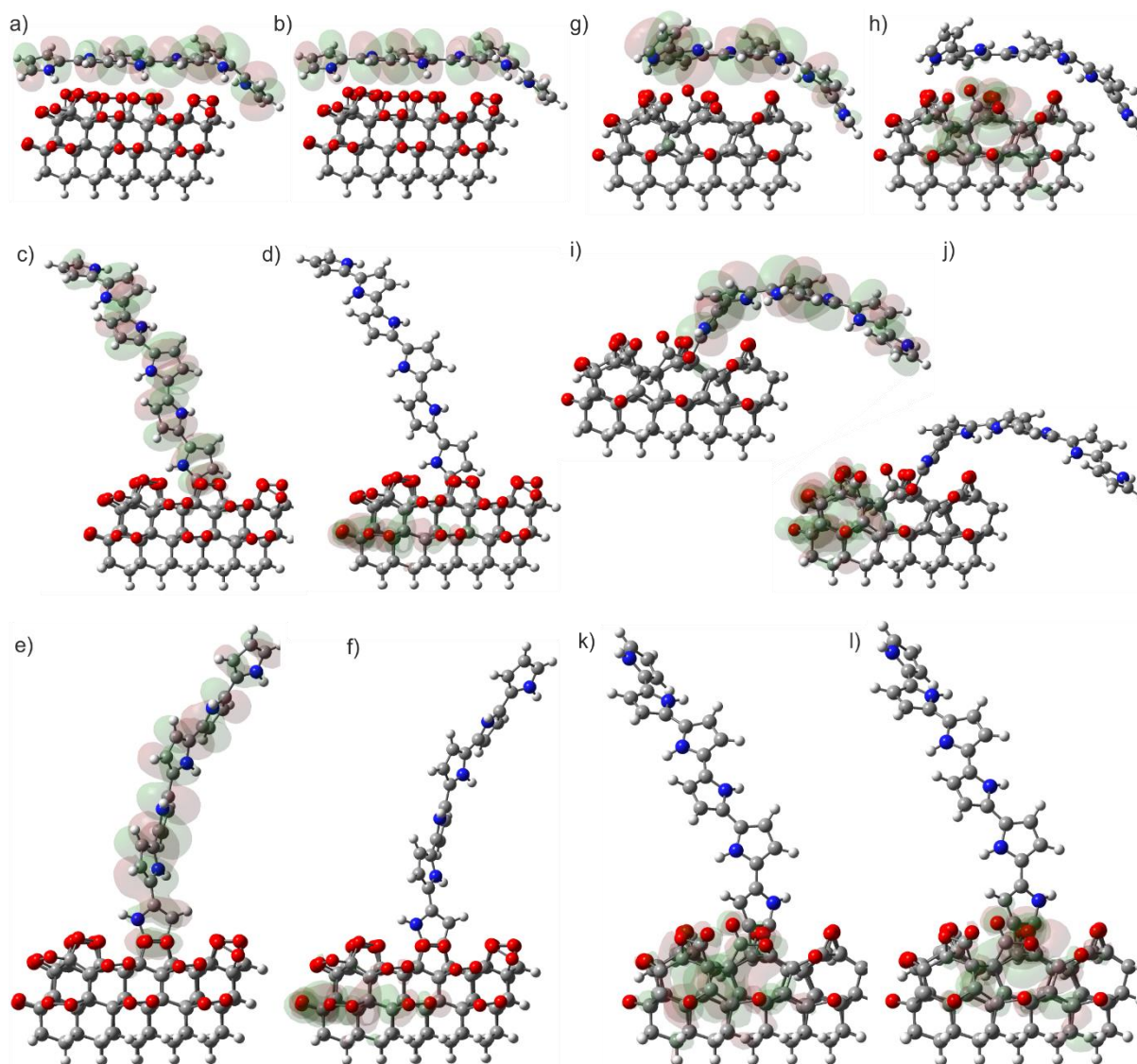


Figure S2: Optimized structures of **PPy** on **O-terminated 1×1 (100) ND edge slab**: physisorbed HOMO (a) and LUMO (b), one-bond contact HOMO (c) and LUMO (d), two-bond contact HOMO (e) and LUMO (f). Optimized structures of **PPy** on **O-terminated 2×1 (100) ND edge slab**: physisorbed HOMO (g) and LUMO (h), one-bond contact HOMO (i) and LUMO (j), two-bond contact HOMO (k) and LUMO (l). C atoms are grey, H atoms white, O atoms red, N atoms blue. Red and green clouds indicate positive and negative value of the orbital surfaces at the isovalue of $0.01e^{-\text{\AA}^{-3}}$.

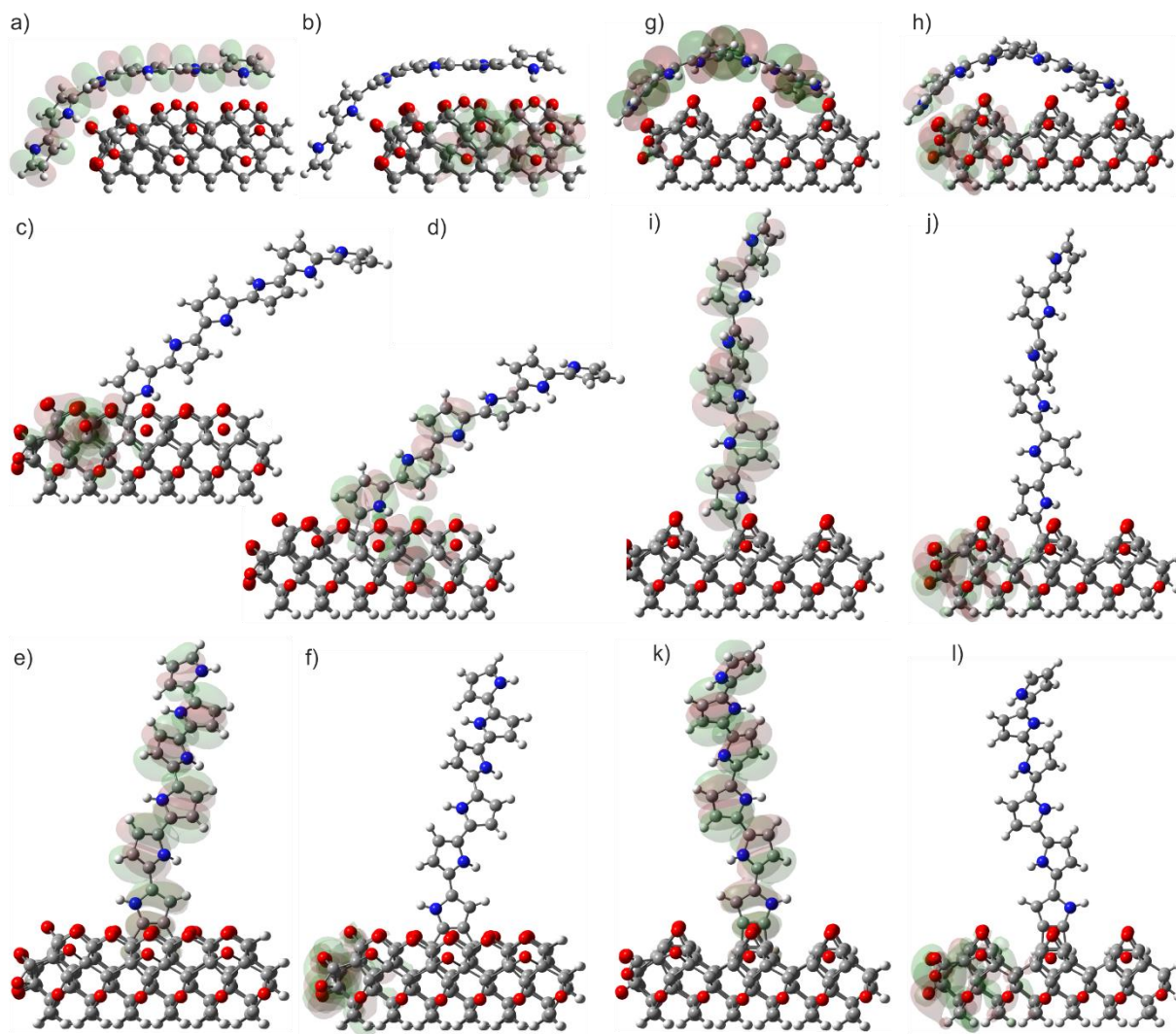


Figure S3: Optimized structures of **PPy** on **OH-terminated 1×1 (111) ND edge slab**: physisorbed HOMO (a) and LUMO (b), one-bond contact HOMO (c) and LUMO (d), two-bond contact HOMO (e) and LUMO (f). Optimized structures of **PPy** on **OH-terminated 2×1 (111) ND edge slab**: physisorbed HOMO (g) and LUMO (h), one-bond contact HOMO (i) and LUMO (j), two-bond contact HOMO (k) and LUMO (l). C atoms are grey, H atoms white, O atoms red, N atoms blue. Red and green clouds indicate positive and negative value of the orbital surfaces at the isovalue of $0.01e^{-\text{\AA}^{-3}}$.

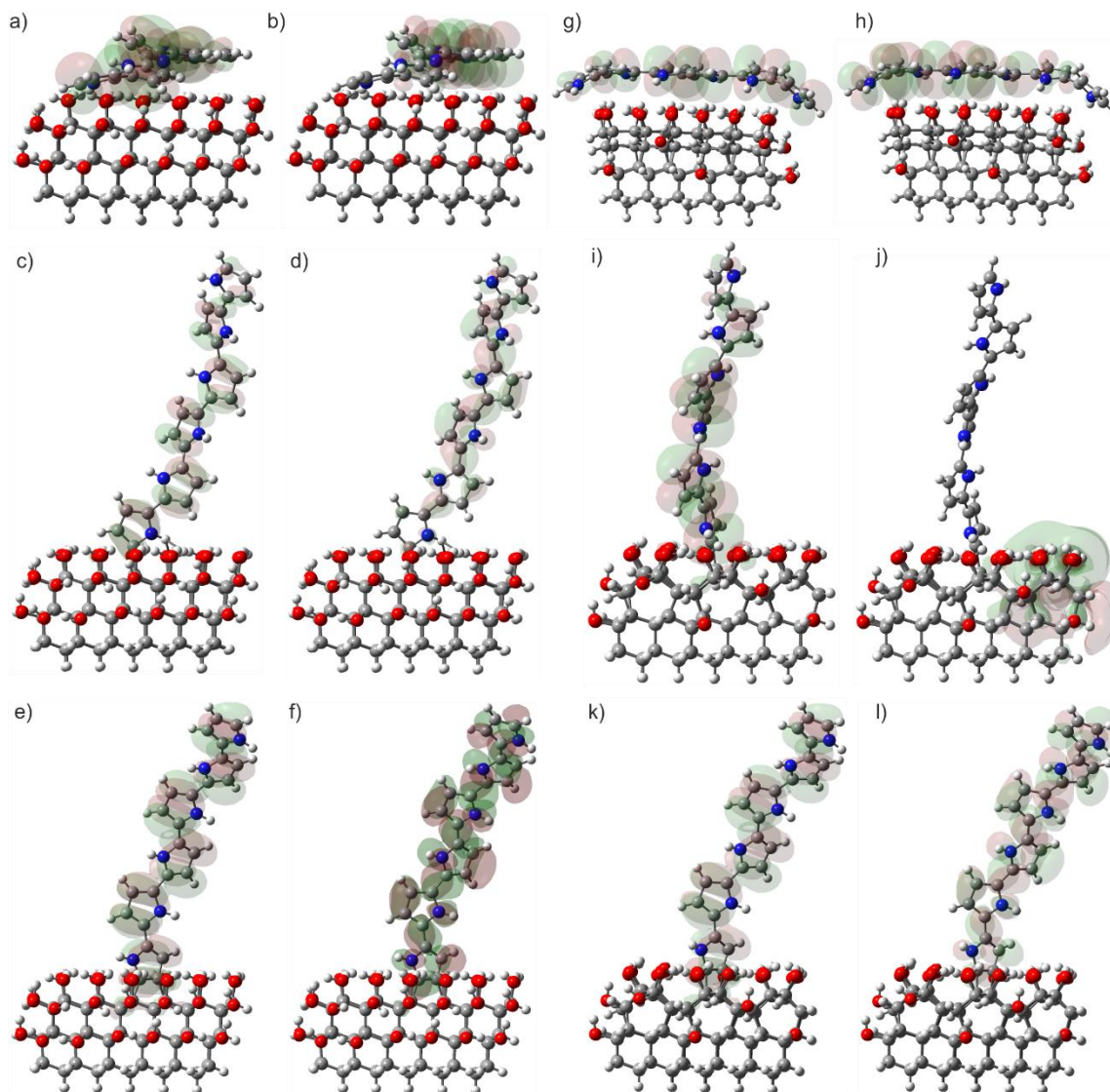


Figure S4: Optimized structures of **PPy on OH-terminated 2×1 (100) ND edge slab:** physisorbed HOMO (a) and LUMO (b), one-bond contact HOMO (c) and LUMO (d), two-bond contact HOMO (e) and LUMO (f). C atoms are grey, H atoms white, O atoms red, N atoms blue. Red and green clouds indicate positive and negative value of the orbital surfaces at the isovalue of $0.01e^{-\text{\AA}^{-3}}$.

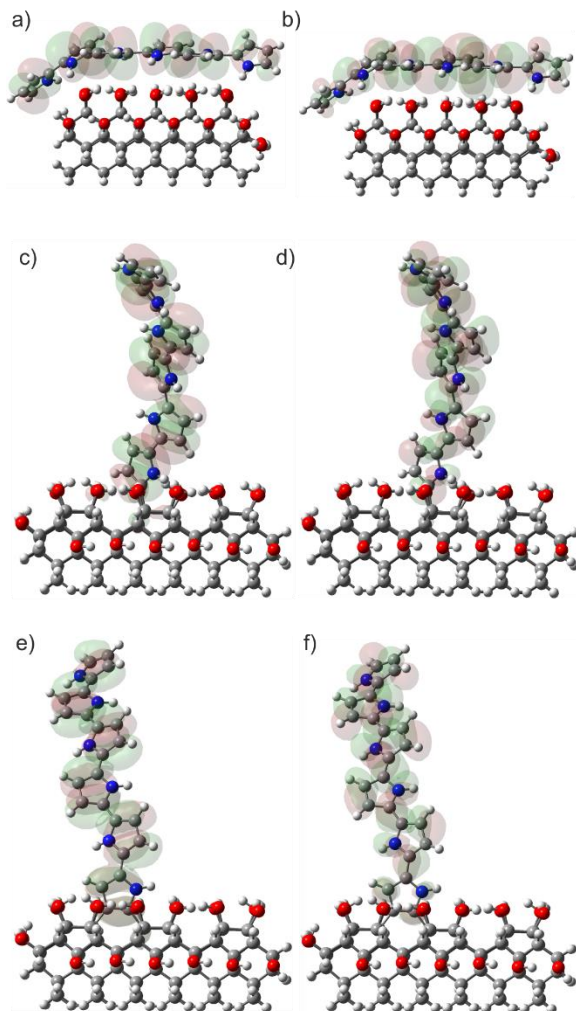


Figure S5: Optimized structures of **PPy** on **COOH-terminated 1×1 (111) ND edge slab**: physisorbed HOMO (a) and LUMO (b), one-bond contact HOMO (c) and LUMO (d), two-bond contact HOMO (e) and LUMO (f). Optimized structures of **PPy** on **COOH-terminated 2×1 (111) ND edge slab**: physisorbed HOMO (g) and LUMO (h), one-bond contact HOMO (i) and LUMO (j), two-bond contact HOMO (k) and LUMO (l). C atoms are grey, H atoms white, O atoms red, N atoms blue. Red and green clouds indicate positive and negative value of the orbital surfaces at the isovalue of $0.01e^{-\text{\AA}^{-3}}$.

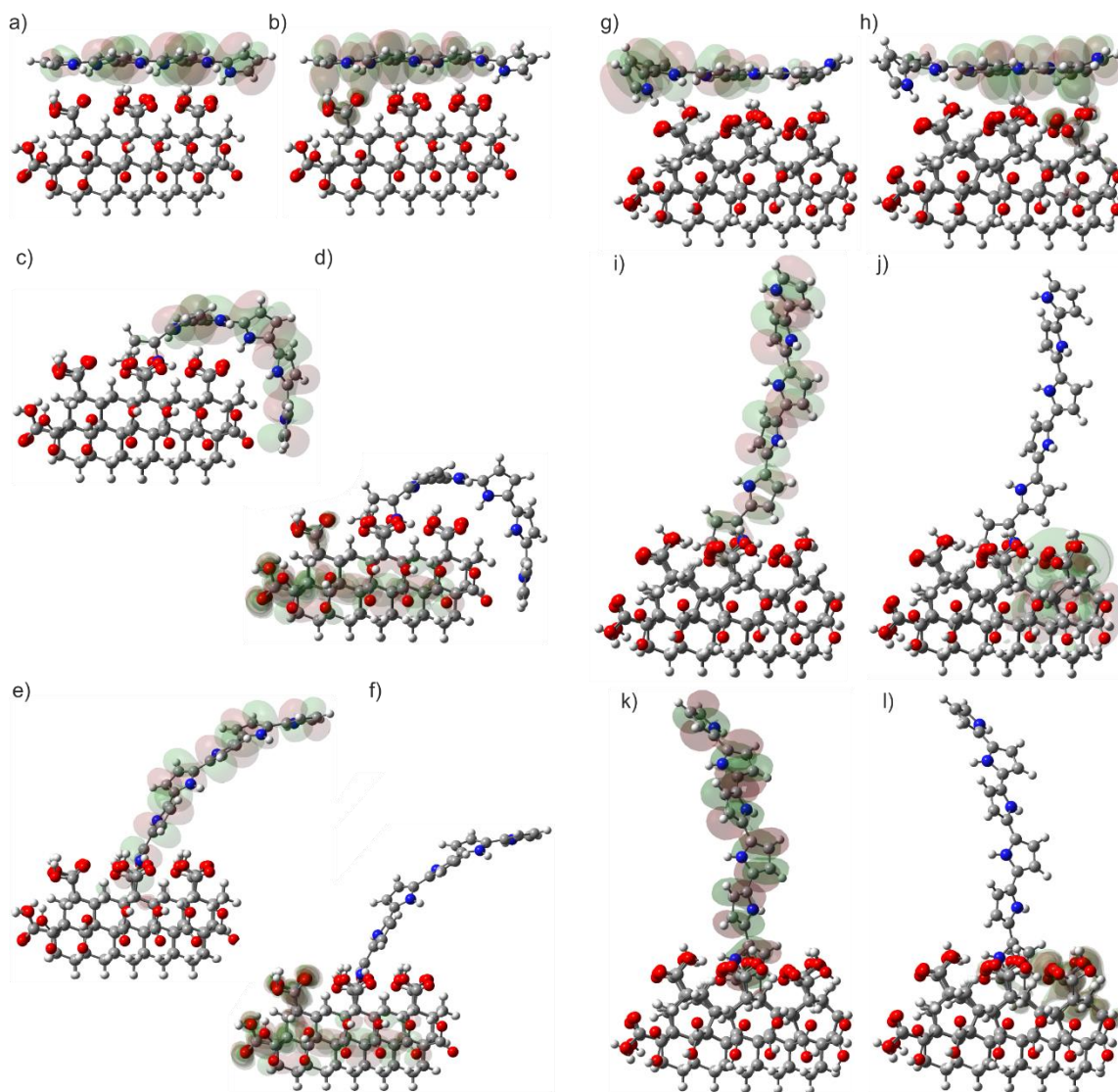


Figure S6: Optimized structures of PPy on COOH-terminated 2×1 (100) ND edge slab: physisorbed HOMO (a) and LUMO (b), one-bond contact HOMO (c) and LUMO (d), two-bond contact HOMO (e) and LUMO (f). C atoms are grey, H atoms white, O atoms red, N atoms blue. Red and green clouds indicate positive and negative value of the orbital surfaces at the isovalue of $0.01e^{-\text{\AA}^{-3}}$.

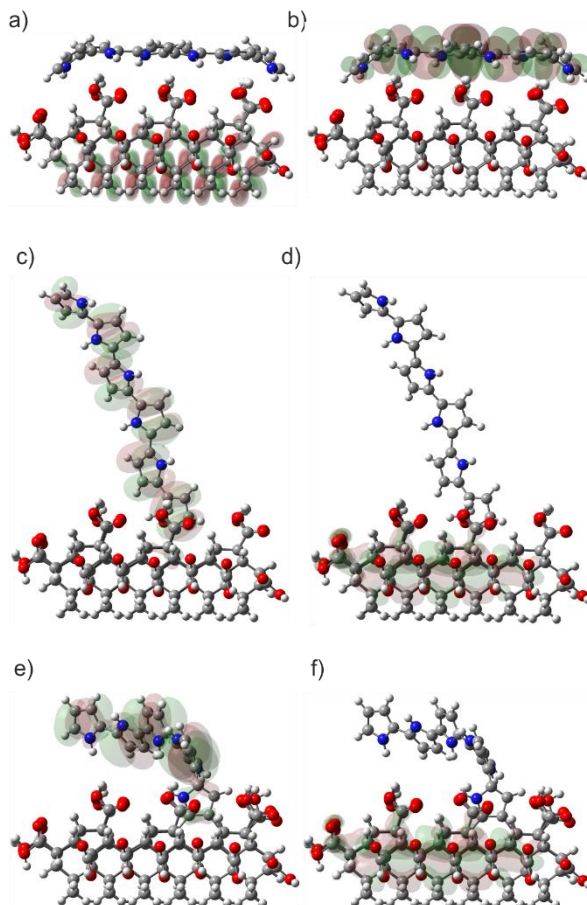


Figure S7: Optimized structures of **PPy** on **anhydride-terminated 1×1 (111) ND edge slab**: physisorbed HOMO (a) and LUMO (b), one-bond contact HOMO (c) and LUMO (d), two-bond contact HOMO (e) and LUMO (f). Optimized structures of **PPy** on **anhydride-terminated 2×1 (111) ND edge slab**: physisorbed HOMO (g) and LUMO (h), one-bond contact HOMO (i) and LUMO (j), two-bond contact HOMO (k) and LUMO (l). C atoms are grey, H atoms white, O atoms red, N atoms blue. Red and green clouds indicate positive and negative value of the orbital surfaces at the isovalue of $0.01e^{-\text{\AA}^{-3}}$.

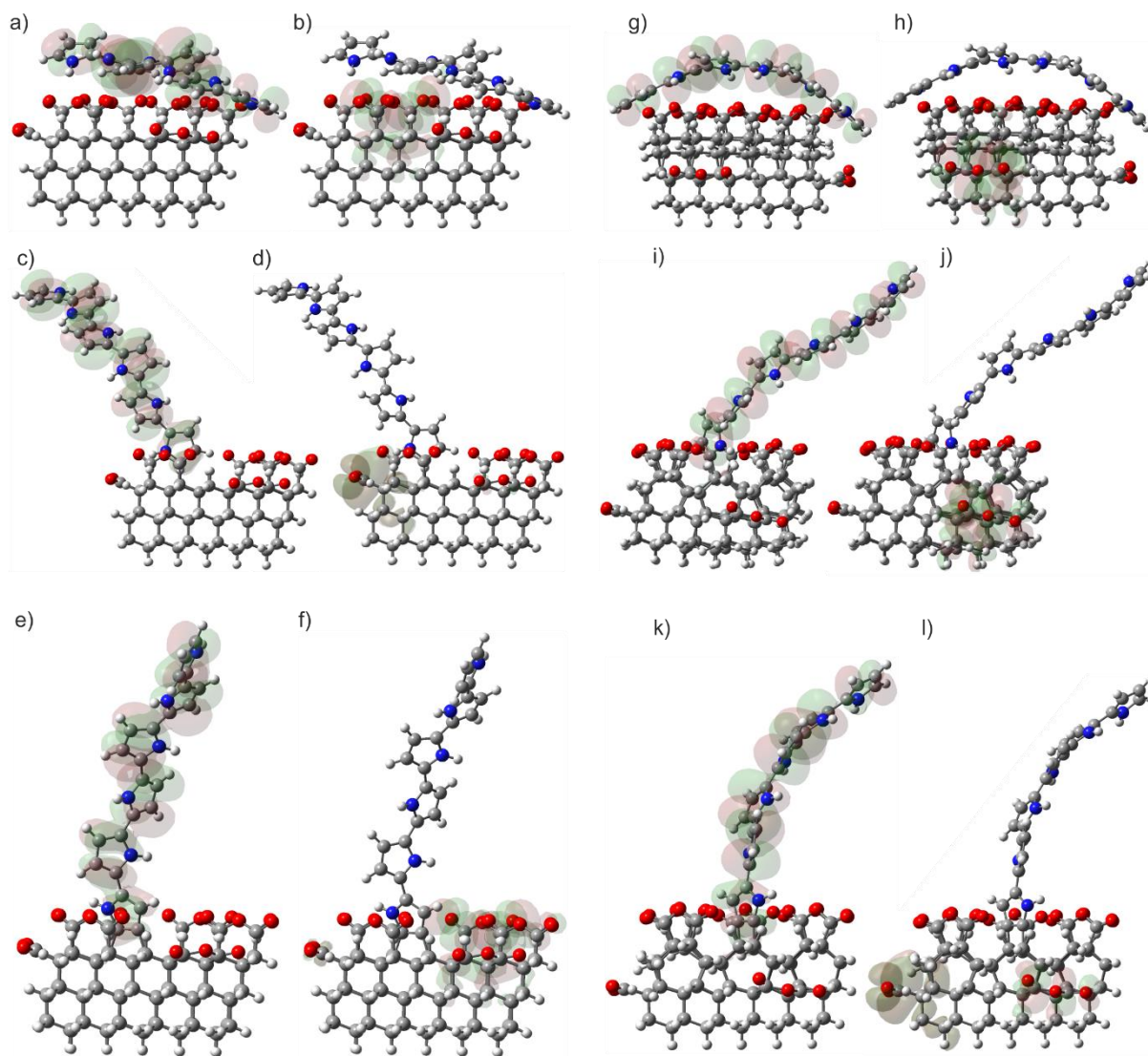


Figure S8: Optimized structures of PPy on anhydride-terminated 2×1 (100) ND edge slab: physisorbed HOMO (a) and LUMO (b), one-bond contact HOMO (c) and LUMO (d), two-bond contact HOMO (e) and LUMO (f). C atoms are grey, H atoms white, O atoms red, N atoms blue. Red and green clouds indicate positive and negative value of the orbital surfaces at the isovalue of $0.01e^{-\text{\AA}^{-3}}$.

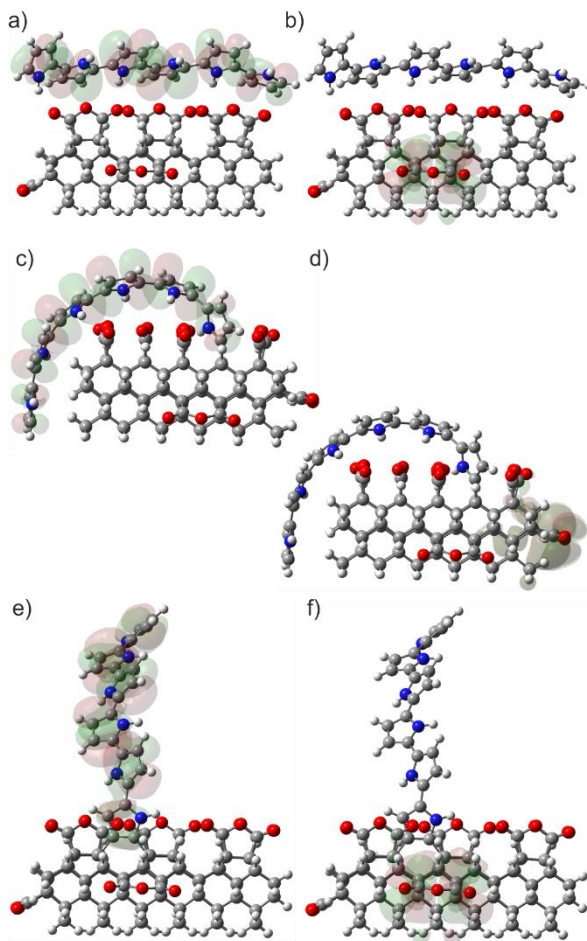


Figure S9: Optimized structures of **PPy on a-C:H ND edge slab**: physisorbed HOMO (a) and LUMO (b), one-bond contact HOMO (c) and LUMO (d), two-bond contact HOMO (e) and LUMO (f). Optimized structures of **PPy on a-C:O ND edge slab**: physisorbed HOMO (g) and LUMO (h), one-bond contact HOMO (i) and LUMO (j), two-bond contact HOMO (k) and LUMO (l). C atoms are grey, H atoms white, O atoms red, N atoms blue. Red and green clouds indicate positive and negative value of the orbital surfaces at the isovalue of $0.01e^{-\text{\AA}^{-3}}$.

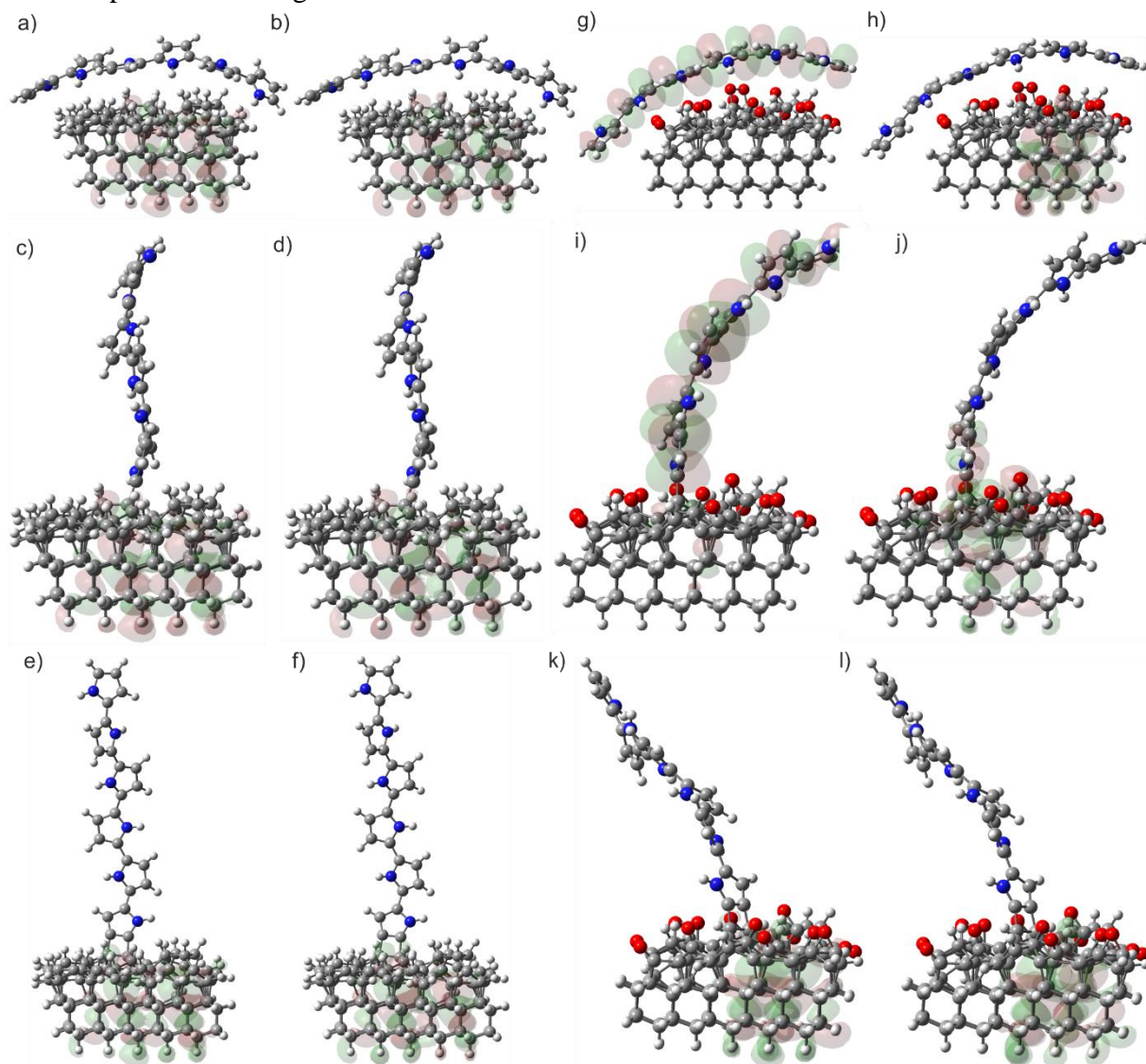


Figure S10: HOMO (blue) and LUMO (red) energy levels of i) **standalone PPy** (dashed lines), ii) standalone O-terminated ND slabs (dot-and-dashed lines), and iii) **PPy physisorbed or chemisorbed** (1-bond, 2-bond) **on O-terminated ND** (full lines) in the case of 1×1 (111) (a), 2×1 (111) (b), 1×1 (100) (c), and 2×1 (100) (d) ND slabs.

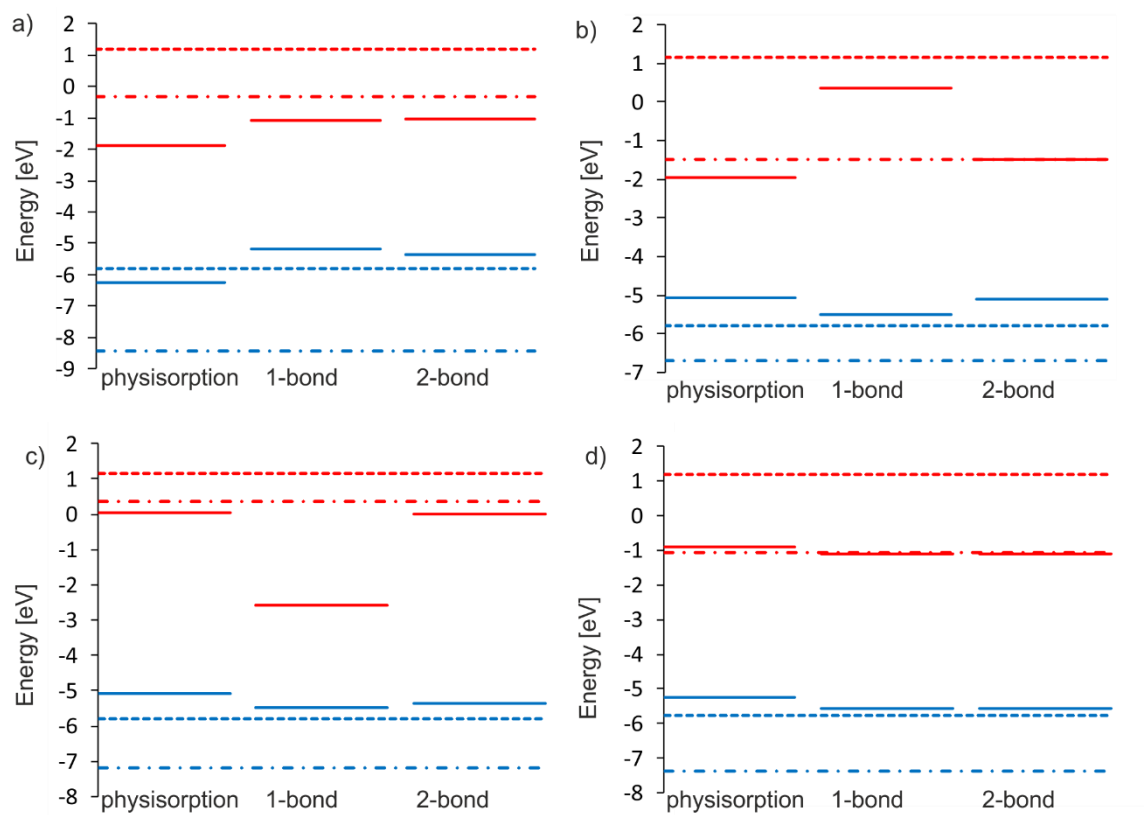


Figure S11: HOMO (blue) and LUMO (red) energy levels of i) **standalone PPy** (dashed lines), ii) **standalone OH-terminated ND slabs** (dot-and-dashed lines), and iii) **PPy physisorbed or chemisorbed (1-bond, 2-bond) on OH-terminated ND** (full lines) in the case of 1×1 (111) (a), 2×1 (111) (b), and 2×1 (100) (c) ND slabs.

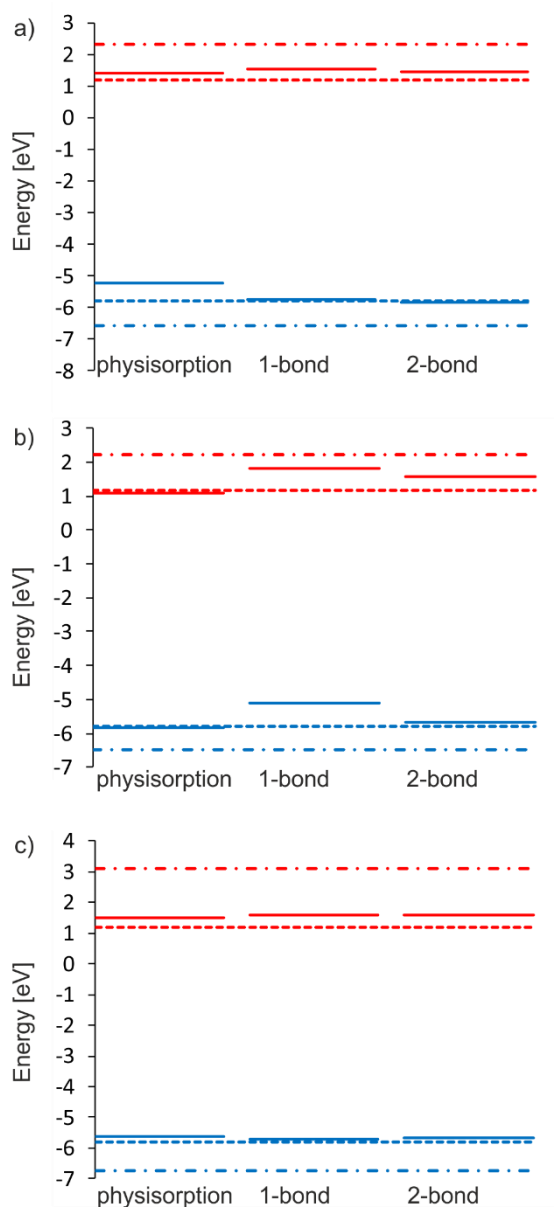


Figure S12: HOMO (blue) and LUMO (red) energy levels of i) **standalone PPy** (dashed lines), ii) **standalone COOH-terminated ND slabs** (dot-and-dashed lines), and iii) **PPy physisorbed or chemisorbed (1-bond, 2-bond) on COOH-terminated ND** (full lines) in the case of 1×1 (111) (a), 2×1 (111) (b), and 2×1 (100) (c) ND slabs.

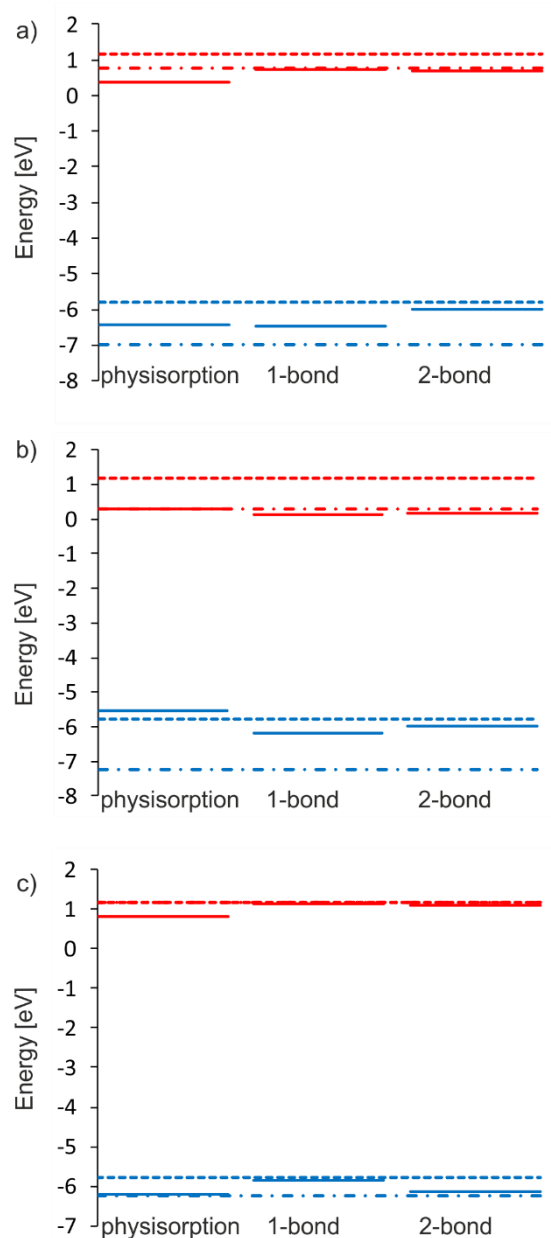


Figure S13: HOMO (blue) and LUMO (red) energy levels of i) **standalone PPy** (dashed lines), ii) **standalone anhydride-terminated ND slabs** (dot-and-dashed lines), and iii) **PPy physisorbed or chemisorbed (1-bond, 2-bond) on anhydride-terminated ND** (full lines) in the case of 1×1 (111) (a), 2×1 (111) (b), and 2×1 (100) (c) ND slabs.

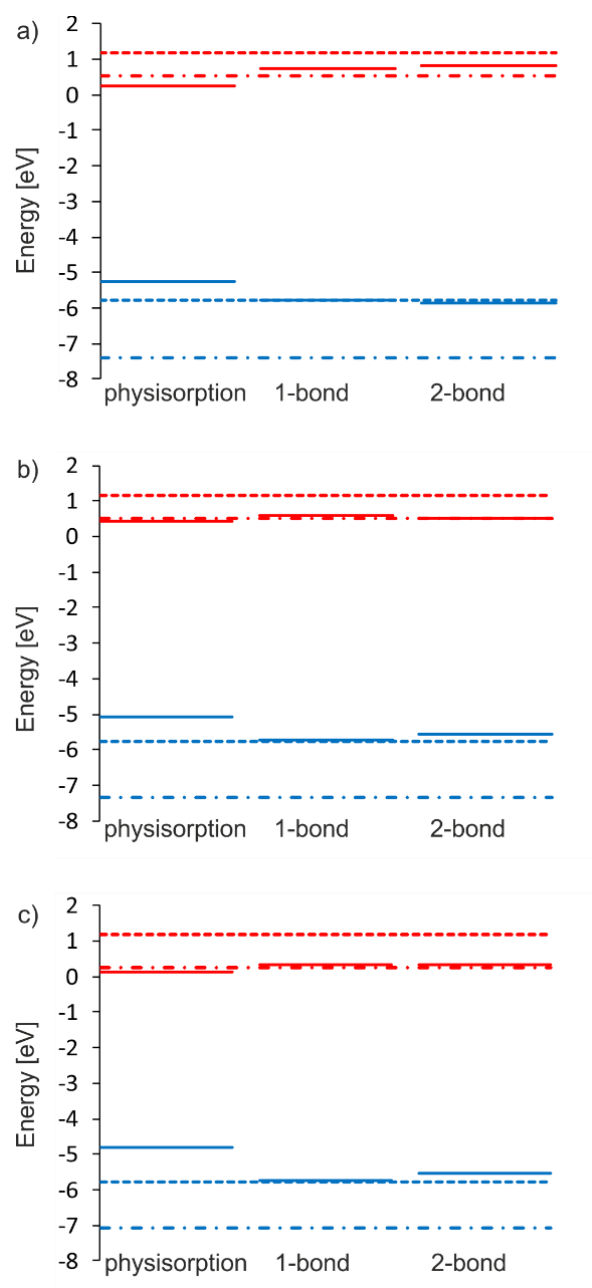


Figure S14: HOMO (blue) and LUMO (red) energy levels of i) **standalone PPy** (dashed lines), ii) **standalone ND slabs with amorphous surface layer** (dot-and-dashed lines), and iii) **PPy physisorbed or chemisorbed (1-bond, 2-bond) on a-C:H** (a) and **a-C:O** slabs (b) (full lines).

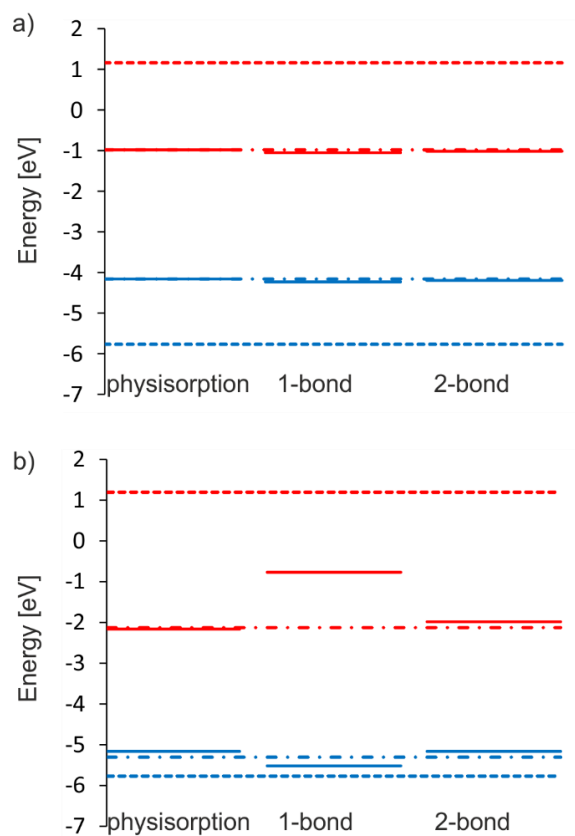


Figure S15: Bond length vs binding energy (E_b) for the PPy-ND chemisorbed structures indicated by blue dots.

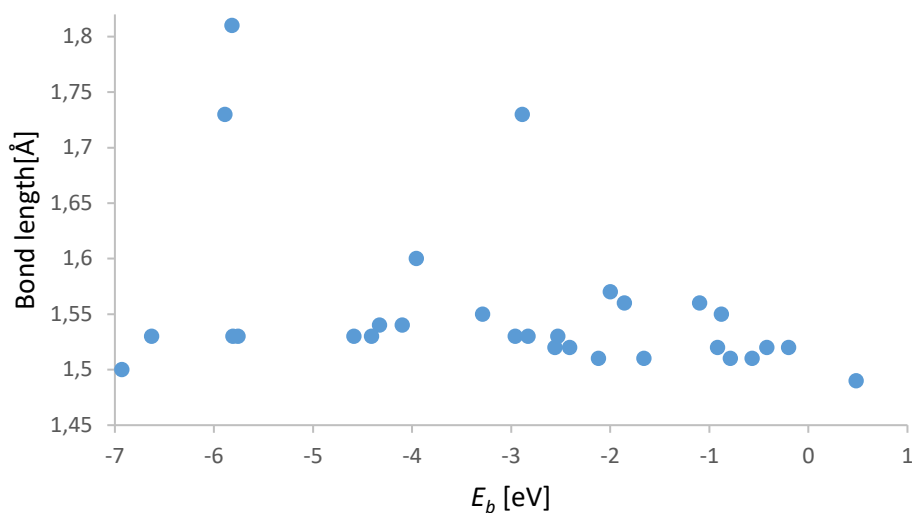


Figure S16: Bond length vs interaction energy (E_{int}) for the PPy-ND structures indicated by blue dots.

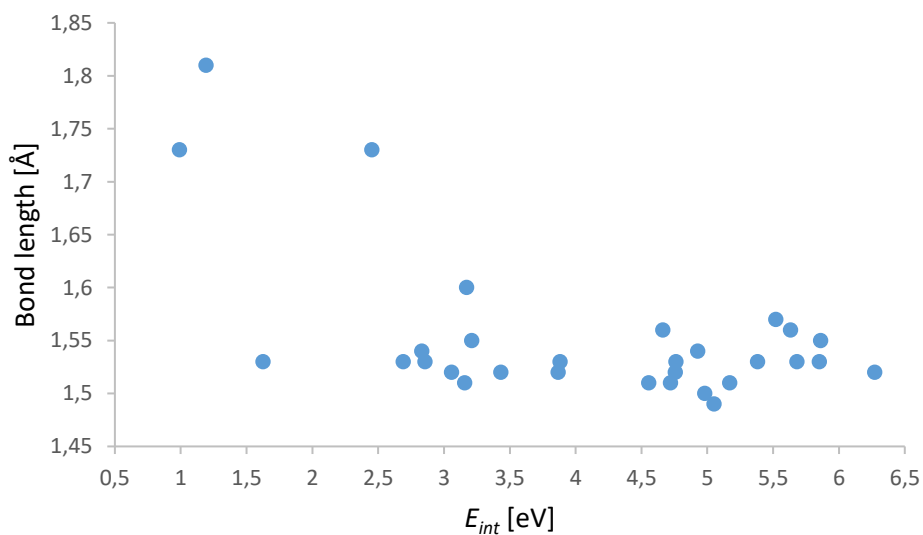


Figure S17: Interaction energy (E_{int}) vs binding energy (E_b) for the PPy-ND structures indicated by blue dots.

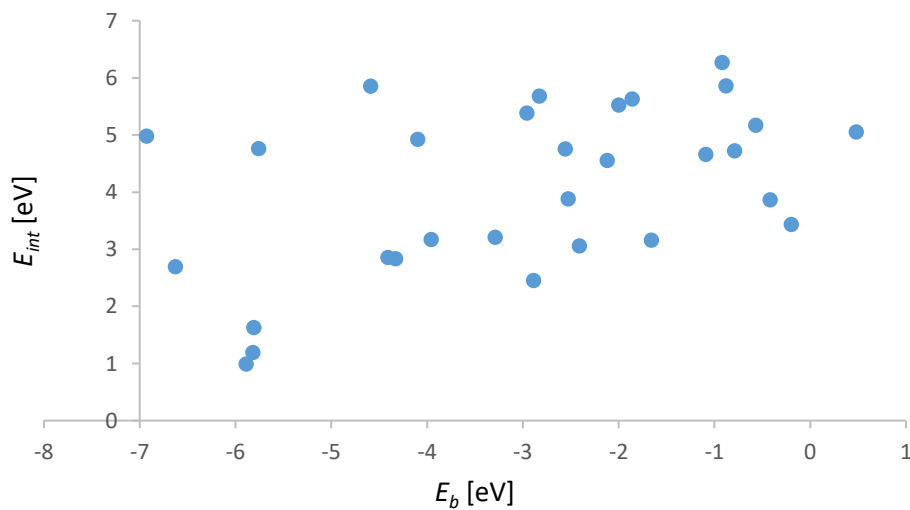


Figure S18: Charge transfer (Δq) vs bond length for the PPy-ND structures indicated by blue dots.

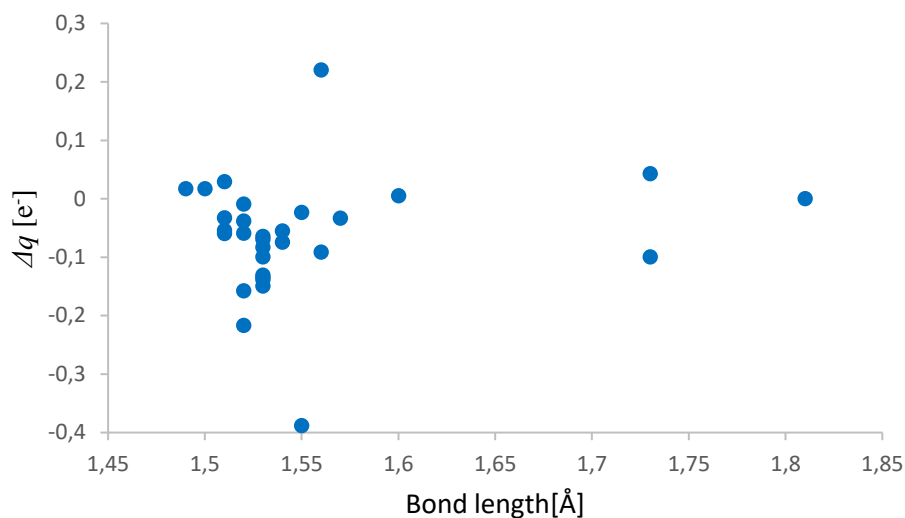


Figure S19: Charge transfer (Δq) vs interaction energy (E_{int}) for the PPy-ND structures indicated by blue dots.

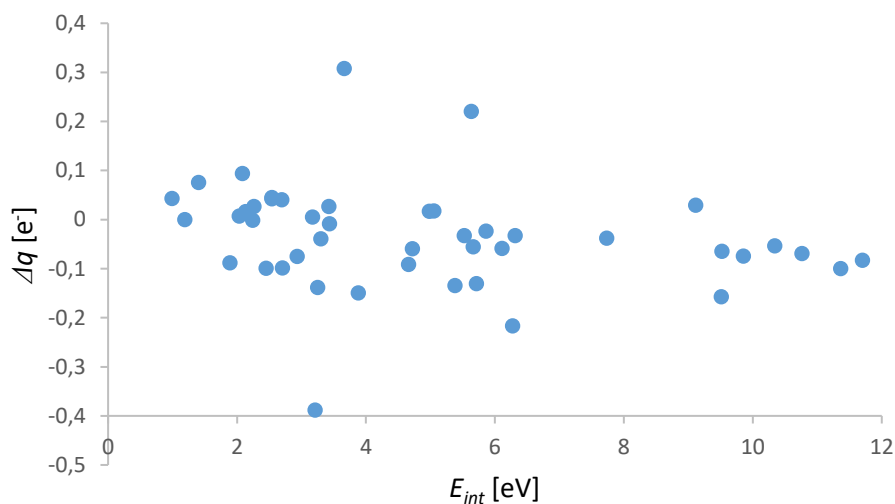


Figure S20: Charge transfer (Δq) vs HOMO-LUMO gap for the PPy-ND structures indicated by blue dots.

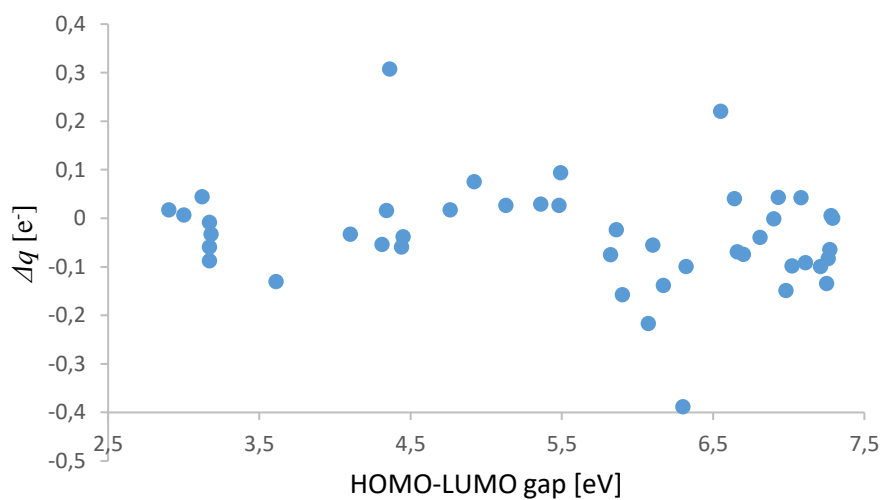


Table S1: Summary of bond lengths between **PPy and O-terminated ND**: ND-PPy bond length [\AA], number of (n) and bond length [\AA] of hydrogen bonds formed between NH groups in PPy and O atoms on ND surface for various bonding configurations. Py heterocycles are numbered from the ND edge (physisorbed PPy) or from the bond with ND (chemisorbed PPy).

PPy-ND structure	Type of bond	Bond length [\AA]	n	Py 1	Py 2	Py 3	Py 4	Py 5	Py 6
1×1 (111), peroxides	physisorption	-	3	3.73; 1.54	-	1.85	-	-	-
1×1 (111), peroxides	1-bond	1.57	1	3.01	-	-	-	-	-
1×1 (111), peroxides	2-bond	1.51; 1.51	0	-	-	-	-	-	-
2×1 (111), epoxides	physisorption	-	2	2.04	-	-	-	2.10	-
2×1 (111), epoxides	1-bond	1.55	1	2.18	-	-	-	-	-
2×1 (111), epoxides	2-bond	1.52; 1.53	0	-	-	-	-	-	-
1×1 (100), ethers	physisorption	-	2	-	1.62	-	2.99	-	-
1×1 (100), ethers	1-bond	1.50	1	2.68	-	-	-	-	-
1×1 (100), ethers	2-bond	1.46; 1.56	0	-	-	-	-	-	-
2×1 (100), epoxides	physisorption	-	1	-	-	-	3.12	-	-
2×1 (100), epoxides	1-bond	1.51	0	-	-	-	-	-	-
2×1 (100), epoxides	2-bond	1.51; 1.52	0	-	-	-	-	-	-

Table S2: Summary of bond lengths between **PPy and OH-terminated ND**: ND-PPy bond length [\AA], number of (n) and bond length [\AA] of hydrogen bonds formed between NH groups in PPy and O atoms on ND surface for various bonding configurations. Py heterocycles are numbered from the ND edge (physisorbed PPy) or from the bond with ND (chemisorbed PPy).

PPy-ND structure	Type of bond	Bond length [\AA]	n	Py 1	Py 2	Py 3	Py 4	Py 5	Py 6
1×1 (111)	physisorption	-	2	2.02	2.94	-	-	-	-
1×1 (111)	1-bond	1.81	3	2.25; 2.32; 2.72	-	-	-	-	-
1×1 (111)	2-bond	1.51; 1.54	0	-	-	-	-	-	-
2×1 (111)	physisorption	-	2	2.76	2.63	-	-	-	-
2×1 (111)	1-bond	1.73	0	-	-	-	-	-	-
2×1 (111)	2-bond	1.52; 1.54	0	-	-	-	-	-	-
2×1 (100)	physisorption	-	1	1.89	-	-	-	-	-
2×1 (100)	1-bond	1.60	2	1.66; 3.03	-	-	-	-	-
2×1 (100)	2-bond	1.52; 1.53	0	-	-	-	-	-	-

Table S3: Summary of bond lengths between **PPy and COOH-terminated ND**: ND-PPy bond length [\AA], number of (n) and bond length [\AA] of hydrogen bonds formed between NH groups in PPy and O atoms on ND surface for various bonding configurations. Py heterocycles are numbered from the ND edge (physisorbed PPy) or from the bond with ND (chemisorbed PPy).

PPy-ND structure	Type of bond	Bond length [\AA]	n	Py 1	Py 2	Py 3	Py 4	Py 5	Py 6
1×1 (111)	physisorption	-	4	-	2.25	-	2.09	2.51	2.02
1×1 (111)	1-bond	1.56	3	1.65	-	2.71	2.13	-	-
1×1 (111)	2-bond	1.52; 1.55	1	2.02	-	-	-	-	-
2×1 (111)	physisorption	-	2	2.63	2.76	-	-	-	-
2×1 (111)	1-bond	1.73	0	-	-	-	-	-	-
2×1 (111)	2-bond	1.52; 1.54	0	-	-	-	-	-	-
2×1 (100)	physisorption	-	3	-	2.06	-	2.52	-	2.34
2×1 (100)	1-bond	1.53	1	2.57	-	-	-	-	-
2×1 (100)	2-bond	1.53; 1.53	0	-	-	-	-	-	-

Table S4: Summary of bond lengths between **PPy and anhydride-terminated ND**: ND-PPy bond length [\AA], number of (n) and bond length [\AA] of hydrogen bonds formed between NH groups in PPy and O atoms on ND surface for various bonding configurations. Py heterocycles are numbered from the ND edge (physisorbed PPy) or from the bond with ND (chemisorbed PPy).

PPy-ND structure	Type of bond	Bond length [\AA]	n	Py 1	Py 2	Py 3	Py 4	Py 5	Py 6
1×1 (111)	physisorption	-	3	2.00	-	1.98	-	-	2.26
1×1 (111)	1-bond	1.56	0	-	-	-	-	-	-
1×1 (111)	2-bond	1.52; 1.53	0	-	-	-	-	-	-
2×1 (111)	physisorption	-	1	2.04	-	-	-	-	-
2×1 (111)	1-bond	1.55	0	-	-	-	-	-	-
2×1 (111)	2-bond	1.53; 1.54	0	-	-	-	-	-	-
2×1 (100)	physisorption	-	3	2.04	-	2.29	-	2.85	-
2×1 (100)	1-bond	1.52	2	2.61	-	-	1.93	-	-
2×1 (100)	2-bond	1.52; 1.52	0	-	-	-	-	-	-

Table S5: Summary of bond lengths between **PPy and NDs with an amorphous surface layer**: ND-PPy bond length [\AA], number of (n) and bond length [\AA] of hydrogen bonds formed between NH groups in PPy and O atoms on ND surface for various bonding configurations. Py heterocycles are numbered from the ND edge (physisorbed PPy) or from the bond with ND (chemisorbed PPy).

PPy-ND structure	Type of bond	Bond length [\AA]	n	Py 1	Py 2	Py 3	Py 4	Py 5	Py 6
a-C:H	physisorption	-	0	-	-	-	-	-	-
a-C:H	1-bond	1.52	0	-	-	-	-	-	-
a-C:H	2-bond	1.51; 1.52	0	-	-	-	-	-	-
a-C:O	physisorption	-	3	-	2.02	-	2.14; 2.77	-	-
a-C:O	1-bond	1.49	1	1.90	-	-	-	-	-
a-C:O	2-bond	1.49; 1.53	0	-	-	-	-	-	-

Table S6: Summary of binding energy (E_b), interaction energy (E_{int}), charge transfer (Δq), and HOMO-LUMO gap of **PPy on O-terminated NDs**. ND structure without PPy bonding (“none”) corresponds to a standalone ND.

ND surface structure	PPy bonding	E_b [eV]	E_{int} [eV]	Δq [e^-]	HOMO-LUMO gap [eV]
1×1 (111), peroxides	physisorption	3.66	3.66	0.31	4.36
1×1 (111), peroxides	1-bond	-2.00	5.52	-0.03	4.10
1×1 (111), peroxides	2-bond	-0.57	10.34	-0.05	4.31
1×1 (111), peroxides	none	-	-	-	8.07
2×1 (111), epoxides	physisorption	2.54	2.54	0.04	3.12
2×1 (111), epoxides	1-bond	-0.88	5.86	-0.02	5.86
2×1 (111), epoxides	2-bond	-4.41	5.71	-0.13	3.61
2×1 (111), epoxides	none	-	-	-	5.21
1×1 (100), ethers	physisorption	3.42	3.42	0.03	5.13
1×1 (100), ethers	1-bond	-6.93	4.98	0.02	2.90
1×1 (100), ethers	2-bond	-2.12	9.11	0.03	5.36
1×1 (100), ethers	none	-	-	-	7.56
2×1 (100), epoxides	physisorption	2.13	2.13	0.02	4.34
2×1 (100), epoxides	1-bond	-0.79	4.72	-0.06	4.44
2×1 (100), epoxides	2-bond	-0.42	7.73	-0.04	4.45
2×1 (100), epoxides	none	-	-	-	6.34

Table S7: Summary of binding energy (E_b), interaction energy (E_{int}), charge transfer (Δq), and HOMO-LUMO gap of **PPy on OH-terminated NDs**. ND structure without PPy bonding (“none”) corresponds to a standalone ND.

ND surface structure	Type of bond	E_b [eV]	E_{int} [eV]	Δq [e^-]	HOMO-LUMO gap [eV]
1×1 (111)	physisorption	2.69	2.69	0.04	6.64
1×1 (111)	1-bond	-5.82	1.19	0.02	7.29
1×1 (111)	2-bond	-5.76	9.52	-0.06	7.27
1×1 (111)	none	-	-	-	8.88
2×1 (111)	physisorption	2.24	2.24	-0.002	6.90
2×1 (111)	1-bond	-5.89	0.99	0.04	6.93
2×1 (111)	2-bond	-6.63	5.38	-0.13	7.25
2×1 (111)	none	-	-	-	8.71
2×1 (100)	physisorption	2.54	2.54	0.04	7.08
2×1 (100)	1-bond	-3.96	3.17	0.01	7.28
2×1 (100)	2-bond	-4.59	11.7	-0.08	7.26
2×1 (100)	none	-	-	-	9.81

Table S8: Summary of binding energy (E_b), interaction energy (E_{int}), charge transfer (Δq), and HOMO-LUMO gap of **PPy on COOH-terminated NDs**. ND structure without PPy bonding (“none”) corresponds to a standalone ND.

ND surface structure	Type of bond	E_b [eV]	E_{int} [eV]	Δq [e ⁻]	HOMO-LUMO gap [eV]
1 × 1 (111)	physisorption	3.30	3.30	-0.04	6.81
1 × 1 (111)	1-bond	-1.09	4.66	-0.09	7.11
1 × 1 (111)	2-bond	-4.10	9.85	-0.07	6.70
1 × 1 (111)	none	-	-	-	7.77
2 × 1 (111)	physisorption	2.93	2.93	-0.07	5.82
2 × 1 (111)	1-bond	-2.89	2.45	-0.10	6.32
2 × 1 (111)	2-bond	-5.81	3.25	-0.14	6.17
2 × 1 (111)	none	-	-	-	7.54
2 × 1 (100)	physisorption	2.70	2.70	-0.10	7.02
2 × 1 (100)	1-bond	-2.53	3.83	-0.15	6.98
2 × 1 (100)	2-bond	-2.83	11.36	-0.10	7.21
2 × 1 (100)	none	-	-	-	7.41

Table S9: Summary of binding energy (E_b), interaction energy (E_{int}), charge transfer (Δq), and HOMO-LUMO gap of **PPy on anhydride-terminated NDs**. ND structure without PPy bonding (“none”) corresponds to a standalone ND.

ND surface structure	Type of bond	E_b [eV]	E_{int} [eV]	Δq [e ⁻]	HOMO-LUMO gap [eV]
1 × 1 (111)	physisorption	2.08	2.08	0.09	5.49
1 × 1 (111)	1-bond	-1.86	5.63	0.22	6.55
1 × 1 (111)	2-bond	-2.96	10.76	-0.07	6.66
1 × 1 (111)	none	-	-	-	7.92
2 × 1 (111)	physisorption	2.26	2.26	0.03	5.48
2 × 1 (111)	1-bond	-3.29	4.29	-0.39	6.3
2 × 1 (111)	2-bond	-4.33	5.66	-0.06	6.1
2 × 1 (111)	none	-	-	-	7.83
2 × 1 (100)	physisorption	1.40	1.40	0.08	4.92
2 × 1 (100)	1-bond	-0.92	6.27	-0.22	6.07
2 × 1 (100)	2-bond	-2.56	9.51	-0.16	5.90
2 × 1 (100)	none	-	-	-	7.32

Table S10: Summary of binding energy (E_b), interaction energy (E_{int}), charge transfer (Δq), and HOMO-LUMO gap of **PPy on NDs with an amorphous surface layer**. ND structure without PPy bonding (“none”) corresponds to a standalone ND.

ND surface structure	Type of bond	E_b [eV]	E_{int} [eV]	Δq [e ⁻]	HOMO-LUMO gap [eV]
a-C:H	physisorption	1.89	1.89	-0.09	3.17
a-C:H	1-bond	-0.20	3.43	-0.01	3.17
a-C:H	2-bond	-2.41	6.11	-0.06	3.17
a-C:H	none	-	-	-	3.17
a-C:O	physisorption	2.03	2.03	0.01	3.00
a-C:O	1-bond	0.48	5.05	-0.12	4.76
a-C:O	2-bond	-1.66	6.31	-0.03	3.18
a-C:O	none	-	-	-	3.17